TECHNISCHE UNIVERSITÄT MÜNCHEN

Department Chemie
Lehrstuhl für Theoretische Chemie

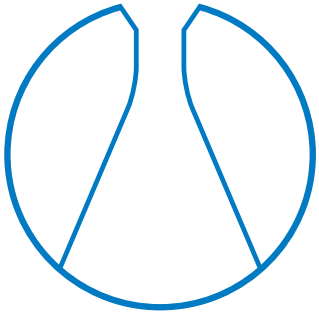

First-Principles Description of the Isomerization Dynamics of Surface-Adsorbed Molecular Switches

DISSERTATION

Reinhard Johann Maurer

TECHNISCHE UNIVERSITÄT MÜNCHEN

Lehrstuhl für Theoretische Chemie

First-Principles Description of the Isomerization Dynamics of Surface-Adsorbed Molecular Switches

Reinhard Johann Maurer

Vollständiger Abdruck der von der Fakultät für Chemie der Technischen Universität München zur Erlangung des akademischen Grades eines

Doktors der Naturwissenschaften (Dr. rer. nat.)

genehmigten Dissertation.

Vorsitzender : Univ.-Prof. Dr. Ville Kaila

Prüfer der Dissertation:

1. Univ.-Prof. Dr. Karsten Reuter
2. Univ.-Prof. Dr. Johannes Barth
3. Univ.-Prof. Dr. Peter Saalfrank, Universität Potsdam (schriftliche Beurteilung)
3. Univ.-Prof. Moniek Tromp, Ph.D. (mündliche Prüfung)

Die Dissertation wurde am 28.11.2013 bei der Technischen Universität München eingereicht und durch die Fakultät für Chemie am 15.01.2014 angenommen.

Für Katja

Unsere gemeinsame Verrücktheit hält mich bei Vernunft

Abstract

The constant pursuit of miniaturization of electronic devices has reached the point, where further integration may only be achieved if individual molecules constitute the main functional units of such devices. Corresponding functional molecular switches can be triggered via light or electrical stimuli. Unfortunately, current design strategies of such molecules are based on trial and error and more often than not the molecular function is quenched by overly strong coupling to the environment. This thesis attempts a full parameter-free first-principles description of the key variables that determine surface-adsorbed molecular switching. This is done on the prototypical testcase of photo-induced isomerization of coinage metal adsorbed Azobenzenes. Herefore specifically the effects of differing substrate and molecular functionalization are investigated. Employing dispersion-corrected Density-Functional Theory, a correct model of the structure and energetics of adsorbed Azobenzene is established. Including the lateral interactions in high coverage situations and vibrational anharmonicity, an excellent agreement with experiment can be reached and a solid benchmark of the method is given. Drastic implications on the mechanism follow from ground-state isomerization paths. An unbalanced adsorption of different geometries leads to an effective loss of bistability and the switching function at reactive surfaces. These results suggest that future molecular device design will have to focus on functionalization that accounts for a balanced stabilization of all intermediate states. Recent experiments revealed a photo-induced switching mechanism for tetra-*tert*-butyl functionalized Azobenzene (TBA) at Au(111). It is believed that isomerization is triggered by excitation from the metal *d*-bands rather than from the adsorbate states followed by subsequent charge-transfer between substrate and adsorbate. In order to further investigate the detailed photo-isomerization dynamics, an efficient approach to low lying excited states of large adsorbate systems based on a recently proposed variant of the Δ-Self-Consistent-Field method has been established. The method yields a topologically correct description of excited-state potential energy surfaces and a qualitative account of hybridization and image charge effects. A systematic comparison between excited states that are involved in gas-phase and substrate-mediated excitations enables a rationalization of the effects of functionalization and substrate adsorption. The resulting picture suggests that although the electronic dynamics are fundamentally different from the gas-phase, the nuclear dynamics will follow similar mechanisms. Finally, possible paths towards the explicit dynamical simulations of the photoisomerization mechanism are outlined.

Kurzfassung

Die fortschreitende Miniaturisierung elektronischer Bauteile gelangt mit der Zeit in Dimensionen, in denen einzelne Moleküle funktionale Grundeinheiten repräsentieren. Entsprechende funktionale Schaltermoleküle können mit Licht oder Elektronen in verschiedene Zustände überführt werden, jedoch basieren derzeit übliche Strategien zur Entwicklung solcher molekularen Systeme auf empirischen Versuchsreihen und einfachen Rezepten. Sehr oft führt dies dazu, dass die intrinsische molekulare Funktionalität durch zu starke Wechselwirkung mit der Umgebung verloren geht. Diese Arbeit beschreibt mittels parameterfreier Simulation auf Basis quantenmechanischer Methoden die wichtigsten Variablen, die die Schaltfähigkeit von Molekülen an Oberflächen bestimmen. Am Beispiel der photo-induzierten Isomerisierung von Azobenzenen an Münzmetalloberflächen werden insbesondere die Effekte verschiedener Oberflächen und variabler Adsorbatfunktionalisierung analysiert. Mit Hilfe dispersionskorrigierter Dichtefunktionaltheorie wird hierbei ein akkurates Modell der Struktur und Energetik adsorbierter Azobenzene erstellt. Insbesondere die Berücksichtigung lateraler Wechselwirkungen in hohen Packungsdichten und der Struktureffekte anharmonischer Molekülschwingungen erlauben eine genaue Beschreibung in Einklang mit der experimentell beobachteten Struktur und bestätigen damit die Zuverlässigkeit des Modellierungsansatzes. Die Untersuchung von Reaktionspfaden entlang entscheidender Freiheitsgrade ergibt, dass auf reaktiveren Oberflächen als Gold geometrisch inkonsistente Adsorption die Schaltfunktion durch Aufhebung der Bistabilität verhindert. Zukünftige Ansätze zur Entwicklung funktionaler Adsorbate sollten daher die gleichmäßige Stabilisierung aller involvierten Geometrien anstreben. Im Falle von tetra-*tert*-butyl-Azobenzen adsorbiert an Au(111) konnte experimentell eine photoinduzierte Schaltfunktion nachgewiesen werden. Jedoch liegt die Vermutung nahe, dass der zugrundeliegende Mechanismus auf elektronischen Anregungen aus dem Substrat statt aus dem Adsorbat basiert, die in weiterer Folge einen Ladungstransfer zwischen Molekül und Oberfläche induzieren. Um die Details des photo-induzierten Schaltprozesses weiter zu untersuchen, wurde eine effiziente Methode zur Berechnung niedrig liegender Anregungen großer Adsorbate auf Basis der kürzlich vorgeschlagenen „linear expansion Δ-Self-Consistent Field“ Methode entwickelt. Diese erlaubt eine qualitativ korrekte Beschreibung der Topologie der angeregten Zustände, sowie der substratinduzierten Hybridisierungs- und Bildladungseffekte. Ein systematischer Vergleich der beteiligten angeregten Zustände in den Schaltprozessen des isolierten und des adsorbierten Moleküls erlaubt eine Rationalisierung der Substrat- und Funktionalisierungseffekte. Die Resultate lassen vermuten, dass die elektronischen Mechanismen in adsorbierten Molekülen anders sind, dass jedoch die Kernbewegungen ähnlichen Regeln wie in der Gasphase folgen. Zuletzt werden mögliche Wege zur Beschreibung der expliziten nicht-adiabatischen Moleküldynamik des Photoisomerisierungsmechanismus erläutert.

Contents

Abbreviations

ΔSCF-DFT Delta-Self-Consistent-Field Density-Functional Theory

2PPE 2-Photon-Photoexcitation

Ab Azobenzene

BOA Born-Oppenheimer Approximation

CC Coupled Cluster

CI Conical Intersection

CI(SD) Configuration Interaction (Singles and Doubles)

cn clamped nuclei approximation

DBA para-di-*tert.*-butyl-Azobenzene

DFA Density-Functional Approximation

DFT Density-Functional Theory

DOF degree of freedom

EA Electron Affinity

FC Franck-Condon

Fig. Figure

FLOPS Floating Point Operation per second

GAOs Gaussian-type Atomic Orbitals

GGA Generalized Gradient Approximation

HK Hohenberg-Kohn

HOMO Highest Occupied Molecular Orbital

HP Hartree Product

IP Ionization Potential

LDA Local Density Approximation

leΔSCF linear expansion Delta-Self-Consistent Field

LUMO Lowest Unoccupied Molecular Orbital

MOs Molecular Orbitals

NAC non-adiabatic coupling

NAOs Numerical Slater-type Atomic Orbitals

NEXAFS Near-Edge X-Ray Absorption Finestructure Spectroscopy

PP Pseudopotential

RI Resolution of Identity

RMSD Root Mean Square Deviation

SAOs Slater-type Atomic Orbitals

sc self-consistent

SCF Self-Consistent Field

SM Sum Method

STA Sudden Transition and Averaging

TBA 3,3',5,5'-tetra-*tert*-butyl-Azobenzene

TD-DFT Time-Dependent Density-Functional Theory

TD-KS Time-Dependent Kohn-Sham

TSH Tully's Surface Hopping

USPP Ultrasoft-Pseudopotential

vdW van der Waals

xc exchange-corelation

ZPE Zero Point Energy

1 Introduction

Starting from the middle of the 20th century, electronic devices used for any kind of communication technology, computers, or power electronics immensly improved in terms of complexity and integration. This has led to supercomputers in the year 2005 (1 Peta-Floating Point Operation per second, FLOPS) being 1 billion times faster than the fastest computer in 1961 (1.2 Mega-FLOPS, IBM 7030 'Stretch' at Los Alamos National Laboratory, New Mexico, USA). Standard smart phones in the year 2013 have a computing power exceeding 1 Giga-FLOPS. The main source of this success is the constant miniaturization of the main active component of any electronic device - the transistor. Current computers contain microprocessors with many million transistors per mm^2, where the size of each transistor is in the sub-micrometer regime. With this integration density, the smallest components already only consist of some 1000s of atoms. It is therefore easily to be expected that in the future single atoms or molecules can act as the main building blocks of electronic devices [1, 2]. Such molecular nanotechnological devices may ultimately enable data storage or logical operations on atomistic length scales. With this in mind it is very easy to dream up many more possible applications of such molecular machinery ranging from nanosensors [3] and molecular functionalized surfaces [4] to single molecular machines [5].

A key ingredient of molecular nanotechnology is the ability to selectively stimulate reversible changes on the single molecule level. Molecules fulfilling this prerequisite have been termed molecular switches - molecular representations of binary 'ON' and 'OFF' operations [6]. These changes can be in the form of discrete modifications to the molecular conformation, the chemical state, the magnetic state, or in fact any other measurable molecular property. Embedded in a matrix [7] or adsorbed at well-defined surfaces [8], such molecules should be switchable individually or in domains, and the corresponding changes have to be detectable in terms of simple electric or spectroscopic changes. Prospective systems will have to have very high chemical and physical stability at ambient conditions to ensure a sufficiently high number of switching events during a life cycle. In order to meet such requirements, a large effort has to be undertaken to ensure intelligent chemical design and physical characterization of possible candidate molecules, as well as the effect of an embedding environment on the function.

The function of molecular switches depends on a delicate interplay of different quantum molecular interactions within the molecule and with the underlying substrate. Often enough a well understood efficient switching mechanism in the gas-phase or solution is not observed in an adsorbed state. A systematic characterization and design at the atomic-scale can presently only happen at reduced complexity and controlled conditions; this can be achieved in a *surface science* approach. Hereby, small amounts of molecules are adsorbed on specific facets of clean single crystal surfaces in ultra high vacuum. Under these ideal conditions, the effect of the surface on the geometry and electronic structure of the molecule and *vice versa* can then be studied by a variety of spectroscopic techniques as well as quantum molecular simulation methods. The success of this approach has been highlighted by the award of the nobel price in Chemistry for Gerhard Ertl in 2007[1].

[1] www.nobelprize.org

Employing this approach, a large variety of molecular switches is currently investigated for their functionality. This includes molecules that undergo changes due to chemical reactions [9], conformational changes [10], or magnetic spin transitions [11, 12]. The means to induce switching range from light irradiation to thermal activation [13] and inelastic electron tunneling [14]. Some of the most successful examples include surface-adsorbed molecules, acting as molecular motors [15, 16], rotors [17], and even molecular cars [18]. In all cases, to achieve function in a surface-mounted state, interactions with the substrate should be strong enough for an ordered structure to be formed, but weak enough for the switching ability not to be quenched. Especially on metal surfaces the latter is a big concern. Nevertheless, metal surfaces are specifically appealing as substrates, due to the direct electronic contact, but also due to the electronic coupling that might introduce new switching pathways and mechanisms.

Current research on promising molecular switches is often based on trial and error. A detailed understanding of the corresponding nuclear and electronic dynamics involved in molecular switching processes on surfaces is a prerequisite for a rational design of functioning devices. Quantum theory based simulation of mindfully chosen prototypes is able to aid the understanding of surface-mounted molecular switching processes. With computers constantly multiplying in speed and size, current methods allow to tackle nanotechnologically relevant large-scale systems with good accuracy. Nevertheless, a large number of approximations on different levels have to be applied to enable the description of hundreds or thousands of particles. For such a modelling approach to be reliable it has to be constantly benchmarked against experiment.

In this context, this work will investigate metal surface-adsorbed molecular switching on the example of a particular molecular switch, namely Azobenzene adsorbed to coinage metal surfaces. Azobenzene (H_5C_6-N=N-C_6H_5, Ab) and diazenes in general are prototypical examples of conformational binary molecular switches. The two different conformers, E(trans)-Azobenzene and Z(cis)-Azobenzene, can be reversibly photoswitched with two different wavelengths in solution [19, 20]. In contrast, the molecule and its various derivatives have shown a strong dependence of the switching function on different underlying substrates or differing chemical derivation. The above mentioned quenching of the photoswitching ability is observed for Azobenzene upon adsorption to coinage metal surfaces [21–23]. Overly strong coupling to the surface might drastically reduce the lifetime of the excited states by allowing fast energy transfer, and was correspondingly cited as one possible reason for the observed loss of switching function [24–26]. In addition to the electronic coupling, steric hindrance might also prevent molecular motion. A corresponding approach to lift off the molecule by derivatizing it with bulky spacer groups has led to the successful switching of 3,3',5,5'-tetra-*tert*-butyl-Azobenzene (TBA) on Au(111), although with drastically reduced efficiency compared to the solution [21, 26]. A detailed analysis of the TBA molecule and Azobenzene adsorbed on the Au(111) surface has revealed that the position of the central photochromic diazo-bridge is barely affected by the bulky spacer groups [27]. Therefore, pure sterical decoupling arguments fail to explain the regained switching function. To add to this discrepancy, experimental evidence points to a strongly modified light-induced mechanism for metal-mounted switching in the case of TBA [28].

Analyzing all above observations in detail, this work aims for a parameter-free description and conceptual understanding of the key factors that decide on the survival of molecular function upon surface adsorption. Therefore, a first-principles based quantum molecular description is established including the geometrical, electronic, and dynamical factors that determine the transient functional behavior. Based on an accurate structural model for Azobenzene and TBA, a detailed and comparative analysis of the prerequisites that govern the photo-induced switching function will be conducted. Extracting the main ingredients that form a functioning adsorbed molecular switch will enable to formulate general rules to rational design strategies for future functioning devices.

Structure and Objectives of this Work

Part I of this thesis will set the stage by giving a concise introduction to the methods and numerical tools that are used in this work and that served as a basis for further developments and implementations. This may only serve as a reference to the great pioneering works in the corresponding fields though. Chapter 2 is specifically concerned with the general problem of describing a molecular many-body system in the framework of quantum mechanics and how few approximations can make a seemingly unfeasible task numerically tractable. Whereas the canonical way of systematically improving and expanding electronic wave functions gives rise to so-called wave function or Post-Hartree-Fock methods, chapter 3 presents an intriguingly simple way of how to represent the many-body problem in a very different way, namely in the form of Density-Functional Theory, which, together with its extensions, forms the main theoretical body underlying this work. The main concern of this work is the description of adsorption phenomena on idealized, extended coinage metal surfaces. Chapter 4 shows another example of how a theory, namely the theory of the solid state, can break a problem such as the description of an infinitely extended surface down to describing its smallest irreducible unit. The methods described in the above chapters represent the main tool set with which chemists or physicists study the chemical and physical properties of molecular systems in equilibrium.

Part II will focus on the photo-induced isomerization dynamics of isolated Azobenzene in the gas-phase. One particular reason for the choice of this molecule as a prototypical test case is the vast amount of experimental and theoretical work on its isomerization mechanism. A corresponding literature review is attempted in chapter 5. The main focus of this thesis is the description of surface-mounted light-induced molecular switching of large organic molecules. Therefore, one important objective is to **find a numerically highly efficient way to calculate electronic excited states**. In chapter 6 the Delta-Self-Consistent-Field Density-Functional Theory (ΔSCF-DFT) method of calculating low lying excited-state energies is analysed for its ability to describe excited states of gas-phase Azobenzene that are relevant to the photoisomerization process.

Part III focuses on the ground-state structural and electronic properties of Azobenzene adsorbed to coinage metals. The fact that many experimental and several theoretical works have laid the grounds for this work, motivates a second more in-depth review of recent literature on metal-adsorbed switching, which is given in chapter 7. This is followed by a detailed investigation of the two stable ground-state isomers of Azobenzene and its derivative tetra-*tert*-butyl-Azobenzene in terms of adsorption structure and energetics (Chapter 8) with a specific focus on **establishing an accurate structural model** on the basis of very recent advances in the account of dispersion interactions between the adsorbate and the substrate. In chapter 9 **the quality of the established structural model is confirmed** by a detailed comparison to structural data from X-ray standing wave experiments. Excellent agreement can be achieved by additionally accounting for the structural changes due to ambient experimental conditions. In the final chapter of this part (chapter 10), the thermodynamic stability of the two ground-state isomers is investigated in terms of the thermal reaction pathways between them. From this, the **gain and loss of important prerequisites to adsorbed switching** can be rationalized and furthermore possible **rational design strategies are formulated**.

The final part IV of this work focuses on the electronic excited states and explicit isomerization dynamics of surface adsorbed Azobenzene molecules. Current computer infrastructures, as much as they have advanced, still do not enable the application of current accurate excited state methodologies on adsorbate systems of this size. Based on the assessment of the ΔSCF-DFT method in chapter 6 and a recent approach put forward by Gavnholt *et al.* [29] **an efficient ap-**

proach to low lying electronic excitations of metal adsorbed molecules is established (chapter 11). Employing this methodology, the **excited-state potential energy landscape along important pathways is characterized** in chapter 12 and, based on this, first conclusions on the mechanism are drawn. The final chapter of this part attempts to analyse and put together all necessary ingredients to **establish an explicit excited-state dynamics simulation setup** that is able to describe the transient nuclear and electronic dynamics associated with adsorbed molecular switching.

The work is concluded in chapter 14; additional material is found in the appendices.

Part I

Theoretical Background

2 Quantum Many-Body Theory

This and the following chapters present a short account of the theoretical foundations on which this work is laid. Descriptions closely follow the books of Szabo and Ostlund [30], Fetter and Walecka [31], and Parr and Yang [32]. For more detailed descriptions the reader is referred to these works. This short review builds on the basic knowledge of quantum mechanics and quantum molecular model systems that is conveyed and described, for example, in the books of McQuarrie [33] or Kutzelnigg [34].

2.1 The Electronic Problem and the Schrödinger Equation

The simultaneous movement of interacting electrons and nuclei in molecular systems is within quantum mechanics described by the Schrödinger equation [35]. Including all important interaction terms, the Schrödinger equation gives an accurate account of quantum many-particle systems in the non-relativistic limit. The equation reads[1]

$$i\frac{d}{dt}\Psi(\mathbf{r}_1,\ldots,\mathbf{r}_N,t) = \hat{H}\Psi(\mathbf{r_1},\ldots,\mathbf{r_N},t), \tag{2.1}$$

with $\Psi(\mathbf{r}_1,\cdots\mathbf{r}_N,t)$ being the many-body wave function of the system; this function depends on all spatial coordinates $\mathbf{r}_i$ and on time t. $\hat{H}$ represents the Hamiltonian or energy operator of the system, consisting of two terms:

$$\hat{H} = \sum_{i=1}\hat{T}(\mathbf{r}_i) + \sum_i\sum_{i>j}V(\mathbf{r}_i,\mathbf{r}_j), \tag{2.2}$$

where $\hat{T}(\mathbf{r}_i)$ is the kinetic energy operator of particle i and V is the potential energy between two interacting particles i and j; sums run over all particles or pairs of particles. Quantum mechanical spin is not explicitly contained in non-relativistic non-magnetic Hamiltonians, but enters as wave function variable via boundary conditions[2]. If the system is in a stationary, time-independent state, the Schrödinger equation reduces to the eigenvalue equation:

$$\hat{H}\Psi_i(\mathbf{r_1},\ldots,\mathbf{r_N}) = E_i\Psi_i(\mathbf{r_1},\ldots,\mathbf{r_N}). \tag{2.3}$$

The eigenvalue spectrum of this equation corresponds to the energies of the ground and excited states E_i with corresponding eigenfunctions Ψ_i. The only interaction considered between particles is the Coulomb interaction.

The Hamiltonian of a general molecular system containing N electrons and M nuclei can be written in explicit form as

$$\hat{H} = \underbrace{-\sum_{i=1}^{N}\frac{1}{2}\nabla_i^2}_{\hat{T}_{\text{electrons}}} \underbrace{-\sum_{A=1}^{M}\frac{1}{2M_A}\nabla_A^2}_{\hat{T}_{\text{nuclei}}} \underbrace{-\sum_{i=1}^{N}\sum_{A=1}^{M}\frac{Z_A}{r_{iA}}}_{V_{\text{elec-nuc}}} \underbrace{+\sum_{i=1}^{N}\sum_{j>i}^{N}\frac{1}{r_{ij}}}_{V_{\text{elec-elec}}} \underbrace{+\sum_{A=1}^{M}\sum_{B>A}^{M}\frac{Z_AZ_B}{R_{AB}}}_{V_{\text{nuc-nuc}}}. \tag{2.4}$$

[1] This equation is expressed in atomic units as are all equations below, if not stated otherwise. Consult Szabo and Ostlund [30], p.41 or the webpage physics.nist.gov for more details on atomic units.

[2] In this work, spin is subsummed with spatial variables in the vectors $\mathbf{r}$.

The terms of the Hamiltonian include, in this order, the kinetic energy of the electrons, the kinetic energy of the nuclei (with M_A being the mass of nucleus A in multiples of the electron mass), the potential due to attractive Coulomb interaction between nuclei and electrons (with Z_A being the atomic number of nucleus A), the potential due to repulsive Coulomb interaction between electrons, and the potential due to repulsive interaction between nuclei (r and R correspond to the respective distances between electrons and nuclei).

Solving the time-independent Schrödinger equation (eq. 2.3) of a quantised system yields a set of total energies and wave functions; all observables of the system can be cast as functionals of these wave functions. Unfortunately, there is no analytical solution to this problem for more than two particles (i.e. systems that are bigger than the hydrogen atom). Moreover, the wave functions are high-dimensional functions of $3 \cdot (\mathrm{N+M})$ spatial variables and a numerical evaluation with reasonable accuracy is problematic already just on the level of storing such objects in computer memory.

A standard quantum mechanical approach to such a complex system is to partition the problem into simple mathematically feasible subsystems; if interactions are weak or negligible the subsystems can be mathematically separated. Such a separation can often be done for the quantum motion of both electrons and nuclei, because of different time and length scales in which they move.

2.2 The Born-Oppenheimer Approach

The Hamiltonian of a molecular system can be separated into an electronic and a nuclear part, coupled via the electron-nuclear attraction term:

$$\hat{H} = \underbrace{\hat{T}_{\mathrm{elec}} + V_{\mathrm{elec-elec}}}_{\text{electronic}} + \underbrace{\hat{T}_{\mathrm{nuc}} + V_{\mathrm{nuc-nuc}}}_{\text{nuclear}} + V_{\mathrm{elec-nuc}}. \tag{2.5}$$

Since the mass of the smallest atomic nucleus is approximately 1800 times bigger than the mass of an electron, to every move of an atomic nucleus the electronic motion is almost instantaneously equilibrated; within the reference frame of the electrons, the nuclei seem frozen. It is therefore a common approximation to set the nuclear kinetic energy to zero [36] (clamped nuclei approximation or cn in what follows); $V_{\mathrm{elec-nuc}}$ now only has the positions of the electrons as variables and $V_{\mathrm{nuc-nuc}}$ is a constant term. The coupling therefore vanishes and the two subsystems can be separated into an electronic Hamiltonian and a nuclear Hamiltonian, and two distinct eigenvalue problems, which are only parametrically connected.

After this separation, the electronic Hamiltonian and the corresponding Schrödinger equation can be written as

$$\hat{H}^{\mathrm{cn}}_{\mathrm{elec}} = -\sum_{i=1}^{N} \frac{1}{2}\nabla_i^2 + \sum_{i=1}^{N}\sum_{j>i}^{N} \frac{1}{r_{ij}} - \sum_{i=1}^{N}\sum_{A=1}^{M} \frac{Z_A}{r_{iA}} \tag{2.6}$$

$$\text{and} \quad \hat{H}^{\mathrm{cn}}_{\mathrm{elec}}\Phi(\mathbf{r};\mathbf{R}) = E^{\mathrm{cn}}_{\mathrm{elec}}(\mathbf{R})\Phi(\mathbf{r};\mathbf{R}). \tag{2.7}$$

Here $\mathbf{r}$ and $\mathbf{R}$ represent the set of variables of the electrons and atomic nuclei. The atomic positions only enter as parameters, leaving the electronic energy E_{elec} a parametric function of these positions. The electronic energy, including the nuclear-nuclear repulsion, therefore acts as a potential in which the atomic nuclei move and the corresponding problem of molecular

translations, vibrations, and rotations can be solved on this potential via[3]:

$$\hat{H}_{\text{nuc}} = -\sum_{A=1}^{M} \frac{1}{2M_A}\nabla_A^2 + \sum_{A=1}^{M}\sum_{B>A}^{M} \frac{Z_A Z_B}{R_{AB}} + E_{\text{elec}}^{cn}(\mathbf{R}) \tag{2.8}$$

$$\text{and} \quad \hat{H}_{\text{nuc}} \cdot \chi(\mathbf{R}) = E_{\text{nuc}} \cdot \chi(\mathbf{R}). \tag{2.9}$$

What generally is referred to as the Born-Oppenheimer Approximation (BOA) is a cooking recipe based on the cn-approximation[4]: After having solved the electronic Schrödinger equation, one may propagate the nuclear dynamics employing the nuclear Schrödinger equation. Herein, only the masses of the nuclei enter. The so-called adiabatic approximation (or sometimes also called Born-Huang approximation [38]) takes the total wave function in a product Ansatz:

$$\Psi(\mathbf{R}, \mathbf{r}) = \chi(\mathbf{R})\Phi^{\text{cn}}(\mathbf{r}; \mathbf{R}), \tag{2.10}$$

where only one specific electronic state has been chosen. When solving for χ employing the variational principle one ends up with an (often negligible) adiabatic correction term, adding to the nuclear BOA-Schrödinger equation [37]. Often the terms adiabatic or Born-Oppenheimer are used interchangably in literature.

The Born-Oppenheimer (or the adiabatic) approximation is the basis for the notion of a potential energy surface and fundamental to all chemical bonding concepts. It has proven to be valid for the description of ground state phenomena and thermal reaction processes. For the description of systems with close lying electronic states or systems with fast dynamic changes between electronic states (non-adiabatic transitions) as can be found in photochemical or photophysical processes[5], the assumptions underlying the BOA are not valid and results based on this approximation will be qualitatively wrong. In what follows, a short summary is given on how nonadiabatic corrections or fully nonadiabatic treatments proceed on the basis of the BOA. These approaches will be discussed in more detail in chapter 13 of this thesis.

When subsystems interact (such as electrons and nuclei via $V_{\text{elec}-\text{nuc}}$), the full wave function can be represented as a linear combination of the corresponding subsystem wave functions [40]. The full interacting molecular wavefunction can therefore be written as

$$\Psi(\mathbf{R}, \mathbf{r}) = \sum_i \chi_i(\mathbf{R})\Phi_i(\mathbf{r}; \mathbf{R}), \tag{2.11}$$

where the χ_i act as expansion coefficients for the linear combination of the electronic wave functions and the sum runs over all possible ground and excited electronic states.

This so-called 'Born-representation' can be inserted into the full time-dependent Schrödinger equation (eq. 2.1) of the molecular system. Multiplying from the left with an electronic wavefunction $\bar{\Phi}_j$, integrating over the electronic degrees of freedom and changing to a Dirac representation of the integral[6] the result reads:

$$\langle\Phi_j| \sum_i (\hat{T}_{\text{nuc}} + \hat{H}_{\text{elec}}^{\text{cn}})\chi_i|\Phi_i\rangle = \langle\Phi_j| \sum_i i\frac{d}{dt}\chi_i|\Phi_i\rangle\,. \tag{2.12}$$

[3]Symbols depicting wave functions are defined as follows: Ψ symbolizes a molecular many-body wave function or a non-interacting product of single-particle wave functions, Φ and χ symbolize electronic and nuclear many-body wave functions, ψ symbolizes a non-interacting single-electron wave function, and ϕ symbolizes a mathematical basis function.

[4]For a detailed analysis of the often confusing and erroneous usage of the terms BOA and adiabatic approximation in literature and on how the BOA is associated with a publication of Born and Oppenheimer from 1927 mentioning it only as a sidenote, see Kutzelnigg [37] or a workshop lecture summary of Prof. Kutzelnigg (in german): http://tagung-theoretische-chemie.uni-graz.at/en/past-workshops/workshop-1997/

[5]or in general in metallic systems at finite temperature [39]

[6]For a description of the Dirac 'Braket' notation consult Szabo and Ostlund [30].

The wave functions span a complete space ('Hilbert' space) of orthonormal eigenfunctions. Applying orthonormality and reformulating the previous equation one arrives at:

$$\sum_i \langle \Phi_j | \hat{T}_{\text{nuc}} | \Phi_i \rangle \cdot \chi_i + E_j^{\text{elec}} \chi_j = i \frac{d}{dt} \chi_j. \tag{2.13}$$

We can now rewrite this as the following coupled set of equations for the nuclear wave functions χ_i:

$$(\hat{T}_{\text{nuc}} + E_j^{\text{elec}}) \chi_j - \sum_i \hat{\Lambda}_{ij} \cdot \chi_i = i \frac{d}{dt} \chi_j, \tag{2.14}$$

where $\hat{\Lambda}_{ij} = \delta_{ji} \hat{T}_{\text{nuc}} - \langle \Phi_j | \hat{T}_{\text{nuc}} | \Phi_i \rangle$ are the nonadiabatic coupling operators. Introducing the explicit form of the nuclear kinetic energy operator we can rewrite $\hat{\Lambda}_{ij}$ as

$$\hat{\Lambda}_{ij} = \frac{1}{2M} (2\mathbf{F}_{ij} \cdot \nabla + G_{ij}), \tag{2.15}$$

where

$$\mathbf{F}_{ij} = \langle \Phi_i | \nabla \Phi_j \rangle \tag{2.16}$$

is the derivative coupling vector and

$$G_{ij} = \langle \Phi_i | \nabla^2 \Phi_j \rangle \tag{2.17}$$

is the second-order scalar coupling. These two quantities specify the coupling between atomic and electronic motion. As can be seen from eq. 2.14, states mix during the time propagation of χ_j, depending on the effect of Λ_{ij}. Setting off-diagonal elements of Λ_{ij} to zero one arrives back at the adiabatic approximation, where the molecular wavefunction reduces to a simple product and different electronic states do not interact.

2.3 Wavefunctions, Orbitals, and Basis

Properties of Electronic Wave Functions

Employing the BOA[7], the problem of solving the molecular Schrödinger equation is reduced to the many-body problem of simultaneously moving electrons in a static potential due to the nuclei. At this point it is time to discuss the properties of electronic wave functions (eigenvector solutions of the electronic Schrödinger equation). As mathematical objects, wave functions complying with quantum theory have to be smooth, multiply differentiable, and square-integrable over the definition space. An electron can only be fully characterized if all defining quantum numbers are included in the description. The description established up to this point does not include any spin. However, wave functions describing electrons have to be antisymmetric with respect to particle exchange in order to correctly describe the fermionic character of electrons and to comply with the Pauli principle.

[7] The wave function superscript cn will be dropped in the following.

Expanding the Many Body Wavefunction

As seen in the previous chapter, partitioning subsystems mindfully can decide upon the mathematical feasibility of a problem. In this spirit, the electronic Hamiltonian can be seen as consisting of independent 1-electron Hamiltonians in the field of the nuclei that interact via an electron-electron repulsion term:

$$\hat{H}_{\text{elec}} = \underbrace{\sum_{i=1}^{N}\left(-\frac{1}{2}\nabla_i^2 - \sum_{A=1}^{M}\frac{Z_A}{r_{iA}}\right)}_{\hat{H}_0=\sum_i \hat{h}_i} + \underbrace{\sum_{i=1}^{N}\sum_{j>i}^{N}\frac{1}{r_{ij}}}_{V_{\text{elec-elec}}}, \tag{2.18}$$

where the $\hat{h}_i$ refer to one-electron Hamiltonians of independent particles. By constructing a non-interacting product state $\hat{H}_0$ and linearly combining the corresponding solutions (due to the electron-electron interaction $V_{\text{elec-elec}}$), one can write down the electronic many-body wave function Φ in a closed form. The simplest possible choice for eigenfunctions of $\hat{H}_0$ are products of the single-electron eigenfunctions of the $\hat{h}_i$, so-called molecular *orbitals*[8]:

$$\Psi^{\text{HP}}(\mathbf{r}_1, \mathbf{r}_2, \ldots, \mathbf{r}_N) = \psi_{E_1}(\mathbf{r}_1)\psi_{E_2}(\mathbf{r}_2)\cdots\psi_{E_N}(\mathbf{r}_N) \tag{2.19}$$

However, such so-called *hartree products* (HP) neither satisfy the antisymmetry requirement of the Pauli principle, nor the indistinguishability of quantum particles:

$$\begin{aligned}\Psi(\mathbf{r}_1, \mathbf{r}_2, \ldots, \mathbf{r}_N)^{\text{HP}} = \psi_{E_1}(\mathbf{r}_1)\psi_{E_2}(\mathbf{r}_2)\cdots\psi_{E_N}(\mathbf{r}_N) \neq \\ \psi_{E_1}(\mathbf{r}_2)\psi_{E_2}(\mathbf{r}_1)\cdots\psi_{E_N}(\mathbf{r}_N) = \Psi^{\text{HP}}(\mathbf{r}_2, \mathbf{r}_1, \ldots, \mathbf{r}_N).\end{aligned} \tag{2.20}$$

It is however possible to construct a normalized linear combination of Hartree products that satisfies this antisymmetry requirement

$$\Psi(\mathbf{r}_1, \mathbf{r}_2, \ldots, \mathbf{r}_N) = -\Psi(\mathbf{r}_2, \mathbf{r}_1, \ldots, \mathbf{r}_N). \tag{2.21}$$

These antisymmetric product wave functions can be expressed in form of determinants, so-called *Slater determinants*:

$$\Psi_{E_1,E_2,\ldots,E_N}(\mathbf{r}_1, \mathbf{r}_2, \ldots, \mathbf{r}_N) = (N!)^{-1/2}\begin{vmatrix}\psi_{E_1}(\mathbf{r}_1) & \psi_{E_2}(\mathbf{r}_1) & \cdots & \psi_{E_N}(\mathbf{r}_1)\\ \psi_{E_1}(\mathbf{r}_2) & \psi_{E_2}(\mathbf{r}_2) & \cdots & \psi_{E_N}(\mathbf{r}_2)\\ \vdots & \vdots & \ddots & \vdots\\ \psi_{E_1}(\mathbf{r}_N) & \psi_{E_2}(\mathbf{r}_N) & \cdots & \psi_{E_N}(\mathbf{r}_N)\end{vmatrix} \tag{2.22}$$

There exists a complete set of orthonormal 1-electron wave functions $\{\psi_{E_i}\}$ that are eigenfunctions of $\hat{h}$ (or at least there exists a set of functions yielding a good account of the physical boundary conditions). The set of all possible N-particle Slater determinants that can be constructed from this orthonormal basis of orbitals again spans an orthonormal eigenfunction space for the operator $\hat{H}_0$.

The interacting electronic many-body wave function Φ_i of eq. 2.7 can be expanded in these non-interacting antisymmetrized product states in the following way:

$$\Phi_i(\mathbf{r}_1, \mathbf{r}_2, \ldots, \mathbf{r}_N) = \sum_{l\neq m\neq\cdots\neq n=0}^{l\neq m\neq\cdots\neq n=\infty} C^i_{E_l,E_m,\ldots,E_n}\Psi_{E_l,E_m,\ldots,E_n}(\mathbf{r}_1, \mathbf{r}_2, \ldots, \mathbf{r}_N). \tag{2.23}$$

[8] The term *orbital* stems from the analytical solution of the hydrogen atom. For a treatment of this problem consult Kutzelnigg [34] or Bethe and Salpeter [41].

The remainder of work lies in solving the Schrödinger equation for the many-body expansion coefficients C_i. To do this efficiently or to make it numerically feasible at all, both the expansion in the space of Slater determinants, as well as the expansion in the space of the 1-electron wave functions have to be defined in a way to be quickly convergent, truncatable, and numerically easy to handle. Different ways of expanding and truncating the many-body wave function gives rise to different quantum chemical methods. Two important examples will be discussed in section 2.4.

Expanding Orbitals in a Complete Function Space - The Basis

The form of the 1-electron eigenfunctions (molecular orbitals) to $\hat{h}$ is known. However, the mathematical form is not ideally suited for numerical evaluation. Fortunately, such molecular orbitals can be constructed from complete orthonormal function spaces, which themselves are well-known solutions to simple systems matching the boundary conditions of the problem; these are then called the *basis functions* or the *basis*. For molecular systems, such as gas-phase Azobenzene, the obvious choice is to construct molecular orbitals as linear combination of atomic orbitals (*LCAO-Ansatz*). These functions can then be either analytical or numerical solutions to the hydrogen-like atom (e.g. 'Slater-type functions', SAOs, or NAOs) or other simple to evaluate functions which approximate these solutions, like Gaussian-type functions (GAOs). More discussion on these localized basis functions can be found in appendix A.

In the case of extended solid systems (e.g. metals) an ideal basis to describe the boundary conditions and the delocalized character of the electrons is a basis of extended functions, such as plane-waves, wavelets [42] or functions that are evaluated directly on a simple real space grid. As main ingredient of the numerics used in this thesis, basis functions of this kind will be discussed in more detail in chapter 4.

The general form of a basis expansion is

$$\psi_i(\mathbf{r}) = \sum_{\mu=1}^{K} c_{\mu i}\phi_\mu(\mathbf{r}), \tag{2.24}$$

with K being the number of basis functions after which the expansion is truncated; such truncation to a finite function space is inevitable to enable computations. Schrödingers eigenvalue equation (or derived eigenvalue problems discussed later) can be represented within such a basis set space and be cast into matrix form to be solved numerically. Converging the solution of the Schrödinger equation with respect to the truncation of the basis (or approaching the 'basis set limit') means increasing the variational dimensionality of the problem and reducing the numerical error associated with the calculation.

2.4 Common Wave Function Approximations

The choice of the wave function to be used defines the quantum chemical method. From the plethora of existing wave function expansions, only those employed in this work will be detailed below. For a description of an exemplary wave function software package, see appendix A.1

The Hartree-Fock Method

The *Hartree-Fock method* (HF) is an approach central to the chemical concept of molecular orbitals (MOs), referring to independent effective quantum states of electrons within a molecular system. MOs govern all 'chemical' thinking and although only strictly meaningful within the HF approach, the idea carries over to the concept of quasi-particles in a many-body molecular

system [43]. Additionally, the HF approximation acts as the basic starting point for many more elaborate wave function expansions, which improve on the description of many-body effects (so-called 'Post-Hartree-Fock methods').

The starting point of HF theory is a wave function consisting of a single non-interacting Slater determinant[9]. One has to find the best possible approximation to the ground state of an N-electron system, described by a single Slater determinant containing the lowest lying molecular orbitals[10]. According to the variational principle the lowest possible energy of such a single determinental wave function

$$\Psi_0(\mathbf{r}_1, \mathbf{r}_2, \ldots, \mathbf{r}_N) = (N!)^{-1/2} \begin{vmatrix} \psi_1(\mathbf{r}_1) & \psi_2(\mathbf{r}_1) & \cdots & \psi_a(\mathbf{r}_1) & \psi_b(\mathbf{r}_1) & \cdots & \psi_N(\mathbf{r}_1) \\ \psi_1(\mathbf{r}_2) & \psi_2(\mathbf{r}_2) & \cdots & \psi_a(\mathbf{r}_2) & \psi_b(\mathbf{r}_2) & \cdots & \psi_N(\mathbf{r}_2) \\ \vdots & \vdots & \vdots & \vdots & \vdots & \ddots & \vdots \\ \psi_1(\mathbf{r}_N) & \psi_2(\mathbf{r}_N) & \cdots & \psi_a(\mathbf{r}_N) & \psi_b(\mathbf{r}_N) & \cdots & \psi_N(\mathbf{r}_N) \end{vmatrix} \tag{2.25}$$

is a functional of this wave function and given by

$$E_0[\Psi_0] = \langle \Psi_0 | \hat{H}_{elec} | \Psi_0 \rangle = \langle \Psi_0 | \sum_a \hat{h} + \sum_{a=1}^{N} \sum_{b>a}^{N} \frac{1}{r_{12}} | \Psi_0 \rangle =$$

$$\sum_a \langle \psi_a | \hat{h} | \psi_a \rangle + \sum_{a=1}^{N} \sum_{b>a}^{N} \left(\langle \psi_a \psi_a | \frac{1}{r_{12}} | \psi_b \psi_b \rangle - \langle \psi_a \psi_b | \frac{1}{r_{12}} | \psi_b \psi_a \rangle \right). \tag{2.26}$$

In the above equation 2.26, the Slater determinant has been expanded in the space of 1-electron orbitals; only three sums over integrals of the 1-electron states and the operators exist, which are not equal to zero. The integrals (denoted by Dirac brakets) run over all definition space of the MOs ψ. The 1-electron operator $\hat{h}$ and the 2-electron operator $1/r_{12}$ only give rise to non-zero integrals for orbital combinations, not differing by more than one and two electrons, respectively. In both cases, integration runs over the spatial and spin coordinates of the involved MOs. The definition of such an integral used in eq. 2.26 is

$$\langle \psi_a \psi_a | \frac{1}{r_{12}} | \psi_b \psi_b \rangle = \int \int d\tau_1 d\tau_2 \psi_a(\mathbf{r}_1) \psi_a(\mathbf{r}_2) \frac{1}{r_{12}} \psi_b(\mathbf{r}_1) \psi_b(\mathbf{r}_2). \tag{2.27}$$

By functional variation under an orthonormality constraint $< \psi_a | \psi_b >= \delta_{ab}$ the functional E_0 can be minimized. The resulting set of effective single-particle integro-differential pseudo-eigenvalue equations are called *Hartree-Fock* equations:

$$\left[\hat{h}(\mathbf{r}_1) + \sum_b \hat{J}_b - \sum_b \hat{K}_b \right] \psi_a(\mathbf{r}_1) = \epsilon_a \psi_a(\mathbf{r}_1), \tag{2.28}$$

where the Fock-operator consists of the sum over the 1-electron operators $\hat{h}$, the *Coulomb operator* $\hat{J}_b$, and the *exchange operator* $\hat{K}_b$, the latter being defined by their effect on an orbital ψ_a such that

$$\hat{J}_b(\mathbf{r}_1) \psi_a(\mathbf{r}_1) = \left[\int d\tau_2 \psi_b^*(\mathbf{r}_2) \frac{1}{r_{12}} \psi_b(\mathbf{r}_2) \right] \psi_a(\mathbf{r}_1) \tag{2.29}$$

[9] This is valid in the case of the *Restricted Hartree-Fock method*; the only variant considered here.

[10] In the following the orbitals are defined as spin orbitals. That means every orbital can have either occupation 1 or 0 and there are two kinds of orbitals $\psi^{\uparrow}$ and $\psi^{\downarrow}$.

and

$$\hat{K}_b(\mathbf{r}_1)\psi_a(\mathbf{r}_1) = \left[\int d\tau_2 \psi_b^*(\mathbf{r}_2)\frac{1}{r_{12}}\psi_a(\mathbf{r}_2)\right]\psi_b(\mathbf{r}_1). \tag{2.30}$$

The eigenfunction solutions ψ_a of this set of equations define quasi-particles, which move in an effective non-local potential $\mathrm{v}^{\mathrm{HF}} = \sum_b(\hat{J}_b - \hat{K}_b)$. Within this potential, every electron thus moves independently in an averaged effective field of all other electrons. The electrons are 'dressed' by the mean interaction with all other particles. The term $\hat{J}$ can be understood as the classical electrostatic energy between two interacting electron densities ('Hartree'-energy), whereas the exchange term is a purely quantum mechanical term that stems from the antisymmetry-requirement. The Hartree-Fock potential depends on all molecular orbitals; the corresponding set of equations is therefore non-linear and has to be solved iteratively by assuming a starting set of orbitals ('guess') and self-consistently converging the MOs and the potential v^{HF}. Therefore, HF-theory is also called a *self-consistent-field* method (SCF). When constructing the molecular orbitals from a truncated basis set, the HF-equations can be cast in a matrix form and solved efficiently in computer algebra for the basis set coefficients $c_{\mu i}$.

The N lowest lying eigenfunction solutions of a N-electron system define the electron density of the system by

$$\rho(\mathbf{r}_1) = \sum_{a=1}^{N} \langle \mathbf{r}|\psi_a\rangle \langle \psi_a|\mathbf{r}\rangle = \sum_{a=1}^{N} \psi_a^*(\mathbf{r}_1)\psi_a(\mathbf{r}_1) \tag{2.31}$$

with $\sum_a |\psi_a\rangle \langle\psi_a|$ being the density operator. These molecular orbitals define the occupied MO space; the higher lying orbitals are called unoccupied or virtual. The eigenvalues of the Hartree-Fock equations ϵ_a correspond to electron addition or electron removal energies ('Koopmans-Theorem'). Starting from the wave functions, the density, and the orbital eigenvalues, all important quantum mechanical observables and properties of molecular systems can be derived.

Although the average interaction and also the Pauli-repulsion between electrons in a molecular system is well described by HF-theory, the interactions due to the collective correlated quantum motion of the electrons is neglected, owing to the fact that the wavefunction only corresponds to a single Slater determinant. As already expressed above, HF-theory also acts as the basic starting point for many-body treatments taking such correlation effects into consideration. One of many definitions of the so-called *correlation energy* is the difference of the correct many-body groundstate energy of a system to the HF-energy of that system. A recipe on how to include this electron correlation in the treatment of molecular systems is given by the *configuration interaction*-Ansatz (CI). In this approach the many-body wavefunction is expanded starting from the groundstate Hartree-Fock Slater determinant by linear combination with excited state Slater determinants. These are generated by replacing occupied by virtual orbitals in the HF-determinant.

$$|\Phi\rangle = C_0|\Psi_0\rangle + \sum_r\sum_a C_a^r|\Psi_a^r\rangle + \sum_{rs}\sum_{ab} C_{ab}^{rs}|\Psi_{ab}^{rs}\rangle + \sum_{rst}\sum_{abc} C_{abc}^{rst}|\Psi_{abc}^{rst}\rangle + \cdots \tag{2.32}$$

were $a, b, c, \ldots$ indices refer to occupied orbitals in the HF ground state and $r, s, t, \ldots$ indices refer to virtual orbitals in the HF solution; correspondingly $|\Psi_a^r\rangle$ refers to a determinant in which orbital a has been replaced by orbital r. Every such excited determinant corresponds to a certain electron configuration, which is mixed into the HF wave function by CI coefficients C. Different levels of Post-Hartree-Fock theory are defined by the level at which this expansion is truncated (i.e. CI single and double excitations (CISD)). Furthermore these methods can be grouped into

two approaches: At one hand these CI coefficients can be calculated, based on fixed basis set coefficients $c_{\mu i}$ previously calculated by Hartree-Fock. For such a method to be accurate, the CI coefficients have to be rather small compared to C_0 in order to pose a small correction to the HF solution ('single reference methods'). In other cases (i.e. bond-breaking events) the HF solution gives a qualitatively wrong account of the electronic structure of the system and CI coefficients may be of the order of the C_0 coefficient. This requires to treat the CI in a small expansion space and the basis set coefficients to be optimized simultaneously to determine the optimal ground-state energy ('multi reference methods').

The Coupled Cluster Approach

A problem with correlation techniques, based on the CI expansion, is that truncation at a certain level of excitation removes many of the nice properties that are for example inherent to HF theory. This includes the property of *size-extensivity*, referring to the ability of a method to predict the ground-state energy of two separate systems and the two systems together at infinite separation to be identical. Lack of this property complicates the calculation of energetics associated with intermolecular reactions, such as the surface adsorption events studied in this work.

The *Coupled Cluster expansion* (CC) offers a different approach to expand the many-body wave function on the basis of a non-interacting reference wave function (HF solution) and can be written as [44]

$$|\Phi_{\mathrm{CC}}\rangle = \exp(T)\,|\Psi_0\rangle = (1 + T + T^2/2 + T^3/3! + \cdots)\,|\Psi_0\rangle\,, \tag{2.33}$$

with T called the cluster operator:

$$T = T_1 + T_2 + T_3 + \cdots + T_n. \tag{2.34}$$

Its components introduce single, double, and triple excitations to the HF reference. Truncating such an expansion for example after double excitations yields

$$|\Phi_{\mathrm{CCSD}}\rangle = \exp(T_1 + T_2)\,|\Psi_0\rangle = (1 + T_1 + T_2 + T_1^2/2 + T_2^2/2 + T_1T_2 + \cdots)\,|\Psi_0\rangle\,, \tag{2.35}$$

where the terms can be defined by their action on the reference wave function in the following way

$$T_1\,|\Psi_0\rangle = \sum_{r,a} t_a^r\,|\Psi_a^r\rangle\,, \tag{2.36}$$

$$\frac{1}{2}T_1^2\,|\Psi_0\rangle = \sum_{r>s}\sum_{a>b} t_a^r t_b^s\,|\Psi_{ab}^{rs}\rangle\,, \tag{2.37}$$

$$T_1T_2\,|\Psi_0\rangle = \sum_{r,a}\sum_{s>t}\sum_{b>c} t_a^r t_{bc}^{st}\,|\Psi_{abc}^{rst}\rangle\,. \tag{2.38}$$

From this it follows that the formal second order expansion contains the same terms as the CISD, but additionally also contains so-called disconnected products of expansion coefficients ('cluster amplitudes') introducing higher lying excitations. These additional terms introduce simultaneous excitations, independent from each other, such as in the case of the T_1T_2 term.

These terms lead to a size-extensive treatment without much additional numerical effort compared to the CI methods, because the disconnected amplitudes can be calculated as products of the connected ones. Nevertheless, these methods are numerically highly intensive and self-consistent calculations including single and double excitations are currently restricted to small organic systems containing first and second row elements. The major part of the correlation energy can already be included at the level of double excitations. Very often higher lying excitations are only included pertubatively as is the case for the CCSD(T) method [45], which is also termed the 'Gold-Standard' of quantum chemistry, typically resulting in errors in the range of 1 kcal/mol for a variety of molecular properties.

The many-body character of the CC methods also gives access to optical response properties such as the calculation of electronically excited states. One such approach, namely the second-order approximate coupled cluster singles and doubles model (CC2) [46] has been employed in this work. It is based on the CCSD approach, where the wave function is defined by

$$|\Phi_{\mathrm{CCSD}}\rangle = \exp\left(T_1 + T_2\right)|\Psi_0\rangle \tag{2.39}$$

and enters the Schrödinger equation in the following way:

$$\left(\hat{H} - E_0\right)|\Phi_{\mathrm{CCSD}}\rangle = E_{\mathrm{corr}}\,|\Phi_{\mathrm{CCSD}}\rangle \tag{2.40}$$

Successively multiplying from the left with $\langle\Psi_0|$, $\langle\Psi_a^r|$, $\langle\Psi_{ab}^{rs}|$, ect., one arrives at the following equations for the correlation energy and the expansion coefficients[11]

$$E_{\mathrm{corr}} = \langle\Psi_0|\hat{H}\exp\left(T_1 + T_2\right)|\Psi_0\rangle \tag{2.41}$$

$$\langle\Psi_a^r|\hat{H}\exp\left(T_1 + T_2\right)|\Psi_0\rangle = 0 \tag{2.42}$$

$$\langle\Psi_{ab}^{rs}|\hat{H}\exp\left(T_1 + T_2\right)|\Psi_0\rangle = 0. \tag{2.43}$$

When expressing $\hat{H}$ in T_1 transformed form

$$\widetilde{H} = \exp\left(-T_1\right)\hat{H}\exp\left(T_1\right) \tag{2.44}$$

the CCSD equations for the coefficients become

$$\langle\Psi_a^r|\widetilde{H} + \left[\widetilde{H}, T_2\right]|\Psi_0\rangle = 0 \tag{2.45}$$

$$\langle\Psi_{ab}^{rs}|\widetilde{H} + \left[\widetilde{H}, T_2\right] + \frac{1}{2}\left[\left[\widetilde{H}, T_2\right], T_2\right]|\Psi_0\rangle = 0, \tag{2.46}$$

where square brackets denote commutation relations. In the case of CC2 the equations for the single excitations are unchanged, but the double excitations are only accounted for in first order, yielding the CC2 doubles equation:

$$\langle\Psi_{ab}^{rs}|\widetilde{H} + \left[\widetilde{H}, T_2\right]|\Psi_0\rangle = 0. \tag{2.47}$$

The thereby resulting set of equations is ideally suited to formulate linear response equations, from which an eigenvalue problem for the excitation energies can be derived. During this work, the CC2 method has been used in connection with the Resolution-of-Identity (RI) approximation [47], where the density is expanded in terms of an auxiliary basis set (For details see appendix A.1).

[11] This is given, if intermediate normalization $\langle\Phi_{\mathrm{CCSD}}|\Psi_0\rangle = 1$ is assumed, see Szabo and Ostlund [30], pp. 231.

3 Density-Functional Theory

The key variable in many-body theory is the wave function. The total energy of any system is a functional of this high dimensional object. In addition to its complicated dependence on all variables of the system, it is a quantity, which is only defined up to an arbitrary phase factor and not a physical observable. Therefore, the question arises wether the many-body problem can be recast on the basis of a more accessible quantity, such as the distribution of electrons in space - the electron density. The following chapter will recapitulate the main works, which have shown that such a reformulation is in fact possible and there exists a Density-Functional theory (DFT) with which a many-body interacting system can be represented by a system of non-interacting quasiparticles in an effective potential. The content of this chapter is mainly based on the books of Parr and Yang [32], Koch and Holthausen [48], and Dreizler and Gross [49]. Sections 3.1 and 3.2 specifically contain ideas from a lecture by E.K.U. Gross in Benasque, Spain (2011). Descriptions in section 3.6 and partly in 3.5 are based on the book of Ullrich [50].

3.1 The Hohenberg-Kohn Theorem

The electronic properties of a molecular system are completely determined by the interactions of the nuclei with the electrons, the so-called external potential $V_{\text{ext}} = V_{\text{nuc-elec}}$. All other terms are system-independent operators. All concepts in the previous chapter are based on the existence of a one-to-one correspondence of this external potential to a many-body wave function. This means that, when knowing the external potential, the Schrödinger equation enables the calculation of a unique wave function and from this wave function it is possible to construct the external potential.

Knowing the wave function one can calculate any observable of the system, also the electron density. Figure 3.1 shows these step-by-step mappings M_1 and M_2. If there exists a one-to-one invertible mapping M_3, which directly connects the external potential and the electron density,

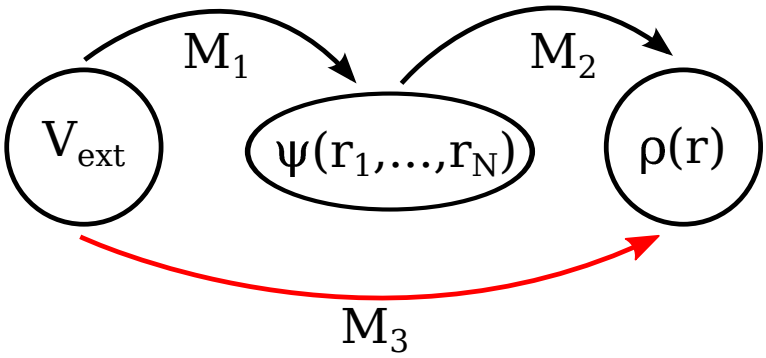

Figure 3.1: Scheme of the mappings involved in going from a wave function-based (Ψ) description (M_1,M_2) to a density-based (ρ description (M_3) of the external potential V_{ext} and the system.

then the electron density can act as the basic quantity of the many-body problem. This is the statement of the *first Hohenberg-Kohn Theorem: There exists an invertible one-to-one mapping between the external potential* V_{ext} *and the electron density* ρ [51]:

$$M3^{-1} : V_{\text{ext}}(\mathbf{r}) \leftarrow \rho(\mathbf{r}). \tag{3.1}$$

This statement can be proven by showing the individual invertibility or bijectiveness of M_1 and M_2. The first proof is given by simply rewriting the electronic Schrödinger equation

$$\begin{aligned} \left(\hat{T} + V_{\text{elec-elec}} + V_{\text{ext}}\right) |\Phi\rangle &= E\,|\Phi\rangle \\ V_{\text{ext}} = E - \frac{\hat{T}\,|\Phi\rangle}{|\Phi\rangle} &- V_{\text{elec-elec}}. \end{aligned} \tag{3.2}$$

Following from this, a given Φ uniquely defines the external potential.

Invertibility of M_2 can be shown by assuming two nondegenerate ground state wave functions Φ and Φ', which satisfy

$$\hat{H}\Phi = E\Phi \qquad \text{and} \qquad \hat{H}'\Phi' = E'\Phi'. \tag{3.3}$$

It is to be shown that if Φ and Φ' are different, then also ρ and ρ' have to be different; if M_3 is bijective, no two wave functions can yield the same density.

When employing the variational principle one arrives at

$$\begin{aligned} E = \langle\Phi|\hat{H}|\Phi\rangle < \langle\Phi'|\hat{H}|\Phi'\rangle &= \langle\Phi'|\hat{H}' + V - V'|\Phi'\rangle \\ E < E' + \int \rho'(\mathbf{r})[V(\mathbf{r}) - V'(\mathbf{r})]d\mathbf{r} & \end{aligned} \tag{3.4}$$

and similarly

$$\begin{aligned} E' = \langle\Phi'|\hat{H}'|\Phi'\rangle < \langle\Phi|\hat{H}'|\Phi\rangle &= \langle\Phi|\hat{H} + V' - V|\Phi\rangle \\ E' < E - \int \rho(\mathbf{r})[V(\mathbf{r}) - V'(\mathbf{r})]d\mathbf{r}. & \end{aligned} \tag{3.5}$$

When now assuming that $\rho = \rho'$, the sum of inequalities 3.4 and 3.5 yields

$$E + E' < E + E' \qquad \text{Contradiction.} \tag{3.6}$$

From this it follows that the electron density is uniquely connected to the external potential, and, in connection with M^{-1}, completely determines all quantities, including the wave functions:

$$\rho \xrightarrow{M_3^{-1}} V_{\text{ext}}[\rho] \xrightarrow{\text{Schrodingereq.}} \Phi_i[\rho]. \tag{3.7}$$

From the Hohenberg-Kohn proof it follows that the total energy of the system can be written as

$$\hat{E}_{\text{HK}}[\rho] = \hat{T}[\rho] + V_{\text{elec-elec}}[\rho] + V_{\text{ext}}[\rho] = \hat{F}[\rho] + \int \rho(\mathbf{r})v_0(\mathbf{r})d\mathbf{r}, \tag{3.8}$$

where F is a universal functional of the density. The external potential, determined by the positions of the nuclei, is the only system-dependent term. One can now variationally optimize this energy functional for a given external potential under the constraint that the density can be represented by a fermionic many-body wave function and that this density integrates to

the number of electrons in the system (density is *N-representable*); the result will be the exact ground-state energy E_0 and the ground-state density $\rho_0(\mathbf{r})$ of the system (*second Hohenberg-Kohn Theorem* or rather Levy's-constrained-search derivation of DFT [52, 53]).

In this chapter it has been shown that quantum mechanical observables can in fact be expressed as functionals of the electron density, a local function of 3-dimensional space (and spin), as opposed to being dependent on a many-dimensional wave function object. Furthermore, there exists a variational principle, from which a universal density-functional for the ground-state energy and the ground-state density of a system can be calculated. Unfortunately, the proof by contradiction yields nothing more and less than this; no clear path on how such a functional should be constructed emerges.

The remaining problem is the formulation of the system-independent kinetic energy and electron-electron repulsion terms in F[ρ]. These terms describe the energy of an inhomogeneous electron gas and can not easily be recast as pure density-dependent terms. Nevertheless, we can expand the functional in powers of the electronic charge e^2:

$$\hat{F}[\rho] = \hat{F}^{(0)}[\rho] + e^2\hat{F}^{(1)}[\rho] + e^4\hat{F}^{(2)}[\rho] + \dots \tag{3.9}$$

By equating coefficients $F^{(i)}$ we can identify $F^{(0)}[\rho] = T_s[\rho]$ as the energy of non-interacting particles (i.e. the kinetic energy of independent electrons). This term can unfortunately not be expressed as a simple functional of the density without any recourse to wave functions. The first order terms correspond to the Coulomb and exchange terms found from Hartree-Fock theory, where only the classical Coulomb term can be expressed as a simple functional of the electron density. All terms of higher-order in the Coulomb interaction and many-body contributions to the kinetic energy are quantum many-body correlation terms between the electrons and can be summarized in a correlation term $\hat{E}_c$ finally yielding the following expression for $\hat{F}$:

$$\hat{F}[\rho] = \hat{T}_s[\rho] + \frac{e^2}{2}\int\int\frac{\rho(\mathbf{r})\rho(\mathbf{r}')}{|\mathbf{r}-\mathbf{r}'|}d\mathbf{r}d\mathbf{r}' + \hat{E}_x[\rho] + \hat{E}_c[\rho]. \tag{3.10}$$

In this expression only the classical 'Hartree'-Coulomb interaction is known. The functionals $\hat{E}_x$ and $\hat{E}_c$ can be expressed in terms of many-body pair-correlation functions, the exchange and correlation (xc) hole functions, for which approximations can be found. The corresponding approximations will be explained in section 3.3. An approach to an expression for the non-interacting kinetic energy and to the construction of trial densities will be presented in the following section.

3.2 The Kohn-Sham Method

After having shown that a reformulation of wave function theory in terms of the density is possible, an explicit expression needs to be found. The problem of wave function theory was the high dimensionality of the parameter space in which a solution to the wave functions had to be found, whereas the actual operator or energy functional was simple to derive. The same problem expressed in terms of density-functional theory operates with very simple three-dimensional functions, but the complexity has been shifted to the terms in the energy functional[1]. This problem can be remedied by applying some derived properties of the Hohenberg-Kohn theorem.

By construction, the Hohenberg-Kohn (HK) mapping associates a function ρ that is a ground-state density with an external potential. Therefore, only densities can be employed, which fulfill

[1] In the authors opinion, complexity is the only quantity that is always conserved. One may only have the chance to partition the problem in a smart way, in order to meet the complicated parts in a later stage.

the mathematical conditions to be connected to an external potential; such densities are called *V-representable* and have to be normalizable, positive, and comply with the Pauli principle [54]. However, it is no contradiction to HK, if the same density is connected to two different external potentials by two different mappings. For example the effective potential in which non-interacting quasi-electrons in the Hartree-Fock-method move might yield the same density as the Coulomb potential in which real many-body electrons move. The two different interactions yield two different Hamiltonians, which map the same density to different external potentials. The above presented V-representability property can be rephrased in the following way: *Let ρ_0 be the ground-state density of electrons (interacting via $\hat{F}$) in an external Coulomb potential. Then there may also exist another local potential such that electrons (interacting via $\hat{F}'$) exposed to it have the same ground-state density ρ_0.* This tells us that all interacting V-representable ground-state densities are also non-interacting V-representable[2]:

$$v_{\text{ext}}[\rho](\mathbf{r}) \quad \xleftrightarrow{\text{HK for interacting particles}} \quad \rho(\mathbf{r}) \quad \xleftrightarrow{\text{HK for non-interacting particles}} \quad v_{\text{s}}[\rho](\mathbf{r}). \tag{3.11}$$

The idea of Kohn and Sham in 1965 [55] (cf. eq. 3.11) was to use this property to calculate the ground-state density of non-interacting electrons in an effective potential v_s in order to then calculate the energy of this density for the fully interacting system described by v_{ext}[3]. One can introduce orbitals ψ_i for such a non-interacting system with which a non-interacting reference wave function, a Slater determinant, is constructed. With this approach the kinetic energy functional can simply be written as

$$\hat{T}_s[\rho] = \sum_{i=1}^{N} \langle \psi_i | -\frac{1}{2}\nabla^2 | \psi_i \rangle \,. \tag{3.12}$$

The corresponding set of equations for these non-interacting 'quasi'-electrons can be written as

$$\left(-\frac{\nabla^2}{2} + v_s \right) |\psi_j\rangle = \epsilon_j \, |\psi_j\rangle \tag{3.13}$$

and the interacting (and non-interacting) ground-state density is constructed via

$$\rho_0(\mathbf{r}) = \sum_{j}^{N} |\langle \mathbf{r}|\psi_j\rangle \, \langle \psi_j|\mathbf{r}\rangle|^2 \,. \tag{3.14}$$

The existence of this set of coupled effective single-particle equations is provided by Hohenberg-Kohn and the (Ensemble-)V-representability theorem [54], not by the variational principle. However, after recourse to the variational principle, the effective 1-particle potential of eq. 3.13 can be defined as

$$v_s[\rho](\mathbf{r}) = v_{\text{ext}}[\rho](\mathbf{r}) + v_{\text{H}}[\rho](\mathbf{r}) + \underbrace{v_{xc}[\rho](\mathbf{r})}_{v_x + v_c}, \tag{3.15}$$

where the three potential terms are defined as the corresponding variational derivatives of the energy functional terms of eq. 3.10 and correlation and exchange have been summed to the

[2] This is only strictly true if one also considers densities which are constructed by a linear combination of Slater determinants, so densities that are Ensemble-V-representable.

[3] This approach is not just restricted to non-interacting particles. So-called adiabatic connections enable a connection to systems with arbitrary degree of interaction. For an example of a different reference system, such as 'strictly'-correlated electrons, see Gori-Giorgi and Seidl [56].

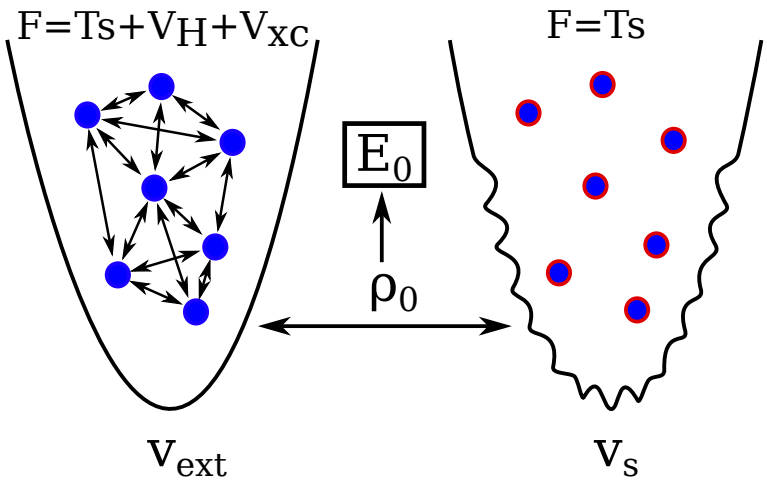

Figure 3.2: Schematic illustration of a real many-body electronic problem (left) and the Kohn-Sham non-interacting system (right) in which the interactions between the molecules are contained in the potential v_s acting on the individual particles.

exchange-correlation potential; specifically the existence of v_{xc} follows from the variational principle:

$$v_i = \left.\frac{\delta E_i[\rho]}{\delta \rho}\right|_{\rho_0}. \tag{3.16}$$

Due to this Kohn-Sham transformation, the problem of interacting electrons in a Coulomb potential has been recast to non-interacting 'quasi-particles' moving independently in a screened, local potential, which accounts for all many-body interactions between electrons (see Fig. 3.2). Therefore it can be argued that these Kohn-Sham eigenvalues and eigenfunctions do have a meaning as effective quasi-electrons of the system, but they can not be associated with electron addition or removal energies, as was the case in Hartree-Fock theory. More on the meaning of Kohn-Sham eigenvalues and eigenfunctions can be found in section 3.5.

Actual calculations are done in terms of a self-consistent field solution of the Kohn-Sham equations, similar as was done for Hartree-Fock theory. All many-body terms in the kinetic energy that are neglected in T_s are subsummed in E_{xc}[4]. This remaining term can be approximated on the level of the exchange-correlation (xc) energy functional or on the level of the xc-potential v_{xc}, which will be the remaining task in the next section.

3.3 Approximations to the Exchange-Correlation Functional

The Kohn-Sham equations (cf. eq. 3.13) present an exact reformulation of a many-body theory in terms of a Density-Functional. The remaining issue is to find an explicit form of $E_{xc}[\rho]$ that accounts for the major effects of Pauli repulsion of same-spin electrons, many-body quantum correlation (instantaneous attraction and repulsion due to quantum fluctuations) and many-body corrections to the kinetic energy of the system. These are strictly non-local properties, which depend on at least two electron coordinates at the same time. Already in the seminal

[4]This can be done in a rigorous way via an adiabatic connection between the interacting and the non-interacting system, see Koch and Holthausen [48], pp. 67

work of Kohn and Sham [55], the authors propose a strictly local approximation to the exchange-correlation energy - the *local-density approximation* (LDA), in which

$$E_{xc}^{\mathrm{LDA}}[\rho] = \int \rho(\mathbf{r})\epsilon_{xc}(\mathbf{r})d\mathbf{r}, \tag{3.17}$$

where ϵ_{xc} indicates the exchange and correlation energy density of a uniform electron gas at density ρ. The corresponding terms for exchange and correlation are split. The exchange term $\epsilon_x(\rho)$ for the homogeneous electron gas is well known (cf. Martin [57], p. 157) and analytic forms for $\epsilon_c(\rho)$ have been parametrized (VWN [58]) on the basis of accurate quantum Monte Carlo calculations by Ceperley and Alder [59]. This seemingly crude approximation has proven to capture a lot of the physics in alkali metals and alkaline earth metals, where delocalized valence electrons and minimal density variations govern the electronic structure of the material. In the case of strongly spatially varying electron densities of atoms, molecules, or transition metals, this approach leads to severe errors in total energies, bond lengths, and density-derived properties.

The LDA approach can be generalized to the description of spin-polarized materials in a *local-spin-density* approach, in which the KS-equations are solved individually for the spin densities and the xc-functional is parametrized with respect to these spin densities (or the total density and the magnetization density).

The main shortcomings of the LDA are due to the so-called *self-interaction error*, the missing *derivative discontinuity* in the v_{xc}, and the wrong asymptotic decay of the xc-functional approximation. Coulomb interaction exists between all electrons, except the electron with itself. In an exact theory (and also in Hartree-Fock theory) it is the exchange term that counteracts self-interactions induced indiscriminantly by the classical Hartree potential. The self-interaction error refers to the problem that the exchange functional is only approximated in the LDA and does therefore not fully cancel with the Hartree potential for a single electron. This leads to a spurious over-delocalization of the KS-orbitals and an underestimation of the kinetic energy, which therefore leads to large errors in the Kohn-Sham eigenvalues. The derivative discontinuity refers to the fact that the energy of a molecular system changes discontinuously at integer numbers of electrons, because the number of electrons can only change in integer values. The energy contribution due to this derivative discontinuity represents the exact difference between the real fundamental gap of a system (the difference between electron affinity and ionization potential) and the gap between Kohn-Sham levels (KS gap). So even at the level of the exact xc-functional the KS-gap is not equivalent to the fundamental gap of the system and the calculation of molecular resonances. (Koopman's Theorem does not hold in DFT). The discontinuous behaviour is not correctly described by LDA (and almost all other current approximations to the xc-functional). Associated with the above mentioned problems is a wrong asymptotic decay of the xc-potential in the LDA. Instead of a Coulomb-like 1/r decay, the simple LDA potential decays exponentially. The premature decay leads to virtual states being described as too weakly bound or even unbound. This is specifically problematic in the context of long-range interactions, such as van der Waals forces, or in general in the description of virtual KS states and excited state properties (see sections 3.5 and 3.6).

One idea to improve xc-functionals, is to expand the dependence of the xc-functional on the density in terms of a Taylor expansion. An explicit dependence of the functional on the density gradient can improve the description of rapidly varying densities. Such *Generalized Gradient Approximation* (GGA) functionals have the general structure:

$$E_{xc}^{\mathrm{GGA}}[\rho] = \int \rho(\mathbf{r})\epsilon_{xc}^{\mathrm{GGA}}(\rho, \nabla\rho)d\mathbf{r}. \tag{3.18}$$

The key idea here is to construct mathematical expressions for $\epsilon_{xc}^{\mathrm{GGA}}$ which satisfy a large number of boundary conditions and exact properties of the xc-functional. This can be done with the help of empirical parameters and empirical data set input, or purely by enforcing mathematical boundary conditions. One such latter functional is the PBE functional which is the main functional approximation used in this work [60]. While these functionals significantly improve total and relative energies, the problem of self-interaction error and missing derivative discontinuity remains.

Further refinement can be achieved by inclusion of exact Hartree-Fock exchange [61]. These *hybrid* functionals are constructed by mixing a fraction of HF exchange with standard functional approximations in the following generic way:

$$E_{xc}^{\mathrm{hybrid}} = aE_{x}^{\mathrm{exact}} + (1-a)E_{x}^{\mathrm{GGA}} + E_{c}^{\mathrm{GGA}} \tag{3.19}$$

This approach specifically removes a large portion of self-interaction error from the description. Typical approximations are the PBE0 functional (GGA=PBE and a=0.25 in eq. 3.19) [62], but the most widely used empirical functional mixture is called B3LYP [63]. These functionals correspond to the current state-of-the-art and main work horses in application to isolated molecular systems. The quality of structural and energetic properties of molecular systems close to equilibrium is particularly high. The introduced explicit dependence on the occupied orbitals is still valid within the context of DFT, because the orbitals themselves are functionals of the density.

A specific class of hybrid functionals - so-called *range-separated hybrids* [64] - correct the wrong asymptotic decay using the knowledge that the exchange potential of Hartree-Fock decays as -1/r. At short electron-electron separation, density-functional approximations (DFAs) to the exchange term, such as the LDA, work quite well, whereas at longer distances exchange effects contribute dominantly to the potential tail. The Coulomb interaction can be split into a short-range and a long-range term and different DFAs for the exchange contribution can be used. A specific subclass for this approach are 'Coulomb-attenuated' functionals in which the amount of Hartree-Fock exchange is increased at larger interelectronic separations (for example as done in the functional CAM-B3LYP) [65].

At this point in time, there is a variety of different paths that are followed in current research to remedy the three main problems that were mentioned earlier. There is a large amount of work currently dedicated to systematically construct xc-functionals on the basis of many-body perturbation theory and the adiabatic-connection dissipation-fluctuation theorem (ACDFT) [66] (e.g. functionals based on the Random Phase Approximation (cRPA) [67]). Recent works also explicitly model the shape of the exchange-correlation hole by enforcing the correct behavior with respect to the above mentioned three points. Such functionals are able to describe bond dissociation events and strongly correlated systems for simple systems [68].

One important issue that is connected with the wrong long-range asymptotics and the insufficiently treated correlation of currently used DFAs is the fact that Van der Waals (vdW) interactions are not correctly described by functionals which do not explicitly include a non-local dependence on unoccupied orbitals (such as the ones mentioned in the last paragraph). The next chapter will focus on common approaches to a correct description of such dispersive interactions, which are of great importance in the context of molecular adsorbates.

3.4 The Description of Van-der-Waals Interactions in DFT

The currently used Density-Functional approximations (DFAs), such as GGAs and Hybrid functionals yield a good description of chemical bonding of different kinds (covalent, ionic, or de-

localized metallic bonding) in equilibrium situations. This is generally not the case for weak, long-ranged intermolecular interactions. Specifically interactions, that are induced by fluctuating polarization of molecules due to the electronic quantum dynamics, are not sufficiently accounted for by local or semi-local DFAs [69]. The correct account of these so-called dispersion or van-der-Waals interactions depends on the approximation to the correlation functional. Here again, the currently used local description of the correlation hole and the wrong asymptotic decay of the corresponding potential, are the main issues connected with this deficiency.

Many different approaches have been used to incorporate van-der-Waals forces into a DFT description [70–72]. Similar to a level-by-level definition of the quality of xc-functionals in DFT coined by Perdew as *Jacob's ladder* [73], Klimeš and Michaelides recently classified DFT-based dispersion methods [72]. The most simple way of accounting for dispersion is by introducing the correct asymptotic $-1/r^6$ interaction between fluctuating dipoles. This can be done by simple empirical pair-potentials with which the total energy is corrected:

$$E_{\mathrm{tot}} = E_{\mathrm{DFT}} - \sum_{A,B} f(r_{AB}^{\mathrm{cut}}, A, B) \frac{C_{6AB}}{r_{AB}^6}. \tag{3.20}$$

In this so-called *DFT-D* approach, dispersion is approximated as a pairwise additive force between all pairs of nuclei A and B. The corresponding coefficients C_{6AB} are tabulated and constant for each element. Additionally these interactions have to be damped to zero at short range (i.e. before a cut-off radius of r_{AB}^{cut}), not to interfere with the DFT description; this is done by the damping function f in eq. 3.20. A widely used set of coefficients (C_{6AB}, r_{AB}^{cut}) are the ones derived by Grimme [74, 75]. Although the basic qualitative features of vdW bound systems can be described with such an approach, very often it overestimates the interaction energy and does not yield correct geometries, specifically for surface-adsorbate systems [76]. Reasons for this are the neglect of any higher-order many-body contributions and also the neglect of screening of long-range interactions by the interjacent density in periodic systems.

Accuracy can be gained by accounting for different chemical environments by rescaling the C_6 coefficients accordingly for each atom [76]. Tkatchenko and Scheffler recently introduced such a scheme ('DFT+vdw(TS)'), which is based on accurate reference atomic polarizabilities and reference atomic C_6 coefficients [77]. The corresponding intermolecular coefficients are calculated as

$$C_{6AB} = \frac{2 C_{6AA}^{\mathrm{eff}} C_{6BB}^{\mathrm{eff}}}{\frac{\alpha_B^0}{\alpha_A^0} C_{6AA}^{\mathrm{eff}} + \frac{\alpha_A^0}{\alpha_B^0} C_{6BB}^{\mathrm{eff}}}. \tag{3.21}$$

The tabulated atomic coefficients are rescaled, based on the atomic volume in the respective environment:

$$C_{6AA}^{\mathrm{eff}} = \left(\frac{V_A^{\mathrm{free}}}{V_A^{\mathrm{eff}}} \right)^2 C_{6AA}^{\mathrm{free}}, \tag{3.22}$$

where the atomic volumes for the free atom and for the atom within the system are calculated from an Atoms-in-Molecules density partitioning scheme (i.e. Hirshfeld partitioning [78]). This idea has already been earlier expressed in the dispersion approach of Johnson and Becke [79, 80]. Accounting for the chemical environment of the atoms significantly improves the description of dispersion interactions between molecules. Nevertheless, in the context of adsorbates on metal surfaces, strong disagreement with experiment remains owing to the neglect of many-body interactions [76].

The two most recent approaches, which yield a very good description of geometries and binding energies for metal-surface mounted adsorbates are *van-der-Waals functionals* (vdw-DF) and the DFT-D type DFT+vdw$^{\text{surf}}$ approach [81]. Van-der-Waals functionals explicitly include a non-local description of correlation that captures the main effects of dispersion [82–84]. Nevertheless, the corresponding calculations are numerically significantly more demanding than simple local DFAs. The recent DFT+vdw$^{\text{surf}}$ approach of Ruiz *et al.* [85] builds on the DFT+vdw(TS) scheme and specifically tackles the problem of many-body screening in metal substrates. Simple pair-wise interactions based on free atom polarizabilities do not capture the correct many-body collective response of a metal substrate due to adsorption of a molecule. By employing the Lifshitz-Zaremba-Kohn theory of the vdW interaction between a solid surface and an atom [86, 87], the authors renormalize the substrate C_6 coefficients, polarizabilities, and vdw radii in order to capture the correct screened interactions. The corresponding effective volume that rescales the C_6 coefficients (eq. 3.22) is calculated with respect to an atom in the bulk, instead of a free atom. This method has been implemented and employed in this work. It will be discussed in more detail in part III of this thesis.

3.5 Electronic Excited States with DFT

The following two sections will discuss extensions of Density-Functional Theory towards the calculation of higher-lying stationary solutions to the many-body electronic problem, meaning electronic excited state energies.

An immediate consequence of the Hohenberg-Kohn Theorem is that the ground-state density determines the potential and subsequently (via the Schrödinger eq. 2.3) all properties of the system including excited state solutions to the many-body problem. Thus, any excited state expectation value is a functional of the ground-state density. The question remains how such functionals are to be realized explicitly. Finding such expressions is already a cumbersome task for excited states in wave function theory, owing to the constraint that an excited state many-body wavefunction has to be orthogonal to the ground-state wave function and to all other excited states. One possible way would be, for example, to reformulate the optical response function (see section 3.6) as an explicit functional of the ground state density.

Since the very early days of DFT, approaches to excited state descriptions have been developed, some of them more rigorous and some of them in a more *ad hoc* manner. The most simple way to approximate electronic excited state energies of the system is to measure the difference between the corresponding occupied and unoccupied ground-state KS-eigenvalues (sometimes called ΔDFT). This corresponds to the excitation energy of the non-interacting reference system though and completely neglects many-body effects, such as the screening of a hole by other electrons or the fact that Kohn-Sham eigenvalues do not correspond to molecular resonances.

An early approach beyond this level is based on work of Slater [88], but also of Gunnarsson, Lundqvist [89], Ziegler, Rauk, Baerends [90], and van Barth [91], but dates back to much earlier calculations even before the formulation of the Hohenberg-Kohn theorem [92]. This approach is termed Delta-Self-Consistent-Field-DFT (ΔSCF-DFT) or Hartree-Fock-Slater-Method.

Let us assume a generalized form of the Kohn-Sham scheme [93], in which the density is defined by

$$\rho(\mathbf{r}) = \sum_{i=1}^{\infty} f_i \left|\psi_i(\mathbf{r})\right\rangle \left\langle\psi_i(\mathbf{r})\right| , \tag{3.23}$$

where the occupation numbers f_i may have arbitrary non-integer values between 0 and 1. The

corresponding energy functional is

$$\tilde{E}[\rho, f_1, f_2, \dots] = \sum_{i=1}^{\infty} f_i \langle \psi_i(\mathbf{r})| -\frac{\nabla^2}{2}|\psi_i(\mathbf{r})\rangle + V_{\text{ext}}[\rho] + E_H[\rho] + E_{xc}[\rho]. \tag{3.24}$$

If this functional is varied with respect to both, the KS-orbitals and the occupations, then the minimum energy and the ground-state Kohn-Sham equations are found at a Fermi distribution, where the lowest lying orbitals are filled. However, if one fixes a set of occupation numbers and varies the KS-orbitals a set of KS-equations results, which is formally identical to the original equations, but the energy representing the stationary point is a function of the occupations f_i and may be regarded as an approximation to the excited state of the interacting many-body system. It can be shown that

$$\left.\frac{\partial \tilde{E}(f_1, f_2, \dots)}{\partial f_i}\right|_{\rho} = \epsilon_i(f_1, f_2, \dots). \tag{3.25}$$

This so-called Janak's theorem yields a way how to describe ionization energies or electron affinities through the following expression

$$E_{N+1} - E_N = \int_0^1 \epsilon_i(f) df. \tag{3.26}$$

The two cases of $f = 0$ and $f = 1$ are described in the realm of ground-state KS-DFT and the corresponding integral can be approximated by its midpoint where the occupation of the system is $f = 0.5$. This is commonly referred to as *Slater's transition-state approach* and is the most simple evaluation of this integral in order to calculate excited state properties [94].

A more direct way would be to define any excitation energy as the difference between two self-consistent solutions of the KS-equations

$$E_{\text{ex}} = E(\{f_i^{\text{EX}}\}) - E_0(\{f_i^{\text{fermi}}\}), \tag{3.27}$$

where one corresponds to an excited state distribution of electrons in the reference system, the other one corresponds to the ground-state Fermi-distribution. This ΔSCF approach is practically done by calculating the self-consistent excited state with the ground-state approximation to the xc-functional. It is surprisingly successful in the description of excited states of atomic and molecular systems, and it has been shown that this approach is formally correct for the lowest lying excited states, which do not belong to the same symmetry as the ground state, such as electronic states of different spin [89, 90, 95]. The variational adaptation of the density due to the excited state occupancy gives an approximate account of screening, higher order exchange, and the excited state kinetic energy. Specifically in the context of charge-transfer excitations [96–98] and the description of atomic and molecular multiplet structure [90, 91], this approach has proven rather useful. Nevertheless, ΔSCF-DFT suffers from a variety of short-comings. Only those excited states are accessible, which can be approximated by a certain set of non-ground state occupations in the non-interacting reference system. In addition, if the excited state has the same symmetry as the ground-state, orthogonality and convergence are hard to achieve, if not impossible.

There is a variety of fundamental works which try to rationalize the success of this approach and put excited state calculations in DFT on a formal basis. Levy and Nagy [99–101] were able to show that a variational principle for individual excited-state functionals exists; these functionals can be varied under the constraint that the target excited state is orthogonal to a number of lower lying states and the ground state. A correspondingly derived excited state Kohn-Sham

scheme can yield the excited state density. Nevertheless the respective xc-functional which depends on both, the individual excited and the ground-state density, is yet to be concretized.

On the basis of a generalized adiabatic connection (GAC) [102], Görling formulated a so-called GAC-Kohn-Sham approach, which gives a justification for the success of ΔSCF-approaches in classic KS-DFT. In this scheme, *every* eigenstate Ψ_i of an interacting many-body system is adiabatically connected to a certain eigenstate Φ_i of a non-interacting reference system, represented by Slater determinants with arbitrary non-groundstate occupations. However, every interacting eigenstate is connected to a different Kohn-Sham system. That means for every electronic state Ψ_i, a separate Kohn-Sham potential $v_{s,i}$ exists. In general, in such a Kohn-Sham scheme the interacting ground state could be connected to an excited eigenstate of the non-interacting system and *vice versa*. In practice such a scheme would have to calculate the GAC-KS solutions for arbitrary states and only at the end one can sort them to find the energetically ordered solutions Ψ_i. Corresponding functionals for this approach would have to depend not only on the density, but also on the GAC label (i.e. they have to be different for different electronic states). Such functionals could be realized by explicitly orbital-dependent xc-functionals. When approximating such functionals with simple local DFAs used in classic KS-DFT, one arrives at ΔSCF-DFT. Therefore the ΔSCF-DFT approach can be seen as an approximate variant of a GAC-KS method, where the important functional state-dependence is ignored. This clearly supports an interpretation of Kohn-Sham eigenstates as zeroth order approximations to molecular resonances.

The most rigorous approach to the inclusion of excited states in static DFT is the ensemble DFT formalism of Theophilou [103] and Gross and coworkers [104, 105]. In this approach the KS-DFT method is generalized to a density and energy functional, constructed as

$$\rho_{w_1,w_2,\ldots} = \sum_w w_i \langle \Phi_i | \hat{\rho} | \Phi_i \rangle \tag{3.28}$$

and

$$\hat{E}_{w_1,w_2,\ldots}[\rho_{w_1,w_2,\ldots}] = \hat{T}_{s,w}[\rho_{w_1,w_2,\ldots}] + E_{H,w}[\rho_{w_1,w_2,\ldots}] + E_{\mathrm{ext},w}[\rho_{w_1,w_2,\ldots}] + E_{xc,w}[\rho_{w_1,w_2,\ldots}], \tag{3.29}$$

where linear combinations of differently occupied Slater determinants Φ_i enter the Kohn-Sham equations and the weight factors w_i are parameters, which determine the state mixing. Excited states Ω_i can be calculated as

$$\Omega_i = \frac{dE_{w_i}}{dw_i}. \tag{3.30}$$

Although this is formally correct and reduces to Kohn-Sham in the limit of one ground-state Slater determinant, this approach shares the same basic problems as the above two mentioned approaches of Levy, Nagy, and Görling, namely that the necessary exchange-correlation functional in some way is explicitly state-dependent. Unfortunately, there is currently no clear way on how to approximate such functionals.

Constrained DFT represents a formally less justified approach, which builds on the variational nature of DFT calculations [106, 107]. It is possible to impose additional boundary conditions on electrons with respect to their spatial distribution or spin state, by adding Lagrange multiplier terms. The corresponding energy functional is then varied with respect to the density and the corresponding Lagrange multiplier. Especially in the context of electron transfer [108] and charge-transfer excitations [109–112], this approach has been applied extensively.

Finally, a very recent and promising approach that somehow can be seen as generalization of ΔSCF-DFT deserves mentioning. In recent years, Ziegler and co-workers have developed a static

DFT approach to excited states based on variational theory ('constricted variational DFT') [113–117]. The approach is based on the electronic ground-state Hessian [118], describing the variation of the Kohn-Sham states by mixing of occupied and virtual orbital spaces. Such variations are only considered up to second order. It is possible to express the density variations and the energy change due to the density variation in a way that closely resembles linear response time-dependent DFT (TD-DFT) as formulated by Casida [119]. Excited states are the stationary points in the energy regime described by the electronic Hessian and can be calculated under the constraint that an integer number of electrons is transferred. This method reduces to, both, ΔDFT and ΔSCF under certain conditions, and also can be related to the Tamm-Dancoff approximation of linear response TD-DFT.

3.6 Time-Dependent Density-Functional Theory

As soon as external perturbations, such as energy transfer through heat or electromagnetic radiation, act on a system, the previously established ground-state Density-Functional theory can not be applied any more. Time-Dependent Density-Functional Theory (TD-DFT) enables the description of the explicit time-dependent response of a system to any external perturbations, but also the description of non-ground-state stationary solutions to the electronic many-body problem (electronic excited states).

The proof that a time-dependent density can be the fundamental variable of a system is given by the Runge-Gross theorem [120]. The theorem expresses that there exists a one-to-one correspondence between a time-dependent density and a time-dependent potential. Similar as in static DFT, this proof alone does not help in actual calculations. So the question arises if it is also possible to describe the time-dependent evolution of a system in terms of effective non-interacting particles. Van Leeuwen [121] was able to rigorously show that for a given time-dependent density $\rho(\mathbf{r}, t)$ of a many-body system with a given particle-particle interaction V, there exists a different many-body system with an interaction V' which yields the same time-dependent density. This corresponds to a time-dependent extension to the Ensemble-V-representability theorem. It therefore does not only imply the Runge-Gross proof (if V'(t)=V(t) $\rightarrow$ ρ'(t)=ρ(t)), but also yields the formal justification for a time-dependent Kohn-Sham approach.

Along the lines of static DFT, we can now formulate the time-dependent Kohn-Sham equations (TD-KS). When starting from an initially time-independent stationary state at time t_0 we may formulate the KS equation in the following way:

$$\left[-\frac{\nabla^2}{2} + v_s[\rho](\mathbf{r}, t)\right] \psi_j(\mathbf{r}, t) = i\frac{\partial}{\partial t}\psi_j(\mathbf{r}, t), \tag{3.31}$$

with the initial condition

$$\psi_j(\mathbf{r}, t_0) = \psi_j^0(\mathbf{r}). \tag{3.32}$$

The density that enters eq. 3.31 is defined as

$$\rho(\mathbf{r}, t) = \sum_{j=1}^{N} |\psi_j(\mathbf{r}, t)|^2 \tag{3.33}$$

The effective potential v_s is given by

$$v_s[\rho](\mathbf{r}, t) = v_{\text{ext}}[\rho](\mathbf{r}, t) + v_H[\rho](\mathbf{r}, t) + v_{xc}[\rho](\mathbf{r}, t). \tag{3.34}$$

When starting from a stationary state, the initial v_s at time $t = 0$ has to be identical with the xc-potential in static Kohn-Sham DFT. The remaining task, as in static DFT, is to find an approximation to the time-dependent xc-potential. A commonly used approximation is the *adiabatic approximation*, where the same time-independent xc-potential from DFT is used in connection with the time-dependent density:

$$v_{xc}^{A}(\mathbf{r},t) = v_{xc}^{0}[\rho_0](\mathbf{r})\Big|_{\rho_0(\mathbf{r})\to\rho(\mathbf{r},t)}. \tag{3.35}$$

Adiabatic refers to a perturbation that changes a system slowly enough for it to remain in an eigenstate of the system; the only time-dependence comes from the electron density. Therefore, the functional has no dependence on or no memory of previous times[5]. In practical applications, one generally employs a DFA known from static DFT, such as the LDA (adiabatic LDA, ALDA). This is a very drastic approximation. The consequence of static DFT was that complex interactions in a simple local potential were mapped into an effective potential, which had a highly non-local spatial dependence. In a wavefunction-based approach to the time-dependent Schrödinger equation, the time-dependence can be encoded in the complex phase of the wavefunction, a time-dependent density is still a real-valued phase-less entity and cannot encode this information. Therefore, in addition to the strong spatial non-locality of the xc-potential, in TD-DFT this potential is also highly non-local in time.

The TD-DFT framework is especially well suited for the calculation of response properties of molecular systems, such as excited state energies or oscillator strengths. When explicitly propagating the TD-KS equations one can extract the many-body response function of the system, including all information on the energies and on the lifetimes of excited states. However, very often such a full solution is not necessary. Especially if the system is in a stationary state and one is only interested in stationary excited state properties. Then one rather succumbs to linear response theory, which describes a systems response to weak perturbations, such as is the case of the photo-induced isomerization of Azobenzene.

The response of a density induced by a time-dependent perturbation potential v_1 can be expanded in a Taylor series and the first-order (linear) density response is given by

$$\rho_1(\mathbf{r},t) = \int dt' \int d\mathbf{r}' \chi(\mathbf{r},t,\mathbf{r}',t') v_1(\mathbf{r}',t'), \tag{3.36}$$

where χ refers to the density-density-response function. The poles of this function yield the excitation energies of the system. A function which has a time-dependence only in form of a time-difference-dependency can also be expressed in terms of a frequency-dependent function. In the framework of TD-KS the Fourier-transformed linear-response equation can be reformulated as

$$\rho_1(\mathbf{r},\omega) = \int d\mathbf{r}' \chi_s(\mathbf{r},\mathbf{r}',\omega) \left[v_1(\mathbf{r}',\omega) + \int d\mathbf{x} \left\{ \frac{1}{|\mathbf{r}'-\mathbf{x}|} + f_{xc}(\mathbf{r}',\mathbf{x}',\omega) \right\} \rho_1(\mathbf{x},\omega) \right], \tag{3.37}$$

where χ_s defines the frequency-dependent density-density-response of the non-interacting reference system expressed in terms of the ground-state KS-orbitals ψ_j^0, KS-eigenvalues ϵ_j and occupations f_j[6]

$$\chi_s(\mathbf{r},\mathbf{r}',\omega) = \sum_{j,k=1}^{\infty} (f_k - f_j) \frac{\psi_j^0(\mathbf{r})\psi_k^{0*}(\mathbf{r})\psi_j^{0*}(\mathbf{r}')\psi_k^0(\mathbf{r}')}{\omega - (\epsilon_j - \epsilon_k) + i\eta} \tag{3.38}$$

[5] Any dependence on future times is forbidden by the condition of causality.

[6] $i\eta$ refers to an infinitesimal complex constant.

and f_{xc} is the xc-kernel defined as

$$f_{xc}(\mathbf{r},t,\mathbf{r}',t') = \left.\frac{\delta v_{xc}(\mathbf{r},t)}{\delta\rho(\mathbf{r}',t')}\right|_{\rho_0(\mathbf{r})} \quad \text{and} \quad f_{xc}(\mathbf{r},\mathbf{r}',\omega) = \int d(t-t')\exp^{i\omega(t-t')} f_{xc}(\mathbf{r},t,\mathbf{r}',t'). \tag{3.39}$$

These equations show that the response of the interacting system can be calculated from the response of the non-interacting system and the xc-kernel. The self-dependence of ρ_1 in these equations implies a necessary self-consistent solution. Knowing ρ_1 and using eq. 3.36 one can calculate the poles (Ω) of χ, which correspond to optical resonances of the system. Casida has derived a set of coupled eigenvalue equations on the basis of the above mentioned density-response, yielding the electronic excited states as eigenvalues [119]. They can be cast into the compact eigenvalue equation (neglecting spin)

$$\sum_{j',k'} \left[\delta_{jj'}\delta_{kk'}(\epsilon_j - \epsilon_k) + (f_k - f_j)K_{jk,j'k'}(\Omega))\right]\beta_{j',k'}(\Omega) = \Omega\beta_{j,k}(\Omega), \tag{3.40}$$

where $K_{jk,j'k'}(\Omega)$ is defined in the following way

$$K_{jk,j'k'}(\Omega) = \int d\mathbf{r}\int d\mathbf{r}'\psi_j^*(\mathbf{r})\psi_k(\mathbf{r})\left[\frac{1}{|\mathbf{r}-\mathbf{r}'|} + f_{xc}(\mathbf{r},\mathbf{r}',\Omega)\right]\psi_{j'}(\mathbf{r}')\psi_{k'}^*(\mathbf{r}'). \tag{3.41}$$

The indices j and k run over all eigenvalues of the ground-state Kohn-Sham solution. If $K_{jk,j'k'}(\Omega)$ is set to zero, this equation simply reproduces differences between KS-eigenvalues (the poles of χ_s). Although, linear response can in principle only yield single excitations, the frequency-dependency[7] of the xc-kernel introduces more solutions than the dimensionality of the eigenvalue problem would suggest. Nevertheless, almost always the xc-kernel is approximated with the adiabatic approximation, in which case this is not given:

$$f_{xc}^A(\mathbf{r},\mathbf{r}') = \frac{\delta v_{xc}^0[\rho_0](\mathbf{r})}{\delta\rho_0(\mathbf{r}')} \tag{3.42}$$

Therefore, in current everyday usage the f_{xc}, an in principle non-local object in space and time, is (when using local xc-functionals) approximated as being completely local and time-independent. This has rather severe consequences on the quality of the excitation energies. Without the frequency-dependency, double and higher-lying excitations can not be described with this approach. Without the spatial non-locality, all the problems of static DFT, such as the wrong asymptotic behavior, the bad quality of virtual KS-states and the missing derivative discontinuity induce errors in the excited state description. This amounts to specifically untrustworthy excited states of non-equilibrium geometries and a complete break-down of the approach for Rydberg [122] or charge-transfer excitations [123, 124]. Some of these problems can be remedied by the improvements on exchange-correlation descriptions mentioned in section 3.3 such as range-separated hybrid functionals [125].

[7] This is equivalent to non-locality in time.

4 Solid State Systems

Solid state systems contain a macroscopic number of electrons and atoms, but their properties are determined on the atomistic scale. The periodicity of crystalline solid state systems such as metal surfaces enables to extract all important information on the system from the smallest repeated unit - the unit cell. In the following the necessary conditions on wave-function or DFT-based descriptions of such systems and the methods, that are used in this work, are described.

4.1 Crystal Lattices and Periodic Wave Functions

In a periodic system, the translational symmetry of the unit cells is described by primitive translation vectors in real space

$$\mathbf{R} = \sum_{i=1}^{3} n_i \mathbf{a}_i \qquad n_i \in \mathbb{Z}_0, \tag{4.1}$$

where $\mathbf{a}_1, \mathbf{a}_2, \mathbf{a}_3$ are the lattice vectors of the unit cell. These vectors span an infinite lattice of periodically repeated unit cells. Associated with this lattice, one can define a reciprocal unit cell via

$$\mathbf{b}_1 = \frac{2\pi}{\Omega}\mathbf{a}_2 \times \mathbf{a}_3 \qquad \mathbf{b}_2 = \frac{2\pi}{\Omega}\mathbf{a}_3 \times \mathbf{a}_1 \qquad \mathbf{b}_3 = \frac{2\pi}{\Omega}\mathbf{a}_1 \times \mathbf{a}_2, \tag{4.2}$$

where

$$\Omega = \mathbf{a}_1 \cdot |\mathbf{a}_2 \times \mathbf{a}_3| \quad \text{and} \quad \mathbf{a}_i \cdot \mathbf{b}_j = 2\pi\delta_{ij} \tag{4.3}$$

and a corresponding reciprocal lattice as

$$\mathbf{G}_m = \sum_{i=1}^{3} m_i \mathbf{b}_i \qquad m_i \in \mathbb{Z}_0. \tag{4.4}$$

Unit cells are generally not unique in their definition; Wigner-Seitz cells, however, can be uniquely defined[1]. In reciprocal space this Wigner-Seitz cell is called 1st Brillouin zone.

All functions of a periodic system have to obey the translation symmetry via periodic boundary conditions

$$\hat{T}_{\mathbf{R}} f(\mathbf{r}) = f(\mathbf{r} + \mathbf{R}) = f(\mathbf{r}). \tag{4.5}$$

In the above equation, $\hat{T}_{\mathbf{R}}$ is a translation operator to the translation vector $\mathbf{R}$. In periodic systems, it commutes with the Hamiltonian of the system, therefore implying that the two operators share a common spectrum of eigenfunctions. The eigenvalue problem of the symmetry

[1] The Wigner-Seitz cell is defined as the unit cell, constructed by the planes that perpendicularly bisect the vectors from the origin of the cell to the origin of the adjacent cell.

operator, defined in eq. 4.5, leads to the so-called *Bloch* condition on all possible periodic wave functions, which states

$$\psi_{n\mathbf{k}}(\mathbf{r}) = u_{n\mathbf{k}}(\mathbf{r})e^{i\mathbf{k}\cdot\mathbf{r}}, \tag{4.6}$$

where

$$u_{n\mathbf{k}}(\mathbf{r}) = u_{n\mathbf{k}}(\mathbf{r}+\mathbf{R}) \tag{4.7}$$

and

$$\mathbf{k} = \frac{n_1}{N_1}\mathbf{b}_1 + \frac{n_2}{N_2}\mathbf{b}_2 + \frac{n_3}{N_3}\mathbf{b}_3, \tag{4.8}$$

where n_i are integer numbers and N_i is the number of unit cells. This means that all periodic wave functions have to be products of lattice periodic functions $u_{n\mathbf{k}}$ and $\mathbf{k}$-modulated plane waves. The translational symmetry thereby induces an additional quantum number to the wave function, which is represented by reciprocal wave vectors $\mathbf{k}$. These wave vectors are only allowed to take discrete values following eq. 4.8. However, if the number of unit cells N is macroscopic, the $\mathbf{k}$-vectors become quasi-continuous. The electronic eigenspectrum is determined by both, band index n and wave vector $\mathbf{k}$; this is often visualized as band structure $E_n(\mathbf{k})$. For every $\mathbf{k}$ there exists a discrete set of eigenstates; for this reason, all observables of the system have to be averaged over $\mathbf{k}$-space

$$\langle f \rangle = \frac{1}{N_\mathbf{k}} \sum_\mathbf{k} f(\mathbf{k}). \tag{4.9}$$

Numerically this is done with a finite stencil, the $\mathbf{k}$-grid. Optimal sampling grids have been specified in literature [126–128].

The function $u_{n\mathbf{k}}$ has to be expanded in a finite basis set, which complies with eq. 4.7. The most simple choice of $u_{n\mathbf{k}}$ is a plane wave, but many different types of functions can be used as basis sets (see Martin [57], pp. 236).

4.2 Plane Waves and the Pseudopotential Method

The functions $u_{n\mathbf{k}}$, expanded in a complete plane wave basis set, can be written

$$u_{n\mathbf{k}} = \frac{1}{\sqrt{\Omega}} \sum_m c_{n,m}(\mathbf{k}) \cdot e^{i\mathbf{G}_m \cdot \mathbf{r}}, \tag{4.10}$$

where m labels a reciprocal lattice vector. The corresponding 1-particle KS reference wave functions $\psi_{n\mathbf{k}}$ are

$$\psi_{n\mathbf{k}} = \frac{1}{\sqrt{\Omega}} \sum_m c_{n,m}(\mathbf{k}) e^{i(\mathbf{k}+\mathbf{G}_m)\cdot\mathbf{r}}, \tag{4.11}$$

where $\mathbf{G}_m$ specifies a reciprocal lattice vector, characterizing the basis function. This basis has the advantage that it is orthonormal. Introducing it into the Kohn-Sham equations one arrives at a set of simple matrix equations for the coefficients c at different points in $\mathbf{k}$-space

$$\sum_{m'} \left(\frac{1}{2}|\mathbf{k}+\mathbf{G}_m|^2 \delta_{mm'} + \tilde{v}_s(\mathbf{G}_m - \mathbf{G}_{m'}) \right) c_{n,m'}(\mathbf{k}) = \epsilon_{n\mathbf{k}} c_{n,m}(\mathbf{k}). \tag{4.12}$$

In this equation, the kinetic energy is a diagonal sum over squares of reciprocal lattice vectors and $\tilde{v}_s$ refers to the Fourier transform of the Kohn-Sham potential (i.e. the potential in reciprocal space). The number of basis functions that are included in expansion 4.11 can be specified in form of the maximal kinetic energy of the plane waves that are included

$$\frac{1}{2}(\mathbf{k}+\mathbf{G}_m)^2 \leq E_{\text{cut}}, \tag{4.13}$$

with the basis being constructed independently at different $\mathbf{k}$-points.

The disadvantage of this basis lies in its smooth delocalized functions. Very large energy cutoffs are needed to correctly describe the large wavefunction gradients, density fluctuations, and wavefunctions close to the nucleus. However, the core electrons do not contribute strongly to chemical bonding and it is therefore a common choice to solve the problem only for the valence electrons and restrain the core electron density to the density of the isolated atom in the molecular environment, which is called the *frozen core approximation*.

This can be done via pseudopotentials [129] (PP), which replace the strong Coulomb potential of a bare nucleus by an effective ionic potential of a pseudo-atom that includes the effects of the core electrons. These PPs need to correctly describe the scattering properties of the atom, while the correct nodal structure of the valence electron wave functions has to be retained. Pseudopotentials are typically generated from *ab-initio* calculations of isolated atoms. The corresponding pseudopotentials and pseudo-waves are then optimized to be as smooth and simple as possible within a certain core-radius and to ideally agree with the all-electron wave functions outside of this radius. This is done independently for different angular momenta and the corresponding 'non-local' pseudopotential can be expressed in a so-called *Kleinman-Bylander* form [130]

$$\hat{V}_{PS} = V_{\text{loc}}^{PS}(\mathbf{r}) + \sum_{ij} |\beta_i\rangle\, B_{ij}\, \langle\beta_j|\,, \tag{4.14}$$

where the highest considered angular momentum is defined to be the local part of the PP $V_{\text{loc}}^{PS}(\mathbf{r})$ and the $|\beta_i\rangle$ are individual projection operators for each angular momentum channel. These PPs are optimized to be maximally transferable between different chemical environments. This is especially the case if the all-electron charge within the core region is perfectly reproduced. Such PPs are called *norm-conserving*. However, this constraint can be rather restrictive and specific atomic or molecular states still require a large amount of plane waves for a good representation.

Much more smooth and efficient pseudopotentials can be generated if the norm-conservation criterion is lifted [131]. The so-called *ultra-soft pseudopotentials* (USPPs) are not required to reproduce the correct charge in the core region, the necessary core radius can be larger, and the plane-wave cutoff, necessary to yield a correct description of states, is much smaller. However, the price to pay is the fact that the valence states are not orthogonal any more and a generalized eigenvalue problem arises (as is the case in localized basis sets):

$$\sum_{m'} \left(\frac{1}{2}|\mathbf{k}+\mathbf{G}_m|^2 \delta_{mm'} + \tilde{v}_s(\mathbf{G}_m - \mathbf{G}_{m'}) \right) c_{n,m'}(\mathbf{k}) = \epsilon_{n\mathbf{k}} \hat{S} c_{n,m}(\mathbf{k}). \tag{4.15}$$

where $\hat{S}$ is an overlap operator, guaranteeing orthonormalization of the $\psi_{n\mathbf{k}}$:

$$\langle\psi_{n\mathbf{k}}|\hat{S}|\psi_{n'\mathbf{k}}\rangle = \delta_{nn'}. \tag{4.16}$$

As an example of a numerical implementation of an ultra-soft pseudopotential-plane-wave approach, the CASTEP code was used in this work (see appendix A.3).

Part II

Photodynamics of Gas Phase Azobenzene

5 180 Years of Azobenzene Research in a Nutshell - a Literature Overview

Azobenzene ((E)-diphenyldiazene, H_5C_6-N=N-C_6H_5, in the following 'Ab', Figs. 5.1 and 5.2) and diazenes in general are the most intensively studied representatives of molecular switches [6, 132]. They are prototypical examples of conformational switches and have been in use as chromophores and dyes for a long time. The following chapters of this thesis will focus on the isomerization dynamics of gas-phase Azobenzene and in particular on the correct theoretical description thereof. In order to unequivocally set the stage for the investigation of the structure, energetics, and switching behavior of Azobenzenes adsorbed to coinage metal surfaces, the current chapter will briefly recapitulate the present state of understanding concerning the switching behavior of isolated Ab and its derivatives, as it has emerged from a plethora of previous experimental and theoretical studies.

The first documented synthesis of Ab dates back to the year 1834 [133], the correct elemental formula was given by Hofmann in 1860 [134] and the first correct Lewis structure prediction on the basis of Kekulés theory of aromaticity was given by Glaser in 1866 [135]. Although the structure was known very early, it took until 1937 for the metastable Z-Ab isomer and the isomerism between the two stable conformers to be detected by Hartley [19]. He was able to transform the orange-red E(trans)-Ab isomer (melting point 68°C) via light-irradiation into the yellow Z(cis)-Ab form (melting point 71.4°C) and also reported the corresponding large dipole moment of the second form. This was the starting point for many investigations of this mechanism in solution regarding the adsorption spectrum and quantum yield [136–139]. These works already include first suggestions on the mechanistic details of the photo-induced isomerization process. The first studies, that were purely focusing on the mechanism, postulated excitation to a triplet state and subsequent slow excited state decay [140, 141], although Zimmerman *et al.* already very early rationalized the lack of fluorescence as sign of an internal radiationless conversion from the photo-induced excited state back to the electronic ground state of the molecule rather than an intersystem crossing [142]. Shortly after, Jones and Hammond were able to explicitly exclude the involvement of excited state triplets in the photo-isomerization process [143]. Accurate crystal structure predictions of E-Ab and Z-Ab were given by Brown [144] and Mostad and Rømming [145].

In the following, the experimental data on the Ab photochemistry will be summarized as it emerged from this initial stage of Ab research and the years thereafter. Molecular photoswitching of Ab is characterized by two stable isomers, namely Z-(cis) and E-(trans)Azobenzene, whereby E-Ab is more stable by 0.58 eV [146]. Both states are separated by a sizable ground-state activation barrier of about 1.16 eV for Z-Ab measured in vapour [147] (0.88 - 1.04 eV measured in solvent [148]). Together with the difference in stability this adds up to a thermal activation barrier for E-Ab of 1.50 to 1.75 eV. The UV spectra of both isomers are characterized by a low lying n$\rightarrow \pi^*$ (S1) and a higher lying $\pi \rightarrow \pi^*$ (S2) transition, whereby the lower state is of little intensity in E-Ab due to symmetry-selection rules [20, 132, 149, 150]. The adsorptions occur at about 440 nm (2.82 eV) and 301 nm (4.12 eV) for the S1 and S2 of E-Ab, respectively [147].

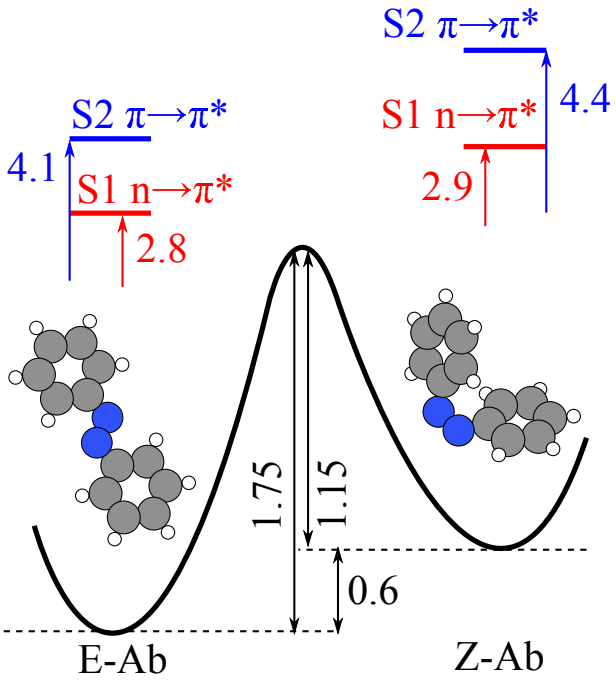

Figure 5.1: Summary of experimental findings on Azobenzene in gas-phase. For references see the main text. Energies are given in eV.

The corresponding excitations for Z-Ab lie at about 420 nm (2.92 eV) [147] and about 280 nm (4.42 eV) [149]. The excitations are not very sensitive to solvent effects and are therefore very similar in solvent and in gas-phase. Both isomers are interconvertable via photoexcitation [19, 132]. Azobenzene can Z→E or E→Z isomerize following excitation to either the S1($n \rightarrow \pi^*$) or the S2($\pi \rightarrow \pi^*$) state [20, 132]. The corresponding quantum yields for E→Z (Z→E) isomerization in *n*-hexane are 0.24 or 0.12 (0.55 or 0.40) following excitation to S1 or S2, respectively [142, 151, 152]. From this it can be seen that a higher switching success rate per photon is achieved for the Z→E backreaction than for the E→Z isomerization, and that the electronic excitation to S1 provides a higher isomerization yield than excitation to S2. Owing to the latter observation it has been argued by Rau [132] that this represents a violation of Kasha's rule[1]. Recently it has been shown that excitation to higher lying states predominantly leads to dissociation [153]. The corresponding experimental facts are summarized in Fig. 5.1.

One may define a second phase of the investigation of Ab photoisomerization, mainly driven by the advent of quantum chemical modelling and advanced time-resolved spectroscopical techniques starting from the late 1960s and early 1970s. It is from this point on that the actual geometric and atomistic details of the isomerization process were studied and discussed.

A vast amount of experimental [154–165] and theoretical [166–187] works have focused on this topic over the past decades and have started a long lasting controversy over the dominating mechanisms [132, 160, 161, 171, 188]. Here, I only explicitly mention the time resolved femtosecond absorption and fluorescence measurements of Satzger and coworkers [163]. The authors measured transient absorption spectra and assigned several time constants to different parts of the isomerization process. For the S1 (S2) isomerization of E-Ab the authors find: τ_1=0.34

[1]Kasha's rule states that fluorescence occurs dominantly from the lowest lying excited state. This is, however, not true if there exist crossings between S0 and S1 and internal conversion can occur. Furthermore, Kasha's rule only strictly applies to simple non-reactive absorption and emission.

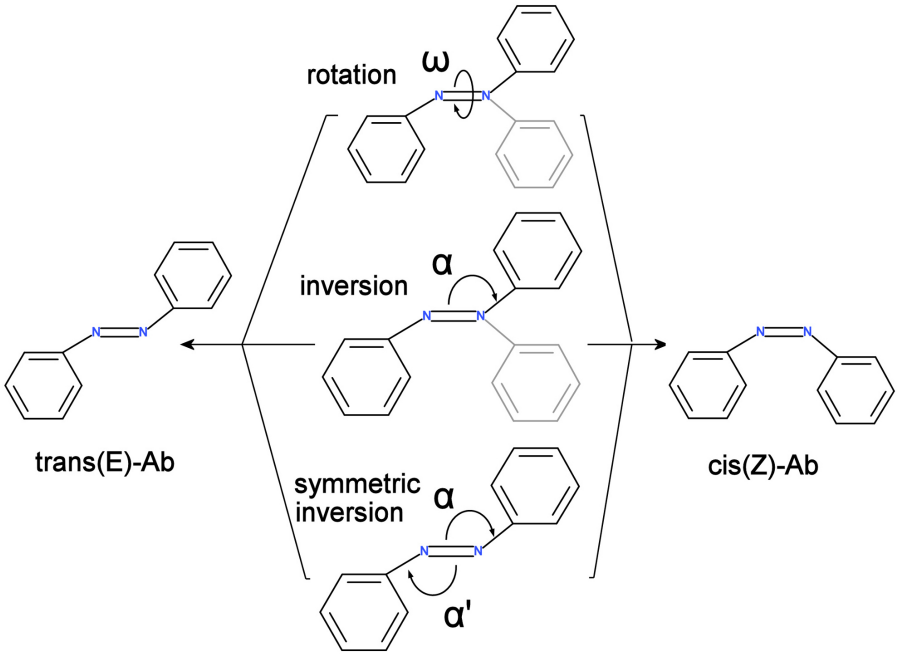

Figure 5.2: Schematic overview of important degrees of freedom in the photoisomerization mechanism of Ab: rotation around the central CNNC dihedral angle ω (upper panel), inversion around one of the NNC angles α (central panel), and a symmetric breathing mode of both CNN angles α and α'.

(0.42) ps, τ_2=3.0 (2.9) ps, τ_3=12 (12) ps. In the case of S2 excitation it was necessary to assign an additional smaller time constant of 0.13 ps. From the similarity of the time constants they concluded that both processes happen over fast nuclear motion from the Franck-Condon (FC) structure to a state crossing or conical intersection (CI) [189] (τ_1), relaxation to the ground state minimum energy structure (τ_2), and further vibrational cooling through the solvent (τ_3). The authors interpret the additional process following S2 excitation as fast initial population transfer from S2 to S1. In this view, both excitation channels thus follow the S1 dynamics. For the isomerization starting from Z-Ab they reach the same conclusion even though the time constants show more subtle differences between S1 and S2 (τ_1=0.17 (0.2) ps, τ_2=2 (1.1) ps, τ_3=10 (14) ps). These experimental values have been confirmed by several other groups even though the corresponding authors came to different interpretations concerning the actual isomerization mechanism [159–161]. The experimental conclusion of immediate population transfer from S2 to S1 is supported by several *ab-initio* studies. From high-level multireference post-Hartree-Fock calculations of the involved PESs, Ishikawa and coworkers [168], as well as Schultz *et al.* [161], also proposed that excitation to S2 is immediately followed by transitions that could involve several states and finally reach the S1 state, from whereon the actual isomerization then follows S1 dynamics. Recently this has been further supported by high level multireference calculations of Conti, Garavelli, and Orlandi [178] and explicit non-adiabatic dynamics simulations for a derivative of Azobenzene by Floß *et al.* [190]. The difference in quantum yield between S2 and S1 dynamics can be explained on the basis of additional decay channels in S2 [178] that do not lead to isomerization and different nuclear dynamics on S1 following deexcitation from S2 [191].

Following the above reasoning, the majority of the isomerization will occur on the S1 electronic state. For the nuclear S1 dynamics several possible pathways have been discussed in

the literature. Figure 5.2 illustrates the most frequently studied degrees of freedom, namely an isomerization around the central CNNC dihedral angle ('rotational pathway') and an isomerization around one of the two CNN angles ('inversion pathway'). The general understanding of the prevalence of these mechanisms has undergone various transitions. The initial belief was that excitation to S1 mainly follows inversion whereas excitation to S2 should follow rotational isomerization [132, 166, 167], this way rationalizing the different quantum yields. However, most of the recent experimental studies [161–163], as well as theoretical studies that either investigated the excited-state potential energy surfaces (PESs) [168, 169, 173, 176, 178] or performed explicit non-adiabatic dynamics simulations [174, 177, 179, 181, 182, 190–193] agree on the dominance of the rotational isomerization following excitation of E and Z-Ab in either S1 or S2 in gas-phase and solvent.

Recent explicit *ab-initio* non-adiabatic dynamics studies have reached very high predictive power and allow a correct interpretation of existing experimental data. Specifically the works of Ciminelli *et al.* [191], Pederzoli *et al.* [185], Böckmann *et al.* [193], and Weingart *et al.* [187] have to be mentioned. The current understanding of the nuclear S1 dynamics is based on a change of the central dihedral angle due to a clockwise or anticlockwise pedal motion of the azo-bridge [185, 187, 193, 194] and differences in the decay pathways between different pro-chiral Z-Ab species [187].

On the basis of the above mentioned large amount of studies and the detailed understanding of the mechanism, Ab is an ideal test case for which the effects of the surface on the switching function can be investigated. For this very reason, a significant amount of experimental effort has been made to design and understand surface-mounted molecular switches based on Ab as the main functional subunit. For a detailed review on the corresponding literature see chapter 7. However, the minimal system sizes that are necessary to describe such a surface-mounted system prohibit the use of explicit on-the-fly nuclear quantum dynamics simulation techniques and the underlying *ab-initio* methodology, that have so much aided the understanding of the gas-phase mechanism. It is therefore necessary to find a highly efficient methodology that enables excited state calculations for the switching process. In the remainder of this part of the thesis, one such efficient but highly approximate scheme, namely the Δ Self-Consistent-Field Density-Functional Theory (ΔSCF-DFT) approach, will be tested for its ability to describe the correct switching dynamics and furthermore for it to be a possible method candidate to be used for the surface-mounted isomerization dynamics.

6 Computationally Efficient Isomerization Dynamics: ΔSCF-DFT and Azobenzene

This chapter assesses the ability of the ΔSCF-DFT method to yield a reliable description of the excited state dynamics of isolated Ab and derivatives with the specific aim towards surface-mounted molecular switches. The work presented in this chapter has been published in *The Journal of Chemical Physics* [195].

6.1 Introduction

This thesis aims for an independent description of surface-mounted molecular switching as provided by material-specific first-principles theory. In order to elucidate the mechanistic details of the switching function, a reliable theoretical method has to be established. Unfortunately, metal-surface mounted switches pose a tremendous challenge to such modeling: On the one hand, the theory obviously needs to accurately describe both molecular ground and involved excited electronic states. Particularly the latter is commonly the realm of numerically highly-demanding correlated wave-function based approaches tractable only for very limited system sizes. On the other hand, the non-trivial influence of the substrate dictates its explicit treatment, which in order to properly describe the metal band structure needs to rely on extended surface structures (see chapter 8). Together with the sheer lateral extension of flat-lying adsorbed molecules like Ab, this gives rise to system sizes that are already at the cutting-edge of what can be tackled with approximate ground-state techniques such as density-functional theory with present-day semi-local exchange-correlation functionals [27, 196–199]. This calls for numerically highly efficient approaches to describe the excited states, which in fact should only impose CPU-costs comparable to those of a semi-local DFT ground-state calculation.

It is self-evident that such approaches will be approximate in nature, and thus need to be carefully scrutinized to assess what can and what cannot be addressed reliably. A careful scrutiny requires accurate references as benchmark though. With only limited and indirect experimental information on excited PES topology available this primarily concerns higher-level theory. Notwithstanding, corresponding techniques might have their own limitations. As little conducive as uncritically applying approximate theories is then to readily dismiss them either for what they are or because of discrepancies with incorrect reference data. With this scope the objective of this chapter is specifically to revisit the reliability of the numerically undemanding DFT-based Δ Self Consistent Field (ΔSCF, cf. chapter 3.5) approach to excited states in the context of the prototypical molecular switch Azobenzene. Apart from perfectly meeting the computational efficiency requirement, this type of constrained DFT [200, 201] technique is particularly appealing as it is readily extended to applications at extended surfaces, even in case of appreciable adsorbate-surface hybridization [29, 202]. Unfortunately, a study by Tiago *et*

al. [173] preceding this thesis work on gas-phase Ab reported qualitatively different ΔSCF PES topologies as compared to Time-Dependent DFT [203] reference data, questioning the usefulness of this approach for an envisioned application to the isomerization mechanism of Ab (and its derivatives) at metal surfaces.

Revisiting the problem, the approximate Coupled Cluster Singles and Doubles (RI-CC2) [46, 47] method is used as additional reference technique (cf. chapter 2.4 and appendix A.1). Its accuracy in describing the lowest lying singlet excitations relevant for the isomerization of gas-phase Ab was already demonstrated by Fliegl *et al.* [170]. For reasons of computational feasibility the here presented benchmark is still exclusively performed for the free molecule in the gas-phase. Nevertheless, the discussion and assessment will also be geared towards the application of ΔSCF to surface mounted Ab. As such, the focus lies on applying a semi-local DFT with a gradient-corrected xc functional (GGA) [60] as ground-state basis for the approach, as such functionals are presently the unbeaten workhorse for metal surface studies.

6.2 Computational Details

All ground-state calculations at the spin-polarized Kohn-Sham (KS) DFT level were performed with the all-electron full-potential DFT code FHI-aims release version nr. 051610 [204] (see appendix A.2). Centrally targeted are results as obtained with the GGA functional of Perdew, Burke and Ernzerhof (PBE) [60] to describe electronic exchange and correlation. In order to assess the effect of different xc treatments additional calculations were performed with the local-density approximation functional in the parameterization by Perdew and Wang [205] and with the hybrid functional B3LYP [61, 63]. FHI-aims employs hierarchical basis sets consisting of atom-centered numerical orbitals (see appendix A.2). A 'tier 2' basis set with the internal default tight settings was used for the numerical integrations. From test calculations at the 'tier 3' basis set level it can be concluded that calculated relative energies (and the ensuing ΔSCF excitation energies) are converged to within 2 meV at these numerical settings. The code also offers a standard implementation of the ΔSCF approach [89, 95, 102][1] to obtain approximate excited states. To make full excited state PES scans and geometry optimizations tractable within ΔSCF the existing implementation of discrete constraints was modified to a Gaussian smeared constraint that affects the population of all KS states within a defined small energy window of 0.01-0.02 eV width. At generally insignificant changes of the total energy, this allows to also readily converge systems with degenerate KS states that otherwise lead to significant convergence problems in the SCF procedure. The actual constrained geometry optimizations in both ground and excited states were then performed in combination with a locally modified version of the Atomic Simulation Environment (ASE, see appendix A.4) [206]. The corresponding constraint optimization procedure is based on internal coordinate constraints [207]. Forces were hereby relaxed to below a threshold value of 10 meV $Å^{-1}$.

In the most straightforward ΔSCF realization, singlet excitations are mimicked by enforced population changes within one spin channel, while triplet excitations are modeled through appropriate occupation changes in both spin channels. In terms of the Ab frontier orbitals (*vide infra*), the singlet S1 state would thus result from the enforced occupation of the KS lowest unoccupied molecular orbital (LUMO) and the enforced depopulation of the KS highest occupied molecular orbital (HOMO) within one spin channel, while the triplet T1 state would result from the enforced occupation of the KS LUMO in one spin channel and the enforced depopulation of the KS HOMO within the other spin channel (see Fig. 6.1). However, earlier detailed work [90, 91, 201, 208] has demonstrated that the resulting single determinants of KS orbitals yield a

[1] This implementation is due to Matthias Gramzow, Fritz-Haber Institut Berlin.

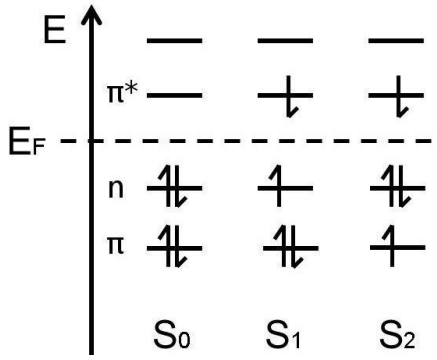

Figure 6.1: Molecular Orbital scheme showing the occupation rearrangements for the S1 and S2 singlet excited states.

particularly inaccurate description precisely of low lying singlet states as are of central interest here. This owes to the fact that present-day local and semi-local xc functionals only evaluate the electron density that is symmetry-broken with respect to the true multi-determinantal singlet states. A possible remedy that will be employed in this chapter is the so-called "sum method" (SM) of Ziegler *et al.* [90], in which the multiplet corrected energy of the singlet state is calculated from the single-determinant singlet and triplet energies as $E_{\mathrm{S}}^{SM} = 2E_{\mathrm{S}} - E_{\mathrm{T}}$. A second possibility is to calculate a singlet state simply using non-spinpolarized DFT calculations, in which case the magnetization density is zero everywhere in space [201, 209]. In such restricted DFT calculations the occupations of the involved doubly-degenerate KS states are then simply varied by ± 1. While this approach lacks a proper formal justification, it is particularly appealing in the context of the envisioned calculations for surface-mounted Ab, as there non-spinpolarized DFT would represent a significant saving in computational time.

The TD-DFT [210] and RI-CC2 calculations [46, 47] used to assess the performance of the ΔSCF approach were done with TURBOMOLE V6.2 [211] (see appendix A.1). TD-DFT calculations were hereby done for the same xc functionals as in the ΔSCF case, as well as for the long-range corrected CAM-B3LYP functional [65], which is presently not available in FHI-aims nor in TURBOMOLE. The CAM-B3LYP calculations were therefore performed with the GAMESS code [212]. In addition to these excited-state calculations TURBOMOLE V6.2 was employed to obtain the constrained PBE geometries for the PESs in Section 6.3. For these and the TD-DFT calculations a gaussian basis set of triple zeta quality (def2-TZVP) with polarization functions from the Ahlrichs series of basis functions [213], and the resolution of identity (RI) approximation [214] was used. The estimated basis set error of the relative energies and excitation energies lies within 10-20 meV as estimated from a quadruple zeta basis set. For the TD-DFT calculations the maximum value of the eucledian norm of the residual vector for the transition density matrices was set to $1 \cdot 10^{-6}$. For the RI-CC2 calculations the basis set was def2-TZVPP, which was previously shown to yield highly accurate excitation energies for the Ab system [170]. With respect to the higher def2-QZVPP basis set the uncertainty in the calculated relative and excitation energies can be estimated to be about 60 meV.

6.3 Ground and Excited State PES Topology

As established in preceding detailed quantum chemical work, the centrally targeted low lying excitations, S1 and S2, have largely singly excited character at least at the Franck-Condon (FC) structures, and can be viewed as $n \rightarrow \pi^*$ (HOMO to LUMO) and $\pi \rightarrow \pi^*$ (HOMO-1 to

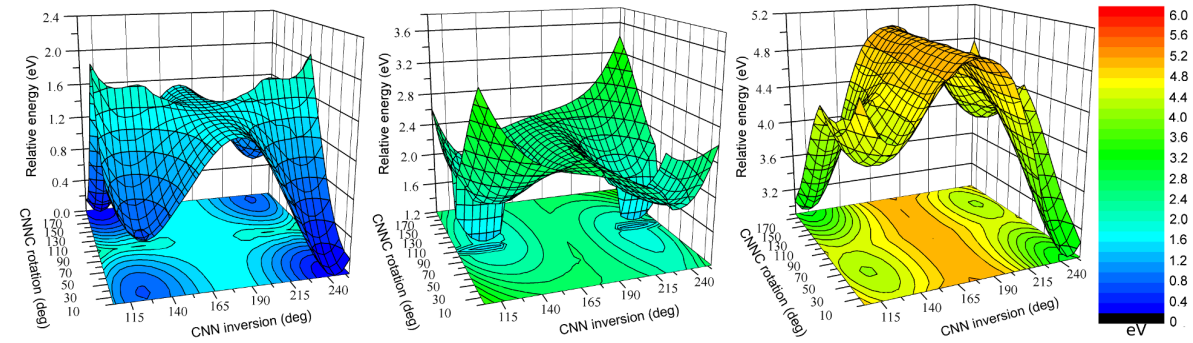

Figure 6.2: Two-dimensional relaxed ΔSCF-DFT(GGA-PBE) PES scans of rotation around the dihedral CNNC angle ω and inversion around one of the two CNN angles α, cf. Fig. 5.2. Shown are the ground state S0 (left), the first excited state S1 (center), and the second excited state S2 (right). Energies relative to the zero reference E-Ab ground state energy are given in eV.

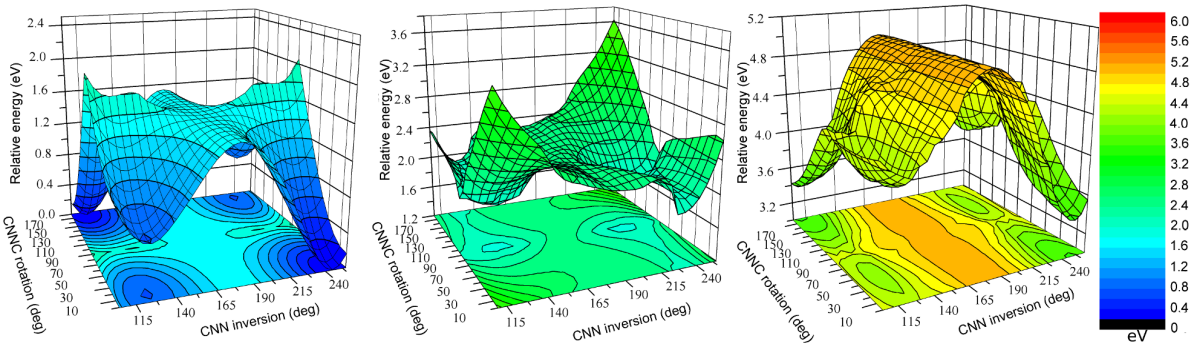

Figure 6.3: Two-dimensional relaxed TD-DFT(GGA-PBE) PES scans of rotation around the dihedral CNNC angle ω and inversion around one of the two CNN angles α. Shown are the ground state S0 (left), the first excited state S1 (center), and the second excited state S2 (right). Energies are given in eV.

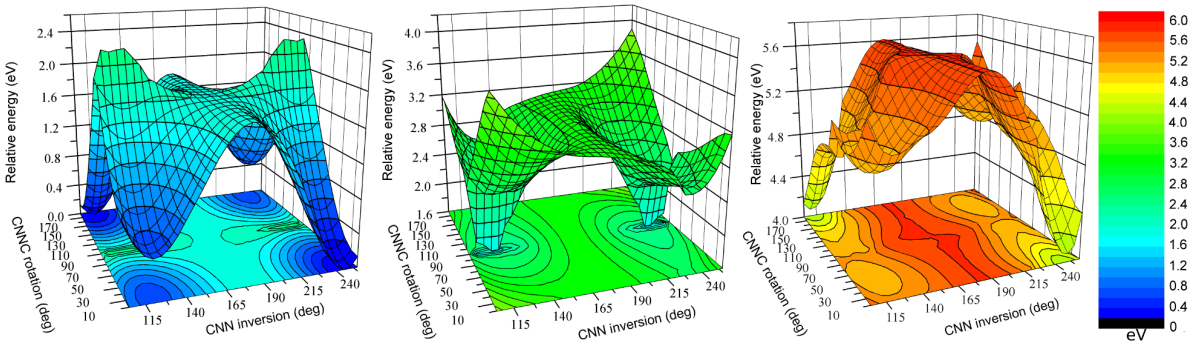

Figure 6.4: Two-dimensional relaxed RI-CC2 PES scans of rotation around the dihedral CNNC angle ω and inversion around one of the two CNN angles α. Shown are the ground state S0 (left), the first excited state S1 (center), and the second excited state S2 (right). Energies are given in eV.

LUMO) transitions, respectively [170, 178]. In SM-corrected ΔSCF one accordingly models the two singlet excitations by modifying the populations of HOMO and LUMO (S1) and HOMO-1 and LUMO (S2), respectively. Figure 6.2 shows correspondingly obtained two-dimensional PES scans along the dihedral CNNC angle ω and along one of the two CNN angles α (cf. Fig. 5.2). Every point on the PES corresponds to a molecular geometry, in which the values for these two angles were constrained to the specific value, while all other degrees of freedom of the Ab molecule are those as resulting from a full geometry optimization in the ground-state[2]. Rather than a state-specific geometry optimization, this allows to clearly disentangle geometric and electronic effects and thereby to directly compare different methods as all are evaluated for the same geometry (The same procedure applies to the results in Fig. 6.5 below). The PESs shown in Fig. 6.2 are for the GGA-PBE xc functional, and we obtain essentially the same topologies for the three surfaces with the LDA or B3LYP. The only difference are more or less constant offsets between the three surfaces depending on the level of xc treatment, which is why we restrict the presentation for the moment to the GGA-PBE case and return to the xc discussion in the next section when focusing on the vertical excitation energies. Figures 6.3 and 6.4 present the same PES scan as was shown in Fig. 6.2, but calculated with TD-DFT(GGA-PBE) and RI-CC2, respectively. The overall topology with all three methods agrees strikingly well. The systematic offset of the two DFT based methods compared to RI-CC2 can be nicely seen from the color scheme. The excited state barriers seem to agree within all three methods, only the S1 inversion barrier calculated with TD-DFT(GGA-PBE) appears rather low.

Qualitatively, the overall obtained topology of S0, S1, and S2 is perfectly consistent with the prevalent understanding of the Ab photochemistry as summarized in the preceding chapter 5. The ground-state PES is dominated by the two metastable states, E-Ab and Z-Ab, separated by sizable barriers along both the rotation and inversion pathway. In contrast, the S1 PES does not exhibit a barrier along the rotational pathway, which after photoexcitation of either E-Ab or Z-Ab should thus quickly lead the system to the well-known conical intersection (CI) region around mid-rotation. Moreover, the S1-FC region at E-Ab is rather flat, while the S1-FC region at Z-Ab is very steep. This is consistent with the experimentally reported longer excited-state lifetime of E-Ab compared to Z-Ab, and is also in line with the reported lower S1 quantum yields for E→Z than for Z→E isomerization. Finally, the closeness of the S2 minima to the respective S0-S2 FC structures, as well as the separation of these minima by large barriers along both inversion and rotation suggests that isomerization after S2 excitation does indeed not occur on the S2 surface, but rather via deexcitation along CIs in other degrees of freedom than those scanned here, followed by motion on the S1 surface.

For a more quantitative comparison a one dimensional PES cut is more instructive. Figure 6.5 compiles these scans along the two prevalently discussed isomerization pathways, the rotational one following motion around the dihedral angle ω and the inversion one following motion along one of the two CNN angles α, cf. Fig. 5.2[3]. The basis of these one-dimensional PES scans are again optimized ground-state geometries, in which the corresponding angle was frozen and all other degrees of freedom were fully relaxed.

The topological similarity, meaning the relative energetics within each PES, for the three methods is rather striking. At the ground-state it is reflected by an almost quantitative agreement of the inversion barrier computed with DFT(GGA-PBE) and RI-CC2, 1.52 eV and 1.74 eV, respectively. These values match also nicely with experiment and previously reported values of

[2]These two-dimensional PES cuts have been sampled with a dense regular grid and the presented continuous curves are interpolated between these points

[3]All potential energy surface scans of the inversion coordinate α presented in this thesis take α as defined in a Z state of the molecule. Therefore, α above 180° corresponds to the complementary angle to the one that would be measured. This is done for consistent definition and ease of visualization.

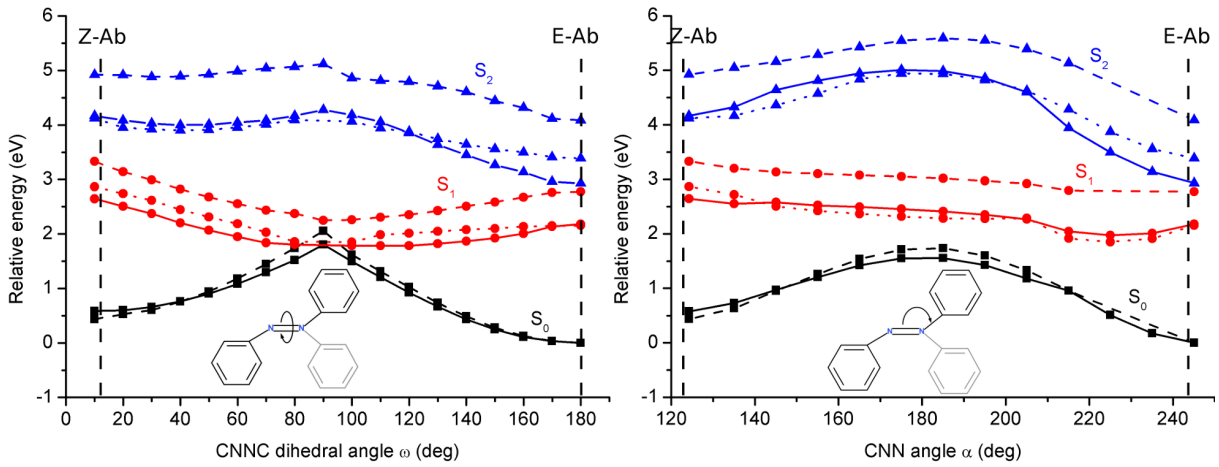

Figure 6.5: PES scans along the rotational (left) and inversion (right) pathway, cf. Fig. 5.2. Shown are the groundstate (S0, black), first (S1, red), and second (S2, blue) excited states, calculated each time with ΔSCF(GGA-PBE) (solid line), TDDFT(GGA-PBE) (dotted line), and RI-CC2 (dashed line). The given inversion angle α above 180° corresponds to the complementary angle to the one that would be measured.

1.5 eV (DFT(LDA) [173]) and 1.74 eV (DFT(B3LYP) [176]). Only slightly lower quantitative consistency is achieved for the S0 rotation barrier, for which the computed values are 1.81 eV and 2.05 eV at DFT(GGA-PBE) and RI-CC2 level of theory, while values of 1.65 eV (CASSCF/PT2 [169]) and 2.18 eV (DFT(B3LYP) [176]) can be found in literature. At the RI-CC2 reference, the rotation pathway is dominated by the well known CI seam between S0 and S1 state around midway rotation [169, 171, 173, 176]. The residual gap obtained in the present calculations, cf. Fig. 6.5, is hereby caused by the geometries that were optimized at the DFT level. For the inversion pathway RI-CC2 reveals no intersection between S0 and S1 along the here displayed PES cut. Also this is in agreement with preceding work, which either did not find any near-degeneracies between states on the inversion pathway or found them only at very high energies compared to the CI seam on the rotation pathway [169]. In both cases, i.e. rotation and inversion pathway, ΔSCF-DFT(GGA-PBE) and TD-DFT(GGA-PBE) correctly reproduce the existence viz. non-existence of S1 and S0 state degeneracies. At the S2 surface, the large barrier along the inversion pathway is again rather well reproduced by the three methodologies, 2.08 eV (ΔSCF(GGA-PBE)), 1.55 eV (TD-DFT(GGA-PBE)), 1.50 eV (RI-CC2) when measured from E-Ab, or 0.84 eV (ΔSCF(GGA-PBE)), 0.82 eV (TD-DFT(GGA-PBE)), 0.67 eV (RI-CC2) when measured from Z-Ab. The same holds for the barrier along the rotation pathway on S2, where the corresponding values are 1.35 eV (ΔSCF(GGA-PBE)), 0.71 eV (TD-DFT(GGA-PBE)), 1.03 eV (RI-CC2) when measured from E-Ab.

Furthermore, the excellent agreement of the three methods (ΔSCF, TD-DFT, RI-CC2) with respect to the topology also extends to other parts of the PES not contained in the hitherto presented scans. This is nicely demonstrated by table 6.1, which compiles selected structural parameters of the ground-state E-Ab and Z-Ab states, as well as of those minimum energy structures on the S1 and S2 states that are obtained after optimization from the E-Ab and Z-Ab FC structure. At the ground-state level the known excellent performance of the DFT GGA-PBE functional in describing both geometry and relative energetics of both E-Ab and Z-Ab isomers as compared to both higher-level theory and experiment can be reproduced. Optimization in the S1 state with FC E-Ab as starting structure yields a minimum at similar geometries within

Table 6.1: Optimized geometry parameters of E and Z Ab in ground (S0) and excited (S1, S2) states, cf. Fig. 6.5 for the definition of the azo-bridge bond length d_{NN} and the two angles ω and α. Additionally shown are the relative energies ΔE of the corresponding states with respect to the ground-state E-Ab zero reference. None of the methods identified a stable minimum after optimization from S1 Z-Ab, which is why the corresponding entries have been left blank in the table.

	method	Trans (E)				Cis (Z)			
		ω	α	d_{NN}	ΔE	ω	α	d_{NN}	ΔE
		(deg)		(Å)	(eV)	(deg)		(Å)	(eV)
S0	DFT(GGA-PBE)	180	115	1.26	0	12	124	1.25	0.58
	RI-CC2	180	114	1.27	0	7	121	1.27	0.47
	CASSCF/PT2 [169]	180	115	1.24	0	4	123	1.24	0.52
	Exp [145, 155]	180	114	1.25	0	0	122	1.25	0.6 [215]
S1	ΔSCF(GGA-PBE)	180	130	1.25	1.67	–	–	–	–
	TD-DFT(GGA-PBE)	180	131	1.24	1.53	–	–	–	–
	RI-CC2	180	128	1.26	2.26	–	–	–	–
	CASSCF/PT2 [169]	180	129	1.25	1.95	–	–	–	–
S2	ΔSCF(GGA-PBE)	180	113	1.36	2.53	18	127	1.31	3.60
	TD-DFT(GGA-PBE)	180	111	1.34	3.15	30	122	1.31	3.65
	RI-CC2	180	110 /113	1.37	4.06	–	–	–	–
	CASSCF/PT2 [178]	180	113	1.35	4.05	8	129	1.29	5.55

ΔSCF(GGA-PBE), TD-DFT(GGA-PBE), and RI-CC2, which in turn compare nicely to the CASSCF optimized geometry reported by Cembran *et al.* [169]. The d_{NN} bond length at this minimum energy geometry is essentially unchanged with respect to ground-state E-Ab, as one would intuitively expect for a transition depopulating the non-bonding n HOMO orbital. In contrast, in terms of energetics the different methodologies yield again a large scatter and this point will be elaborated in the next section. In the S2 state an equivalent situation is obtained. Excellent agreement in the geometries is contrasted by strong discrepancies in the energetics for both minimum energy structures obtained after optimization from the FC E-Ab and FC Z-Ab. With respect to the angular degrees of freedom both these minimum energy structures exhibit values in close correspondence to their S0 counterparts. They differ largely in their strongly activated d_{NN} bond though. This is again congruent with the expectations for a transition depopulating the π-bonding HOMO-1 orbital and supports the already mentioned interpretation that deexcitation from S2 occurs via CIs in other degrees of freedom than those relevant for the isomerization process.

6.4 Excitation Energies of E-/Z-Azobenzene

As already mentioned in the preceding section, equivalent S0, S1, and S2 topologies to those just discussed are obtained when using different xc functionals in the DFT, ΔSCF, and TD-DFT calculations. *Cum grano salis* corresponding PESs essentially exhibit global vertical shifts with respect to each other as further illustrated in Fig. 6.6 for the inversion pathway. This allows us to focus the discussion of the different levels of theory on single prominent points on the PES, suitably the vertical excitation energies as there experimental data is also available as reference. Table 6.2 summarizes the corresponding data. The benchmark against the experimental vertical excitation energies at E-Ab and Z-Ab emphasizes the known high accuracy achieved by the

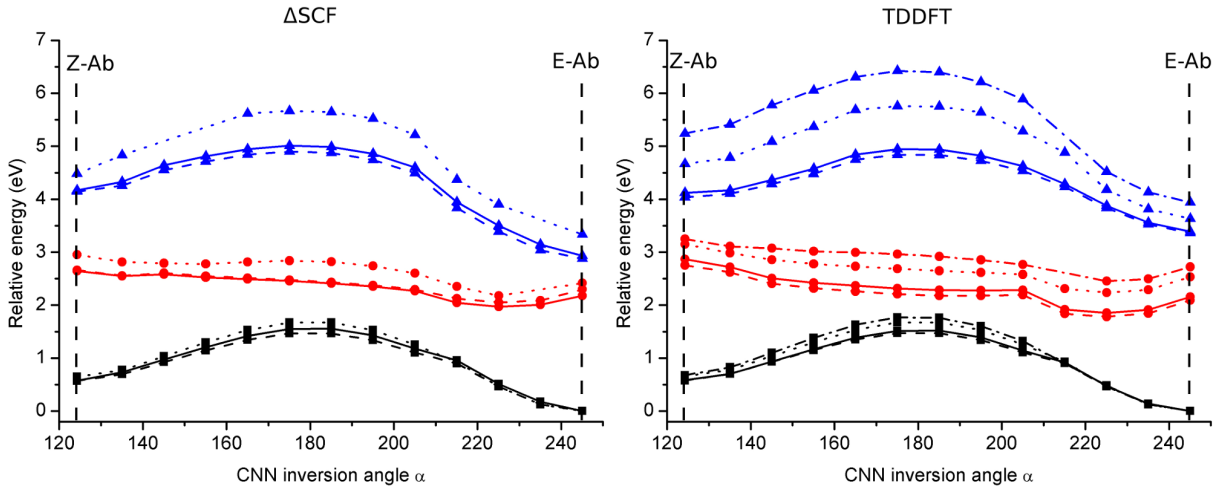

Figure 6.6: PES scan along the inversion pathway, calculated with ΔSCF-DFT (left side) and TD-DFT (right side). Shown are the groundstate (S0, black), first (S1, red), and second (S2, blue) excited states, calculated each time with an LDA (dashed line), GGA-PBE (straight line), and B3LYP (dotted line) functional. Also shown for the TD-DFT case is the pathway calculated with the CAM-B3LYP functional (dashed-dotted line).

Table 6.2: Vertical excitation energies for S1 and S2 excitation at E-Ab and Z-Ab at the different levels of theory and from experiment.

method	Trans (E)		Cis (Z)	
S0→	S1	S2	S1	S2
	(eV)		(eV)	
ΔSCF(LDA)	2.30	2.88	2.10	3.56
TD-DFT(LDA)	2.09	3.36	2.19	3.46
ΔSCF(PBE)-not spin pol.	2.27	2.75	2.13	3.54
ΔSCF(PBE)	2.21	2.98	2.10	3.63
TD-DFT(PBE)	2.15	3.39	2.29	3.43
ΔSCF(B3LYP)	2.41	3.33	2.30	3.83
TD-DFT(B3LYP)	2.53	3.63	2.49	4.01
TD-DFT(CAM-B3LYP)	2.72	3.94	2.58	4.56
RI-CC2	2.84	4.07	3.00	4.51
CASSCF/PT2 [178]	2.53	4.23	2.72	4.49
Exp. [147, 216]	2.82	4.12	2.92	4.68

RI-CC2 approach for the two low lying Ab singlet excitations [170] and justifies its use as a theoretical reference method in our study. In contrast, TD-DFT and ΔSCF based on present-day local and semi-local functionals yield excitation energies that are dramatically too low, as had already been noticed in preceding work for this molecule [170, 173]. This concerns predominantly the S2 excitation which at Z-Ab is underestimated by more than 1 eV.

While thus unsatisfactory on the absolute scale, the similarity of the results produced by ΔSCF and TD-DFT as long as they are based on the same functional is notable. The differences are with ~ 0.4 eV largest for S2 E-Ab, while for the other three excitations listed in table 6.2 the two methods match to within 0.1-0.2 eV. To one end this is due to the sum-rule correction we employ for ΔSCF, which yields a spin purified state that is better comparable to TD-DFT [97]. The plain spin-mixed ΔSCF approach instead yields excitation energies for the two states that are typically about 0.3 eV lower than the spin-purified ones. This would further increase the difference to the corresponding TD-DFT values and, worse, also to experiment. Table 6.2 furthermore indicates that simple non-spin polarized ΔSCF calculations [201] are also in this system an alternative, effective way of tackling the multi-determinantal singlet problem. The corresponding values do not differ much from the sum-method corrected ones, and come at a significantly lower computational cost. Himmetoglu *et al.* recently showed that a non-spin-polarized (NSP) treatment can in fact yield a better description than the sum-method corrected (SMC) results [209]. The authors argue that the better description in the case of NSP is based on the fact that it corresponds to an ensemble density approach of mixed singlet and triplet states as well as other contributions.

To the other end the obtained similarity of ΔSCF-DFT and TD-DFT results is connected to the pronounced single-particle character of the S1 and S2 excitations, which in turn is also the rationalization for the high accuracy of the RI-CC2 method [170]. This is most obvious for the S1 state, which is essentially described by a single excitation over the entire PES range scanned and which is thus most straightforwardly mimicked in ΔSCF-DFT. However, it also holds to some extent for the S2 state, which is of a more collective nature in the sense that it exhibits multiple significant TD-DFT excitation amplitudes. As apparent from the afore described moderate deviations even this can still be relatively well described by single-excitation ΔSCF-DFT due to its desirable ability to account for orbital relaxation (*vide infra*).

Despite the similarity, the absolute performance of both methods when based on local and semi-local functionals against RI-CC2 and experiment is still a concern. Particularly the deviation in the S2 Z-Ab vertical excitation energy exceeds the one commonly found for low lying singlet excitations in organic molecules [97, 122, 124]. Visual inspection of the involved frontier orbitals, cf. Fig. 6.8 below, suggests that this might be related to some charge-transfer (CT) aspect of the excitations, which in particular for S2 around Z-Ab shifts charge between the central azo-group and the phenyl-moieties. This interpretation receives some quantitative support by an evaluation of Tozer's CT Λ-parameter [122] that is defined in the context of linear response TD-DFT calculations. This parameter is defined as

$$\Lambda = \frac{\sum_{i,a} \beta_{i,a}^2 \langle \psi_i | \psi_a \rangle}{\sum_{i,a} \beta_{i,a}^2}, \tag{6.1}$$

where $\beta_{i,a}$ defines the eigensolutions of the linear response equations, the TD-DFT amplitudes (see eq. 3.40 in chapter 3.6).

Measuring the spatial overlap in a given excitation, Λ values towards unity indicate that occupied and virtual orbitals involved in the excitation occupy increasingly similar regions of space. In contrast to Rydberg and CT excitations such 'short-range excitations' should then be

much better amenable to TD-DFT based on local or semi-local xc functionals [122, 123, 203]. For the present case, it is indeed precisely for S2 and around Z-Ab that the the lowest Λ-values of around 0.5 are obtained, while for S1 and for S2 towards E-Ab Λ-values lie consistently around 0.7 or higher. Further support for the CT picture comes then also from the larger reduction of the underestimation of S2 at Z-Ab when going to the hybrid functional level. Whereas for S1 and S2 at E-Ab the admixture of exact exchange reduces the error with respect to the RI-CC2 from $\sim 0.7\,\text{eV}$ to $\sim 0.4\,\text{eV}$, at Z-Ab the S2 error goes from the larger $\sim 1.1\,\text{eV}$ equally down to $\sim 0.5\,\text{eV}$, cf. table 6.2. At the level of the Coulomb-attenuated CAM-B3LYP functional this remaining deviation is then further reduced to the order of $0.1\,\text{eV}$ throughout. Also this is consistent with the interpretation of some overall CT character of the low lying singlet excitations, which this functional with its varying degree of exact exchange at short and long range is specifically supposed to tackle [119, 217–219]. At this functional level the agreement reached with respect to experiment is thus essentially *en par* with that of the correlated wave function reference techniques, and it can be speculated that the same would approximately hold for CAM-B3LYP-based ΔSCF-DFT (which unfortunately is presently not available to us).

6.5 TD-DFT and the Inversion Path Barrier - The Benefits of ΔSCF-DFT

The good agreement of ΔSCF-DFT, TD-DFT, and RI-CC2 in terms of overall PES topology particularly around mid-inversion might come as a bit of a surprise in view of earlier studies that reported significant discrepancies for this [173] or for π-bond twisting paths of comparable molecules [125, 220, 221]. In such cases deviations between ΔSCF and TD-DFT are often readily attributed to the "simplicity" of the prior theory. Alternatively, "collective" character of an excitation as judged from the existence of several significant TD-DFT amplitudes is also cited as reason for the failure of "single excitation" restricted ΔSCF-DFT. In turn, when it comes to differences between TD-DFT and higher level wave function theories, the deficiency of semi-local TD-DFT to deal with CT-character of excitations is a frequently encountered rationalization. Instead, in the present case yet another difficulty of TD-DFT applies, namely state-crossings, and this can easily lead to wrong assessments, in particular as one finds the allegedly "simpler" theory ΔSCF to be significantly more robust with respect to this issue.

Table 6.3 compiles the TD-DFT amplitudes for the second excited state at the two minima E and Z-Ab and at mid-inversion geometry. Improving the xc-functional gives in addition to improved absolute excitation energies only minor changes of the amplitudes or of orbital overlap. At the mid-inversion geometry none of the applied xc-functionals remedy the state crossing of the HOMO-1 and HOMO-2 orbitals. Starting from the B3LYP functional one also finds artificial orbital rearrangements at the E and Z-Ab geometries. It seems that higher level xc-functionals are able to systematically improve the description of excited states within TD-DFT, but none of the currently used exchange-correlation descriptions is able to correctly describe the KS state ordering in the ground state.

The S2 topology that was found around mid-inversion shows a sizable barrier and is similar for ΔSCF, TD-DFT and RI-CC2 (compiled in Fig. 6.5). This would not be the case if one would simply plot the values following the transition from the second highest occupied to the lowest unoccupied orbital without considering the orbital character in the case of TD-DFT. Instead, the excitation was chosen that exhibits the largest amplitude for the targeted transition between the π and π^* KS orbitals. Table 6.3 shows the corresponding n-th excitations for the mid-inversion point. As shown in Fig. 6.7 the two procedures do not lead to the same result around mid-inversion, and only the approach that tracks the correct transition yields a PES topology that is

Table 6.3: TD-DFT amplitudes as well as Λ values [122] of the S2 excited state for E-Ab (E), Z-Ab (Z), and the transition state around inversion (I) for the different applied xc-functionals. Only contributions > 0.05 are shown. '#th Exc.' corresponds to the number of the excitation at which the $\pi \rightarrow \pi^*$ state was found.

xc-func	LDA			PBE		
	E	I	Z	E	I	Z
#th Exc.	2	5	2	2	5	2
transition \ Λ	0.74	0.63	0.58	0.75	0.65	0.54
H-1[a] →L	0.78	–	0.66	0.82	–	0.40
H-2→L	0.20	0.74	–	0.16	0.68	–
H-3→L	–	0.20	–	–	0.24	0.15
H-4→L	–	–	–	–	–	–
H→L	–	–	–	–	–	–
H→L+1	–	–	0.25	–	–	0.45
H→L+3	–	–	–	–	–	–
xc-func	B3LYP			CAM-B3LYP		
	E	I	Z	E	I	Z
#th Exc.	2	6	2	2	4	2
transition \ Λ	0.76	0.57	0.64	0.79	0.60	0.65
H-1[a] →L	–	–	0.89	–	0.10	0.57
H-2→L	–	0.26	–	–	0.53	–
H-3→L	–	–	–	–	–	0.07
H-4→L	–	0.56	–	–	0.18	0.12
H→L	0.99	–	–	0.99	–	0.14
H→L+1	–	–	0.06	–	–	–
H→L+3	–	0.15	–	–	–	–

[a] H: HOMO, L: LUMO

in agreement with both ΔSCF and the reference RI-CC2 data. In contrast, the approach that merely monitors the HOMO-1 to LUMO TD-DFT excitation yields a very wide plateau-region along the inversion path, precisely as reported previously by Tiago *et al.* [173] for this system.

The source for this difference is clearly apparent from Fig. 6.8, which shows the evolution of the energetic position of the GGA-PBE KS frontier orbitals along the inversion pathway. At both E-Ab and Z-Ab these orbitals exhibit the ordering HOMO-1 (π), HOMO (n), and LUMO (π^*) as intuitively expected from the $n \rightarrow \pi^*$ (HOMO to LUMO) and $\pi \rightarrow \pi^*$ (HOMO-1 to LUMO) character of S1 and S2, respectively. However, around mid-inversion the ground-state KS orbital energies of the states that at E-Ab and Z-Ab correspond to HOMO-1 and HOMO-2 cross. Inspection of the TD-DFT amplitudes reveals that the correct $\pi \rightarrow \pi^*$ TD-DFT excitation then corresponds to a transition primarily between this HOMO-2 level and the LUMO (cf. table 6.3).

Here, it is intriguing to note that also in Hartree-Fock as the basis for the RI-CC2 reference, the frontier orbital ordering does not correspond to the aforementioned π, n, and π^* sequence. Still, the two lowest energy RI-CC2 excitations anywhere on the PES parts scanned in this study have predominant amplitude just exactly for the transitions expected, i.e. $n \rightarrow \pi^*$ for S1 and $\pi \rightarrow \pi^*$ for S2. As such the TD-DFT result which places the $\pi \rightarrow \pi^*$ transition at a higher lying excitation than the second transition around mid-inversion has to be interpreted as the inability

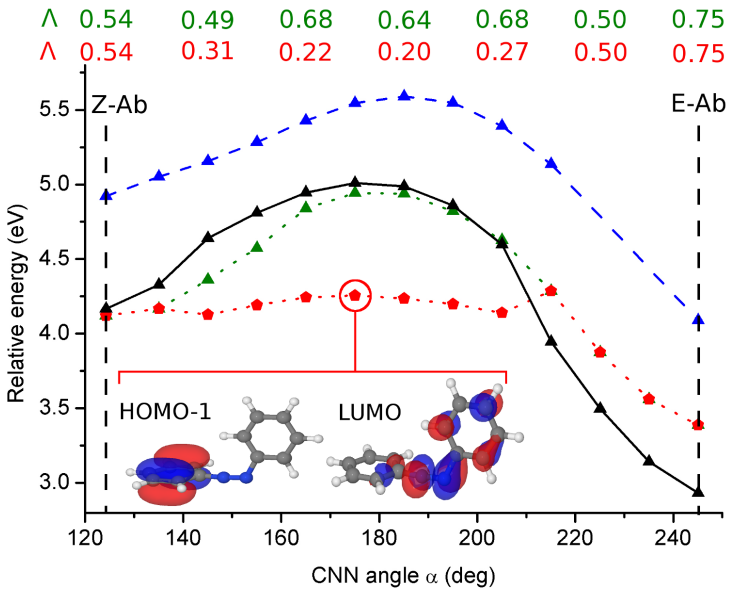

Figure 6.7: Scan along the inversion pathway, comparing the S2 PES as calculated with TD-DFT(GGA-PBE) when following the HOMO-1→LUMO excitation (red, dotted line) and when following the transition with predominant $\pi \rightarrow \pi^*$ character (green dotted line). Only the latter approach yields the correct PES topology with sizable barrier around mid-inversion as compared to RI-CC2 (dashed line) and ΔSCF-DFT(GGA-PBE) (solid line). Also shown are the CT Λ-values [122] for the two TD-DFT curves (see text), as well as the LUMO and the "wrong" HOMO-1 orbital at mid-inversion. These nicely reveal the pronounced CT-character of this transition.

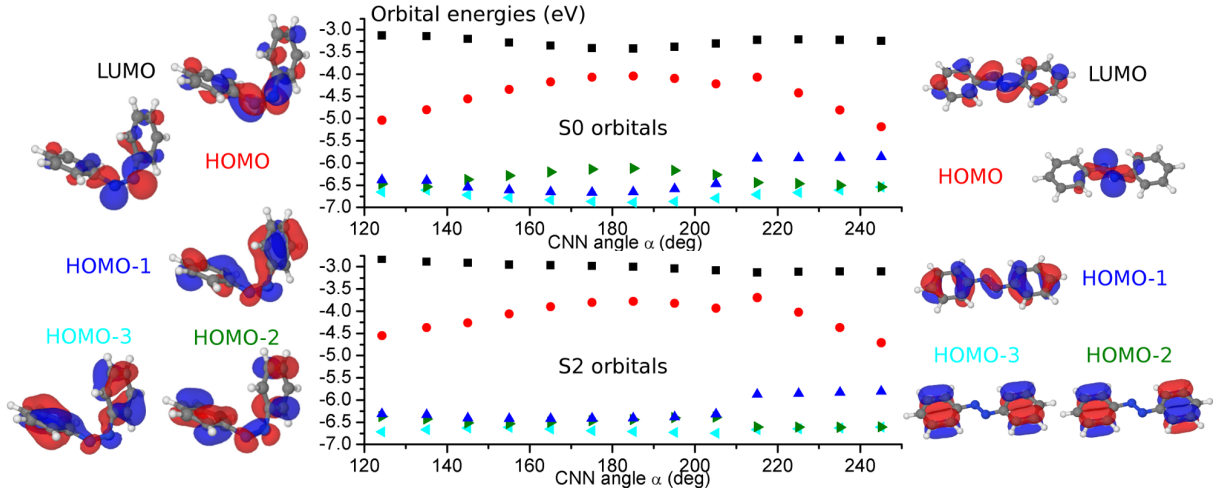

Figure 6.8: Energetic positions of GGA-PBE KS frontier orbitals along the inversion pathway as resulting from a self-consistent ground-state calculation (upper panel) and as resulting from a self-consistent ΔSCF-DFT calculation for the S2 excitation (lower panel). Additionally shown are the corresponding KS ground-state orbital shapes at Z-Ab (left) and E-Ab (right).

of current xc-functional approximations to correctly describe the ground-state orbital ordering. Connected with that is the inability of linear-response TD-DFT based on adiabatic semi-local xc-kernels to cope with ground-state orbitals offered by GGA-PBE. This is then also consistent with the observation that in TD-DFT the S2 excitation typically exhibits larger amplitudes for more than one single-particle transition (cf. table 6.3).

Intriguingly, the allegedly simpler theory ΔSCF-DFT is much less affected by this limitation as it allows for orbital relaxation under the excitation constraint. Figure 6.8 demonstrates that the self-consistent orbitals obtained under the S2 population constraint no longer exhibit any state crossing along the inversion pathway. Once self-consistency is achieved, the constraint of a depopulated HOMO-1 and a populated LUMO leads always to a situation, where the HOMO-1 corresponds to the π state and the LUMO to the π^* state, i.e. the computed excitation energy corresponds indeed exactly to the transition that was envisioned. This type of robustness was found to hold for both S1 and S2, everywhere on the PES parts that were scanned, and for whatever xc-functional that was used. Especially for dynamical simulations or mappings of larger parts of the PESs this is an important asset. It is also particularly remarkable as at the hybrid functional level (B3LYP and CAM-B3LYP) the ordering of the ground-state KS levels differs from expected π, n, π^* sequence essentially everywhere on the PES parts scanned. This made it rather cumbersome to track the correct transitions in TD-DFT, which, however, was the prerequisite to obtain the consistent agreement of the TD-DFT PES topologies with respect to ΔSCF-DFT and RI-CC2 reported above. For corresponding method comparisons the ease with which unidentified state-crossings can impair the TD-DFT results is hereby particularly consequential, as it may readily lead to wrong assessments. Discrepancies between TD-DFT and ΔSCF that in reality are due to an unidentified state-crossing in TD-DFT may lead to the dismissal of the allegedly 'simpler' ΔSCF theory [173]. As shown in Fig. 6.7, the switch of the excitation character induced by the state-crossing around mid-inversion gives furthermore rise to small Λ values for the wrong TD-DFT transition. This bears the danger to assign the discrepancy in the PES topology of this transition with respect to the RI-CC2 reference incorrectly to the deficiency of present-day functionals in describing CT excitations.

6.6 Conclusion and Outlook to Surface-Mounted Azobenzene

In summary, a systematic investigation of ground- and low lying singlet excited-state PESs that are of relevance for the isomerization dynamics of gas-phase Azobenzene is presented in this chapter. The results demonstrate that sum-method corrected ΔSCF yields global PES topologies, i.e. relative energetics within one PES, that agree very well with those of TD-DFT at the same xc-functional level and with accurate RI-CC2 reference data. Previous contradictory reports concerning the agreement of ΔSCF and TD-DFT suffered from unresolved state crossings in the TD-DFT calculations [173], while the orbital relaxation possible in ΔSCF makes this approach very robust with respect to this issue. The now unanimously obtained PES topologies of S0, S1 ($n \rightarrow \pi^*$) and S2 ($\pi \rightarrow \pi^*$) states are furthermore quite consistent with existing experimental data concerning the photo-isomerization mechanism.

When based on the same xc-functional sum-method corrected ΔSCF and TD-DFT agree to within 0.1-0.2 eV for the S1 state that is most relevant for the isomerization of free Ab, and to within 0.4 eV for the S2 state. This suggests ΔSCF as a promising route to larger Ab-containing systems, where TD-DFT becomes computationally untractable. This concerns predominantly surface-mounted Ab, where calculations for the adsorption at coinage metals indicate that the low lying excited states largely retain their molecular character [196]. Particularly appealing in this context is that the correct PES topology for gas-phase Ab can be obtained already at

the level of semi-local xc functionals, which are presently the unbeaten workhorse for metal adsorption studies. Furthermore, it can be concluded that the neglect of spin in non-spin-polarized calculations does not significantly alter the qualitative features observed for the two investigated pathways. Specifically in the context of metal-adsorbed molecular switches, neglect of spin corresponds to a significant gain in computational efficiency.

Notwithstanding the correct description of the excited-state topology, at this level of xc treatment the vertical excitation energies produced by ΔSCF and TD-DFT are grossly underestimated. An analysis attributes this primarily to some charge-transfer character of the S1 and S2 excitations, which the local functionals are unable to grasp. As to be expected, hybrid (B3LYP) and even more so long-range corrected hybrid (CAM-B3LYP) functionals improve on this situation. Conserving the overall topology they primarily induce global upward shifts of the excited-state PESs, leading to vertical excitation energies at the CAM-B3LYP level that are roughly *en par* to the correlated wave function reference techniques.

Whereas the reduction of self-interaction error achieved with the advanced functionals is of paramount importance to adequately describe the molecular excitations, one has to recognize that mere admixture of exact exchange does not seem to be the right pathway for adsorption at metal surfaces (at least when judged from the few seminal ground-state studies performed to date. [222–224]). There, semi-local functionals are still more or less the only tractable approach. For the following application to surface-mounted Ab this dictates a cautious approach carefully assessing what can and what cannot be addressed with semi-local functional based ΔSCF. The present results justify the applicability of the method and encourage to search for a description of surface-mounted molecular switching of adsorbed Ab based on a methodological ΔSCF extension, which will be presented later in this work (see chapter 11).

Part III

Structure and Reactivity of Adsorbed Azobenzene

7 Surface Adsorbed Molecular Switches - a Literature Overview

Current research on functioning surface-adsorbed molecular switches is still in a very early phase. Trial and error based functionalization of molecules and variation of substrates keeps the percentage of successfully switchable adsorbates at a low level. Nevertheless, already many interesting functioning systems have emerged, such as artificial molecular motors or machines [225, 226] and optically contractable polymers [227]. In the context of so-called smart materials, molecular switches have been used for surface functionalization that enables the reversible switching between different properties, such as hydrophilicity or hydrophobicity [4, 228, 229]. Specifically the field of molecular electronics [230], with the target of further integrating logical [8, 16] and storage devices [1, 7, 231, 232] down to the molecular level, has been a central research focus. Although the above examples represent great successes, they can only be seen as first steps to what is possible in the future. However, an indispensible requirement is a detailed understanding of the factors that govern the switching function and a clear control of the delicate balance of interactions between molecule and environment that will sustain this function.

One reason why in many of the above mentioned examples Diazenes or Azobenzenes represent the optically active unit is that the gas-phase mechanism is, by now, quite well understood (see chapter 5 of this thesis). Its ability to change conformation upon light irradiation depends not only on the efficient excited-state reaction channel, but more fundamentally on the sheer fact that two meta-stable states coexist in the ground state and are reasonably stable at ambient conditions. Therefore, surface adsorption can alter the function in terms of the excited-state lifetime and reaction channel due to coupling and hybridization with substrate degrees of freedom and also on the level of the basic structural prerequisites to switching by introducing steric hindrance or insufficient stability.

The persistence or loss of function of Azobenzene and its derivatives directly adsorbed to noble metal surfaces, such as close-packed facettes of coinage metals, have been intensively studied [10, 233–236]; no light-induced switching of pure Ab on Ag(111) [1] or Au(111) [21] was ever observed. The lack of photo-induced function has been attributed to three main factors: overly strong coupling to the surface, quenching the excited states involved in the isomerization, and steric hindrance due to strong dispersion interactions between the phenyl rings of the molecule and the underlying surface. However, successful induction of switching of Ab on Au(111) via resonant electron tunneling through a Scanning Tunneling Microscopy (STM) tip [14], suggests that the above mentioned factors apply differently to the two substrates. In all experimental studies, corresponding switching has been verified either by strong changes to spectral features or by visual inspection of STM topograph changes.

Molecular functionalization strategies to decouple the photochromic azo-moiety from the

[1] To the best of knowledge of the author, there exists no literature reference on this subject. Therefore, no clear statement can be made. However, the lack of this data, the lack of function for TBA on Ag(111) (see main text), and private communications from the respective experimental community suggest that the switching function is quenched.

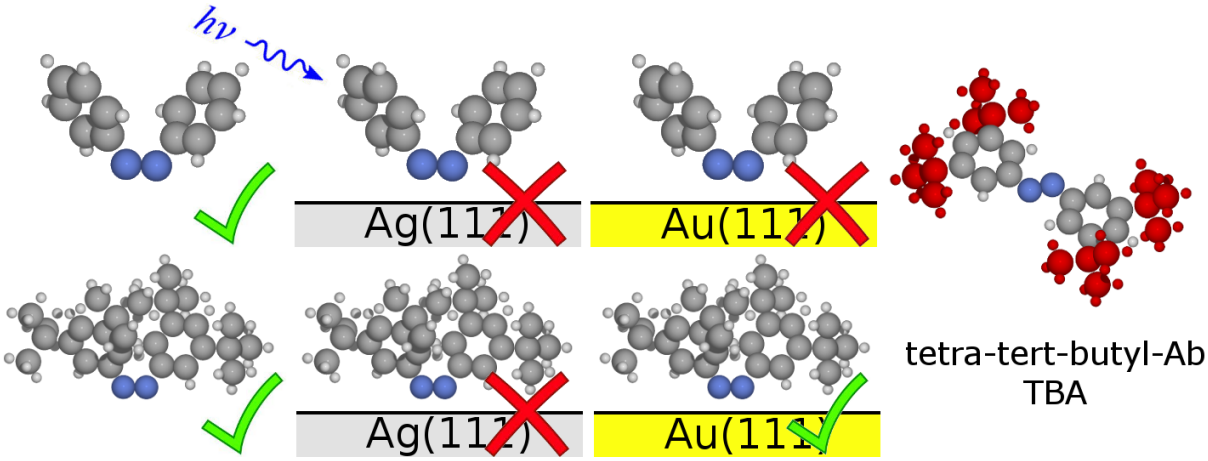

Figure 7.1: Schematic summary of the experimentally observed photo-induced switching function (✓) or non-function (×) of Azobenzene and tetr.-*tert*-butyl-Azobenzene (TBA) in gas-phase and adsorbed to Ag(111) or Au(111) surfaces.

surface follow the basic ideas of either geometrically decoupling the central photochromic azo-bridge from the surface with spacer groups [13, 21, 237] or introducing a modified switching process via strongly chemically active functional groups [234–236]. Comstock *et al.* [21] tested the former by analysing the photoswitching behavior of Azobenzene and Ab substituted with *tert.*-butyl groups at the two phenyl *para* positions and the four *meta* positions (DBA and TBA) when adsorbed to Au(111). The authors were able to detect a switched state of TBA after 1 hour of irradiation with UV light, whereas no isomerization was observed for Ab and DBA. The reason for a functioning photo-induced isomerization of TBA in contrast to DBA and Ab has been related to the electronic decoupling of the central azo-moiety, therewith reduced substrate effects on the excited-state lifetime, and the optical absorption properties. It should be noted at this point that all three molecules represent functioning molecular switches in gas-phase or solvent and could be switched by an STM tip when adsorbed to a Au(111) surface [14, 21, 237]. Fig. 7.1 summarizes the ability or inability to switch upon light-irradiation for Ab and TBA adsorbed to Ag(111) and Au(111).

The photo-switching ability of E-TBA on Au(111) is very sensitive to changes to the molecule or the substrate: only minimally different derivatization of the molecule can modify the switching behavior of an overlayer [238, 239], TBA on slightly more reactive surfaces such as Ag(111) [240] or on Au(100) [22] shows no function. Supression of the photoswitching ability can be observed, not only for small changes to the derivation of the phenyl rings, but also upon modification of the central azo-bridge: the function is lost when replacing the azo-bridge (N=N) with an imine group (C=N) [241][2] or a stilbene group (C=C) [241].

The isomerization mechanism appears furthermore to be strongly modified compared to the gas-phase, exhibiting a reduced efficiency and photon yield; a maximum of 50% of all molecules switch after 7 hours of irradiation [243]), compared to more than 90% of molecules in gas-phase or solvent [132] and the effective cross section of the reaction is orders of magnitude smaller than in the gas-phase [26, 243]. The change in electronic structure of the adsorbate can be verified by STM topographs [243], 2-Photon-Photoexcitation (2PPE signatures of the molecular resonances [26], and changes in the work function [13]. The photoswitched state can be clearly identified

[2]However, "switching" of tetra-*tert*-butyl-Imine can be achieved by variation of temperature and coverage [242].

as the molecular Z-TBA state by structural predictions from Angular Resolved Near-Edge X-Ray Absorption Finestructure (NEXAFS) experiments [244]. In contrast to the gas-phase or solvent situation, photo-induced backreaction from this Z-TBA state to E-TBA is much less efficient and does not happen in the visible regime, but rather with photon energies in the same energy regime as the E-to-Z transition does [243]. A corresponding drop in switching efficiency can already be understood in terms of simultaneously induced switching in both directions, as is supported by the reduced E/Z ratio at the photostationary state. Additionally, backreaction from Z to E-TBA can also be induced by small increases in the substrate temperature; a corresponding thermal activation energy of 0.24±0.03 eV has been measured by Hagen *et al.* [245]. This thermal Z-to-E barrier is reduced by a factor of 4 compared to the corresponding gas-phase barrier [246]. As an additional interesting property of the isomerization mechanism, a strong temperature dependence of the effective photoisomerization cross section has been found; by increasing the temperature of the substrate from 30 to 200 K, the cross section increases drastically by two orders of magnitude (as does the E/Z ratio, see the PhD thesis of S. Hagen [247], pp. 94). From the two possible reasons, a barrier in the excited state separating E and Z-TBA or a strong beneficial influence of vibrational excitation in the ground state, the former can be excluded: the observed T-dependence can not be described by a single-barrier process. From High Resolution Electron Energy Loss Spectroscopy (HREELS) measurements [248, 249] and DFT-based calculation of the vibrational spectrum of TBA adsorbed to Au(111) [199] it is known that the lowest lying vibrational modes involve bending motions of the phenyl rings and the central azo-bridge with respect to the surface. Analytical fitting of the temperature dependence to individual vibrational states supports the experimental observation and suggests that vibrational activation of molecular butterfly motion can strongly enhance switching rates.

The above mentioned experimental results suggest an overall situation that strongly differs from the gas-phase due to geometrical distortion, electronic coupling with the substrate, and a reduced excited-state lifetime, and raise questions regarding the geometric and electronic mechanisms that underly surface-adsorbed photo-switching. The possibility of a purely geometry-based reason for TBA switching and Azobenzene non-switching has been the initial motivation behind introducing bulky spacer groups. However, a recent detailed analysis of the TBA molecule and Azobenzene adsorbed on the Au(111) surface has revealed that the position of the photochromic azo-bridge is barely affected by the bulky spacer groups [27, 199, 250]. The electronic structure and geometry of Ab and TBA on Ag(111) and Au(111) has been experimentally studied by the groups of Prof. Petra Tegeder, Prof. Martin Wolf, Prof. Martin Weinelt, and Prof. Stefan Tautz[3] [13, 23, 26–28, 198, 240, 241, 244]. It has been shown in these works that the electronic structure of the metal substrate plays an important role in the loss and recovery of the molecular switching function. The photoisomerization cross section of TBA on Au(111) shows a strongly different dependence on incidence energy than the gas-phase molecule (see Fig. 7.2, bottom right). Whereas in gas-phase, distinct resonances trigger the isomerization, the adsorbed species shows an initial linear increase in isomerization cross section (<2.2 eV) and an energy region of constant cross section (2.2 eV-4.4 eV), followed by a second region of linear increase (>4.4 eV). Tegeder and co-workers rationalize this energy dependence with a substrate-mediated photo-isomerization mechanism rather than a switching based on intramolecular excitations [26, 28]. Fig. 7.2 reproduces the main results of the corresponding publications. In this mechanism, the incidence photon excites electrons from the metal and generates hot holes. The lower energy bound of the region of constant cross section corresponds to the upper edge of the metal *d*-band, an energy region of increased density-of-state sustaining long-lived holes [251]. The number of

[3]University of Heidelberg, Fritz-Haber Institute of the Max-Planck Society, Free University of Berlin, and Research Center Jülich

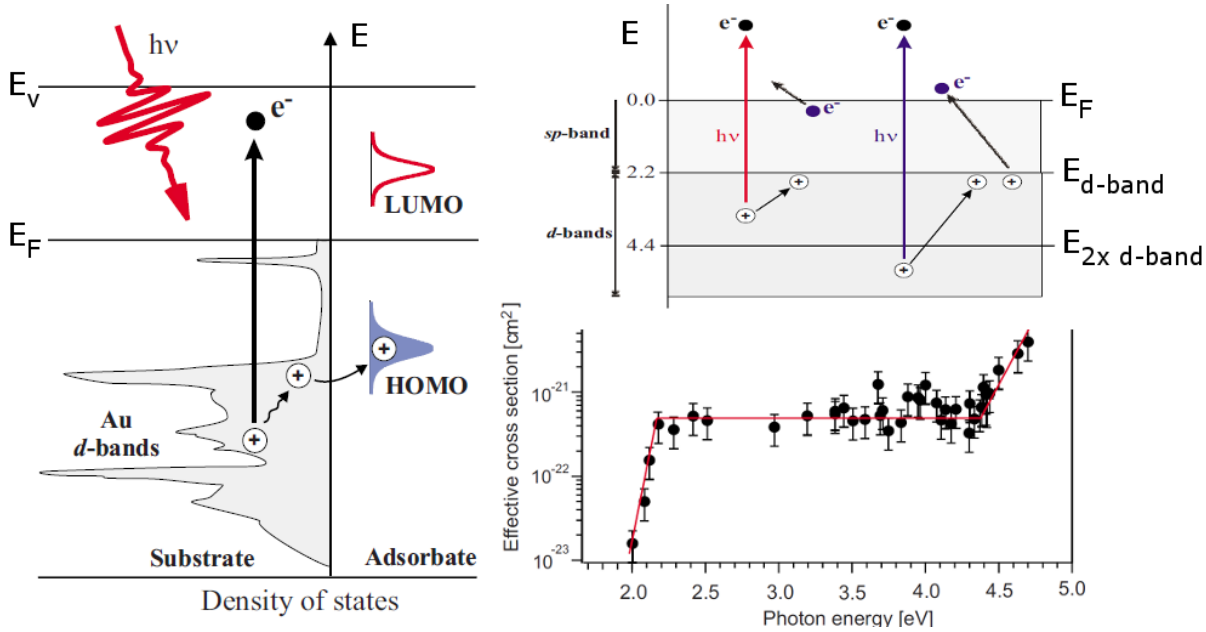

Figure 7.2: (left) Possible alternative mechanism for surface-adsorbed molecular switching. Incident electrons generate hot holes in the metal substrate, which are transferred to the HOMO of the molecule and induce nuclear motion; (bottom right) The photoisomerization cross section as a function of photon energy; (top right) The high density-of-states in the *d*-band region and the therefore increased hole concentration explains the constant cross section between 2.2 and 4.4 eV. The region beyond 4.4 eV corresponds to multi-hole generation. Figures reproduced with permission from Hagen *et al.* [26].

holes that can be generated depends on the available states and their position with respect to the Fermi level. Starting from these 2.2 eV, holes are generated in the localized *d*-bands, which within a few femtoseconds (fs) relax to the upper *d*-band edge. Starting from the energy corresponding to twice the *d*-band onset, double excitation processes can occur. The hole-diffusion to the *d*-band edge can be understood in terms of a level-by-level ladder-climbing process (or intra-band transitions). The corresponding overlap of this upper *d*-band edge in Au(111) with the highest occupied molecular orbital (HOMO), which can be inferred from the experimental positions of the molecular resonances [26, 240], leads to a non-vanishing probability of charge-transfer, where the hole is quenched by an electron from the HOMO, therefore generating a so-called cationic resonance state in the molecule, which subsequently drives the isomerization. The prevalent assumption for the ensuing molecular motion is that, although the coupling to the metallic degrees of freedom will drastically reduce the lifetime of this state, the kinetic energy gained by the motion on the excited-state PES might suffice to enable the transition to the Z-Ab state [252, 253]. Similar mechanisms have been proposed in the context of photo-induced desorption processes [254–256]. Such a substrate-mediated mechanism might further support the strong temperature dependence of the switching cross-section: if the switching ability sensitively depends on the excess kinetic energy with respect to the ground-state barrier, which, in the simplest case, corresponds to the sum of the incidence photon energy and the thermal vibrational energy minus the barrier height, this energy will be higher, the more thermally activated the molecule will be. This model also has been used to rationalize the strong substrate and functionalization dependence in terms of the relative overlap between the metal *d*-bands and the occupied molecular states [23, 28].

Not much is known about the atomic degrees of freedom involved in surface-mounted TBA switching. On the basis of STM topographs and chiral mapping, Comstock *et al.* [257] have argued that the isomerization must follow a predominantly planar inversion of the central CNN bending angle α (cf. definition in Fig. 5.2) rather than the rotational mechanism that is believed to be dominant in gas-phase. However, at present, the experimental data supporting electronic and geometric suggestions to the mechanistic details are rather scarce. Much insight can therefore be gained by a detailed first-principles investigation of the surface photo-induced isomerization process, scrutinizing the feasibility of the suggested substrate-mediated electronic dynamics, the connected nuclear reaction channels, as well as further aiding the understanding of the effects of differing substrate activity and adsorbate functionalization on the switching ability.

First-principles modelling of such large molecular adsorbate reactions and involved excited states is sparse in literature. This relates to the large system size, the high computational expense and the difficulty of simultaneously describing the delocalized metallic band structure and the localized molecular orbitals. An important prerequisite for an *ab-initio* simulation of the excited-state dynamics involved in photoisomerization is a detailed understanding of the adsorption geometries of the ground-state equilibrium structures. A corresponding model of Ab and TBA adsorption geometries on coinage metals has been established in the doctoral thesis of Erik McNellis and builds an important starting point to this work [27, 196–199, 250]. It was herein established that a correct description of Azobenzene molecular adsorption necessitates a full account of dispersion interactions, which are not correctly treated by Density-Functional Theory calculations based on standard semi-local exchange-correlation functional approximations - the currently unbeaten work horses for large-scale models of surface-adsorption [198]. Furthermore, it was shown on the example of TBA on coinage metals that purely structural arguments to design functioning molecular switches can be misleading [199].

The qualitative differences observed between gas-phase and surface-mounted molecular switching as well as the vast amount of experimental data and preliminary work motivate the study of corresponding mechanistic details. This includes a detailed analysis of the ground-state equilibrium structures (chapter 8), coverage dependence (chapter 9), and stability (chapter 10), as well as excited-state potential energy surfaces involved in the isomerization (chapter 12); the topics of the remainder of this thesis.

8 Azobenzene on Ag(111) and Au(111): Structure and Energetics

In this chapter the basic structural modelling approach of this thesis is introduced and corresponding calculations on the minimum energy structures and ground-state adsorption energetics of surface-mounted Azobenzenes are presented and compared to literature.

8.1 Introduction and Modelling Approach

The most basic prerequisite for an investigation of molecular switching on metal surfaces is an accurate prediction of the molecular structure. The computational approach of this thesis is based on density functional theory calculations of adsorbed molecules on metal surface slabs as is shown schematically in Fig. 8.1. Along lateral directions the surface slab is repeated periodically, whereas orthogonal to the surface a large enough vacuum region separates two slab images in order to simulate an extended surface. This approach enables to study, both, the structural equilibrium properties of this system and possible isomerization pathways.

This thesis will make strong use of the structural model for Azobenzene adsorption to coinage metal surfaces that has been developed in the PhD thesis of Erik McNellis [250]. As established by Refs. [196, 197] the adsorption geometry of Azobenzene is determined by several major effects: A possible covalent-type attractive interaction between the central azo-bridge and the surface, an energetic penalty due to the distortion of the molecule upon adsorption, a repulsive force contribution due to the Pauli repulsion between the closed-shell phenyl groups and the substrate, and a strong atractive van-der-Waals (vdW) interaction of the molecule with the substrate. However, the most dominating contribution is the van-der-Waals interaction between the phenyl groups and the surface. Unfortunately, current semi-local exchange-correlation approximations in DFT lack a correct description of long-range dispersive interactions.[1] Especially the efficient pairwise additive DFT-D type vdW correction by Tkatchenko and Scheffler [77] has proven to yield accurate adsorbate geometries, albeit at a certain overbinding for Azobenzene and TBA on coinage metals [198, 199]. The reason for this overestimation can be found in the derivation of the corresponding C_6 coefficients. These are derived from atomic polarizability data and therefore will not correctly capture the collective many-body response of a bulk metal, which will lead to a significant screening of van-der-Waals interactions in deeper-lying substrate layers [85, 198]. For this reason, this work will also employ the recent dispersion correction scheme by Ruiz *et al.* [85] which implicitly accounts for many-body screening. Mercurio *et al.* [198] have instead estimated this effect by simply reducing the van-der-Waals interactions of the molecule with the substrate to the first layer. Following this intuitive approach the authors find a strong reduction of the adsorption energy and an increase in vertical adsorption height both further to the agreement with experimental measurements. However, for the case of the 3,4,9,10-perylene-

[1] For a description of currently employed schemes to include dispersion interactions see chapter 3.4 of this thesis or Klimeš and Michaelides [72]

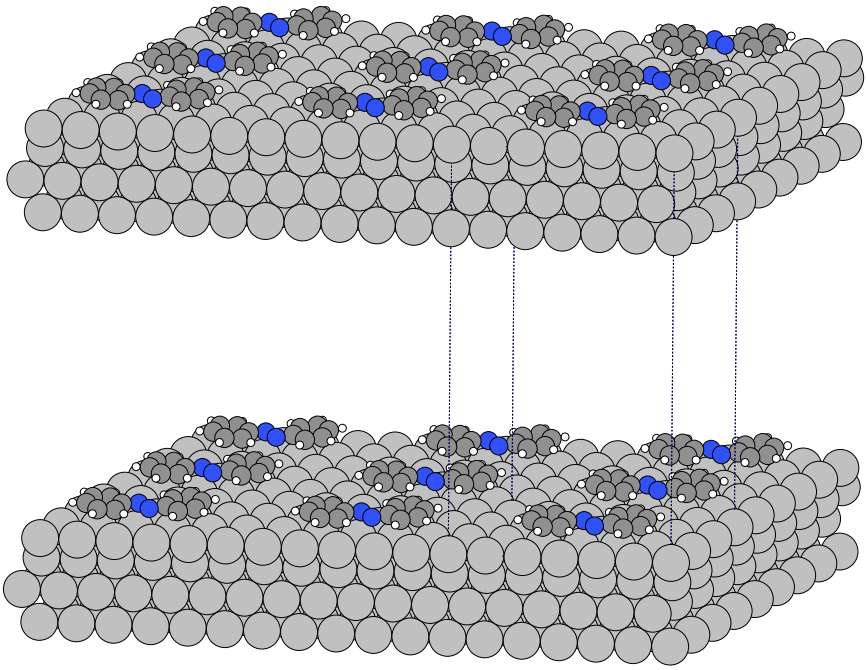

Figure 8.1: Perspective view of a surface supercell of Azobenzene on Ag(111) and its corresponding neighboring image cells along the three lattice coordinates.

tetracarboxylic acid dianhydride (PTCDA) and benzene adsorbed to close packed coinage metal surfaces the novel scheme leads to a reduction of adsorption height connected with a small increase in adsorption energy [81, 85]. In both cases this also leads to an excellent agreement with experimental data. This apparent contradiction shows that the inclusion of many-body response to the description of dispersion interactions can not be understood in terms of simple weakening of the molecule-surface bond.

For this reason, this chapter shortly revisits the adsorption structure and energetics of single adsorbed Azobenzene and TBA molecules on Ag(111) and Au(111) surfaces as predicted by dispersion-corrected Density-Functional Theory calculations by employing one correction scheme implicitly accounting for screening due to many-body response and one scheme neglecting this effect.

Computational Details

All supercell calculations in this and the following chapters have been performed with the pseudopotential plane wave code CASTEP-6.0.1 [258, 259][2] using standard library ultrasoft pseudopotentials [131]. Exchange and correlation were treated with the semi-local PBE functional

[2]For more details see appendix A.3

Table 8.1: vdw(TS) and vdw^{surf} coefficients used in this work: Unscreened [77] and screened C_6 coefficients (in hartree $\cdot$ bohr^6) [85], polarizability α (in bohr^3), vdW radii R_{vdW} (in bohr) and the ratio between free and bulk atomic volume.

		C_6	α	R_{vdw}	V_{free}/V_{bulk}
vdw(TS)	Ag	339.0	50.600	3.820	1.000
	Au	298.0	36.500	3.860	1.000
vdw^{surf}	Ag	122.0	15.360	2.570	0.9419
	Au	133.9	15.620	2.910	0.9452

[60]. Two dispersion correction schemes have been used in this work, namely the Tkatchenko and Scheffler (DFT+vdw(TS)) [77] dispersion correction scheme and the latest scheme by Ruiz *et al.* (DFT+vdw^{surf}) [85]. The latter has been implemented into the current DFT+vdw(TS) module [196] in CASTEP in form of a minor modification (see appendix A.3). Both schemes use a Hirshfeld atoms-in-molecules partitioning scheme [78, 196] to calculate effective atomic volumina and rescale the C_6 coefficients according to the surrounding density, therewith accounting for different bonding environments. In addition to renormalized C_6 coefficients for the substrate atoms, the novel scheme by Ruiz *et al.* employs a different reference to rescale these coefficients. Whereas the original scheme employs the free atom volume as a reference, the vdw^{surf} scheme uses bulk atom volumina as reference. A corresponding proportionality factor between free and bulk metal atom is used to modify the existing implementation. These proportionality constants have been calculated from converged bulk supercell calculations employing the same computational setup as detailed below. Table 8.1 lists the vdw parameters used in this work.

The detailed system setup, computational parameters and convergence settings are heavily based on the structural model established by McNellis [27, 196, 197, 199, 250]. All calculations were performed with (6x4) and (6x5) frozen (111)-oriented 4-layer surface slabs of Ag and Au with 350 eV or 450 eV plane wave cutoff for Azobenzene and 3,3'5,5'-tetra-*tert*-butyl-Azobenzene (TBA), respectively. The used lattice constants for Ag and Au are 4.14 Å and 4.19 Å, respectively [197, 260]. In all calculations the long-range Au(111) surface reconstruction is neglected, due to the fact that a dominant part of the reconstructed surface remains in form of close packed facets [261, 262]. For both surfaces the frozen substrate is believed to be a good approximation due to only minimal structural changes upon adsorption. In the employed large surface unitcells, lateral interactions between the adsorbate and its periodic images are minimal at the DFT level, and longer-ranged vdW interactions between adsorbate molecules are explicitly switched off in the DFT-D correction in order to simulate a low-coverage situation at low computational expense. Spin polarization was not taken into account. The vacuum region was chosen to exceed 20 Å. Contrary to the calculations in Refs. [27, 196, 197, 199], all energy differences and adsorption energies were calculated for these 4-layer metal slabs at a (8x4x1) Monkhorst-Pack **k**-space integration grid [126] for Azobenzene systems and a (6x4x1) grid for TBA systems. Relative energies and adsorption energies are converged to ± 25 meV with respect to plane-wave cutoff, **k**-space integration, and vacuum spacing. Additional details on computational parameters that have been set throughout this work can be found in appendix A.3. Molecular geometries were generated by geometry optimization using delocalized internal degrees of freedom [263] down to a maximum force component of 25 meV/Å. Calculations of the gas-phase molecules have been performed in (40Å×40Å×40Å) and (50Å×50Å×50Å) rectangular supercells for Ab and TBA with the electronic structure calculated only at the Γ-point of the first Brillouin zone.

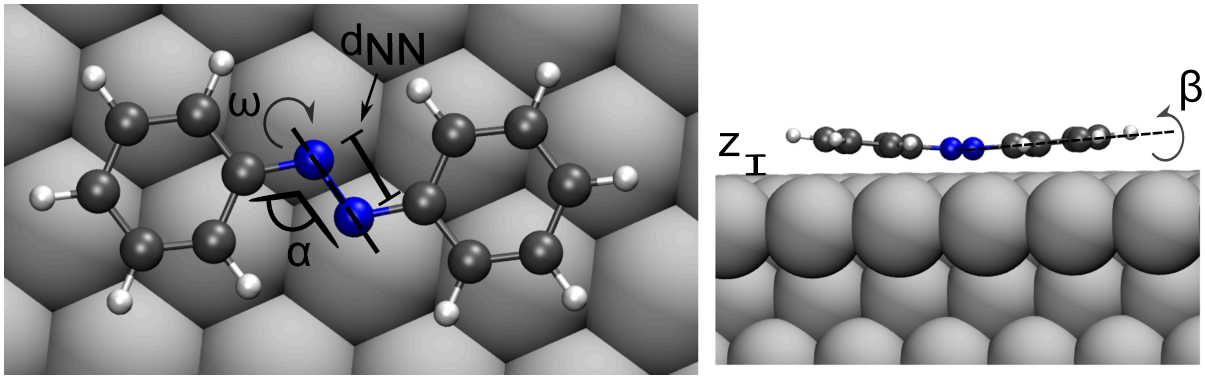

Figure 8.2: Definition of structural parameters of adsorbed Azobenzene. ω defines the central CNNC dihedral angle, $\alpha(\alpha'$,not shown) define the two CNN bending angles, d_{NN} is the distance between two N atoms, z is the vertical height of the central azo-bridge above the first (frozen) surface layer, and β (β', not shown) are torsional angles between the azo-bridge and the phenyl rings (NNCC), which describe the tilting motion of the phenyl groups.

Table 8.2: Structural parameters of the two minimum energy structures of Azobenzene in gas-phase and adsorbed on Ag(111) and Au(111) surfaces. Listed are the vertical distance z from the surface, the NN bond length in Å, and the central dihedral angle ω, as well as both CNN angles α and α'.

method		E-Ab				Z-Ab			
		z	d_{NN}	ω	α/α'	z	d_{NN}	ω	α
	Ab@	(Å)			(deg)	(Å)			(deg)
PBE+vdw(TS)	gas-phase	-	1.26	180	115/115	-	1.25	12	124/124
	Ag(111)	2.95	1.31	177	115/115	2.11	1.34	44	122/122
	Au(111)	3.25	1.30	180	115/115	2.45	1.29	19	124/126
PBE+vdw$^{\mathrm{surf}}$	Ag(111)	2.52	1.34	173	114/114	2.10	1.35	50	121/121
	Au(111)	2.98	1.30	179	115/115	2.38	1.29	19	124/126

8.2 Azobenzene on Ag(111) and Au(111)

McNellis *et al.* [197] have identified the optimal adsorption sites of Azobenzene and TBA on coinage metals as 1:1 coordination of the central azo-bridge over a bridge site of the surface. These sites are mainly determined by the DFT potential energy surface, because of a minimal additional PES corrugation induced by the dispersion correction. The modification of equilibrium molecular structures upon adsorption can be decisive for a possible molecular switching function. The most central parameters to characterize the structure of Azobenzene and TBA are described in Fig. 8.2, namely the central dihedral torsion ω, the two central bending angles α,α' of the phenyl rings, the azo bond length d_{NN}, the vertical adsorption height z, and the twisting angles β and β' of the two phenyl rings with respect to the surface. However, for Ab on Ag(111) or Au(111) our calculations show that in a low coverage adsorption geometry the phenyl rings maximize van-der-Waals interactions and optimally align to the surface.

The corresponding structural parameters for E and Z-Azobenzene are presented in table 8.2 with graphical representations in different views in Fig. 8.3. In general, the structural modification upon adsorption is larger for adsorption on Ag(111) than on Au(111) and larger

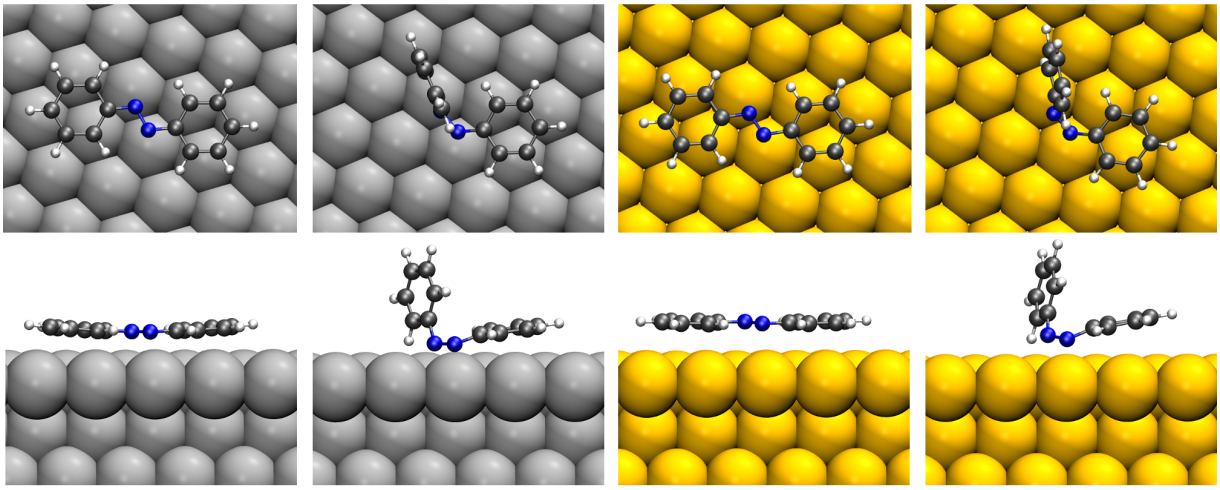

Figure 8.3: The DFT+vdw^{surf} calculated equilibrium ground-state geometries of E-Ab and Z-Ab on Ag(111) and Au(111) in different views from atop and from alongside the surface. From left to right: E-Ab and Z-Ab on Ag(111), E-Ab and Z-Ab on Au(111).

for Z-Ab than for E-Ab. This can be seen from changes in ω and d_{NN} due to adsorption, while the central bending angles α and α' are unchanged. Specifically the structure of Z-Ab is strongly modified due to adsorption to Ag(111). Vertical adsorption heights are systematically higher on Au than on Ag. On both surfaces, the adsorption energy of E-Ab is larger than for the Z-Ab isomer (see table 8.3). In all geometries the phenyl rings maximize the interaction area with the underlying surface. For this reason the Z-Ab geometries are found to be asymetric with one ring adsorbed to the surface and the other phenyl ring being in an upright position. This is in contrast to the symmetrically adsorbed Z-Ab geometry that was found by McNellis *et al.* [196]. The corresponding adsorption energies that are found in this work are only about 0.05 eV higher than this symmetric structure though, suggesting a very low energy penalty with respect to a total rigid azimuthal rotation of the molecule on the surface.

Analysis of the adsorption energies shows that almost all of the total interaction energy stems from the dispersion correction. This is significantly higher in the case of E-Ab than for Z-Ab. The corresponding contributions from the xc-functional are always repulsive for E-Ab and attractive for Z-Ab. This can be understood in terms of Pauli repulsion of the closed-shell E-Ab molecule with the underlying surface, as well as an energetic penalty due to the distortion of the gas-phase geometry. In the case of Z-Ab these repulsive effects are counteracted by a small attractive covalent-type contribution stemming from the interaction of the azo-bridge with the surface. This follows exactly the findings and interpretations of McNellis *et al.* [196, 197]. Due to the stronger stabilization of E-Ab compared to Z-Ab upon adsorption, the relative stabilities are changed, with the metastable Z-Ab isomer being less stable after adsorption then was the case in gas-phase (see table 8.4).

We now compare the differences between the two dispersion corrections. Ab geometries calculated with DFT+vdw^{surf} systematically exhibit a lower vertical adsorption height than the DFT+vdw(TS) structures. This is connected to an increase of the van-der-Waals contribution to the adsorption energy on Ag(111) and a decrease on Au(111). However, the total adsorption energy is only minimally affected due to a simultaneous increase of Pauli repulsion stemming from the reduced distance. Upon inclusion of the many-body collective response of the substrate all dispersion parameters change significantly. The C_6 coefficients are reduced to a third of the free atom value, but so are the polarizability and the van-der-Waals radius of the metal atom

Table 8.3: Adsorption energies of the two minimum energy structures of Azobenzene adsorbed on Ag(111) and Au(111) surfaces. Shown are the total adsorption energy and the two contributions from the dispersion correction and the DFT-GGA part. All energies are given in eV.

method		E-Ab			Z-Ab		
	Ab@	E_{ads}	E_{PBE}	E_{vdw}	E_{ads}	E_{PBE}	E_{vdw}
PBE+vdw(TS)	Ag(111)	1.65	-0.10	1.75	1.46	0.16	1.30
	Au(111)	1.61	-0.01	1.62	1.29	0.11	1.18
PBE+vdw$^{\text{surf}}$	Ag(111)	1.70	-0.30	2.00	1.45	0.06	1.39
	Au(111)	1.44	-0.10	1.54	1.23	0.16	1.07

Table 8.4: Relative stability of the Z-Ab isomer compared to the E-Ab isomer for Azobenzene in gas-phase and adsorbed to Ag(111) and Au(111). All energies are given in eV.

Ab@	E(E-Ab) - E(Z-Ab)	
	PBE+vdw(TS)	PBE+vdw$^{\text{surf}}$
gas-phase	0.58	0.58
Ag(111)	0.70	0.77
Au(111)	0.83	0.73

(see table 8.1). Therefore the above mentioned changes to the geometry can be understood by reduced equilibrium vdW distances, the corresponding minimal change in energy by an interplay of reduced distance, reduced interaction strength, and increased Pauli repulsion. Additionally, the reduced equilibrium interaction distance of the azo-bridge on the surface leads to a further weakening of the azo-bond as can be seen by larger NN bond distances. Specifically on Silver this is connected with further deviations from the gas-phase geometry in terms of the central dihedral angle ω.

In general, the structural deviations, with the exception of the vertical adsorption height, compared to DFT+vdw(TS) are not large, giving an *a posteriori* justification for the structural model devised by McNellis *et al.* [196]. However, the deviations to the experimentally observed adsorption heights are much larger upon inclusion of the substrate many-body response and screening effects. These differences will be further explained below. The differences between the adsorption energy of both conformers, E-Ab and Z-Ab, are increased on Ag(111) and reduced on Au(111), leading to a further relative de-stabilization and stabilization of Z-Ab on Ag(111) and Au(111), respectively (cf. Fig. 8.4).

The inspection of the minimum energy structures of the two conformers does not yet allow strong statements on the reactivity or implications regarding the photoisomerization. However, both structures can be found as stable minima of the potential energy surface, although Z-Ab on Ag(111) is strongly modified towards a possible rotational transition state structure. This shows that the most important prerequisite to molecular switching, namely the existence of two stable structures in the ground state, is still satisfied at 0 K. This is not the case for more strongly interacting surfaces such as Cu(111) [197].

As already detailed in chapter 7, introduction of bulky spacer groups at *meta* positions of the phenyl rings does reinstate the switching function for this TBA molecule on Au(111). The corresponding minimum energy structures at low coverage will be analyzed in the following section.

Table 8.5: Structural parameters of the two minimum energy structures of tetra-*tert*-butyl-Azobenzene (TBA) in gas-phase and adsorbed on Ag(111) and Au(111) surfaces. Shown are the vertical distance z from the surface, the NN bond length d_{NN} in Å, and the central dihedral angle ω, as well as both CNN angles α and α'. Geometry parameters are defined as for the Ab molecule in Fig. 8.2.

method		E-TBA				Z-TBA			
		z	d_{NN}	ω	α	z	d_{NN}	ω	α
		(Å)		(deg)		(Å)		(deg)	
PBE+vdw(TS)	gas-phase	-	1.30	179	115/115	-	1.29	8.3	120/121
	Ag(111)	3.07	1.30	169	115/115	2.09	1.33	28.7	120/122
	Au(111)	3.09	1.30	169	115/116	2.38	1.29	8.2	123/124
PBE+vdw$^{\mathrm{surf}}$	Ag(111)	2.35	1.34	155	114/114	2.07	1.33	29.7	120/122
	Au(111)	2.67	1.30	166	114/118	2.31	1.29	8.7	122/124

8.3 TBA on Ag(111) and Au(111)

For Ab adsorbed to Ag(111) and Au(111) the adsorption height was dictated by the vdW interactions of the phenyl groups in the case of E-Ab and the optimal adsorption height of the azo-bridge in the case of Z-Ab. Introducing four *tert*-butyl-legs, the adsorption height of the phenyl rings is increased and the corresponding adsorption of E-TBA is now given by a balance of attractive vdW contributions from the phenyl rings and from the azo-bridge, as well as the additional repulsive contributions from the bulky side groups. Investigating the central structural parameters in table 8.5, one finds that the adsorption height of the azo-bridge of E-TBA and Z-TBA on both surfaces is almost unchanged compared to the unsubstituted Ab. This has been identified by McNellis *et al.* [27] as a failed attempt to a geometric decoupling of the central photochromic moiety. The general structural changes upon adsorption such as increased d_{NN} and modified dihedral angle ω can also be seen in the case of TBA. Even though, the adsorption height of the azo-bridge is not at all affected by the additional side groups, the structural deviations from the gas-phase TBA structures are less pronounced as was the case in Azobenzene. Specifically the Z-TBA structure on Au(111) seems to be less affected by adsorption, compared to plain Ab, in terms of unchanged d_{NN} and unchanged ω compared to the gas-phase (see Fig. 8.2 for definition and Figs. 8.4 and 8.5 for TBA geometries).

The corresponding adsorption energetics suggest very similar trends as in Ab adsorption (see table 8.6), although at much larger absolute adsorption energies. This is predominantly due to the larger vdW contributions from the additional side groups. However, this is accompanied by strongly increased repulsive Pauli contributions stemming from the closed-shell nature of the molecule. In summary, both factors lead to adsorption energies that are systematically increased by about 1 eV compared to Ab. The size and large number of degrees of freedom of this molecule also suggest a large influence of vibrational zero point energy (ZPE) contributions to the adsorption energy and the relative isomer stability. Corresponding calculations suggest that this effect is of the order of about 0.1 eV. The effect translates to the relative stabilities by Z-TBA being de-stabilized relative to E-TBA upon adsorption (see table 8.7), similar as was the case for adsorbed Ab.

Compared to experimental adsorption energies obtained from temperature programmed desorption (TPD) measurements the computed adsorption energies from DFT+vdw(TS) strongly overshoot these numbers at low coverage for both Ab and TBA (E-Ab@Ag(111): 1.08±0.05 eV,

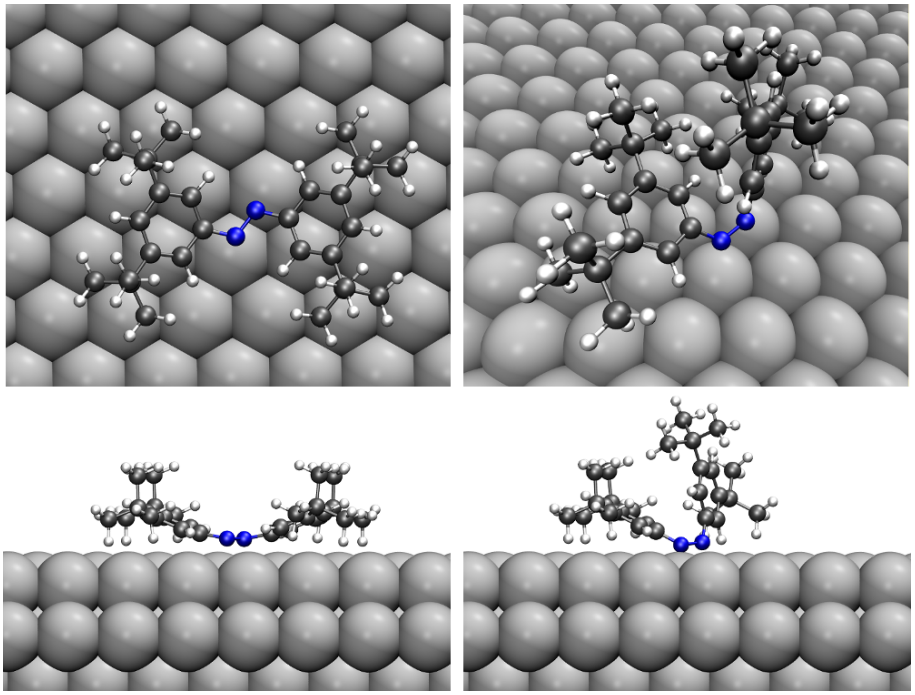

Figure 8.4: Calculated equilibrium ground-state geometries of E-TBA and Z-TBA on Ag(111) in different views from atop and alongside the surface, calculated with vdw^{surf}.

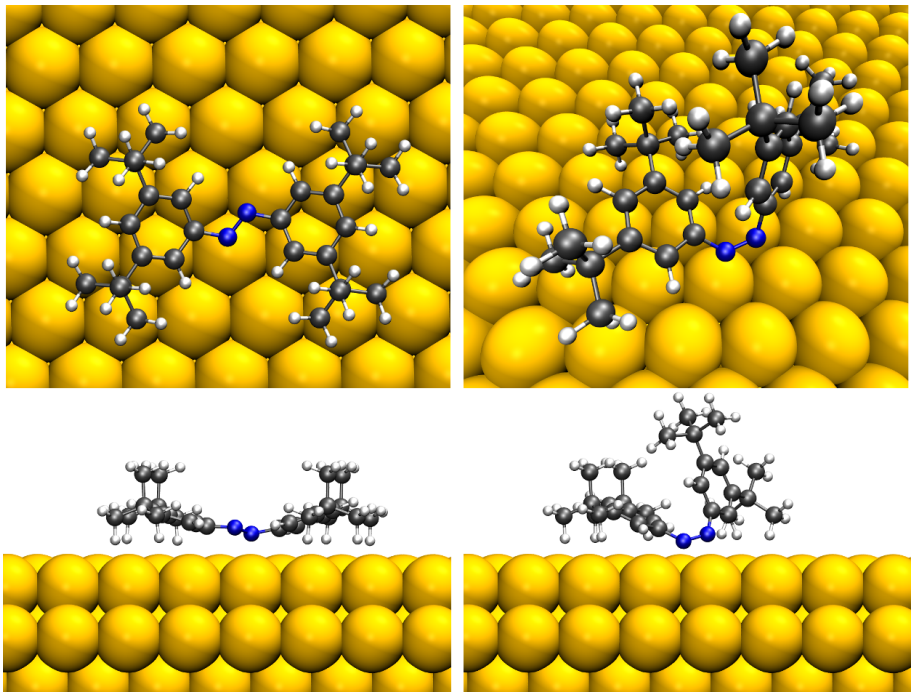

Figure 8.5: Calculated equilibrium ground-state geometries of E-TBA and Z-TBA on Au(111) in different views from atop and from alongside the surface, calculated with vdw^{surf}.

Table 8.6: Adsorption energies of the two minimum energy structures of TBA adsorbed on Ag(111) and Au(111) surfaces. The total adsorption energy is the sum of the vdW contribution and the DFT-GGA contribution. In addition, the energetic correction due to the vibrational zero point energy is given. All energies are given in eV.

method		E-TBA				Z-TBA			
		E_{ads}	E_{PBE}	E_{vdw}	E_{ZPE}	E_{ads}	E_{PBE}	E_{vdw}	E_{ZPE}
PBE+vdw(TS)	Ag(111)	2.66	-0.46	3.12	0.09	2.47	0.06	2.41	-0.01
	Au(111)	2.65	-0.37	3.02	0.13	2.41	0.20	2.21	0.11
PBE+vdw$^{\text{surf}}$	Ag(111)	2.28	-0.20	2.48	-	2.16	0.04	2.12	-
	Au(111)	2.22	-0.44	2.66	-	2.08	0.17	1.91	-

Table 8.7: Relative stability of the Z-TBA isomer compared to the E-TBA isomer for TBA in gas-phase and adsorbed to Ag(111) and Au(111). Energies with and without zero point energy correction are shown. All energies are given in eV.

	E(E-TBA) - E(Z-TBA)			
	PBE+vdw(TS)		PBE+vdw$^{\text{surf}}$	
Ab@	ΔE	$\Delta E + E_{\text{ZPE}}$	ΔE	$\Delta E + E_{\text{ZPE}}$
gas-phase	0.36	0.27	0.36	0.27
Ag(111)	0.54	0.55	0.47	-
Au(111)	0.59	0.52	0.49	-

E-TBA@Ag(111): 1.69±0.15 eV) [198, 199]. Upon inclusion of the screening effects within the substrate in the vdw$^{\text{surf}}$ scheme, the adsorption energies are significantly reduced up to about 15% for all structures on both surfaces. Similar as in Ab adsorption, the structures show strongly reduced vdW interaction at much reduced vertical adsorption height and therefore also increased Pauli repulsion. However, the vertical adsorption height as predicted by the DFT+vdw(TS) scheme was almost identical for Ab and TBA adsorbed to Ag(111) and TBA on Au(111), namely about 3 Å. When applying the DFT+vdw$^{\text{surf}}$ scheme one finds very different vertical adsorption heights for TBA on both surfaces (cf. table 8.5) differing by about 0.3 Å. The bent structure that is induced by the bulky spacer legs leads to a stronger covalent bonding character (d_{NN} and ω deviate more from the gas-phase) compared to Ab adsorption. This can also be seen from the fact that the repulsive interaction from the density functional part is not strongly increased and for adsorption on Ag(111) is even reduced. Furthermore, the difference between the adsorption heights of E-Ab and E-TBA on Ag(111) differs only by about 0.2 Å.

Whereas the results obtained by DFT+vdw(TS) give no clear geometric sign of 'decoupling' due to the additional bulky spacer groups [27], DFT+vdw$^{\text{surf}}$ suggests geometric and energetic effects, which can be seen as supporting the coupling to the surface but also as weakening it. Whereas the vertical adsorption height is reduced compared to pure Ab and the absolute adsorption energy is increased, the central geometric parameters deviate less from the gas-phase reference than was the case for underivatized Azobenzene.

8.4 Conclusion to Chapter 8

In this chapter, the main modelling approach of this thesis has been presented and the structural changes upon adsorption of Azobenzene and TBA have been investigated. Employing the very recent vdW correction approach of Ruiz *et al.* [85], the adsorption heights and adsorption energies are significantly reduced compared to dispersion correction approaches that are based on free atom reference data. However, the retrieved adsorption energies still overestimate recent experimental data by about 30%. These remaining deviations might still be due to the crude description of exchange and correlation at short distances that is given by the semi-local treatment or might even stem from a more fundamental disagreement between the simulations and the experimental reference. Some concern has recently been put forward that current models that are used to analyse TPD data yield significantly overestimated adsorption energies compared to heats of adsorption from adsorption calorimetry measurements [85, 264, 265].

Another concern is based on the underestimation of vertical adsorption heights when compared to measurements performed with x-ray standing wave experiments [266]. The experimentally measured vertical height of TBA on Ag(111) is 3.21±0.05Å [27], which is, as was the case for Azobenzene on Ag(111), much higher than the minimum energy geometry that is found employing the DFT+vdw$^{\text{surf}}$ scheme. Including the effect of the collective substrate response into the dispersion correction increases the deviations between simulation and experiment for the molecules that have been considered here, but proved to give an accurate account of the adsorption height for other systems, such as PTCDA on Ag(111) [85]. In contrast, the simple 1-layer reduced interaction model employed by Mercurio *et al.* [198] suggests a lower adsorption energy and a higher vertical height of the molecule and therein agrees with the experimental x-ray standing wave analysis of that time. These somewhat contradictory observations force us to postpone strong conclusions on the accuracy of the structural modelling approach to the following chapter, in which a detailed analysis of the experimental and computational results will be given. On the general effect of the collective many-body substrate response, no simple answer can be given whether inclusion leads to higher or lower adsorption energies. This is due to the influence of different bonding contributions in systems such as adsorbed benzene (almost pure vdW), adsorbed PTCDA (strong covalent bonding contribution), or adsorbed Azobenzene (mixed vdW and covalent contributions).

The current knowledge of the structure and energetics of the adsorbed Azobenzene species on coinage metals is also not sufficient to conclude on the photoisomerization ability or in general on the reactivity and thermal stability of the two conformers. A detailed investigation of thermal stability and possible transition pathways will be conducted in chapter 10 of this thesis.

9 Theory and Experiment on the Test Stand: Azobenzene on Ag(111)

This chapter presents the *ab-initio* part of a collaborative work together with the Peter-Grünberg institute at the research center Jülich (group of Prof. Tautz), the Free University Berlin (group of Prof. Tegeder), and the Fritz-Haber institute of the Max-Planck society (group of Dr. Tkatchenko). This work was recently published in *Physical Review B* [267] and *Frontiers in Physics* [268]. The here presented detailed comparison of x-ray standing wave experimental data with Density-Functional theory calculations supports the validity and the predictive power of the latter.

9.1 Introduction

Precise experimentally determined structures of large organic adsorbates are indispensable for the detailed understanding of their wide-ranged functionalities, but also for the benchmarking of *ab-initio* electronic structure calculations [269, 270].

As already mentioned in the previous chapter, vdW interactions are substantial and critically influence the adsorption geometry [271–274] of large molecules with polarizable π-electron systems. Efficient semi-empirical dispersion correction schemes are particularly promising [275] and are the method of choice in this thesis [77, 85]. Nevertheless, the approximate nature of such approaches necessitates reliable experimental benchmark structures. This holds in particular for adsorption at metal surfaces, where the non-local collective substrate response (many-body electronic screening) requires advancements beyond the traditional pairwise summation of vdW interactions in these schemes [85, 198]. The dispersion correction approach by Ruiz *et al.*, that is applied in the present and the previous chapter 8 accounts for such collective response effects and reduces the error in adsorption height to approximately 0.1 Å for a variety of molecules [81, 85, 276, 277]. However in the case of Azobenzene and TBA the deviations from experiment further increase compared to the earlier dispersion correction schemes based on free atomic reference data [198].

In this chapter a re-analysis of the experimental data of Mercurio *et al.* [198] will be presented and compared to *ab-initio* calculations that account for lateral interactions in high coverage situations. This leads to a complete reconciliation of the above mentioned contradiction and proves an accurate geometrical description for Ab systems on coinage metals. However, at this level of accuracy, a new issue arises: Experiments for structure determination are often carried out close to room temperature, while in dispersion-corrected DFT treatments the ground state (at 0 K) is normally calculated. The complex internal vibrational structure of large organic adsorbates which may sensitively influence the experimental time-averaged geometry is thus neglected.

Inclusion of such thermal expansion effects into dispersion-corrected DFT calculations is indeed necessary to reach quantitative agreement between experiment and theory, as will be shown in section 9.5 of this chapter. Hence, benchmarking at the current level of sophistication

requires the careful analysis of finite-temperature effects. Otherwise misleading conclusions with respect to the DFT+vdw accuracy might be obtained.

9.2 Summary on Normal Incidence X-Ray Standing Wave Results

The experiments serving as benchmarks have been carried out on Azobenzene adsorbed at Ag(111), using the normal incidence x-ray standing wave technique (NIXSW). NIXSW is an established method to determine the adsorption geometry (in particular adsorption heights) of large organic adsorbates [266, 278]. The Ab/Ag(111) system has been studied by NIXSW before and the results were compared to the DFT+vdw(TS) approach to conclude on the importance of (then untreated) electronic screening effects [198]. The main experimental details underlying the results presented here can be found in the PhD thesis of Giuseppe Mercurio [279] and Refs. [198, 267, 268]. The measurements have been performed in ultra-high vacuum at 210 K on Ab on Ag(111) coverages close to one monolayer. From the NIXSW signal, coherent positions P_c and coherent fractions F_c of the atoms can be retrieved. P_c defines the average adsorption height of a species, while F_c quantifies the corresponding height distribution. A coherent fraction of 1 means that all photoemitters of a certain species have precisely the same adsorption height above the relevant family of Bragg planes, while a coherent fraction of 0 indicates a homogeneous distribution of the photoemitters throughout the Bragg spacing. In general, $F_c < 1$ due to unavoidable structural disorder [280], adsorbate and substrate thermal vibrations. However, the coherent fractions of different chemical species also contain information about the internal geometry of the adsorbate. The NIXSW analysis underlying the here presented results uses this information by including differences between the F_c of different species. This is a major advancement compared to the previous analysis, where the F_c have not been taken into account [198].

In the present case of Ab/Ag(111), NIXSW provides coherent positions $P_c^{\mathrm{C}} = 0.27 \pm 0.02$, $P_c^{\mathrm{N}} = 0.26 \pm 0.02$ and coherent fractions $F_c^{\mathrm{C}} = 0.34 \pm 0.03$, $F_c^{\mathrm{N}} = 0.48 \pm 0.12$. The general procedure to determine the structure parameters (P_c, F_c) and their error bars is described in Mercurio *et al.* [280]. Details on the analysis can be found in Mercurio [279]. While the respective coherent positions are identical within the errors, the coherent fraction of C is 29% smaller than the one of N. This difference can only be caused by an internal structural distortion of Ab.

Two internal degrees of freedom are considered and varied in order to model (P_c, F_c): the torsion angle ω and the phenyl ring twist angle β (see Fig. 8.2 for a definition), defined as dihedral angles CNNC and CCNN, respectively. It is impossible to explain the ratio F_c^C/F_c^N in a model in which ω is the only internal degree of freedom of the molecule, because any distortion along ω that would lead to a decrease of F_c^{C} would at the same time result in an increase of the coherent position P_c^{C} which is related to the average adsorption height of the carbon atoms. Hence, an additional degree of freedom must be considered to explain the measured NIXSW structure parameters. A plausible choice is the dihedral angle β, because for small angles ω, a finite β would broaden the carbon distribution essentially without changing the average carbon height. Note that this broadening could in principle be due to a *static* distortion of the molecule and/or due to its vibrational *dynamics*. However, for a purely dynamical reduction of the average coherent fraction F_c^{C} by 29 % an unreasonably large C vibrational amplitude of the order ± 0.30 Å (with fixed N atoms) would be required. Therefore, it can be assumed that the major effect behind the different coherent fractions is due to a static distortion upon adsorption.

Requiring $F_c^{\mathrm{C}_i} = F_c^{\mathrm{N}_i}$ and constructing the molecular geometry such that the measured values for P_c^{C}, P_c^{N}, F_c^{C}, F_c^{N} are obtained, an adsorption geometry with z of 2.97 ± 0.05 Å, a tilt

Table 9.1: Summary of experimental and computational results for the central structural parameters of Azobenzene adsorbed to a Ag(111) surface. The structural parameters are defined in Fig. 8.2. Phase LC refers to the low coverage adsorption limit. Phase A refers to the indermediate coverage limit at 1.17 molecules per nm^2 calculated with and without anharmonic finite-temperature correction.

		z (Å)	ω (°)	β (°)
phase LC	DFT+vdw(TS)	2.95	178.2	−0.6
($T = 0$ K)	DFT+vdW^{surf}	2.61	175.5	−2.0
phase A	DFT+vdw(TS)	3.26	172.5	18.6
($T = 0$ K)	DFT+vdW^{surf}	2.81	168.3	15.4
phase A	DFT+vdw(TS)	3.23	171.2	17.3
($T = 210$ K)	DFT+vdW^{surf}	2.98	171.0	17.7
experiment	NIXSW	2.97	180.7	17.7
($T = 210$ K)		±0.05	(+2.3/−2.2)	(+2.4/−2.7)

angle ω of 180.7°, and a torsion angle β of 17.7° can be found (cf. table 9.1).

This structure is far from the low-coverage situation that was analysed in chapter 8 of this thesis. A possible rationalization for this is a strong effect on the structure due to lateral interactons between adsorbate molecules at the high coverage situation in experiment; this will be analyzed in the following.

9.3 Computational Details

Coverage Dependent DFT+vdw Calculations

The basic computational setup presented in chapter 8.1 has also been employed here.

A variety of different surface unit-cells with a varying number of molecules was used to simulate different Ab coverages. Table 9.2 shows the cells taken into consideration, as well as the different **k**-grids used [126]. The **k** point and energy cutoff settings were chosen to guarantee convergence with respect to those parameters.

The adsorption energies of Ab in each cell and the adsorption energies per surface area calculated with DFT+vdw(TS) and DFT+vdW^{surf} are reported in table 9.2. The corresponding geometry parameters are reported in table 9.3. For a definition of the dihedral angles ω and β, see Fig. 8.2. Since the DFT-calculated high-coverage geometries have nonplanar phenyl rings (for $\omega \neq 0°$), two dihedral angles β' and β'' are defined as CCNN and NNCC, where one C is bound to the azo-bridge and the other one is the neighbouring C in the corresponding phenyl ring. Additionally, the average between both dihedral angles is given as β.

Table 9.2: List of cells used to calculate different coverages of adsorbed Ab overlayers on the Ag(111) surface. n: number of Ab molecules per cell; k-grid: Monkhorst-Pack grid [126]; area/Ab: surface area per Ab molecule; E_{ads} (DFT+vdw(TS)): adsorption energy *per molecule* and adsorption energy *per surface area* calculated with DFT+vdw(TS); E_{ads} (DFT+vdw$^{\text{surf}}$): adsorption energy *per molecule* and adsorption energy per surface area calculated with DFT+vdW$^{\text{surf}}$.

phase	cell	n	k-grid	area/Ab	E_{ads} (DFT+vdw(TS))		E_{ads} (DFT+vdw$^{\text{surf}}$)	
				(Å^2)	(eV)	(eV/nm^2)	(eV)	(eV/nm^2)
LC	(6×7)	1	(4×4×1)	359.6	1.67	0.47	1.72	0.48
	(5×6)	1	(4×6×1)	256.8	1.68	0.65	1.71	0.67
	(3×6)	1	(6×4×1)	154.1	1.70	1.10	1.76	1.14
	(3×5)	1	(8×4×1)	128.4	1.74	1.35	1.76	1.37
A	(2×5)	1	(8×4×1)	85.6	1.46	1.71	1.33	1.55
	(5×5)	3	(4×4×1)	71.3	1.26	1.76	1.07	1.50
	(3×5)	2	(8×4×1)	64.2	1.16	1.80	0.94	1.47
	(4×5)	3	(6×4×1)	57.1	1.38	2.43	1.20	2.10
B	(5×5)	4	(4×4×1)	53.5	1.39	2.60	1.21	2.25
	(2×5)	2	(8×4×1)	42.8	0.69	1.60	0.54	1.27

Table 9.3: Geometry parameters of Ab calculated with DFT+vdw(TS) and DFT+vdW^{surf} for each cell. z: average adsorption height of N atoms above the surface Bragg plane; z_{N1}-z_{N2}: difference of the adsorption heights of the two N atoms with respect to the surface; ω, β, β'/β'': dihedral angles; In case of cells with more than one AB molecule per cell, the listed geometry parameters refer to the average over all molecules in the cell.

			vdw(TS)					vdw^{surf}				
cell	area/Ab	Ab/area	z	z_{N1}-z_{N2}	ω	β	β'/β''	z	z_{N1}-z_{N2}	ω	β	β'/β''
	(Å^2)	(nm^{-2})	(Å)	(Å)	(deg)	(deg)	(deg)	(Å)	(Å)	(deg)	(deg)	(deg)
$(6\times7)_1$	359.6	0.28	2.95	0.00	178.2	-0.6	-0.4/-0.9	2.61	0.02	175.5	-2.0	-1.7/-2.3
$(5\times6)_1$	256.8	0.39	2.96	0.00	177.2	-1.2	-1.2/-1.1	2.63	0.02	175.7	-2.1	-2.0/-2.2
$(3\times6)_1$	154.1	0.65	2.97	0.00	179.0	-0.7	-0.2/-1.2	2.58	0.01	175.0	-1.8	-1.5/-2.2
$(3\times5)_1$	128.4	0.78	2.95	0.01	177.0	-1.2	-1.3/-1.1	2.61	0.02	175.3	-2.4	-2.2/-2.5
$(2\times5)_1$	85.6	1.17	3.26	0.00	172.5	18.6	16.6/20.6	2.81	0.00	168.3	15.4	13.0/17.8
$(5\times5)_3$	71.3	1.40	3.56	0.14	167.2	32.4	28.8/36.0	3.47	0.04	168.7	34.2	31.1/37.3
$(3\times5)_2$	64.2	1.56	3.52	0.21	164.2	39.8	35.2/44.3	3.56	0.23	166.3	41.7	37.7/45.8
$(4\times5)_3$	57.1	1.75	4.40	1.06	186.8	-26.2	-24.6/-27.8	4.32	1.14	186.8	-25.8	-24.2/-27.4
$(5\times5)_4$	53.5	1.87	4.48	1.11	185.1	-20.4	-19.0/-21.7	4.39	1.07	185.1	-20.2	-18.9/-21.6
$(2\times5)_2$	42.8	2.34	5.47	1.42	180.7	-0.4	-0.3/-0.6	5.39	1.42	180.7	-0.9	-0.8/-1.0

Anharmonic Correction to the Ab Geometry

To determine the average Ab geometry at 210 K in the $(2\times5)_1$ cell ($\mathbf{R}_{210\mathrm{K}}$) the following steps were taken. Note that all DFT calculations in the procedure described below were performed with both PBE+vdw(TS) and PBE+vdW$^{\mathrm{surf}}$.

Step 1: Normal modes were calculated for the DFT-calculated 0 K geometry of Ab/Ag(111) in the $(2\times5)_1$ cell that is given by the 24×3-dimensional position vector $\mathbf{R}_0$, spanned by the 24 atoms and 3 directions in space. The following steps 2 to 5 were carried out for each harmonic mode with frequency ν_i $(=1,\ldots,72)$ and displacement eigenvector $\mathbf{e}_i = \left(\frac{1}{\sqrt{m_1}}\tilde{\mathbf{e}}_i^1,\ldots,\frac{1}{\sqrt{m_{24}}}\tilde{\mathbf{e}}_i^{24}\right)$. $\tilde{\mathbf{e}}_i^I$ $(I=1,\ldots,24)$ are three-dimensional displacement vectors of the individual Ab atoms, mass-weighted by $\sqrt{m_I}$ with the corresponding atomic masses m_I, such that the 72 vectors $(\tilde{\mathbf{e}}_i^1,\ldots,\tilde{\mathbf{e}}_i^{24})$ form an orthonormal set.

Step 2: $\mathbf{R}_0$ was displaced along $\mathbf{e}_i$ and $-\mathbf{e}_i$ by the average mode amplitude $\langle \mathrm{A}_i\rangle$ at $T=210$ K:

$$\langle \mathrm{A}_i\rangle = \frac{\sqrt{2k_{\mathrm{B}}T}}{\nu_i}, \tag{9.1}$$

with k_{B} equal to the Boltzmann constant, providing the two respective geometries $\mathbf{R}_0+\langle \mathrm{A}_i\rangle\mathbf{e}_i$ and $\mathbf{R}_0-\langle \mathrm{A}_i\rangle\mathbf{e}_i$. Analogously, two additional Ab geometries, $\mathbf{R}_0+\frac{\langle \mathrm{A}_i\rangle}{2}\mathbf{e}_i$ and $\mathbf{R}_0-\frac{\langle \mathrm{A}_i\rangle}{2}\mathbf{e}_i$, were constructed.

Step 3: For each of the above five Ab geometries $\mathbf{R}_0+\Delta\mathbf{R}_i$ (with $\Delta\mathbf{R}_i = -\langle \mathrm{A}_i\rangle\mathbf{e}_i, -\frac{\langle \mathrm{A}_i\rangle}{2}\mathbf{e}_i$, $0, +\frac{\langle \mathrm{A}_i\rangle}{2}\mathbf{e}_i, +\langle \mathrm{A}_i\rangle\mathbf{e}_i$) the corresponding DFT energy $E^{\mathrm{DFT}}(\mathbf{R}_0+\Delta\mathbf{R}_i)$ was calculated.

Step 4: The resulting five data points $E^{\mathrm{DFT}}(\mathbf{R}_0+\Delta\mathbf{R}_i)$ were fitted with a Morse potential [88]:

$$V_i(r_i) = D_i\left[1-\exp\left(-a_i r_i\right)\right]^2, \tag{9.2}$$

where r_i is the (mass-weighted) displacement from the equilibrium, D_i and a_i describe respectively the depth of the potential and its curvature at the minimum. Going one step beyond the harmonic regime, the vibrational modes are thus represented by an uncoupled set of anharmonic potentials $V_i(r_i)$. Fig. 9.1 shows an example of such an anharmonic potential for one selected mode.

Step 5: The equation of motion in each Morse potential $V_i(r_i)$ was integrated over one period T_i. For energies E smaller than D_i, the equation of motion of the Morse potential $V_i(r_i)$ is [88]:

$$a_i r_i(t) = \log\left[\frac{1-\cos\theta\cos\left(2\pi\nu_i t\sin\theta\right)}{\sin^2\theta}\right], \tag{9.3}$$

where θ is the phase angle determined by the initial conditions (with $\cos^2\theta = E/D_i$), t is the time variable and $E=k_{\mathrm{B}}T=18$ meV at $T=210$ K. As a result of the integration one obtains $\langle r_i\rangle$, which deviates the more from 0 the stronger the anharmonicity is. $\mathbf{R}_0+\langle r_i\rangle\mathbf{e}_i$ would be the time-averaged Ab geometry at 210 K if only mode i were active.

Step 6: The average Ab geometry at 210 K ($\mathbf{R}_{210\mathrm{K}}$) with all possible active modes was calculated by adding all time-averaged displacements to the 0 K geometry:

$$\mathbf{R}_{210\mathrm{K}} = \mathbf{R}_0 + \sum_{i=1}^{72}\langle r_i\rangle\mathbf{e}_i. \tag{9.4}$$

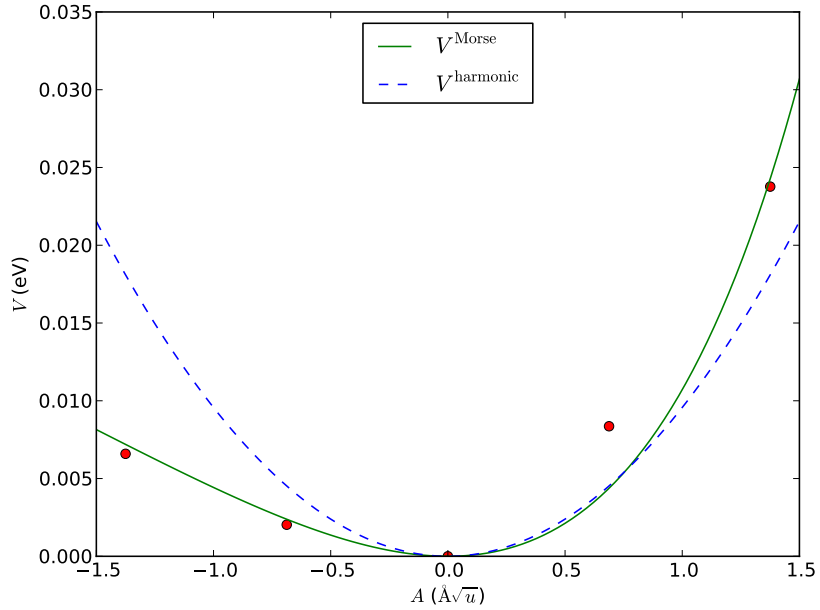

Figure 9.1: Example of a harmonic potential (blue dashed line) and an anharmonic fit (green line) to explicit DFT data (red squares) of geometries distorted along the harmonic eigenmode no. 4 of the Azobenzene structure in a (2x5) Ag(111) cell calculated with DFT+vdw$^{\mathrm{surf}}$.

Only modes with energies below 100 meV contribute significantly to the sum in equation (9.4). $\mathbf{R}_{210\mathrm{K}}$ is the finite-temperature DFT geometry that can be compared to the NIXSW-determined experimental geometry. The corresponding geometry parameters are reported in table 9.3.

9.4 Coverage Dependence of the Adsorption Geometry

A torsion angle β of more than 17° is difficult to rationalize for a single molecule adsorbed on the surface without neighbours. Yet, all previous calculations have been carried out for single molecules (while the above mentioned experiment is performed on a condensed layer). One therefore needs to analyze the coverage- and packing-dependence of the adsorption geometry of Ab/Ag(111) theoretically. The optimized adsorption geometries for a range of different surface unit-cells are determined (see table 9.3), with one Ab per (6×7) cell representing the low-coverage (LC, far left point in Fig. 9.2) limit and two Ab molecules in a (2×5) cell leading to the highest considered molecular surface density.

The PBE+vdW$^{\mathrm{surf}}$ results compiled in Fig. 9.2 show that the adsorption geometry indeed varies substantially with increasing molecular surface density. While in the LC limit the adsorbed molecule is essentially flat, the tilt and torsion angles ω and β increasingly change with the packing density. As a consequence of the internal distortion of the molecule, the vertical adsorption height of the azo-bridge also increases; this tendency continues beyond the critical coverage of 1.56 Ab $\cdot$ nm^{-2} at which the now nearly upright molecules start to flatten out again within the increasingly dense overlayer. The flattening of the upright molecule implies an asymmetric position of the azo-bridge, i.e. different vertical adsorption heights of the two nitrogen atoms, with a concomitant lifting from the surface (cf. table 9.3).

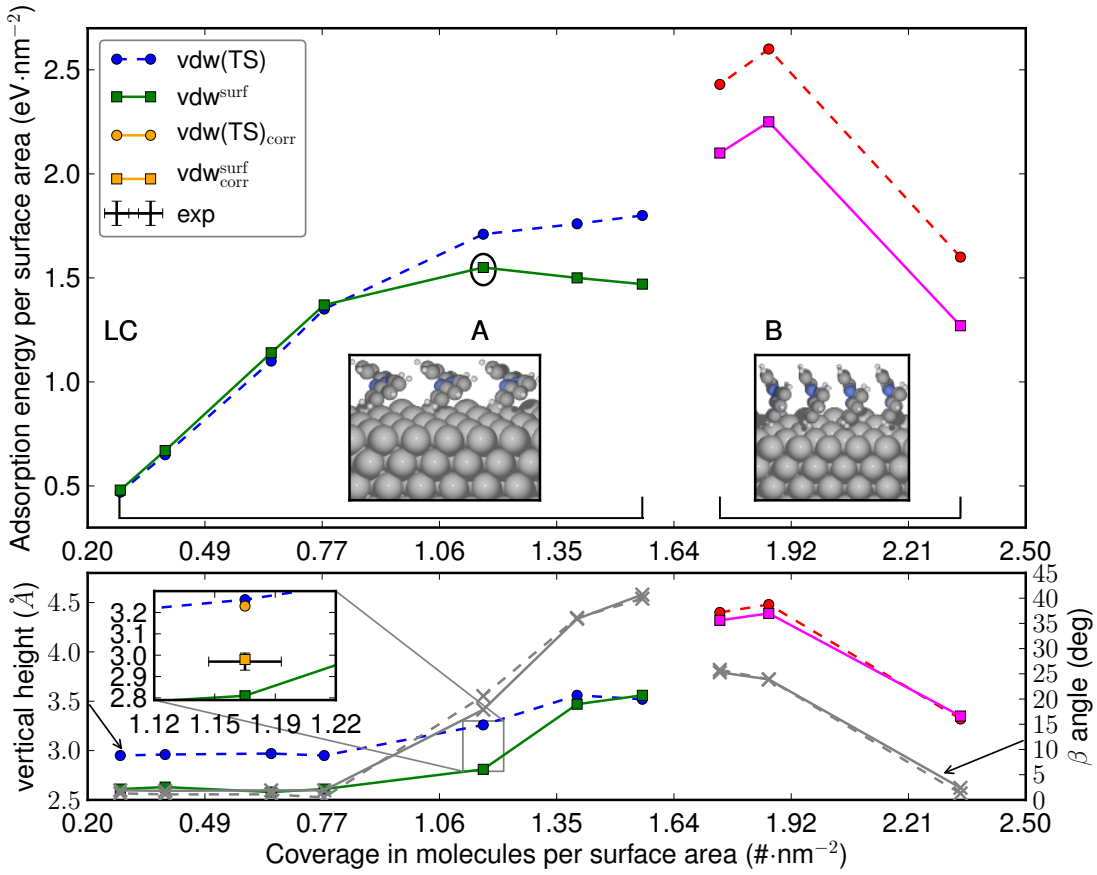

Figure 9.2: (top) Adsorption energy per surface area (in eV) for Azobenzene adsorbed to Ag(111) at different surface coverages, given in molecules per nm^2. These energies have been calculated with DFT+vdw(TS) (green, purple) and DFT+vdw$^{\text{surf}}$ (blue, red). The two sets of curves, green / blue and red / purple mark different phases, A and B, of adsorbate structure. These differences are depicted in two insets. (bottom) Vertical height (in Å) and β angle (in deg) as function of the surface coverage. An inset shows a zoom on the coverage of 1.17 molecules per nm^2: The vertical height is given for the two dispersion corrected methods and the corresponding two anharmonically corrected structures at 210 K.

With most of the adsorption energy of the flat Ab molecule in the LC limit originating from dispersive interactions with the substrate, the binding energy *per molecule* naturally decreases in the distorted high density structures (cf. table 9.2). Due to the denser packing, the adsorption energy *per surface area* E_{ads}/area nevertheless increases and reaches a maximum at 1.17 Ab $\cdot$ nm^{-2}. The intermolecular vdW interactions in the high density phases further increase E_{ads}/area, which reaches a second maximum at a density of 1.87 Ab $\cdot$ nm^{-2}. The calculations therefore predict the existence of two optimum packing densities, a phase A (in Fig. 9.2 indicated by a circle) at 1.17 Ab $\cdot$ nm^{-2} and a phase B at 1.87 Ab $\cdot$ nm^{-2}. Qualitatively similar findings are obtained with the DFT+vdw(TS) scheme. In detail, however, there are decisive differences. For example, vdw(TS) fails to predict the maximum of E_{ads}/area corresponding to phase A.

To decide which structure — if any of the above — corresponds to the experimental one, the calculated ground-state geometries are compared to experiment (table 9.1). Phase LC can be ruled out, both because of its small torsion angle, and because of the sample preparation

procedure which yields dense layers. The average adsorption height of N atoms in phase B is 4.39 Å, which is inconsistent with the experimental value of 2.97 Å or — modulo a Bragg spacing — 5.32 Å. It can therefore be concluded that the NIXSW experiment has been carried out on a structure similar to phase A. This conclusion is consistent with the expectation that neither of the two dispersion-correction schemes will work reliably at the packing density of phase B that is close to the one of the molecular crystal. There even the vdW$^{\text{surf}}$ scheme will overestimate lateral interactions [281], because higher-order many-body terms between adsorbates are neglected [282]. This neglect will contribute to a spurious stabilization of phase B in the here employed DFT+vdW$^{\text{surf}}$ calculations.

In table 9.1 the geometry parameters of phase A are summarized. At 0 K the vdW$^{\text{surf}}$ scheme yields a height of $z = 2.81$ Å at tilt $\omega = 168.3°$ and torsion $\beta = 15.4°$, while the vdw(TS) scheme predicts $z = 3.26$ Å, $\omega = 172.5°$, and $\beta = 18.6°$. With regard to β, this corresponds to a good agreement of the ground-state calculation with the experimental result ($\beta = 17.7°$). In contrast, the calculated adsorption heights of the azo-bridge are 0.16 Å too small for vdW$^{\text{surf}}$ and 0.29 Å too large for vdw(TS). It is clear from chapter 8 that the inclusion of collective substrate response has a large impact on the predicted adsorption height z. The inclusion improves the description of the vertical height, although the height is still not perfect, and the calculated ω is too small.

These remaining differences can be understood in terms of the different descriptions. While the *ab-initio* calculations are done at the absolute ground state (0 K), the experiment is done at a significant temperature of 210 K. The corresponding thermal energy will modify the aparent equilibrium structure if low lying vibrational modes of the system show a large anharmonicity. In the following this effect will be investigated using the geometry correction approach explained in section 9.3.

9.5 Finite Temperature Effects on the Adsorption Geometry

The predictions of the DFT+vdW$^{\text{surf}}$ theory can be substantially improved towards a quantitative agreement with experiment, if the effect of finite temperature is taken into account. In particular, as mentioned above, the anharmonic contributions to the vibrational motion may modify the time-averaged geometries that are experimentally observable [266]. This can be demonstrated by explicitly calculating the harmonic vibrations for the adsorbed Ab molecule at the optimum density of 1.17 Ab $\cdot$ nm^{-2} (Phase A), both at DFT+vdW$^{\text{surf}}$ and DFT+vdw(TS) levels. The anharmonic regimes of these modes are then mapped at energies that are accessible at the experimentally employed 210 K, by distorting the molecule along the corresponding vibrational eigenvectors. To this DFT data, a Morse potential [88] is fitted for every harmonic mode. The analytically integrated motion in the Morse potentials yields the shifts of the average positions at 210 K relative to the harmonic minima. Summing these shifts over all vibrational modes, one finally arrives at an anharmonically corrected geometry for the adsorbed Ab molecule. Note that the vibrational dynamics of the substrate is taken into account in the fitting of the photoelectron yield profiles of the NIXSW experiment at the level of Debye-Waller theory [283], with parameters from Sears and Shelley [284][1]

With this procedure one arrives at the following finite-temperature (210 K) structures for the vdW$^{\text{surf}}$ (vdw(TS)) schemes: $z = 2.98$ Å (3.23 Å), $\omega = 171.0°$ (171.2°), and $\beta = 17.7°$ (17.3°) (see table 9.1). Dominated particularly by the low-energy adsorbate-substrate stretching modes, anharmonic effects primarily affect the vertical height z. In the case of vdW$^{\text{surf}}$, the azo-bridge is lifted by 0.17 Å into almost perfect agreement with the measured value of 2.97 ± 0.05 Å. At the same time, the larger vertical adsorption height of the azo-bridge allows the molecule to flatten

[1] For details on this see Mercurio *et al.* [267, 268].

out again under the influence of the van der Waals interaction with the metal (increase of ω), and to twist further as a result of intermolecular interactions (increase of β). Both tendencies bring the calculated geometry closer to experiment, although the calculated ω remains too small. In the case of the DFT+vdw(TS) result, on the other hand, anharmonicity affects z and β only mildly, because z is too large already in the 0 K calculation; moreover, it has an adverse effect on ω, because it brings the molecule closer to the surface (see the inset in Fig. 9.2). Overall, the quality gap between vdW$^{\text{surf}}$ and vdw(TS) is therefore widened by the inclusion of anharmonic vibrational effects.

9.6 Conclusions to Chapter 9

A detailed re-assessment of the experimentally obtained geometry of Azobenzene on Ag(111) and the underlying analysis has shown that neglecting the signal coherence leads to a loss of information on the internal molecular and overall adsorption structure. The corresponding experimental structure that has originally been obtained in the work of Mercurio *et al.* [198] was based on the assumption of a flat adsorption structure, where internal degrees of freedom have been neglected. The analysis presented in section 9.2 reveals a structure that can not be understood without accounting for lateral adsorbate-adsorbate interactions at close distance.

Corresponding calculations on the coverage dependence of the electronic and geometric properties of Ab on Ag(111) show that the most recent DFT+vdw$^{\text{surf}}$ method is able to predict an energetically favoured phase at intermediate geometries, which agrees nicely with experiment in terms of the vertical adsorption height and the phenyl ring twisting angle. This finally also lifts the riddle of chapter 8, where the inclusion of the many-body substrate response into the DFT dispersive treatment further increased the disagreement with experiment for Ab on Ag(111), while yielding excellent agreement for other molecular adsorbates in literature. Since the vdW$^{\text{surf}}$ scheme leads to a reduction of both the dispersion coefficients *and* the van der Waals radii, it may counterintuitively decrease the adsorption height compared to DFT+vdw(TS). This is exactly what was observed for the LC phase studied in the previous chapter. However, in the specific case of Ab on Ag(111), the effects of high surface coverage on the adsorption geometry are immense. Dense molecular packing and the associated molecular distortion increases the vertical height again by 0.20 Å. The remaining differences between experiment and theory can then be understood by inclusion of anharmonic finite-temperature effects which lead to an even further increased apparent height of the molecule.

This rigorous benchmark shows that the DFT+vdW$^{\text{surf}}$ scheme in fact captures the essential physics of both covalent and dispersive contributions to the adsorption process and represents a valid modelling approach to the structure of large π-conjugated molecules. Specifically in the context of this thesis, the corresponding description of the molecular structure and ground-state energetics yields a good starting point for a subsequent description of excited state or dynamical properties. This methodological basis motivates in the following to seek for a detailed description of the thermal ground-state stability of the Azobenzene conformers.

10 Bistability Loss - Azobenzene (Non-)Switching on Coinage Metals

In the previous chapters we have established the corresponding state-of-the-art in literature and a methodology that correctly predicts the adsorption structure of Azobenzene and TBA on coinage metals. This chapter now investigates the ground-state potential energy surfaces associated with an isomerization process in more detail and focuses on the thermal stability of the minimum energy structures and the transition states connecting them. The corresponding results rationalize the observed stability decrease and function loss for Ab on Ag(111). The main part of the work presented here was published in the journal *Angewandte Chemie International Edition* [285].

10.1 Introduction and Computational Details

As already mentioned, many unsuccessful attempts towards adsorbed molecular switching have been reported. Experimentally, different approaches to the design of functioning molecular switches have been seeked out, the most straightforward approach beeing molecular functionalization aiming to further decouple the photochromic moiety, in our case the azo-bridge, both spatially and electronically. This has been a standard strategy to regain the switching function of molecular switches, viewing excited-state quenching at the metal surface as central reason for the loss of function upon adsorption. TBA is one of the most prominent examples in which functionalization has enabled successful switching on a Au(111) surface [13, 243]. However, as pointed out by McNellis *et al.* a pure spatial decoupling can not be the reason for the regained switching function [27] and corresponding photoswitching of TBA adsorbed to Ag(111) has not been achieved [240].

The unsuccessful attempts to switch both Ab and TBA at the Ag(111) surface indicate that factors other than photochromic decoupling might also be important. Several explanations why switching of TBA on other metal surfaces is not observed have been formulated [23, 28], but no unified picture specifying how surface interaction changes the stability and reactivity of metal-mounted azocompounds has yet been reached. At this point it is helpful to recall that the most basic prerequisite to a possible switching function is the existence of two metastable states at the experimentally applied conditions. It is intriguing to realize that no study has hitherto addressed the possibility that the absence of surface mounted switching could as well simply stem from a modified ground-state stability.

On the basis of the Ab gas-phase isomerization pathways investigated in chapter 6 and the minimum energy structures of the adsorbed species calculated in chapter 8, the following chapter will investigate this point by studying the effect of coinage metal surface adsorption on the ground-state barriers between the E and Z-Ab geometries. The corresponding results suggest that surface adsorption modifies the Ab ground-state stability in a way to *de facto* remove bistability and therewith allow immediate thermal re-isomerization from the previously

metastable state. This implies an unbalanced stabilization of the minimum energy structures and the barrier states due to adsorption.

Computational Details

The minimum energy pathways presented below have been generated using sequential constrained optimization [263] down to a maximum force component of 25 meV/Å. The rotational and inversional minimum energy pathways have been sampled with a dense set of points for Azobenzene on Ag(111) and Au(111) in a low coverage regime. All computational settings are identical to the ones used in chapter 8 and have been detailed there. The corresponding structures have been optimized using both dispersion correction schemes, DFT+vdw(TS) and DFT+vdw^{surf}. Rotational transition state structures were validated by a Quadratic Synchronous Transit (QST) transition state optimization [286, 287]. Due to convergence issues close to the inversion transition state only structures very near to the transition state can be given. Molecular projected Densities-of-State (MOpDOS) were calculated with a locally adapted version of CASTEP and a post-processing tool following the scheme described by McNellis *et al.* [197] (for more details see chapter 11.3 and appendix A.3). The adsorption energies for the transition state are defined by reference to the energy of the corresponding gas-phase transition state structure. Vibrational zero point energy contributions have been calculated for selected structures of the gas-phase molecule and the adsorbed molecules by imposing a frozen surface approximation and calculating the harmonic vibrational spectrum for the molecular degrees of freedom by finite differences.[1]

10.2 Groundstate Barriers of Ab on Ag(111) and Au(111)

As detailed in chapters 8 and 9, the vast amount of mechanistic studies of Ab isomerization in gas-phase and solution mainly focuses on two different mechanisms [167, 169, 176, 178, 195]: A dihedral rotation of one phenyl group around the central azo-bridge and an initially planar inversion around one of the CNN bond angles, cf. Fig. 5.2 and 10.1. In terms of the actual dynamics, symmetric breathing motions of both CNN angles might also play an important role in reaching low lying isomerization channels [171, 176]. The present consensus points towards a dominance of a rotational pedal motion leading to successful isomerization upon photoexcitation [181, 193]. Nonetheless, in the ground state both mechanisms show significant barriers, 1.8 and 1.5 eV for rotation and inversion, respectively, as seen from the more stable E-Ab state (see chapter 6). The rotational barrier maximum also coincides with a state crossing with the first singlet excited state [169]. Exactly these barriers generate two stable ground state basins between which switching can occur, by posing thermal barriers that cannot be overcome at standard ambient conditions.

Recomputing these barriers for Ab adsorbed to Ag(111) and Au(111) one finds the inversion barrier (iTS-Ab) and the potential energy surface along a symmetric inversion mode almost unchanged compared to the gas-phase case. In contrast and as shown in Fig. 10.2, the rotational barrier in the case of Ab on Ag(111) is drastically reduced by about 1 eV with respect to the E-Ab isomer. In addition, the metastable Z-Ab isomer changes its minimum energy geometry towards a higher dihedral angle and destabilizes by another 0.2 eV as compared to E-Ab, i.e. while Z-Ab is 0.5 eV higher in energy in the gas-phase, it is 0.7 eV at the surface.

[1] This has been done using the corresponding module in the Atomic Simulation Environment, see appendix A.4.

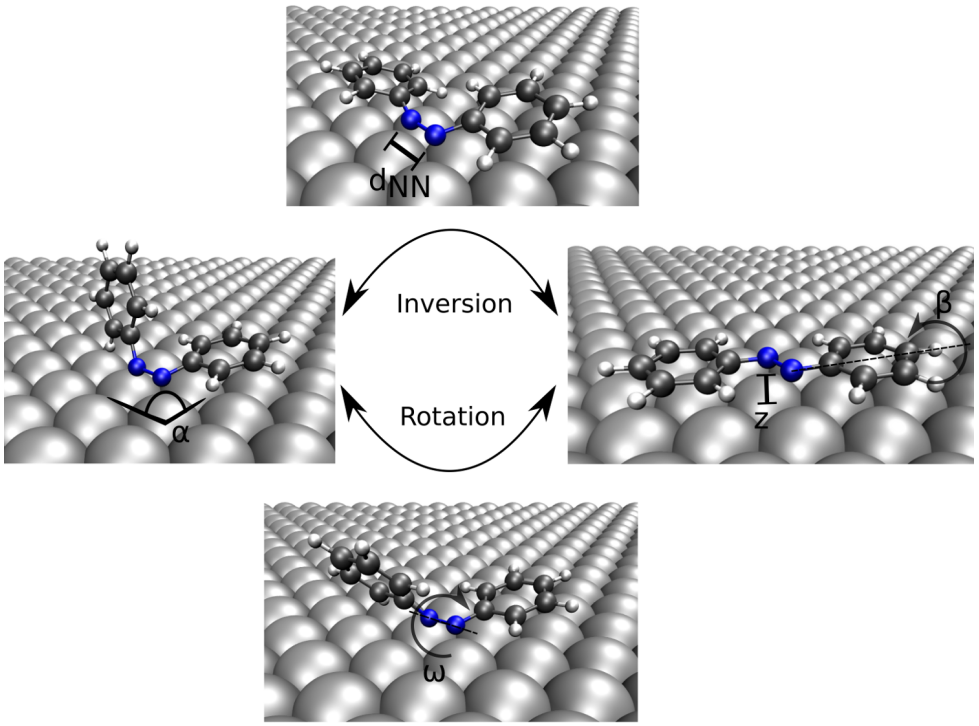

Figure 10.1: DFT+vdw(TS) calculated Azobenzene on Ag(111) minimum energy geometries and transition state structures along rotation and inversion coordinates. Also shown are the geometry parameter definitions already given in Fig. 8.2.

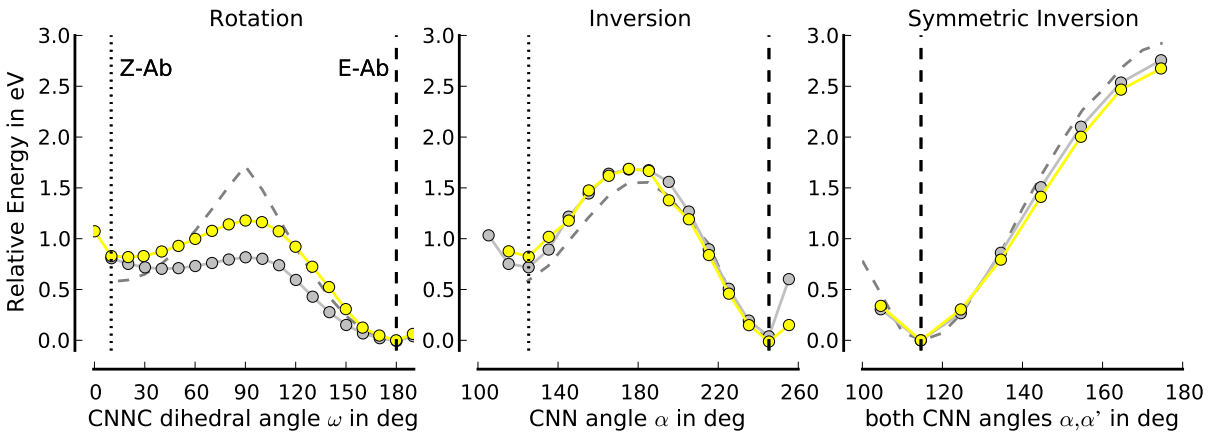

Figure 10.2: Minimum energy isomerization paths along the rotation (left), inversion (center), and symmetric inversion (right) coordinates. Shown are DFT+vdw(TS) calculated ground-state curves for the molecule in the gas phase (grey dashed line), adsorbed to a Ag(111) surface (grey), and adsorbed to a Au(111) surface (yellow).

Table 10.1: Relative energies of the rotational (rTS-Ab) and inversion (iTS-Ab) barrier geometries and Z-Ab compared to E-Ab calculated with pure DFT and vdw(TS) dispersion corrected DFT, as well as vdw^{surf} corrected DFT. Energies are given for the geometries in gas-phase and adsorbed on Ag(111) and Au(111).

	DFT+vdw(TS)				DFT*				DFT+vdw^{surf}			
	E-Ab	rTS	iTS	Z-Ab	E-Ab	rTS	iTS	Z-Ab	E-Ab	rTS	iTS	Z-Ab
Ab@	in eV				in eV				in eV			
gas-phase	-	-	-	-	0	1.67	1.51	0.58	-	-	-	-
Ag(111)	0	0.82	1.69	0.70	0	0.49	1.56	0.33	0	0.80	1.77	0.77
Au(111)	0	1.19	1.70	0.83	0	0.95	1.54	0.47	0	1.03	1.58	0.73

*: Pure DFT adsorption energies have been evaluated at the DFT+vdw(TS) geometries.

Table 10.2: Uncorrected and zero point energy corrected DFT+vdw(TS) energy difference between the rotational barrier structure (rTS-Ab) and the Z-Ab structure for gas-phase Azobenzene and adsorbed at Ag(111) and Au(111). Energies are given in eV.

Ab@	E(rTS-Ab)-E(Z-Ab)	$[E + E_{\mathrm{ZPE}}$(rTS-Ab)]-$[E + E_{\mathrm{ZPE}}$(Z-Ab)]
gas-phase	1.09	1.02
Ag(111)	0.12	0.05
Au(111)	0.38	0.38

These effects together leave the re-isomerization from Z-Ab back to the more stable E-Ab with a minimal zero-point energy corrected barrier of 50 meV, while simultaneously minimizing potential restrictions in the DFT description of the barrier region. Without even entering into the details of the light or electron driven excitation *per se*, already this insignificant barrier alone is enough to explain why Ab at Ag(111) will not switch - the fundamental bistability prerequisite to the switching function is simply lost. In particular, even if a very efficient photo-excitation mechanism from the E-state to the Z-state existed, the strongly vibrationally activated ground-state Z-Ab isomer resulting from the isomerization would still not be sufficiently stable to be observed. This is in perfect agreement with the fact that no stable Z-Ab isomer of Azobenzene on Ag(111) has been reported so far. In the case of Ab adsorbed to Au(111) the remaining barrier of 0.38 eV might very well be sufficient to stabilize the molecule thermally, due to the fact that hitherto employed experimental temperatures are far below room temperature and non-adiabatic effects on the metal surface such as energy dissipation via phonons or to a small extent also via low-lying electron-hole pair excitations [288] will cool the molecule considerably. This is furthermore supported by the fact that, although Ab on Au(111) does not switch via light-irradiation, it can be switched via inelastic electron tunneling through a STM tip [14].

Table 10.1 summarizes the relative energetics calculated for Azobenzene in gas-phase and adsorbed to both surfaces. Compared to the gas-phase both dispersion correction schemes show that upon adsorption the rotational transition state (rTS-Ab) is strongly stabilized with respect to E-Ab, while Z-Ab is always slightly destabilized and the inversion transition state is almost unaffected. The barrier reduction due to adsorption is less pronounced on Au(111) than on Ag(111) (see also table 10.2). No qualitative differences can be observed between the two applied dispersion correction schemes concerning both effects. In the case of the DFT-vdw^{surf} scheme the molecules are more closely bound to the surface and the barrier reduction effect is

Table 10.3: Adsorption energies referenced to the gas-phase (in eV), calculated at DFT, DFT+vdw(TS) and DFT+vdw^{surf} level for the two minimum energy structures and the rotational (rTS-Ab) and inversion (iTS-Ab) barrier geometries of Azobenzene adsorbed on Ag(111) and Au(111).

	Adsorptionenergies in eV					
	@Ag(111)			@Au(111)		
	DFT*	DFT+vdw(TS)	DFT+vdw^{surf}	DFT*	DFT+vdw(TS)	DFT+vdw^{surf}
E-Ab	-0.10	1.65	1.70	-0.01	1.61	1.45
Z-Ab	0.16	1.46	1.45	0.11	1.29	1.23
rTS	1.04	2.41	2.49	0.66	1.96	1.99
iTS	-0.13	1.46	1.44	-0.03	1.37	1.37

*: Pure DFT adsorption energies have been evaluated at the DFT+vdw(TS) geometries.

more pronounced. The DFT contribution to the relative stabilities, which includes the covalent bonding effects as well as Pauli repulsion due to the closed-shell nature of the molecule, shows that these effects are the main reason for the reduction of the rotational barrier and actually lead to an additional stabilization of the Z-Ab conformer compared to the E-Ab structure[2]. The effect of the dispersion interactions on top of this is that the E-Ab structure is strongly stabilized compared to the rTS-Ab and Z-Ab structures.

When considering the relative stabilities of adsorbed molecules, one may ask about the effect of surface adsorption on the vibrational zero-point-energy contribution to the total energy. Table 10.2 shows the relative basin depth and therefore the thermal stability of the Z-Ab structure with and without ZPE correction. As already mentioned in chapter 8, ZPE corrections for Ab are very small and do not change the relative energies drastically. Only for Ab@Ag(111) the ZPE contribution further reduces the barrier to the above mentioned 0.05 eV, whereas for Ab@Au(111) the corrections almost cancel out.

All structures that might represent important points in the dynamical switching process, namely both minima E-Ab and Z-Ab as well as both possible transition states rTS-Ab and iTS-Ab are affected by the adsorption in very different ways and their relative stabilities are modified in an unbalanced fashion. This intriguing effect is clearly seen in the adsorption energies of the corresponding structures shown in table 10.3. When referencing the adsorption energy to the corresponding geometrical state in the gas-phase, one finds that the rTS-Ab structure shows by far the highest adsorption energy compared to all other structures. The DFT-based contribution to the adsorption energy shows that these additional 0.66 and 1.04 eV for Au(111) and Ag(111) surface adsorption purely stem from a covalent interaction between the adsorbate and the surface around this rotational transition state, while all other structures only show minimal covalent character in the case of Z-Ab or even repulsive contributions due to dominating Pauli repulsion effects. Such large DFT-contributions to the overall adsorption energy point towards an actual chemisorbed state in the case of rTS-Ab, while all other structures have rather to be termed mostly physisorbed due to the dominating vdW contributions. Interestingly, this strong difference in the chemical bonding properties between Z-Ab and rTS-Ab can not bee seen from the vertical height (cf. table 10.4). Both structures show very similar vertical adsorption heights, which are significantly lower than what is found for the E-Ab or iTS-Ab structures.

To summarize, the reason for the strong preferential reduction of the rotational barrier lies

[2]In fact the E-Ab structure is destabilized with respect to all other structures, due to the fact that it is almost purely bound by dispersive interactions.

Table 10.4: Calculated structural parameters of the two minimum energy structures and the rotational (rTS-Ab) and inversion (iTS-Ab) barrier geometries of Azobenzene in gas-phase and adsorbed on Ag(111) and Au(111) surfaces. Shown are the vertical distance z from the surface, the NN bond length d_{NN} in Å, and the central dihedral angle ω, as well as both CNN angles α and α' (see Fig. 8.2 for definition).

		gas-phase			@Ag(111)				@Au(111)			
		d_{NN} Å	ω deg	α/α' deg	z Å	d_{NN} Å	ω deg	α/α' deg	z Å	d_{NN} Å	ω deg	α/α' deg
vdw(TS)	E-Ab	1.26	180	115/115	2.95	1.31	177	115/115	3.25	1.30	180	115/115
	Z-Ab	1.25	12	124/124	2.11	1.34	44	122/122	2.45	1.29	19	124/126
	rTS-Ab	1.28	90	125/125	2.05	1.38	90	119/118	2.06	1.36	90	119/121
	iTS-Ab	1.23	176	175/117	2.47	1.27	149	175/119	2.93	1.25	166	175/120
vdw^{surf}	E-Ab	-	-	-	2.35	1.34	155	114/114	2.67	1.30	166	114/118
	Z-Ab	-	-	-	2.07	1.33	29.7	120/122	2.31	1.29	8.7	122/124
	rTS-Ab	-	-	-	2.05	1.38	90	118/119	2.05	1.36	90	118/120
	iTS-Ab	-	-	-	2.33	1.28	158	175/119	2.50	1.25	157	175/120

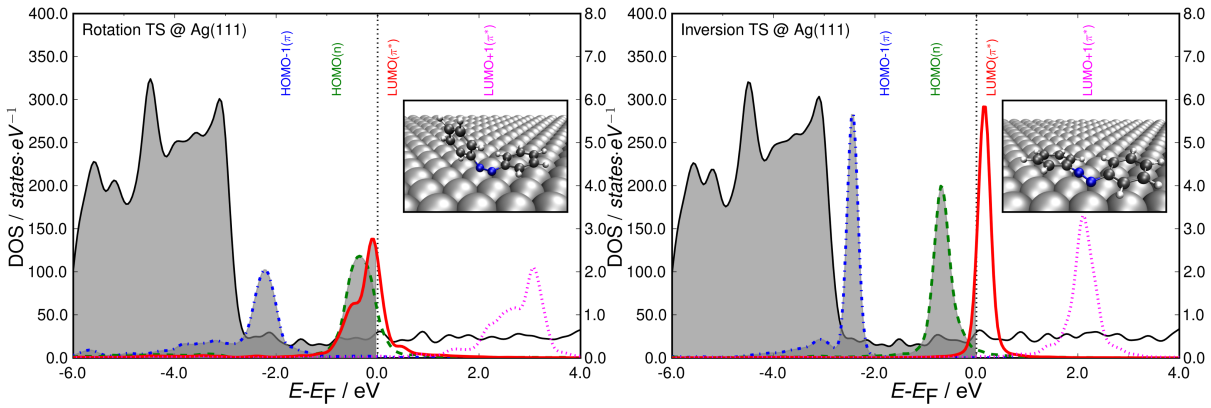

Figure 10.3: Calculated density-of-states (DOS) for the transition states (TS) along rotation (left) and inversion (right) isomerization of Ab on Ag(111) surface. Also shown is the DOS projected onto the molecular frontier orbitals (MOpDOS), as well as the TS geometries including important structural parameters as insets. The dotted line marks the Fermi level and the grey shaded area the occupied bands.

in the formation of a strong chemisorption bond along this pathway when going from E-Ab to Z-Ab. Whereas at both minimum energy structures and the inversion transition state the surface stabilization results to more than 90 % just from dispersive interactions, the adsorption energy at the rTS-Ab structure comes to 40 % from the semi-local DFT functional. Geometrically this covalent bond contribution at the rTS is indicated by a significant reduction of the vertical height and an elongation of the bond length of the central azo-bridge, from 2.95 Å at E-Ab to 2.05 Å and from 1.31 Å at E-Ab to 1.38 Å, respectively.

This leaves only to answer why this state shows such a strong covalent bonding to the metal surfaces, while all others do not. The effects on the electronic structure of the two transition state structures can nicely be discerned from the density-of-states (DOS) and molecular-orbitals

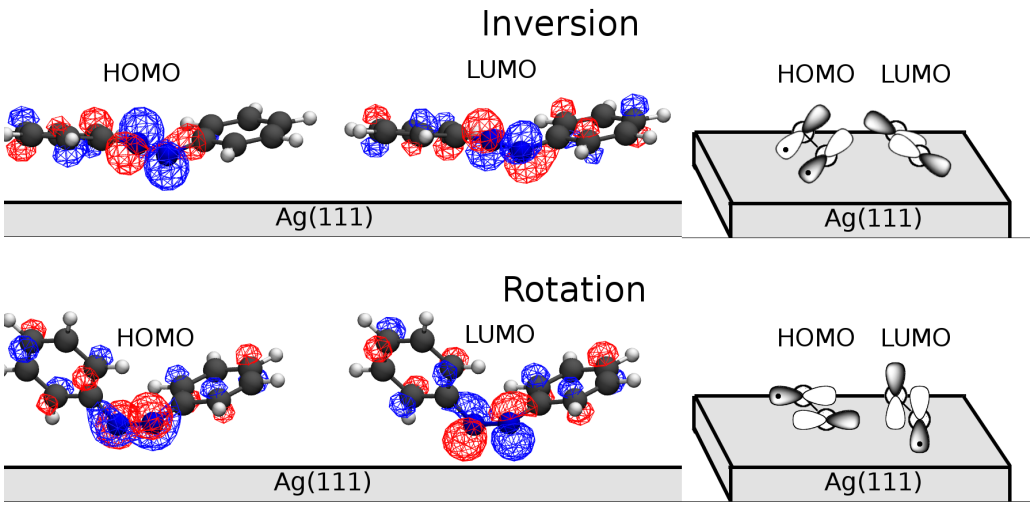

Figure 10.4: HOMO and LUMO orbital shape of Ab at Ag(111) for the inversion (top) and rotational (bottom) transition state. Shown are both calculated isosurfaces (left) and schematic representations of the orbitals centered on the azo-bridge (right).

projected from this density-of-states (MOpDOS) shown in Fig. 10.3. At the iTS-Ab structure, the frontier orbitals exhibit only the same minimal broadening due to the interaction with the metal bands as had been found before for the two minimum energy structures [197]. The small amount of charge transferred to the LUMO shows that in all these cases the surface interaction can be understood in the classic Dewar-Chatt-Duncanson π-donor-π*-acceptor model for bonding between metals and conjugated organics [289, 290]. Along the rotational path the frontier orbitals show instead a much stronger broadening and splitting. At the rTS the LUMO and HOMO are in fact almost degenerate and situated slightly below the Fermi level. The situation is thus highly reminiscent of a diradical state or open-shell Singlet, known to be a highly active chemical intermediate for example in Diels-Alder reactions [291]. Visualizing the corresponding gas-phase molecular frontier orbitals at the surface adsorbed geometry, as done in Fig. 10.4, then immediately shows that both HOMO and LUMO orbitals have a nonbonding character and are perfectly arranged to interact with localized metal *d* states, as opposed to the orbitals found in the inversion barrier structure.

To summarize, when following the pathway from the E-Ab structure to the 90° twisted rTS-Ab geometry the azo double bond is broken and a degenerate diradical state is formed. While in the gas-phase this state is exactly the reason why such a high barrier is formed, for a metal-surface mounted molecule such a state will never exist. Due to the close contact to a continuum of available metal electrons, the molecule is immediately stabilized by a charge-transfer from the surface and the chemical bond that is formed therewith. This effect is more pronounced at the more active Ag(111) surface than on Au(111).

10.3 The Effect of Spacer Groups on the Barrier - TBA on Ag(111) and Au(111)

Whereas the non-switching of Ab on Ag(111) can simply be rationalized by a loss of the bistability prerequisite due to a strong coupling of the isomerization transition state, the question remains what the effect of the bulky *tert.*-butyl groups is that enables molecular switching of

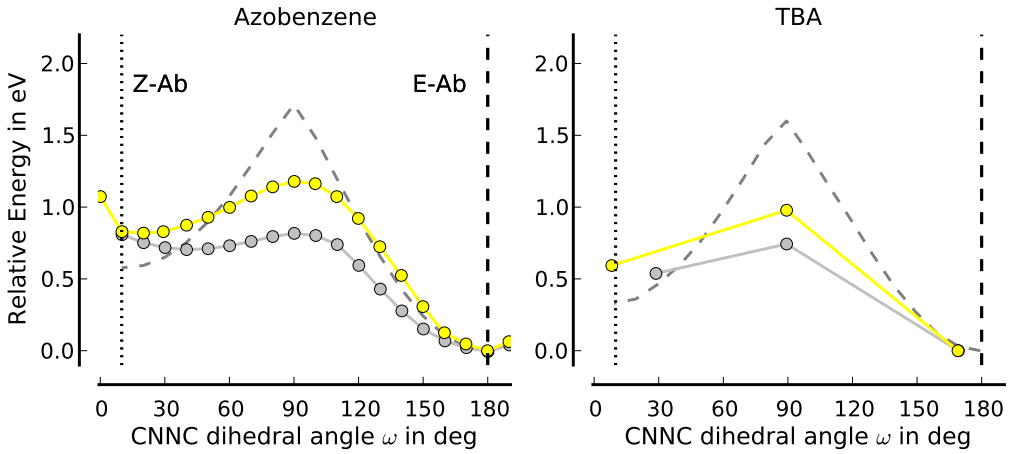

Figure 10.5: Minimum energy paths along the rotational coordinate for Azobenzene (left) and TBA (right) in gas-phase (dashed line) and adsorbed at Ag(111) (grey circles) and Au(111) (yellow circles). In the case of TBA only the minimum energy structures and the optimized transition states are shown. Calculations have been performed with the DFT+vdw^{surf} approach.

Table 10.5: Relative energies of the rotational (rTS) barrier geometry and Z-TBA in reference to E-TBA calculated with DFT+vdw(TS) and DFT+vdw^{surf}. Energies are given for the geometries in gas-phase and adsorbed on Ag(111) and Au(111). Results are not zero point energy corrected.

	DFT+vdw(TS)			DFT+vdw^{surf}		
	E-TBA	rTS	Z-TBA	E-TBA	rTS	Z-TBA
Ab@	Barriers in eV					
gas-phase	0	1.60	0.29	-	-	-
Ag(111)	0	0.74	0.54	-	-	-
Au(111)	0	0.98	0.59	0	0.93	0.49

TBA on Au(111).

The corresponding minimum energy paths along the rotational pathway for Ab and TBA and the relative energies of the TBA derivative on Ag(111) and Au(111) are shown in Fig. 10.5 and table 10.5. Preliminary results on the inversional pathway show no significant modifications from the gas-phase behavior upon adsorption and therefore further investigations have not been pursued. The gas-phase stability, as well as the ground- and excited-state potential energies of TBA are almost identical to Azobenzene in the regions that are relevant for the photoisomerization with the exception of a modified relative stability of the Z-TBA conformer. Due to the additional bulky spacer groups the increased intramolecular van-der-Waals interactions lead to an energetic difference of about 0.3 eV compared to E-TBA. The effects upon surface adsorption are almost identical to what was found for pure Azobenzene adsorbed to Ag(111) and Au(111). Relative to the E-TBA structure, the rotational transition state is strongly stabilized due to the covalent interaction and the Z-TBA structure is destabilized.

The much larger number of molecular degrees of freedom leads to a stronger contribution of the vibrational zero-point-energy to the total energy of the system as has already been shown for the adsorpion energies of the TBA equilibrium structures by McNellis and co-workers [199]. Correspondingly, the trends are similar as for adsorbed Azobenzene, but the effects are larger

Table 10.6: Uncorrected and zero point energy corrected DFT+vdw(TS) energy difference between the rotational barrier structure (rTS-TBA) and the Z-TBA structure for gas-phase TBA and adsorbed at Ag(111) and Au(111). Energies are given in eV.

Ab@	E(rTS-TBA)-E(Z-TBA)	$[E + E_{\mathrm{ZPE}}$(rTS-TBA)]-$[E + E_{\mathrm{ZPE}}$(Z-TBA)]
gas-phase	1.31	1.02
Ag(111)	0.21	0.00
Au(111)	0.38	0.36

Table 10.7: Calculated structural parameters of the two minimum energy structures and the rotational (rTS-TBA) barrier geometry of TBA in gas phase and adsorbed on Ag(111) and Au(111) surfaces. Shown are the vertical distance z from the surface, and the NN bond length d_{NN} in Å, and the central dihedral angle ω, as well as both CNN angles α and α'.

		gas-phase			@Ag(111)				@Au(111)			
		d_{NN} Å	ω deg	α/α' deg	z Å	d_{NN} Å	ω deg	α/α' deg	z Å	d_{NN} Å	ω deg	α/α' deg
vdw(TS)	E-TBA	1.30	179	115/115	3.07	1.30	169	115/115	3.09	1.30	169	115/116
	Z-TBA	1.29	8.3	120/121	2.09	1.33	28.7	120/122	2.38	1.29	8.2	123/124
	rTS-TBA	1.32	89	121/122	1.99	1.37	89	119/120	-	-	-	-
$\mathrm{vdw}^{\mathrm{surf}}$	E-TBA	-	-	-	2.35	1.34	155	114/114	2.67	1.30	166	114/118
	Z-TBA	-	-	-	2.07	1.33	29.7	120/122	2.31	1.29	8.7	122/124
	rTS-TBA	-	-	-	2.06	1.35	89	120/120	2.00	1.35	90	119/120

(see table 10.6). The remaining rotational barrier with respect to Z-TBA on Ag(111) of 0.21 eV vanishes completely after accounting for the vibrational ZPE.

Therefore, the loss of bistability and switching function on Ag(111) is not affected by the addition of bulky spacer groups. This result again is consistent with the fact that no Z-conformer of TBA on Ag(111) has been experimentally found and photo-induced switching has not been observed [240]. The only effect of the spacer groups that can be inferred from the energetics and the geometric parameters (see table 10.7) is that the *tert.*-butyl groups lift off the E-TBA molecule and reduce the dispersion interactions of the phenyl rings. The E-TBA state is therefore destabilized relative to all others. On the basis of these ground-state energetics, no clear answers can thus be given on why photoswitching of TBA on Au(111) occurs, while no such switching is observed for Ab on Au(111).

10.4 Bistability Loss - Implications to Adsorbate Switching Ability and Molecular Design

From the above established understanding many conclusions can be drawn in the context of currently used functional molecular design strategies. The two most often used strategies, namely a modification of the substrate and a geometrical decoupling via molecular functionalization have been investigated in the example of Azobenzenes on coinage metals. The first strategy targets the overall interaction strength of the molecule with the substrate in order to re-instate the known gas-phase behavior. The second one aims at a spatial and electronic decoupling of the

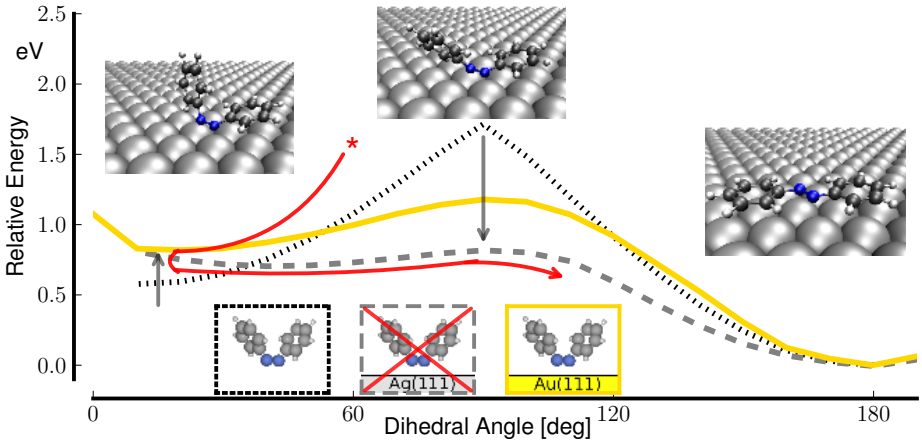

Figure 10.6: Schematic view of the rotational pathway for Azobenzenes in gas-phase and adsorbed at Ag(111) and Au(111) surfaces. Upon adsorption to a Ag(111) surface, a vibrationally hot intermediate structure can not be stabilized in the Z(cis) basin.

photochromic moiety. In the following it will be summarized again how these strategies modify the ground-state stability in the case of Azobenzene.

A general problem of Azobenzene adsorption on Ag(111) is an overall adsorbate-substrate interaction that is too large. This is specifically true for the rotational transition state structure that is additionally stabilized by a covalent bond with the substrate electrons that is formed when the pro-diradical state arises. By reducing the electron availability and therewith the stabilization of the diradical state through charge transfer this overly strong stabilization could possibly be reduced. On the substrate side this is effectively achieved by a lowered Fermi energy level (higher work function or electronegativity), as e.g. realized at the Au(111) surface. Indeed, this partly re-establishes the rotational barrier as is shown in Fig. 10.6. The resulting depth of 0.36 eV for the metastable Z-Ab basin is still much reduced compared to the gas-phase (1.02 eV) though. The bistability is thereby re-instated and switching is in principle possible again. However, the same process of going from a more active surface to a more inert one, has also further destabilized the Z-Ab conformer. So the surface adsorption is still unbalanced in the sense that E_{ads}(rTS-Ab) > E_{ads}(E-Ab) > E_{ads}(Z-Ab).

Another route to achieve a more balanced binding of all involved geometries could be via molecular functionalization. In the present case this has been pursued by adding bulky spacer groups that enforce a reduced van-der-Waals interaction of the phenyl rings with the surface. Our calculations show that this is completely ineffective in terms of reducing the interaction strength of the rotational transition state or the Z-Ab isomer. The corresponding relative energies are almost identical to the pure Azobenzene case. So the envisioned decoupling of the photochromic moiety can not be achieved by this approach [27]. On the other hand, the reduced interactions of the phenyl rings with the surface lead to a reduced stabilization of the E-TBA isomer as compared to all other structures. Correspondingly, the effect in our relative-energy picture is that the Z-TBA isomer is at least stabilized to 0.59 eV above E-TBA. This is exactly the gas-phase energy difference between the E and Z-Azobenzene conformers. Hence, when going from Ab adsorbed on Ag(111) to TBA adsorbed on Au(111), the substrate replacement re-enabled switching by increasing the barrier height. The functionalization additionally stabilized the meta-stable state, in order to finally end up with a situation that is very close to the gas-phase case, with the difference of a, still, significantly reduced barrier.

Both experimental strategies are generally believed to lead to simple changes to the overall interaction strength. This study shows that this must be replaced by a more differentiated picture that accounts separately for the effects on both metastable states and the relevant transition state structures. Both strategies indeed improved the previous adsorption situation for the studied Azobenzene system, but in an unbalanced way. Future functional molecular design should thus focus on different strategies that balance the interactions in all important intermediate geometries. Only this could garantee that modifications to the ground-state stability and reactivity are minimal and do not hamper the important prerequisites that are necessary to enable a successful excited-state switching process.

In the special case of TBA on Au(111), where switching is successful, one might imagine different ways to further increase the efficiency of the photo-induced molecular switching, which will depend on the mechanism that is believed to underlie the process. If one thinks in terms of the gas-phase isomerization mechanism, a further increase of the rotational barrier is important to ensure minimal changes to the gas-phase dynamics. In terms of a substrate-mediated excitation process, as discussed by Tegeder *et al.* [28] and summarized in chapter 7, a corresponding barrier should be large enough to still stabilize a meta-stable state, but small enough that a kinetically activated but prematurely deexcited intermediate may cross it. In such a mechanism it will also be important to efficiently enable the charge-transfer process or hole-quenching in the substrate, while in the context of the gas-phase mechanism it should be avoided as much as possible.

In both cases a selective tuning of the barrier is important. Substrate-modification from Ag(111) to Au(111) was able to do this in the studied Ab system, but is a general strategy that will affect both meta-stable and intermediate structures. Another well-known strategy to modify the electron-availability or work-function of the substrate might be the use of electron-withdrawing co-adsorbates, such as halogenated self-assembling monolayers [292, 293]. Such co-adsorbates could deplete electrons from the first layer and thereby reduce the chemical interaction of the rotational transition state, but at the same time contribute lateral dipole-dipole and van-der-Waals interactions to the functional molecule that induce preferential changes to the other conformations. This strategy appears to be a promising route. It opens a multitude of possible ways to modify the underlying ground-state energetics, but at the same time also increases the complexity of the system. Therefore, possible coadsorbate candidates have to be studied in detail in the future.

10.5 Conclusions to Chapter 10

In conclusion, our calculations on the Ab system indicate that thermal isomerization of surface-adsorbed molecules including double bond twisting events generally proceed via barrier geometries that couple much stronger to the surface than the minimum energy or other transition state structures. The ensuing lowering of the ground-state barriers might be sufficiently strong to eliminate the bistability prerequisite for switching, as illustrated here for Azobenzene and TBA at Ag(111). Without doubt, molecular functionalization must centrally target a tuned interaction of the photochromic moiety with the underlying metal to prevent ultra-fast quenching of excited states important for the isomerization. However, as shown here, a second goal must also be to achieve a balanced surface interaction of all geometries involved in the isomerization process. Quite naturally this calls for a paradigm change to current molecular switch design strategies.

For the present case of Azobenzene-derivatives at noble metal surfaces this amounts to specifically aim at a selective destabilization of the diradical rotational transition state. As

an intriguing and hitherto not pursued route this could be achieved by further reducing the substrate electron availability e.g. through electron demanding coadsorbates that increase the work function or that lead to selective inter-adsorbate dipole-dipole interactions.

A large amount of insight can thus be gained just on the level of the ground-state potential energy surfaces. In the present case this provides a full understanding of Ab and TBA non-switching on more active surfaces including Ag(111), and the fact that very subtle changes to the molecule or the environment can decide on opening a reaction channel or closing it. However, the successful switching of TBA on Au(111) in contrast to the unsuccessful switching attempts of unsubstituted Ab on the same surface are still to be understood and this can not happen on the level of the ground-state energetics. In order to unravel the subtle differences in the dynamics and the excited-state potential energy surfaces of Ab and TBA on Au(111), in the next part of this work we seek a corresponding approach to the description of excited states.

Part IV

Photodynamics of Adsorbed Azobenzene

11 An Efficient Approach to Excited States of Metal Adsorbed Molecules: Linear Expansion Δ-SCF-DFT

The current chapter reviews and augments a recently proposed ΔSCF-DFT based scheme to calculate electronically excited states of surface adsorbed molecules and enables its use for large complex adsorbate molecules such as adsorbed Azobenzene and derivatives. The main part of this chapter has been published in *The Journal of Chemical Physics* [294].

11.1 The Need for an Efficient Excited State Approach

Functional organic adsorbates, such as the molecular switch Azobenzene investigated in this thesis, pose a big challenge to current *ab initio* methodologies. This specifically relates to their large size and the complexity of the mechanisms that govern the function. While the first challenge requires highly efficient and computationally tractable modelling techniques, the latter enforces the same to be accurate for equilibrium and non-equilibrium configurations, as well as for derived properties such as electronic excited states. Only then can such an approach describe the dynamical details that decide upon the function of such a system.

A plethora of experimental spectroscopy techniques builds a basic data reference for such modelling and gives access to the changes in electronic structure that underlie the excited-state dynamical processes involved in molecular switching; however, often without yielding direct information on the mechanistic details. A long list of first-principles modelling techniques have in turn proven to be valuable tools for the investigation of such mechanistic details, but are generally challenged by the above mentioned large system sizes and the necessity to simultaneously describe localized molecular orbitals and the metallic surface band structure. *Ab initio* quantum mechanical simulations, such as Density-Functional Theory [51, 55] or post-Hartree-Fock approaches [30], have a successful history as such tools in surface science and chemistry. The current state-of-the-art, as we have seen in the foregoing chapters, provides a reliable description of electronic ground-state properties, including adsorption geometries, adsorption energetics, as well as thermal barriers. When it comes to the description of spectroscopy and excited-state properties, quantum chemical approaches are the optimal choice for finite systems or isolating materials, where cluster approximations are possible. They are currently not applicable to metallic systems though, where periodic boundary conditions are necessary to correctly describe the delocalized electronic structure. Applicable excited-state methods for this case include Time Dependent DFT [120, 203, 295], or many-body perturbation theory (MBPT) based methods [296], the latter enabling the description of both, ionic (GW) [297] and neutral (Bethe-Salpeter equation, BSE) [295, 298, 299] electronic excitations. In recent years, computational cost and accuracy of these approaches has tremendously improved. Nevertheless, current computer infrastructure and the remaining accuracy issues of applied density-functional approximations

and self-energy descriptions render systematic excited-state studies of large systems virtually intractable at the time. In this situation, a certain need exists for highly efficient excited-state schemes that, while maybe not fully quantitative, allow for a qualitatively correct description of the major physical effects that govern excited-state processes at surfaces.

Already very early in the history of DFT, attempts to apply and/or generalize the method beyond Hohenberg and Kohn's rigorous proof [51] and towards non-equilibrium excited-state properties have been undertaken. Many of them with the specific aim for a highly efficient description. The most rigorous and major extension was the Runge-Gross proof of a one-to-one correspondence between the time-dependent potential and the time-dependent electron density [120]. Another line of development are functionals generalized to fractional occupation numbers [104, 300], which has led to the standard DFT treatment for metallic systems [301]. Utilizing a Lagrange multiplier formalism, Dederichs *et al.* [106] have shown how to construct constrained density functionals [107], constraining electrons into specific regions of space or spin channels. This very efficient method has been heavily utilized to describe electron-transfer processes [108, 109, 302], but also surface reactions [111, 201]. Another very early approach is based on converging the density with respect to non-equilibrium electron occupations that resemble excitations, so called Delta-Self-Consistent Field DFT (ΔSCF-DFT) [89, 90, 92] that has been reviewed in the context of gas-phase Azobenzene isomerization in chapter 6 of this thesis. This approach, in different variations, has had a comeback in recent years due to its success on molecular charge-transfer excitations [96–98, 195, 202, 209, 303], which are badly described by adiabadic linear-response (lr) TD-DFT using standard semi-local exchange-correlation (xc) kernels [122, 125]. Although in principle without any formal justification, this method has recently been put into context by a number of different works. Ziegler and coworkers identified a close connection to a constrained variational procedure [114–117], which then provides a direct link to lrTD-DFT [115]. Theoretical works by Görling [102] and Ayers *et al.* [100] in turn point towards a possible formal basis for an excited-state density functional and would, at least in the case of the exact xc-functional, justify a corresponding treatment.

In the context of metal-surface adsorbed molecules an interesting extension to ΔSCF-DFT was put forward by Gavnholt *et al.* [29]. This so-called linear expansion ΔSCF (leΔSCF) scheme centers on resonance states that resemble gas-phase adsorbate orbitals, and enforces their occupation in the self-consistent density. This not only provides a well-defined constraint for intra-molecular excitations of the adsorbate, but also enables the description of photoemission and charge-transfer excitations such as the substrate-mediated electron-transfer that is thought to trigger the photoisomerization of TBA adsorbed to Au(111). The method has already been successfully applied to several smaller adsorbate systems [304–306] and promises at least semi-quantitative results, while adding only little computational overhead to ground-state DFT calculations.

In this chapter it will be shown how to establish this leΔSCF approach as an efficient means to the calculation of excited-state potential-energy surfaces (PESs) for large metal-adsorbed molecules. Necessary modifications to the method that enable the calculation of intra-adsorbate, as well as substrate-mediated charge-transfer excitations within the same formalism are presented and tested in the limit of no hybridization with the surface, for gas-phase Azobenzene, but also following a steady increase of hybridization along a vertical Azobenzene binding energy curve on Ag(111).

11.2 Linear Expansion Delta-Self-Consistent Field DFT - Basic Ideas

In the following section we briefly revisit the ΔSCF method and introduce the rationale behind leΔSCF as well as the here employed modification of it.

ΔSelf-Consistent-Field-DFT and leΔSCF-DFT

Detailed descriptions of the ΔSCF-DFT method can be found in the methods part of this thesis (see chapter 3.5) and have also been given numerous times in literature [89, 97, 98, 195, 202]. In the simplest case, excitations are modelled by reordering orbital occupation between states that mainly contribute to a transition. This changed population generates a modified density under which the Kohn-Sham (KS) equations [55] are solved. Singlet excitations are modelled by changing populations within one spin channel, Triplet excitations by switching channels. Certain care has to be taken to ensure the correct calculation of Singlet states. A widely used correction method is Zieglers sum rule [90]: $E_S^{SM} = 2E_S - E_T$. As shown in chapter 6, if the system does not show magnetization and the ground state is a Singlet state, Singlet excitations can also be calculated to a reasonable approximation without taking spin explicitly into account. This has also been shown for the case of O_2 on Al(111) [111] and recently for Iridium complexes [209], the latter work additionally providing a rationalization for the success of this approach.

Corresponding constraints provide a reasonable description of excited states that are well described as single-particle state-to-state transitions, also because the variational adaptation of the KS states with respect to the excited-state density clearly does give additional flexibility. Definition of such single-electron excitation constraints is a simple matter when molecular states can be clearly identified in character and are well separated spatially and energetically. This is almost always the case in minimum-energy structures of isolated organic molecules. More reactive geometries, i.e. transition-state structures, can already contain state degeneracies that hamper convergence. In such a case minimal smearing of the occupation constraint might enable calculation with only a small additional error in energy[1]. In contrast, in the case of the excitation spectrum of molecules interacting with periodic structures, where degeneracies are ubiquitous, such a simple approach will strongly affect the character and the absolute energy of the excitation. In this situation one also has to distinguish between adsorbates interacting with isolating surfaces and adsorbates on metals. In the first case, substrate states are mainly localized and generally exhibit strong hybridization with adsorbate states similar to interactions between two covalently interacting molecules. Such hybridization can in principle completely modify the character and the energy of states, but will again generate states that are localized and can, in the best case, be identified in their character and occupied correspondingly. Therefore a simple ΔSCF approach should still capture the main part of the transition. In the case of transition metal substrates, however, interactions are twofold. Following the Newns-Anderson model [262], chemisorbed molecules will show strong hybridization with *d*-bands, which modifies the character, splitting, and energetic position of the frontier orbitals. Simultaneously, there will also be a weak hybridization due to interaction with *s*- and *p*-bands. This broadens molecular states and spreads their character over many bands in a small energy window. In such a case a simple ΔSCF approach, that occupies the band with the highest overlap compared to a gas-phase molecular state, will miss significant parts of the transition, and therefore strongly underestimate the change in density.

[1] This has been employed in the calculations of chapter 6.

Gavnholt *et al.* [29] have devised the linear expansion ΔSCF (leΔSCF) approach to specifically target such systems. In their approach they do not just define constraints on KS states, but on linear combinations of them. To illustrate this, let us shortly recapitulate the ground-state case for an isolated system (or for an extended system for each **k**-point separately). There the effective one-particle KS equations read

$$\left[-\frac{\nabla^2}{2} + V_{\mathrm{KS}}[\rho]\right] |\psi_i\rangle = \epsilon_i \, |\psi_i\rangle \,, \tag{11.1}$$

where we define the KS potential $\mathrm{V_{KS}}$ acting on the KS auxiliary wavefunctions and the KS eigenvalues ϵ_i. The density on which the KS potential depends on, is constructed from the $\{|\psi_i\rangle\}$ via

$$\rho = \sum_{i}^{\text{states}} f_i \, |\psi_i\rangle \, \langle\psi_i| \,, \tag{11.2}$$

where f_i is the occupation of the state i. In a T=0 K ground-state calculation this results in

$$\rho = \sum_{i=1}^{N_e} |\psi_i\rangle \, \langle\psi_i| \tag{11.3}$$

for a finite system with N_e being the number of electrons of the system, or in case of an extended system

$$\rho = \sum_{\mathbf{k}} w^{\mathbf{k}} \sum_i f_i(\epsilon_F) \, |\psi_i^{\mathbf{k}}\rangle \, \langle\psi_i^{\mathbf{k}}| \,, \tag{11.4}$$

with $w^{\mathbf{k}}$ being the mathematical weight for each **k**-point and ϵ_F being the Fermi energy. In simple ΔSCF calculations one instead constructs the density by replacing one of the states in the sum with another originally unoccupied virtual KS state. In leΔSCF, Gavnholt *et al.* propose to construct so-called resonance states from a linear combination of KS states instead of a single KS state

$$|\tilde{\psi}_c^{\mathbf{k}}\rangle = \sum_{i}^{\text{unocc.}} a_i^{\mathbf{k}} \, |\psi_i^{\mathbf{k}}\rangle \,, \tag{11.5}$$

with expansion coefficients $a_i^{\mathbf{k}}$ defined as

$$a_i^{\mathbf{k}} = \frac{\langle\psi_i^{\mathbf{k}}|\phi_c^{\mathbf{k}}\rangle}{(\sum_i |\, \langle\psi_i^{\mathbf{k}}|\phi_c^{\mathbf{k}}\rangle \,|^2)^{1/2}}, \tag{11.6}$$

where $|\phi_c^{\mathbf{k}}\rangle$ denotes a pre-calculated reference KS state of the corresponding gas-phase adsorbate that ought to be occupied. The excited-state density then follows as

$$\rho = \sum_{\mathbf{k}} w^{\mathbf{k}} \left(\sum_{i=1}^{\text{occ.}} |\psi_i^{\mathbf{k}}\rangle \, \langle\psi_i^{\mathbf{k}}| + \sum_{i,j}^{\text{unocc.}} a_i^{\mathbf{k}} \cdot a_j^{\mathbf{k}*} \, |\psi_i^{\mathbf{k}}\rangle \, \langle\psi_j^{\mathbf{k}}| \right). \tag{11.7}$$

Equation 11.5 thus constructs a new KS state from unoccupied orbitals which resemble the chosen reference state and which are then used to construct the excited-state density. This approach can readily be used to model intra-molecular HOMO-LUMO type excitations, where an equal number of electrons and holes are excited in the adsorbate, but also for adsorbate-substrate charge-transfer, where only a hole or an additional electron is enforced on the adsorbate states. In this case, the occupation of the remaining states has to be adjusted by lowering or increasing the Fermi energy correspondingly in order to conserve the total electron number of the whole

system. This approximation to an excitation can be justified by the large ensemble of substrate electrons which occupy metal bands of very similar character, such that removing one such band from the density should induce only a minor error on the excitation energy. Summarizing the approach, those parts of the reference orbital, which are not yet included in the first N_e-1 ground-state occupied orbitals are constructed from a range of virtual KS states by projecting out components resembling this state and subsequently including them in the density. The ground-state KS procedure is therefore modified in the construction of the density (eq. 11.7) in every SCF step. Following this approach the kinetic energy of the system has to be corrected for the terms due to the newly added constraint orbital [29]. When breaking spin symmetry or including different positions in momentum space (**k**-point sampling) the procedure is followed independently for different spin channels or at different **k**-points. This approach is ideally suited for the description of inverse photo-emission and for diatomics on transition metal surfaces and was shown to outperform spatially constrained DFT approaches as well as simple ΔSCF [29].

A fresh look on leΔSCF

In the following the leΔSCF approach is generalized in two aspects. In a first step to allow for an arbitrary number of constraints constructed from arbitrary reference states without discriminating between occupied and unoccupied states. This provides a more consistent infrastructure for the description of intra-molecular as well as charge-transfer excitations, and might even open the application to systems very different from adsorbate-substrate complexes.

Secondly, the approach should enable the construction of excited-state PESs for large adsorbates in arbitrary geometries, while in the limit of infinite separation between adsorbate and substrate it should retrieve the simple ΔSCF result. In order to achieve this, certain conditions on the reference states $|\phi_c\rangle$ have to be imposed.

Modified Approach It is always possible to expand an arbitrary reference state $|\phi_c\rangle$ in the complete space of KS states of the system under study:

$$|\tilde{\psi}_c^{\mathbf{k}}\rangle = \sum_i^{\text{states}} |\psi_i^{\mathbf{k}}\rangle \langle\psi_i^{\mathbf{k}}|\phi_c^{\mathbf{k}}\rangle \,, \tag{11.8}$$

while at the same time the remaining KS states have to be orthogonalized correspondingly:

$$|\tilde{\psi_i^{\mathbf{k}}}\rangle = |\psi_i^{\mathbf{k}}\rangle - \sum_c^{\text{constr.}} |\phi_c^{\mathbf{k}}\rangle \langle\phi_c^{\mathbf{k}}|\psi_i^{\mathbf{k}}\rangle \,. \tag{11.9}$$

This leaves the subset of $\{|\tilde{\psi_i^{\mathbf{k}}}\rangle\}$ orthogonal to the subset of resonance states $\{|\tilde{\psi_c^{\mathbf{k}}}\rangle\}$, but destroys orthonormality for the complete set of KS states $\{|\tilde{\psi_i^{\mathbf{k}}}\rangle, |\tilde{\psi_c^{\mathbf{k}}}\rangle\}$. We therefore perform an additional orthonormalization on this whole set of KS states. This state transformation is done in every SCF step and yields a set of KS states on which a simple modification of the electron occupation, such as it is done in simple ΔSCF, yields an excited-state density as follows:

$$\rho' = \sum_{\mathbf{k}} w^{\mathbf{k}} \left(\sum_i^{\text{states}\neq\text{constr.}} f_i' \, |\tilde{\psi_i^{\mathbf{k}}}\rangle \langle\tilde{\psi_i^{\mathbf{k}}}| + \sum_c^{\text{constr.}} f_c \, |\tilde{\psi_c^{\mathbf{k}}}\rangle \langle\tilde{\psi_c^{\mathbf{k}}}| \right) \quad , \tag{11.10}$$

where the only boundary condition on eq. 11.10 is that

$$\sum_i^{\text{states}\neq\text{constr.}} f_i' + \sum_c^{\text{constr.}} f_c = N_e \quad . \tag{11.11}$$

In eq. 11.11 the f_c's are given by the aspired constraint definition, while occupations f_i' have to be adapted to conserve the electron number. Due to the modified construction of the KS states and the occupation reordering, there is no need for modification of the density construction routine itself. The modified KS states and excited-state occupations also enter in the calculation of the kinetic energy, which is therefore implicitly treated correctly, again without need of further modification as was necessary in the original implementation of Gavnholt *et al.* in the GPAW package [307, 308]. Constraints are enforced independently in different spin channels and at different **k**-space positions.

This approach only differs from the simple ΔSCF approach by the modification of the KS states, which corresponds to a unitary transformation and forces the resulting KS solution to include the specified resonances. It naturally accounts for the hybridization-induced broadening of the adsorbate KS states at the surface and in all cases includes or removes the *whole* reference state. However, a strong limitation of the method lies in hybridization effects that go beyond broadening. Due to the interaction of the sub-systems (molecule and surface), hybridization of the system can already lead to ground-state occupations that are very different from the separated sub-system case, such as is the case at the rotational transition state structure of Azobenzene adsorbed to Ag(111). The correct treatment of electron transitions then has to start from this occupation and transfer the corresponding amount of electrons effectively. In such as case it is possible that the constraint can not be fully satisfied, because the hybridization is too strong and the molecular reference orbital is already occupied and not a good reference point anymore. In this limiting case the resulting energies can only represent upper bonds to the excitation energies (cf. chapter 12).

Concerning the calculation of energy derivatives, this approach suffers from similar problems as the original implementation of leΔSCF does. The Hellmann-Feynman theorem does not hold due to the additional dependence of the non-variational coefficients of $|\phi_c\rangle$ on the positions of nuclei and the additional entropic contribution due to the excited-state population[2]. A possible formulation of the herewith introduced $|\phi_c\rangle$-'Pulay'-like terms still needs to be developed. Some ideas connected to this issue are formulated in appendix C and D of this thesis.

Generating Suitable Reference States In the leΔSCF scheme an excited-state density is constructed that includes a certain resonance state. All remaining states are variationally relaxed and therefore effectively screen the excitation in the self-consistent (sc) excited-state density. A question that remains is the selection of suitable reference states $|\phi_c\rangle$ from which to construct the resonances. Such reference states could be molecular states of an adsorbate on a surface resembling an excitation (as used in chapter 12 below), localized orbitals of a cluster cut-out that resemble a vacancy, or stemming from the very same system in a different electronic state (as used in chapter 11.4 below). The choice depends very much on the definition of the sub-system and the excitation under study. The projection restricts the resonance state itself to be an input quantity and it cannot change during the self-consistent solution of the KS equations. This stands in stark contrast to simple ΔSCF where the non-self-consistent (non-sc) input orbitals from the ground-state calculation are used to construct the input density and are then iteratively optimized to yield a self-consistent excited-state density (ΔSCF, cf. Fig. 11.1).

In the work of Gavnholt *et al.* the choice of the reference state fell on a virtual ground-state KS state of the gas-phase adsorbate ($\Delta\text{SCF}^{\text{GS}}$). As shown schematically in column 3 of Fig. 11.1, this corresponds to calculating the sc excited-state solution, while forcing the constrained orbital into the non-sc (or ground-state) solution. This might be a valid approximation, if

[2]This contribution also affects forces from simple ΔSCF treatments if significant non-integer occupations arise, although the effect is negligible in organic molecules.

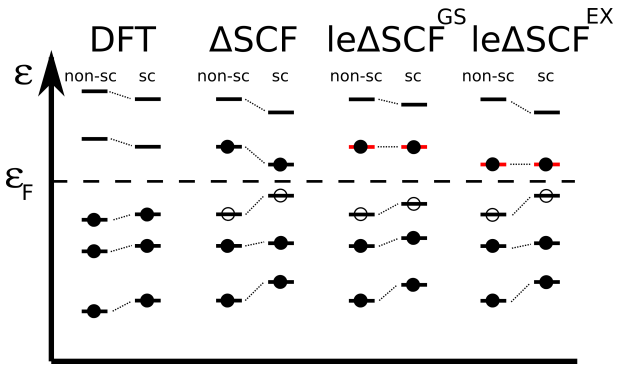

Figure 11.1: Schematic state diagram showing the frontier orbitals in ground-state DFT, simple ΔSCF, leΔSCF with a ground-state reference, and leΔSCF with an excited-state reference. Projected reference states are in red. The excitation is visualized with an electron hole pair (filled and unfilled circles). Schematic orbital positions are shown for the non-self-consistent (non-sc) and the self-consistent case (sc).

the molecular state of interest does not change strongly due to screening in the excited state. Particularly for the description of vertical excitation energies of equilibrium geometries or PESs of small adsorbates where a small number of degrees of freedom defines the KS states, this might be a good choice. This was nicely shown for the calculation of excited-state PESs of small diatomics on transition metal surfaces [29, 304]. The single nuclear degree of freedom in this case reduces the chance of large variations in character and extent of the orbitals between ground-state and excited-state solutions.

However, in many cases this approximation will fail, namely when the ground-state optimized orbital is not a good approximation to the final excited-state KS state. This is in fact the general case for the frontier orbitals of molecules with many degrees of freedom and/or extended π-systems in non-equilibrium geometries, and is especially true when applying standard semi-local exchange-correlation (xc) functionals. In the latter case it is known from lrTD-DFT treatments that the qualitatively wrong description of ground-state molecular resonances in semi-local functionals hampers the description of non-equilibrium geometries and charge-transfer excitations [195, 221, 309]. This problem can to some extent be resolved by including the correct 1/r density-density-response behavior into the xc-functional description [217, 310]. A big strength of the simple ΔSCF approach is in this respect its additional flexibility due to the variational optimization of the orbitals. Although the definition of the excitation itself is primitive compared to lrTD-DFT, the additional variation allows for a consistent-quality description for large portions of PESs and the qualitatively correct description of charge-transfer states and other problematic cases already with a semi-local or hybrid xc-functional [97, 98, 195, 209]. The absolute excitation energies will nonetheless be determined by the quality of the underlying xc functional, meaning that an underestimation of e.g. the HOMO-LUMO gap due to self-interaction error will also carry over to the excited-state description, which could be seen in the comparison between different xc-functionals in Fig. 6.6 of chapter 6.

Some of this ΔSCF flexibility is lost due to the projection inherent in leΔSCF. In order to also ensure a correct sc treatment of the actually constrained orbitals, one has to provide reference states $|\phi_c\rangle$ that are already optimized to the specific excited state of interest. This can for example be done by calculating the simple ΔSCF solution of the excited-state reference system (here the gas-phase molecule) and then including reference states into the leΔSCF calculation that are already in the final excited state (leΔSCF$^{\mathrm{EX}}$, cf. Fig. 11.1). The solution of

this approach would in this case correspond to the simple ΔSCF solution in the limit of zero hybridization.

11.3 Linear Expansion Delta-Self-Consistent Field DFT - Usage, Implementation, and Beyond

Usage

In order to ensure inclusion of relaxation effects of all orbitals and equivalence to ΔSCF, correct reference orbitals have to be chosen. The above mentioned considerations lead to a generalized final-state leΔSCF (leΔSCF$^{\mathrm{EX}}$) approach to arbitrary systems that thus includes the following steps:

- Calculate the electronic ground-state of the system of interest with DFT
- Calculate the excited state of interest in the reference (sub-)system using simple ΔSCF-DFT. From this calculation identify the KS reference states of interest that will be used as $|\phi_c\rangle$
- Calculate the excited state of the system of interest using the ΔSCF reference states $|\phi_c\rangle$ and leΔSCF-DFT

Implementation and Computational Details

The method described in section 11.2 has been implemented in the ultrasoft pseudopotential plane-wave code CASTEP 6.0.1 [258]. The implementation for the ΔSCF scheme constructs the changed set of KS states after every diagonalization step in the SCF procedure and uses a modified Fermi distribution to assign the constraint occupations, adapt the remaining occupations (f_i'), and construct the density from it. The newly constructed resonance KS state replaces the former KS state showing the highest overlap with the reference state. Calculations employing the leΔSCF method as implemented in CASTEP need to be checked for convergence with respect to the standard parameters of plane wave calculations such as plane wave cutoff and k-point sampling, but also with respect to the number of additional virtual orbitals that are explicitly included in the calculation in order to assure convergence of the projections from eq. 11.8. Standard DFT convergence enhancement methods [259, 301, 311] are used for the evaluation of the self-consistent excited-state density. In addition to the modified ΔSCF scheme, simple ΔSCF for gas-phase molecules in a supercell approach has been implemented. This is used for comparison and construction of appropriate excited-state KS reference states. The implementation of the projections in eq. 11.8 enable to use them also for the calculation of Molecular Orbital projected Density-of-States (MOpDOS) following the explanations of McNellis *et al.* [197]. MOpDOS coefficients corresponding to gas-phase reference KS states can be printed out and post-processed for visualization (as has been used in chapter 10). These coefficients in an integrated form also give access to the MO occupations that are used in Fig. 12.1 and 12.2.

Excitations in the following test system have been modelled by effective addition or removal of one electron in the frontier molecular orbitals, namely, the second highest occupied molecular orbital (HOMO-1), the HOMO, and the LUMO of the molecule in order to describe neutral intra-molecular excitations.

The following calculations have been performed using the same settings as detailed in chapter 8. Isolated Azobenzene benchmark calculations of section 11.4 have been run in a

(20Åx20Åx20Å) supercell with a plane-wave energy cut-off of 350 eV and **k**-space sampling only at the Γ-point. The binding energy curve of Azobenzene adsorbed to Ag(111) has been calculated by sequential energy evaluations for the vertically translated equilibrium structure of the molecule on a (6x4) Ag(111) slab. The corresponding dispersion correction scheme used is the DFT+vdw^{surf}. In this corresponding test system not only intramolecular excitations have been calculated, but also corresponding cationic and anionic charge-transfer states by adding or removing electrons from the molecular states and shifting the Fermi level correspondingly. More details on the calculation of reference states can be found in chapter 12.1

... and Beyond: leΔSCF and Self-Energy Corrections to the KS Reference States

The above established methodology presents a highly efficient approach to excited states that should be able to carry the known ability of ΔSCF to describe the potential energy surface topology of gas-phase Azobenzene over to the adsorbed molecule. However, as already pointed out several times in this work, the absolute excitation energies on the level of a semi-local xc-functional description will be systematically underestimated. While this might not influence the dynamics of the excited-state propagation dramatically, de-excitation probabilities will be significantly modified. Furthermore, in a more general context strongly underestimated HOMO-LUMO gaps of adsorbate molecules might even lead to artifical charge-transfer due to an unexpected population of the low lying LUMO, as is known to be the main reason for the long-standing CO puzzle of surface science [224, 312]. In that case an underestimated energetic position of the LUMO leads to a wrong prediction of the most favourable adsorption site for CO on Pt(111) [313][3].

This is a very general problem in the description of adsorbate systems with current DFT methodology. On the level of a semi-local exchange-correlation functional approximation the electronic structure of the metal substrate is, due to very fortuitous error cancellation, described accurately. However the fundamental gap of the molecule is at this level largely underestimated. Adding to this issue, an improved description of the molecular fundamental gap, for example by inclusion of a portion of exact exchange, would in turn yield an unphysical electronic structure of the substrate [222–224, 314].

However, if one were able to use a modified Hamiltonian along the lines of a DFT+U [315–317] treatment and the ideas put forward in the solution of the CO on Pt(111) puzzle by Kresse *et al.* [313] together with the projections that are defined above, one could correct the self-interaction error in the energetic position of the adsorbate orbitals, without interfering with the substrate electronic structure. In addition leΔSCF calculation on top of such a reshaped orbital space might lead to significantly improved absolute excitation energies. This idea is to some extent explicated and tested in appendix D.

11.4 Putting the Method to Use

In this section we apply the proposed method first to the isomerization of the prototypical molecular switch Azobenzene in gas-phase and then investigate the continuous increase of hybridization from the gas-phase to the adsorbed state by calculating the binding energy curve of Azobenzene on Ag(111).

[3] While this is a well known problem for different systems, such as the above mentioned CO on Pt(111), in the case of the rotational transition state structure of Azobenzene adsorbed to coinage metals, the state crossing and population of the LUMO is a physical process that stems from the HOMO-LUMO degeneracy at this geometry and can not be attributed to this issue.

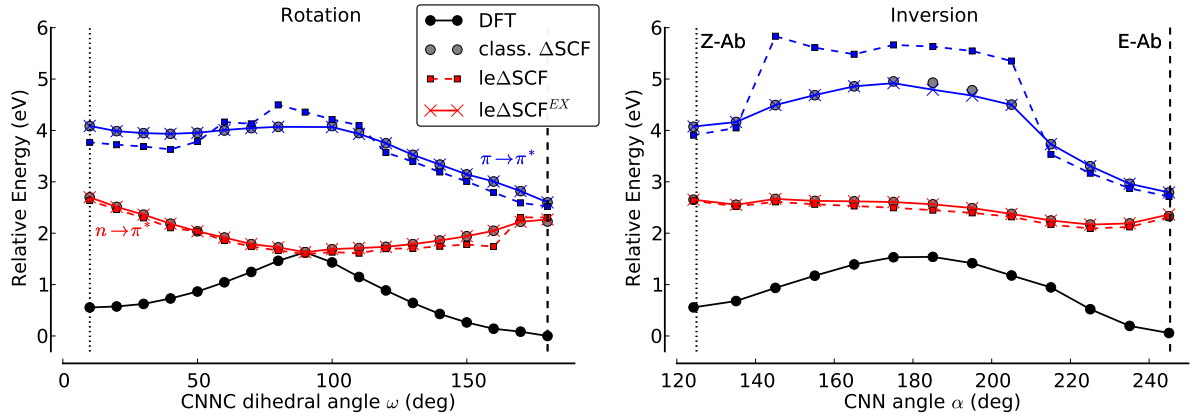

Figure 11.2: Gas-phase Azobenzene PESs along rotation (left) and inversion (right) degrees of freedom for the ground state (black), the first excited n$\rightarrow \pi^*$ state (red), and the second excited $\pi \rightarrow \pi^*$ state (blue). The excited-state curves were calculated with simple ΔSCF (no lines, gray circles), leΔSCF with ground-state reference orbitals (dashed lines, squares) and leΔSCF with excited-state reference orbitals (straight lines, crosses).

Isomerization of Gas Phase Azobenzene

The purpose of this subsection is to demonstrate the equivalence of simple ΔSCF and leΔSCF in the limit of photo-induced E-Z-isomerization of gas-phase Azobenzene.

In chapter 6 it was demonstrated that simple ΔSCF-DFT calculations yield a qualitatively correct description of the involved excited-state PESs. They were shown to be in good agreement with higher level computations (RI-CC2 [46]) and therefore can in principle provide a realistic representation of the mechanisms [195]. Figure 11.2 reproduces these ΔSCF curves (gray filled circles) following the ground-state optimized paths along the two main degrees of freedom. This figure also includes the data obtained when applying the leΔSCF approach as described in the previous section and using the ground-state orbitals of the isolated gas-phase molecule as reference orbitals at every position along the two pathways. Already from visual inspection it is possible to identify regions on both pathways where the difference to ΔSCF is minimal and regions where the topology is not reproduced correctly. The assumption that the constrained states do not change significantly due to the excitation seems sufficiently justified very close to the equilibrium geometries, but fails at the transition-state geometries on the S2 state. In other words, in PES regions where ground-state orbitals are very good approximations to excited-state ones the difference is minimal. In contrast, in regions where due to excitation the orbital character and orbital ordering changes, effects can be quite large. In this respect, it is intriguing to note that the region of biggest error, namely the S2 state at mid-inversion, is also not correctly reproduced by lrTD-DFT when using ground-state PBE orbitals as a starting point (see section 6.5). Both effects have the same source, namely that GGA-DFT derived effective one-particle states are bad approximations to molecular resonances of the interacting many-particle system. This is especially true for virtual states [217, 318].

Also shown in Fig. 11.2 are the curves calculated with leΔSCF when employing reference orbitals that were calculated with the leΔSCF$^{\mathrm{EX}}$ approach detailed above. The corresponding results exactly reproduce the standard ΔSCF curves, because they now include relaxation effects for all KS states. This nicely underscores the importance of including state relaxation in order to generate consistent-quality PESs. Having established the equivalence of the two methods for the gas-phase limit, we now proceed in the next section by investigating the effects of hybridization

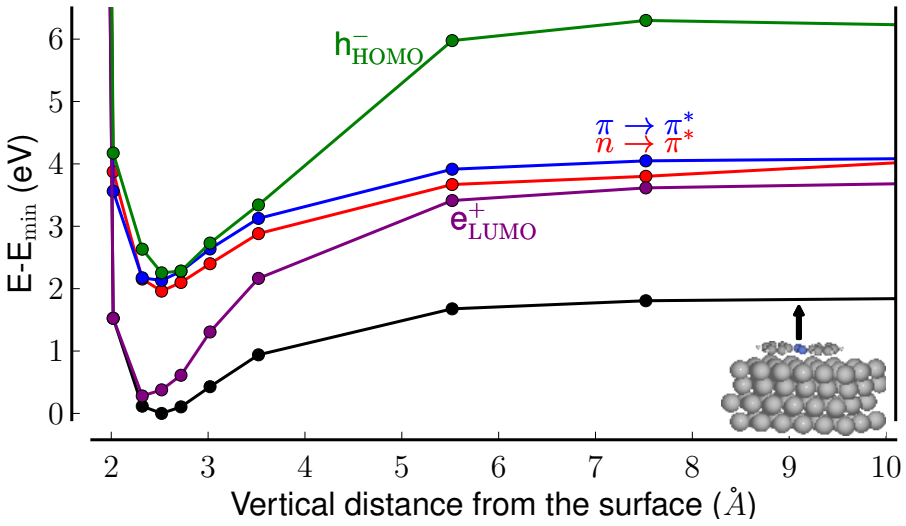

Figure 11.3: Azobenzene adsorbed to Ag(111): Relative energy with respect to the equilibrium adsorption geometry as a function of the vertical adsorption height. Shown are the ground state energy (black curve), the first (n$\rightarrow \pi^*$), and second ($\pi \rightarrow \pi^*$) intramolecular excited states as well as charge-transfer excitations inserting an electron to the LUMO of the molecule (e^-_{LUMO}, purple curve) or removing an electron from the HOMO of the molecule (h^+_{HOMO}, green curve). The small model on the bottom right depicts the dissociation direction orthogonal to the surface.

on the lowest-lying excited states of Azobenzene adsorbed to a metal surface.

Binding Energy Curve of Azobenzene adsorbed to Ag(111)

The above shown calculations of gas-phase molecular excitations with leΔSCF are of no added value compared to simple ΔSCF calculations, with the exception of the proof of equivalence. An actual methodological extension can be found when the molecule is in contact with a substrate that leads to hybridization of the molecular states with the substrate electronic eigenstates. In such a system different excitations can be modelled, namely the intramolecular orbital-to-orbital transitions as have been discussed in the case of gas-phase Ab, but also excitations from the substrate, which lead to cationic or anionic resonance states in the molecule. The first one refers to a hole in the substrate valence bands that quenches an electron from the occupied molecular states, so charge is being transferred from the molecule to the surface (HOMO→substrate, h^+_{HOMO}) and the second one refers to the case where the unoccupied molecular orbitals pick up an excited electron from the conduction bands of the metal (substrate→LUMO, e^-_{LUMO}). In both cases the net charge on the molecule changes. For the gas-phase molecule this would correspond to creating the molecular cation or anion.

Fig 11.3 presents the ground- and excited-state energies of E-Azobenzene on Ag(111) as a function of vertical distance from the surface. The ground-state energetics and geometry are calculated with DFT+vdw^{surf}. At every such geometry four different leΔSCF calculations have been performed to yield the pictured excited-state energies. In these calculations the projected LUMO has been populated while depopulating the HOMO or HOMO-1 (S1, n$\rightarrow \pi^*$ and S2, $\pi \rightarrow \pi^*$), or the LUMO or HOMO occupations have been changed while adapting the Fermi level accordingly (e^-_{LUMO} and h^+_{HOMO}).

Far away from the surface, at distances above 6 Å and beyond, the intramolecular excitations approach the gas-phase limit (gas-phase S1 n$\rightarrow \pi^*$: 2.27 eV , S2 $\pi \rightarrow \pi^*$: 2.75 eV , see chapter

6.4). More accurately put, the values approach the limit of an infinite free-standing molecular layer in the periodic arrangement of the employed supercell geometry, which rationalizes the remaining differences. The corresponding substrate-mediated excitations should in the limit of infinite separation into all directions approach the corresponding anion or cation energies or Ionization Potential (IP) and Electron Affinity (EA) of the molecule as predicted by the PBE functional (IP: 7.82 eV, EA: 1.06 eV [197]). The corresponding value for the IP above 6 Å distance from the surface is 4.37 eV. The value of the electron affinity can be calculated as the difference of the work function (including the potential drop due to the free standing overlayer this amounts to 4.21 eV [197]) and the e^-_{LUMO} state and therefore amounts to 2.36 eV. The substrate-mediated excitation energies are very sensistive to the distance from the substrate and to the interactions with the neighbouring Ab images, as well as the image of the substrate above[4], which rationalizes the rather large remaining deviations to the gas-phase values. This sensitivity stems from the excess charge on the molecule interacting via long-range Coulomb forces with the electron density of the substrate and the neighbouring molecules (induction effects).

When approaching the surface, the intramolecular excitations do not change significantly, whereas e^-_{LUMO} and h^+_{HOMO} are strongly renormalized. Close to the equilibrium geometry the anionic resonance state is only 0.38 eV above the ground state and the cationic resonance state is at 2.52 eV above the ground state. This effect owes to the localized charge on the molecule strongly interacting with the substrate via classical Coulomb interactions; the substrate steadily builds up an image charge at closer distances. Correspondingly, the energy of back-transfer or electron-hole quenching is reduced accordingly. This difference in the renormalization behaviour of intramolecular (or optical excitations) and charge-transfer (or ionic transitions) is well known. It can be very well described at the level of many-body perturbation theory [306, 319, 320], but also with a ΔSCF-type description, whereas linear response TD-DFT treatments fail to capture this effect. It is remarkable that employing such an approximate scheme as leΔSCF, the main physical effects of substrate polarization and state renormalization can in fact be captured.

11.5 Conclusions to Chapter 11 and Outlook

In this chapter an alternative implementation of the leΔSCF method of Gavnholt *et al.* [29] and necessary modifications to enable its application to complex metal-surface chemical reactions have been presented. The current method provides a computationally efficient way to describe low-lying localized excited states in large periodic systems. The correct calculation of molecular reference states that are used to generate the resonances assures a consistent quality description along reaction paths and also sets the connection to simple ΔSCF in the limit of vanishing hybridization between adsorbate and metal substrate. For the example of Azobenzene at a Ag(111) metal surface it was illustrated that the approach yields an account of the stabilization of different types of excitations due the the interaction of large excited-state dipoles or excess charge monopoles with the substrate image charge. As such the method at least qualitatively describes the most important physical effects that arise from the interaction with the electronic structure and charge distributions at the metal surface, and thus allows to discuss surface effects on the molecular functionality beyond the level of surface-modified adsorbate geometries.

The approach presented in this chapter, although approximate in nature, enables a semi-quantitative account of excited-state properties for large-scale systems and might prove to be useful specifically for large hybrid organic/metallic interfaces. While it may never replace theo-

[4]The employed vacuum slab was about 22 Å, therefore a higher vertical distance would lower the excitation energies again.

retically rigorous methods, such as TD-DFT or many-body perturbation theory, it fills a gap in the current methodological spectrum, where these more accurate methods are not yet applicable due to their computational expense or where currently used approximations in the xc-kernel or self-energy description in these methods cause a lack of consistent accuracy. Independent from the development of these schemes there will always be the need for very efficient treatments that allow fast screening on a qualitative or, when solid benchmarking is done, possibly semi-quantitative level.

In the specific case of the photo-isomerization dynamics of metal adsorbed Azobenzenes the leΔSCF method can provide a consistent quality approach to the description of the excited-state potential energy surfaces believed to be involved in the mechanism. The obvious next step that will be pursued in chapter 12 is the investigation of the substrate effect on the excited-state potential energy surfaces of adsorbed Azobenzenes and the entailed dynamics.

12 Electronic Excited States of Azobenzene on Ag(111) and Au(111)

On the basis of the structural model and understanding gained in part III of this thesis and the methodology established in chapters 6 and 11, in this chapter the excited-state potential energy surfaces of adsorbed Azobenzene will be studied. Already on this level, interesting implications on the dynamics can be identified. Section 12.2 has been published in *The Journal of Chemical Physics* [294] alongside with main parts of the previous chapter.

12.1 What Can We Learn from Static Excited State Potential Energy Surfaces?

With the leΔSCF methodology established in the previous chapter we can now study the excited state dynamics that determines the successful photo-induced switching of TBA on Au(111) in contrast to the non-switching of Azobenzene. A first step in this should be a detailed analysis of the excited-state potential energy surfaces involved in this process. Although the leΔSCF method enables such an investigation and the important qualitative effects should be captured, interpreting this data will be an intricate task. The reason for this is the fact that low-lying intramolecular excitations, as well as possibly relevant substrate-mediated excitations will lie in a continuum of substrate excitations and therefore do not fit into the classical definition of an isolated potential energy surface. The minimal energy gaps between such different excitations will efficiently lead to exciton-recombination due to non-adiabatic transitions between these states. This omnipresent non-adiabaticity motivates to think in terms of a general, constant electronic friction leading to decreased excited-state lifetime and energy dissipation from an effective decoupled excited-state potential energy surface [321] and the hope exists that the nuclear motion will dominantly follow a dynamics along such effective PESs.

Mapping such excited-state PESs along important degrees of freedom one can study the changes with respect to the gas-phase PES analogues and discuss the corresponding implications in the context of the two hitherto proposed mechanisms, namely the mechanism based on intramolecular excitations as it is discussed for gas-phase photoisomerization or the substrate-mediated mechanism put forward by Wolf, Tegeder, and coworkers [26, 28].

In the context of intramolecular excitations already changes in the vertical excitation energies from the equilibrium geometries can sensitively modify the switching efficiency. One of the reasons why Azobenzene and diazenes in general are very commonly used units in functional molecules is the fact that back and forth switching between the two involved (meta-)stable states is induced by two very different wavelengths. Correspondingly the isomerization efficiency in solvent is very high, with about 90% of the molecules being switched upon light-irradiation at 444 nm [132]. The smaller the energetic separation between the two isomerization-inducing resonances is, the higher the probability of a simultaneously induced back-reaction. Therefore, the photo-stationary state will be at a much lower isomer ratio. The unbalanced way the

different ground state structures of Ab and TBA were affected by surface adsorption (see chapter 10) suggests that this could also be the case for the excited states and correspondingly could contribute to a reduced switching efficiency, as it is observed for TBA on Au(111) [26, 243].

In the context of a substrate-mediated charge-resonant switching process, the actual curvature and shape of the excited-state potential energy surfaces close to the equilibrium ground-state geometries (Franck-Condon region) will play a crucial role in determining the efficiency of the process. The excited-state lifetime of the adsorbate is strongly reduced by the non-adiabatic friction from the substrate degrees of freedom and premature de-excitation within a very short time window will occur. The success of a switching event depends then crucially on the amount of kinetic energy that can be gained within this time window, where the molecular motion is governed by the electronically excited state, and on wether this energy is sufficient to overcome the ground-state barrier [252, 254–256]. Therefore, significant gradients in the Franck-Condon region and strong activation of a few vibrational modes will be a necessary prerequisite to ensure a high switching rate. In any case, the switching process for TBA on Au(111) is, in terms of quantum yield or cross section, orders of magnitude less efficient then the isomerization in gas-phase or solvent. The high photon fluences that are necessary to induce a significant switching rate suggests that the switching process delicately depends on an ideal initial distribution of vibrational quanta within vibrational modes that drive the switching motion. This is somewhat supported by the strong temperature dependence of the photoswitching cross section. [26]

Computational Details

In this chapter excited-state energies of the minimum energy paths along the rotation and inversion degree of freedom for Ab and TBA on Ag(111) and Au (111) will be presented. In the case of intramolecular excited states (section 12.2), the corresponding geometries are the ones presented in chapter 10, optimized with the DFT+vdw(TS) approach. In the case of the substrate-mediated excitations geometries along these minimum energy paths have been reoptimized using the DFT+vdw$^{\text{surf}}$ approach. It can be assumed that this apparent inconsistency (resulting from the corresponding data being computed at different stages of the thesis work) will not affect the interpretation of the data. Already in chapter 10 it was shown that the change in relative energetics upon inclusion of the many-body collective substrate response is minimal.

The electronic structure convergence criteria employed here are the same as explained in chapter 8, with the only difference of an increased number of unoccupied states that are included in the calculation to ensure a large band space from which the leΔSCF resonance state is constructed. Excitation energy convergence with respect to the number of virtual bands has been assured. The gas-phase reference states have been calculated from the molecular adsorbate geometries in the same supercell geometries and at the same computational settings as the slab calculations with the only difference that the substrate has been removed. Different reference states ϕ_c (cf. chapter 11) have been used for the different leΔSCF excited-state calculations. In the case of the S1 (n$\rightarrow \pi^*$) excitation and the anionic resonance state (e^-_{LUMO}) in which an additional electron is transferred to the projected LUMO of the molecule, the simple ΔSCF gas-phase reference state has been taken from a converged set of S1 excited-state orbitals. Equally, for the S2 ($\pi \rightarrow \pi^*$) excitation the reference state has been taken from a corresponding simple ΔSCF S2 converged set of orbitals. For the cationic resonance state (h^+_{HOMO}), the reference orbitals were calculated from a converged set of orbitals for a molecular system where one electron has been removed from the HOMO, corresponding to a cation. The effective molecular charge of the molecule in this supercell has been counterbalanced by a homogenous charge background. In the case of the ionic resonances, the additional or missing electron in the supercell has been counterbalanced by a corresponding readjustment of the Fermi level. The

error that is assumed to be introduced by this approach tends to zero at large electron numbers and is believed to be negligible at these slab sizes.

The ground-state occupancies of the projected states presented below have been calculated from the integral over the corresponding molecular orbital projected density-of-states up to the Fermi level.

12.2 Intramolecular Excited States

Figures 12.1 and 12.2 reproduce the ground-state paths of Azobenzene on Ag(111) and Au(111) following rotation and inversion. As has been shown in chapter 10, the barrier along inversion is almost unchanged, whereas the rotational barrier is strongly modified. Compared to the gas-phase case, the stability of the Z-Ab isomer is drastically reduced from a basin depth of 1 eV to 0.05 eV or 0.38 eV at Ag(111) and Au(111), respectively [285]. In the context of photo-induced E→Z isomerization, this implies that after deexcitation hot molecules on Ag(111) are liable to thermal re-isomerization to the E-Ab isomer. The bottom panels of Figs. 12.1 and 12.2 show the integrated ground-state occupancies of the projected gas-phase reference orbitals corresponding to the HOMO and LUMO of Azobenzene. For E-Ab and Z-Ab, as well as following geometries along the inversion degree of freedom no considerable charge is added to or withdrawn from these frontier orbitals on Au(111) (cf. Fig. 12.2 on the right). This indicates that the bonding in these molecular geometries is mainly physisorptive. Following the inversion isomerization of Azobenzene on Ag(111) (cf. Fig. 12.1 on the right), we obtain a very similar picture, although the Z-Ab isomer already shows some charge transfer in the ground state. In contrast, following rotation we see that on both surfaces around mid-rotation the LUMO is more than half occupied and the HOMO loses considerable occupation. This is due to an orbital degeneracy of HOMO and LUMO at this point, which exists independent of metal surface adsorption. This leads to the formation of a strongly chemisorbed species at this point, further rationalising the ground state barrier reduction. The shift of the Z-Ab minimum towards higher ω angles (44°) on Ag(111) together with the significant population of the LUMO creates a 'semi-chemisorbed' species at this geometry.

The leΔSCF^{EX} method calculates the first and second excited states of these surface systems by adding an electron to the region of Hilbert space corresponding to the Ab gas-phase LUMO and removing an electron from HOMO or HOMO-1, respectively. The corresponding excited-state curves, cf. Figs. 12.1 and 12.2, along both degrees of freedom show very similar overall topologies compared to the respective gas-phase case. When following inversion on Ag(111) and Au(111), the S1 state is almost unchanged in comparison to gas-phase Azobenzene. A significant lowering of the excitation energy occurs only for geometries close to the Z-Ab minimum. For rotational isomerization, S1 state energies around mid-rotation are reduced simultaneously with the barrier reduction in the ground state, while excitations close to the equilibrium geometries are almost unchanged. The systematic downshift of the S2 state corresponds to a shift of about 1 eV on both coinage metal surfaces all along the pathway, except around the mainly physisorbed E-Ab geometry. Two very important features for the isomerization mechanism in gas-phase are the state-crossings between S0 and S1 at mid-rotation, and between S1 and S2 close to the E-Ab minimum. Both can, in principle, still be observed, suggesting that an intramolecular isomerization mechanism analogous to the gas-phase could also prevail at the surface.

As most intriguing features of surface adsorption, a stronger lowering of the S2 state compared to S1, and a stronger lowering of excitations for all geometries away from the E-Ab equilibrium structure is observed. Both effects can be rationalized by the interaction of the molecular dipole with the image charge that is induced in the underlying metal substrate during

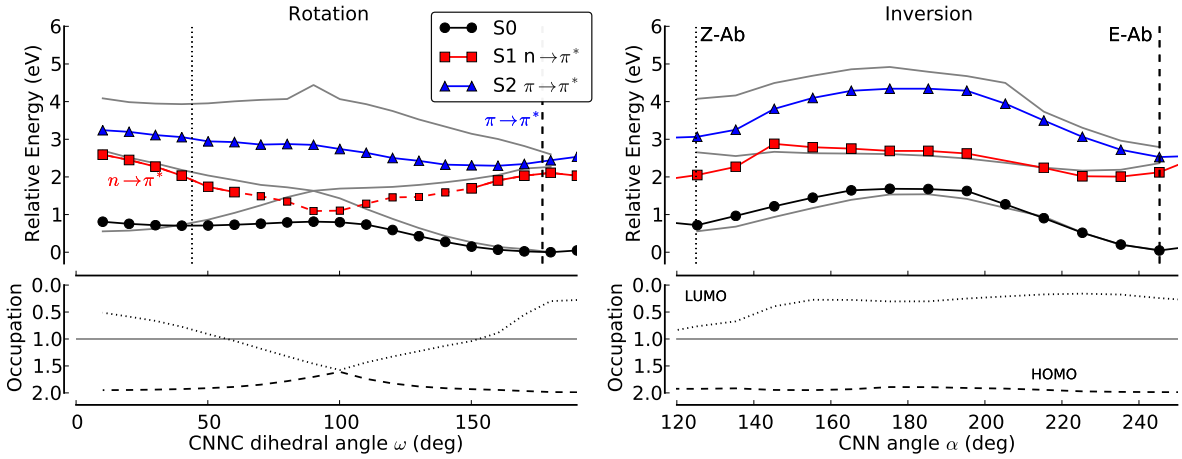

Figure 12.1: Upper panels: Minimum-energy paths of Azobenzene adsorbed on Ag(111) following rotation (left) or inversion (right). Shown are the ground-state energy (black), the first (S1, red), and second (S2, blue) excited states calculated with leΔSCF, as well as the corresponding gas-phase potential energy curves (in gray) calculated with ΔSCF. Regions marked with dashes are of increased inaccuracy due to methodological restrictions further outlined in the text. Vertical dashed and dotted lines on the sides depict the position of E-Ab and Z-Ab minima for the adsorbed molecule. Lower panels: For both degrees of freedom, rotation and inversion, the integrated occupation of the projected gas-phase HOMO (dashed line) and LUMO (dotted line) in the ground state are shown. The horizontal line marks half filling of an orbital.

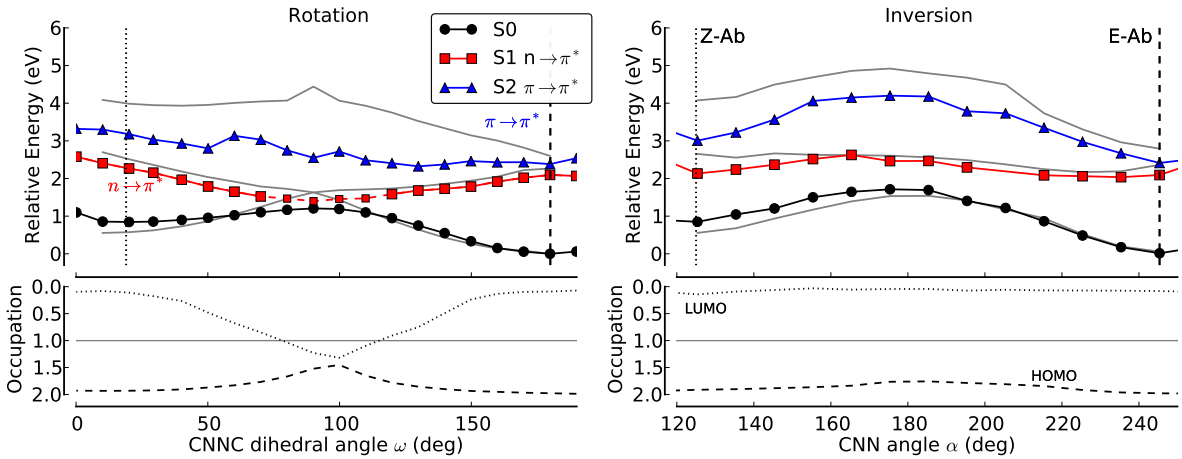

Figure 12.2: Same as Fig. 12.1, but for Azobenzene on Au(111).

Table 12.1: Calculated vertical excitation energies (in eV) for the first Singlet excited state of Z-Ab (S1) and the second Singlet excited state of E-Ab (S2), as well as the difference between them. Reference values shown are taken from experiments in solvent [132, 147] and from high-level quantum chemical (RI-CC2) calculations for the isolated molecule [195].

	Z-Ab S1	E-Ab S2	Energy Difference
Exp.[a]	2.87/2.92	3.89/4.12	1.02/1.2
CC2 @gas[b]	3.00	4.07	1.07
ΔSCF-B3LYP @gas[b]	2.30	3.33	1.03
ΔSCF-PBE @gas[b]	2.10	2.98	0.88
leΔSCF-PBE @Ag(111)	2.03	2.44	0.41
leΔSCF-PBE @Au(111)	2.27	2.38	0.11

[a]: Rau [132] and Andersson *et al.* [147], [b]: Maurer and Reuter [195]

adsorption. Azobenzene in the planar trans configuration shows no significant dipole orthogonal to the surface in the ground and both excited states. Yet, following the isomerization pathways towards the non-planar Z-Ab isomer, the z-component of the dipole in the ground state increases significantly to a gas-phase value of 3.0 Debye (D) [1]. The corresponding excited-state dipole moments for gas-phase Z-Ab are 2.3 D and 4.3 D for S1 and S2, respectively. The stronger polarisation of the S2 excited state thus leads to a stronger interaction of the molecular dipole with the substrate image charge and explains the particularly pronounced lowering of the S2 PES upon adsorption obtained in the leΔSCF^{EX} calculations. An important point to mention here is that the variational treatment in leΔSCF and ΔSCF approaches enables such an image charge build-up due to polarisation effects (opposed to lrTD-DFT treatments), although it should be emphasized again at this point that this is unlikely a quantitative account.

Another effect that modifies excited-state behavior is the hybridization of molecular with surface states. A marker for the strength of hybridization is the change in ground-state occupation of the frontier orbitals, which is found to be much more pronounced for Ab adsorbed on Ag(111) than on Au(111). In regions where orbitals show occupancies very different from the gas-phase, e.g. Z-Ab at Ag(111), we obtain PES changes that are more significant than for regions where occupancies do not change drastically. This effect is especially strong around mid-rotation, where the ground-state occupation of the LUMO already increases beyond one electron on both surfaces. This prohibits the full transfer of one further electron into the LUMO in the leΔSCF^{EX} excited-state calculations and we instead only perform these calculations by enforcing a full two-electron occupation of the LUMO. In Figs. 12.1 and 12.2 these regions are marked with dashed lines to emphasize the expected increased uncertainty due to the concomitant violation of the excitation constraint. These parts of the S1 curves can only serve as an upper estimate to the actual PES topology and attest that such situations of strong hybridization and charge transfer represent a clear limitation to the leΔSCF approach.

Nevertheless, even when only taking them qualitatively, the obtained results clearly show that an explicit treatment of hybridization, charge transfer and image charge effects is necessary to appropriately describe ground- and excited-state PESs of a functional molecule like Azobenzene when adsorbed at metal surfaces. Investigating Ab in a van-der-Waals potential to merely mimick the effect of surface-modified molecular geometries on the switching function, Floß *et al.* [190] recently reported only a small increase in conversion times and decrease of photo-yield

[1] The values for the molecular dipole have been taken from the calculations on the isolated Ab molecule presented in chapter 6 of this thesis.

compared to the gas-phase, while otherwise the photo-isomerization was unaffected. Without yet embarking on actual dynamical simulations, the leΔSCF-obtained PES topologies already indicate that much larger effects are induced by the metal electronic structure. Notably this is the image charge induced lowering of excited-state PESs, which due to the varying degree of state polarization and molecular dipole moment does not occur globally, but differentially "skews" individual state topologies and vertical excitation energies. For the present system this leads to a strong lowering of the S2 state particularly around the Z-Ab geometry.

By itself this image-charge lowering might already rationalize a significantly reduced switching efficiency of the traditional intra-molecular gas-phase isomerization mechanism at the surface: This mechanism proceeds via initial excitation to S2 and fast population transfer to S1 for the E→Z isomerization, as the direct transition to S1 is symmetry forbidden in the E-Ab geometry. The back-reaction Z→E instead involves direct excitation to S1. In the gas-phase the vertical excitation energies for the two reactions differ substantially (cf. Table 12.1) and allow the two isomerizations to be selectively induced by light with two largely differing wave lengths. In contrast, at the surface the leΔSCF^{EX} results suggest that the selective image-charge induced S2 lowering reduces this difference for the two transitions substantially. While in the gas-phase it amounts to more than 1 eV, particularly at Au(111) the difference between E-Ab S2 and Z-Ab S1 reduces to 0.11 eV. Considering an additional state broadening at the surface, this proximity of the two different excitations alone might then already cause a significant loss of switching efficiency via this intra-molecular mechanism as the forward and backward isomerization can simply no longer be selectively triggered. Indeed it has been observed experimentally that the fraction of Z-TBA molecules at the photostationary state is significantly reduced compared to the gas-phase [243], while at the same time the isomerization efficiency of Z-to-E isomerization has become less efficient than the E-to-Z reaction, which is the opposite behavior of the gas-phase situation.

At least qualitatively, these findings should also be robust against the other clear limitation of leΔSCF, namely the one imposed by the employed approximate DFT functional. Already in the gas-phase GGA-PBE based ΔSCF (but also GGA-PBE based lrTD-DFT) severely underestimated absolute vertical excitation energies for Azobenzene compared to accurate quantum-chemical (RI-CC2) calculations [195]. These were primarily global shifts of entire respective excited-state PESs though and largely left topological features like barriers unchanged. Addition of exact exchange can remedy these self-interaction induced shortcomings of the semi-local functional for gas-phase Azobenzene [195]. However, simultaneously it would remove much of the balanced error cancellation in the description of the metal substrate [222, 224]. For metal-surface adsorption there is at present no feasible and equally efficient alternative to semi-local DFT. Starting from the, at least, topologically correct gas-phase PES, leΔSCF merely adds the effect of surface hybridization and polarization. GGA-PBE based leΔSCF excited-state PESs thus have to be seen in light of the self-interaction induced overpolarizability and wrong relative positions of molecular and substrate electronic states, which will affect the observed image charge and hybridization effects upon adsorption. While thus certainly not quantitative, the approach still enables an effective first account of the electronic structure and charge distributions at the metal surface and is thus a viable means to generate further insight into the intricacies of surface functionality of large organic molecules like Azobenzene.

12.3 Substrate-Mediated Excited States

The requirements of potential energy landscapes to be able to support a successful photoswitching mechanism, as the one described by Wolf and Tegeder [28] are very different from the ones

that apply to the mechanism known from gas-phase. A switching function depending on the kinetic energy that can maximally be gained in a short excited-state life time window is determined by an efficient coupling between electronic and nuclear degrees of freedom immediately after vertical excitation from the equilibrium structure and a ground-state barrier that ideally balances between it being small enough to be overcome, but large enough to guarantee sufficient bistability. Therefore, certain changes to the electronic structure and the energy landscape that occur upon adsorption can be of value to the molecular function, whereas in context of an intramolecular process such changes are to be avoided as much as possible. Substrate-mediated ionic resonances have to be specifically analyzed for the following features: significant gradients on the excited-state PESs at the Franck-Condon (FC) points of E and Z-Ab, a barrierless path towards the transition state, and a kinetic excess energy that exceeds the ground state barrier, but does not lead to immediate thermal reisomerization.

The starting point for an investigation of the adsorbed PES topology of ionic resonances are the cation and anion PESs of the gas-phase molecule. Corresponding gas-phase calculations have been reported by Füchsel *et al.* [175] and Leyssner *et al.* [241] in the context of STM- and photo-induced Azobenzene switching on metal surfaces. STM-induced switching can be triggered with negative and positive bias voltage. Therefore, electron removal ('cationic resonance') and electron attachment ('anionic resonance') to the molecule are both viable mechanisms, whereas in the case of photo-induced switching the possibility of an anionic resonance as dominating excitation mechanism can be excluded by experiment [13, 28]. The above mentioned authors report DFT-based anionic and cationic potential energy surfaces of Azobenzene and TBA along rotation and inversion. Just as in the ground-state, these PES show two meta-stable states at very similar positions, although slightly shifted towards smaller α bending angles and ω dihedral angles, closer to the mid-rotation point. Correspondingly, both ionic states show significant gradients at the FC structures of E and Z-Ab and TBA. Additionally upon electron removal or attachment, the rotation and inversion barriers are significantly reduced, although still existent. In general, the ionic surfaces are less corrugated and specifically the cationic PES is much more shallow. It can therefore be argued that in both ionic molecular states, the prerequisites to a substrate-mediated excitation mechanism are in principle given and if only minimal changes to these PESs apply upon adsorption, photo-induced switching *à la* Wolf-Tegeder can be feasible. The absence of these gas-phase features in ions of tetra-*tert*-butyl-stilbene (TBS) has been interpreted as a possible rationalization for the lack of surface-mounted switching for this compound [241].

Fig. 12.3 presents the calculated cationic (in blue) and anionic (in red) resonance states of Ab adsorbed to Au(111) along the minimum energy paths following rotation and inversion. Following the inversion coordinate the two ionic states show two minima around E and Z-Ab and a reduced, but still significant barrier compared to the gas-phase. The here presented excitation energies for the cationic and anionic resonance represent the lowest possibly found energies when exciting from (or to) the Fermi level. Corresponding excitations can also happen at higher photon energies albeit with more excess energy. The cationic resonance is found at higher excitation energy throughout the PES regime considered. At the E-Ab geometry, the corresponding energies (h^+: 1.65 eV, e^-: 1.39 eV) are close to the experimentally found 2PPE molecular resonances (HOMO: 1.77 eV, LUMO: 1.68 eV, absolute energy difference from the Fermi level [23]), albeit at a larger deviation for the excitation to the unoccupied state, owing to the inherent self-interaction in the semi-local DFT based calculations (and possibly also to the difference between the high-coverage situation in experiment and the low-coverage assumed in the here performed calculations). The excited state PESs along rotation show minima at the mid-rotation point, similar to the S1 intramolecular excited state. The gradients around the E and Z-Ab FC points on the excited states are significant in the case of Z-Ab, but minimal

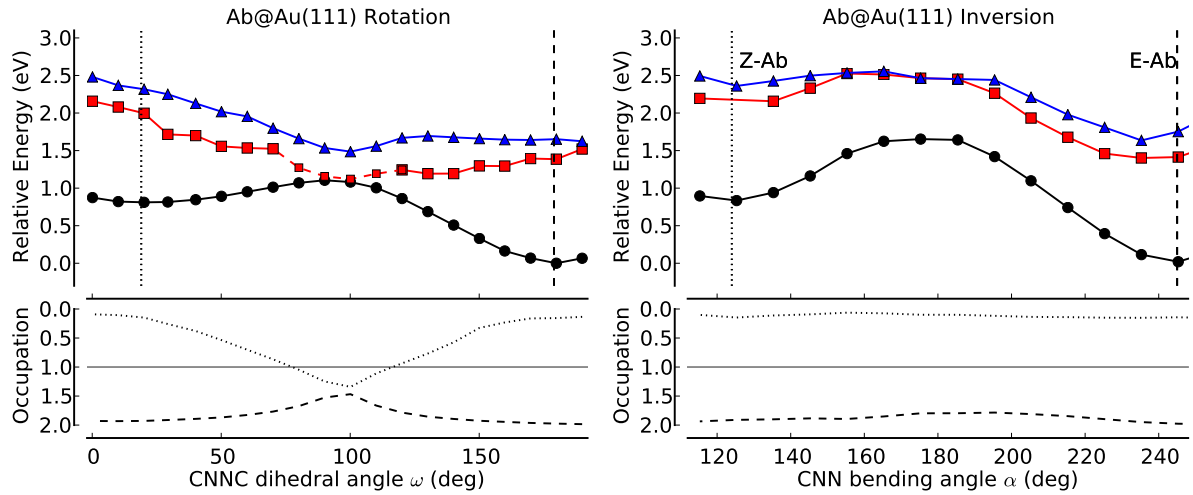

Figure 12.3: Upper panel: Calculated minimum-energy paths of Azobenzene adsorbed on Au(111) following rotation (left) and inversion (right) degrees of freedom. Shown are the ground-state PES (black), an anionic resonance where an electron has been added to the LUMO (red), and a cationic resonance where an electron has been withdrawn from the HOMO of the molecule (S2, blue). Regions marked with dashes are of increased inaccuracy due to methodological restrictions further outlined in the text. Vertical dashed and dotted lines on the sides depict the position of E-Ab and Z-Ab minima for the adsorbed molecule. Bottom panel: See Fig. 12.1 for details.

for E-Ab. The cationic resonance exhibits furthermore an extended plateau region towards the mid-rotation point. It should also be mentioned that, similar to what was found for the intramolecular S1 excitation for the adsorbed molecule, the anionic resonance description is limited by the intrinsic charge-transfer to the LUMO in the ground state at mid-rotation; the corresponding region is marked by dashed lines in Fig. 12.3. In summary, the calculations indicate that along rotation an isomerization could occur barrierless into the ground-state, yet the vibrational activation due to excitation of the E-Ab isomer is very small.

It can be rather insightful to compare the adsorption effect on the ionic PESs on different substrates. When going to a more reactive substrate such as a Ag(111) surface (see Fig. 12.4), strong changes to the excited PESs are apparent. The corresponding paths of cationic and anionic resonance states along rotation are strongly modified, as compared to the gas-phase or to the molecule adsorbed on a Au(111) surface. Owing to the strong adsorption, almost everywhere along the path the LUMO is more than half-filled in the ground state and therefore the anionic resonance excitation constraint in leΔSCF can not be fully satisfied. Correspondingly, the anionic resonance state is systematically downshifted and coincides with the ground state over large portions of the rotational pathway. However and more importantly, the cationic resonance state is systematically shifted upwards on Ag(111) as compared to Au(111) and appears more corrugated with a pronounced minimum at the mid-rotation point. At both FC regions of E and Z-Ab on the cationic resonance state, there is a significant gradient towards the mid-rotation point.

These PES differences between Ag and Au can be understood in terms of the differences in electronegativity (or equivalently in electron affinity) of the underlying surfaces. The electronegativity of the Au surface is higher than that of the Ag surface. Therefore, electrons are harder to detach from the Au surface than from the Ag surface, or in other words, adding electrons to

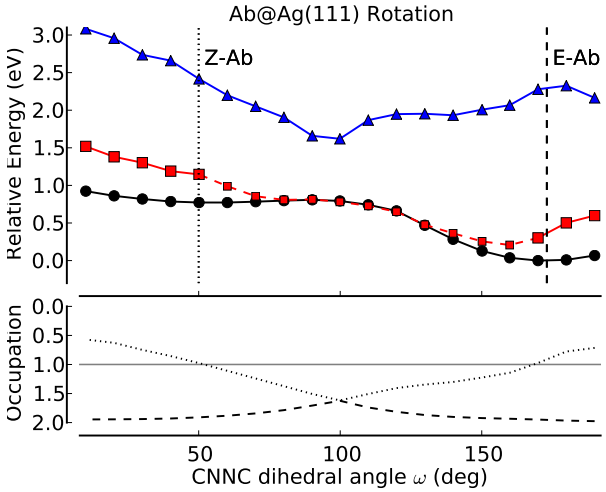

Figure 12.4: Upper panel: Calculated minimum-energy path of Azobenzene adsorbed on Ag(111) following the rotation degree of freedom. Shown are the ground-state PES (black), an anionic resonance where an electron has been added to the LUMO (red), and a cationic resonance where an electron has been withdrawn from the HOMO of the molecule (S2, blue). Regions marked with dashes are of increased inaccuracy due to methodological restrictions further outlined in the text. Vertical dashed and dotted lines on the sides depict the position of E-Ab and Z-Ab minima for the adsorbed molecule. Bottom panel: See Fig. 12.1 for details.

a gold surface is connected to a smaller energetic penalty than for the case of silver. When inducing a cationic resonance state, an electron from the molecule is transferred to the substrate. For the above reasons, the energy that is necessary to do this is higher for Ag than for Au. However, in case of an anionic resonance the situation is reversed. The more electronegative a surface is, the higher the energetic penalty to withdraw electrons from it. Correspondingly, the energy associated with the anionic resonance on the molecule is higher for E-Ab on Au(111) than on Ag(111). This does, however, not hold for the resonances at mid-rotation point. In both cases the chemical bond to the surface efficiently transfers electrons from the substrate to the LUMO of the molecule. Correspondingly, the ground state is already, to some extent, an 'anionic resonance' state; both are energetically equivalent. The closer this charge transfer in the ground state is to a full electron, the smaller the energetic difference between the ground state and the cationic resonance can be. Detaching an electron at the mid-rotation point from the HOMO, effectively yields an S1 ($n \rightarrow \pi^*$) excited Azobenzene molecule. The corresponding S1 excitation energy at mid-rotation, due to the orbital degeneracy, is zero in the gas-phase. The closer the charge-state in the ground state is to the gas-phase, the smaller is the energetic gap between the ground (or anionic) state and the cationic state. The corresponding minimum at mid-rotation on the cationic state, that is observed for the adsorbed species stands in contrast to the barrier exhibited at this point for the gas-phase molecules. It enters due to the significant 'S1' intramolecular excitation character at this point that stems from the charge-transfer in the ground-state. Correspondingly, at this point, the hybridization with the surface completely inverts the topology of the cationic resonance state.

From the above presented PESs for adsorbed Azobenzene, one can infer that the rotational pathway and the corresponding wagging mode of the phenyl rings could be the main dynamical degrees of freedom for isomerization upon photoexcitation. This wagging mode might be efficiently activated by a cationic resonance of the Ab molecule on Ag(111). However, a subsequent

isomerization to the Z-Ab geometry will immediately be followed by a thermal reisomerization. The reason for that is the large amount of excess kinetic energy due to the excitation. When measuring the energy difference between the E-Ab FC region on the cationic resonance state and the ground-state rotational barrier, 1.3 eV excess energy have to be withdrawn by the molecular and substrate degrees of freedom during the isomerization event, otherwise thermal reisomerization to the E-Ab state is imminent. In the case of E-Ab on Au(111) this excess energy only amounts to about 0.4 eV. On the other hand, there is almost no gradient in the cationic resonance state that would induce a corresponding nuclear dynamics towards the Z-Ab isomer. Quite ironically, whereas Azobenzene adsorbed on Ag(111) fulfills the necessary requirements to efficiently activate nuclear motion upon excitation, it might not exhibit the necessary ground-state barrier to maintain a stable Z-Ab state. In contrast in the case of Ab on Au(111) sufficient stability is accompanied by very inefficient mode activation. The inspection of the static PESs therefore suggests that both isomerization processes can at most be highly inefficient.

Introducing bulky spacer groups has enabled switching for the TBA molecule adsorbed on Au(111) [13, 21]. The corresponding ionic resonance states along the rotational transition pathway are shown in Fig. 12.5. The ground-state barrier, similarly as for Ab on Au(111), exhibits a chemisorbed state at mid-rotation and a reduced barrier height (see chapter 10). Nevertheless, the Z-TBA state can be assumed to be sufficiently stable at ambient conditions to prevent immediate thermal reisomerization upon photoswitching. The thermal barrier shows a broad plateau region at mid-rotation, which can be understood in terms of the geometric details of switching: While reducing the dihedral angle ω, the azo-bridge adsorbs more closely to the surface and the substituted phenyl rings maximize dispersion interactions with the substrate for as long as the energetic penalty due to molecule deformation does not exceed the energy gain. After the mid-rotation barrier, one phenyl ring is lifted from the surface and within a range of 20 degree in ω is close enough to the other phenyl ring to be stabilized by van der Waals interactions from π-stacking and the *tert*-butyl side groups. The corresponding energy gain gives the additional stability to the Z-TBA basin as compared to adsorbed Z-Ab. As was the case for Ab on Au(111), the anionic resonance state only coincides with the ground state at the chemisorbed state. Both excited states exhibit a barrierless transition from E-Ab to the mid-rotation point and a minimum at the latter point. However, from the Z-TBA state towards the mid-rotation point, an additional very shallow minimum can be found on both excited states. Considering the accuracy of the employed approach, one may only speak of a plateau region. Around the E-TBA FC region on the cationic resonance state, a significant gradient towards rotation can be found, which is not the case for the Z-TBA FC point. This situation is completely opposite to what was found for Azobenzene adsorbed to Au(111). The excess energy between the E-TBA FC point on the cationic resonance state and the ground state barrier amounts to about 0.5 eV, which is of the order of what was also found for Ab. Summarizing the situation found for TBA isomerization when adsorbed to Au(111), all prerequisites to a substrate-mediated excitation mechanisms thus can be found.

The excited-state topologies of TBA do support the mechanism that was put forward by Tegeder *et al.* in a variety of aspects. The transition from E to Z-TBA involves almost exclusively rotational motion around the central azo-bridge, with the exception of a small, almost isoenergetic phenyl ring twisting (along β) when lifting off the phenyl ring at dihedral angles between mid-rotation and Z-TBA. The PES topology of a cationic resonance in the HOMO that is connected with this motion represents a fairly steep, barrierless descent towards the mid-rotation point. At this point, if not earlier, increased coupling with the substrate is likely to quench the already short-lived excitation and a corresponding motion will have a higher probability for crossing the ground-state barrier than for a momentum inversion to occur. The smaller gradient around the Z-TBA FC region and the correspondingly reduced vibrational activation

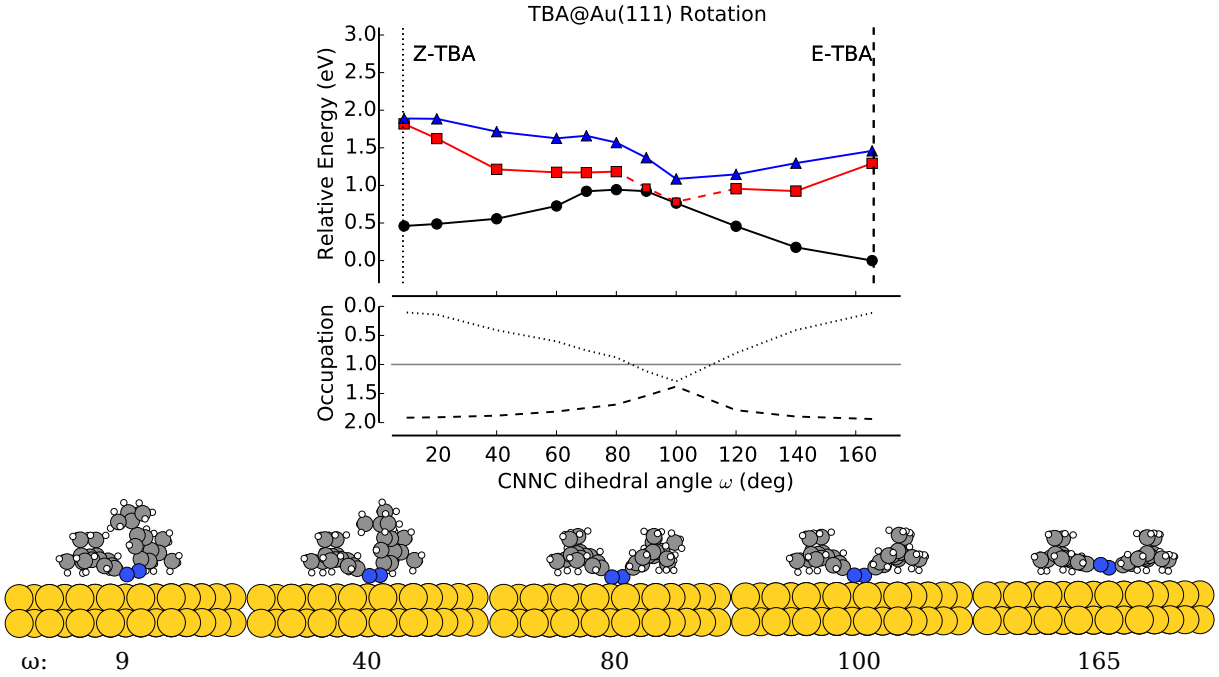

Figure 12.5: Upper panel: Calculated minimum-energy path of TBA adsorbed on Au(111) following the rotation degree of freedom. Shown are the ground-state PES (black), an anionic resonance where an electron has been added to the LUMO (red), and a cationic resonance where an electron has been withdrawn from the HOMO of the molecule (S2, blue). Regions marked with dashes are of increased inaccuracy due to methodological restrictions further outlined in the text. Vertical dashed and dotted lines on the sides depict the position of E-Ab and Z-Ab minima for the adsorbed molecule. Bottom panel: See Fig. 12.1 for details. Below the graph, selected geometries along the rotational minimum energy path are depicted.

of the rotational mode do support the experimentally found minimal photoswitching rate of the Z-TBA isomer. Furthermore, the strong vibrational dependence of the switching rate and the termal reisomerization that are observed, do not qualitatively disagree with the potential energy path that has been found here. A thermal activation of the rotational wagging mode will strongly facilitate a corresponding switching upon photo-excitation.

12.4 Conclusions to Chapter 12

In this chapter, a detailed analysis of the potential energy surfaces calculated with the leΔSCF approach (cf. chapter 11) along hitherto discussed isomerization pathways of adsorbed Ab and TBA has been conducted. The approach does in fact qualitatively account for a range of important effects on excited states that can occur upon adsorption, including electrostatic stabilization via interaction between excited-state dipoles and the substrate image charge, as well as hybridization and charge-transfer in intermediate chemisorbed geometries. Although no quantitative description can be expected from an approximate scheme like leΔSCF, the qualitative topologies of the excited states do enable a first rationalization on why switching may be more favourable on Au(111) than on Ag(111), and in a functionalized molecule (TBA) compared to the pure Azobenzene.

When assuming a photo-induced switching based on the intramolecular excitations known

from gas-phase, the unbalanced stabilization of different molecular geometries that was found in chapter 10 also affects the corresponding first and second excited states. The corresponding result is that unbalanced changes to the excited PES removes the important separation of isomerization-inducing excitation energies between E-to-Z and Z-to-E switching, and therefore reduces the maximally possible photostationary Z/E ratio and switching efficiency that can be achieved without even considering other substrate-effects. Adding to this, the small amount of photons that will excite adsorbates instead of substrate resonances in connection with the minimal lifetime of insufficiently spatially separated electron-hole pairs render a dominant role of intramolecular excitations in the adsorbed photoswitching process improbable.

On the other side, when assuming a substrate-mediated mechanism that involves electron transfer from the molecule to the substrate (or *vice versa*), the qualitative differences between excited-state topologies obtained for the differing substrates and differing molecular functionalization generally support the proposed mechanism by Wolf and Tegeder [28]. An active substrate such as Ag(111) with a significant chemisorption contribution in ground-state bonding will almost fully supress an anionic resonance to the lowest lying molecular state. Isomerization via electron detachment from the highest lying state, although maybe strongly coupled to the relevant vibrational degrees of freedom, is in turn likely to suffer from insufficient excited-state lifetime and ground-state stability. On a more inert substrate such as Au(111), due to the high substrate electronegativity, the ionic excitations are sufficiently separated from the ground state. Notwithstanding, the modifications to their PESs, due to the remaining hybridization (around mid-rotation) and differing dipole-dependent changes (around the minima), leave the corresponding excitations with only minimal vibronic coupling. Strong resonant inelastic electron tunneling might nevertheless induce the necessary excess kinetic energy to propagate the isomerization to a sufficiently thermally stable Z-Ab isomer.

One might think that introducing large functional side groups, as in TBA, might strongly increase the number of degrees of freedom that can be involved in isomerization. However, for the surface adsorbed species this might in fact serve the opposite purpose. The steric hindrance due to bulky spacer groups leaves the rotational isomerization that is induced by a vertical wagging motion of the azo-bridge the only efficient and viable single-mode motion between E and Z states. The PES topologies of the ionic resonance states that have been found for this motion support the substrate-mediated mechanism with fairly-strong vibronic coupling and overall topology. In the case of TBA, both these prerequisites coincide: A significant gradient in the excited state and a sufficient ground-state barrier strongly suggest that photo-induced motion on the excited-state pathway, even if prematurely put back to the ground-state, could be sufficient to overcome the barrier. Subsequently (or better while) the corresponding excess kinetic energy is dissipated via non-adiabatic decay channels opened through electron-hole excitations in the substrate and coupling to the phonons of the substrate. The specific effects of the side groups seem thus multi-facetted and comprise modifications to the potential energy surfaces due to geometrical changes on the azo-bridge (especially at the minima), due to modified stabilization (Z-TBA, rTS are stabilized with respect to E-TBA), and dipolar effects. The additional side groups destabilize the E-TBA isomer and therefore effectively stabilize all other structures. In consequence, the excited-state PESs are shifted downwards for the rotational transition state and the Z-TBA isomer: what was a plateau for the cationic resonance state around the E-isomer geometry in the case of Ab now shows a gradient. In addition to that, the E-isomer, due to the steric hindrance of the side groups, lies at lower ω and therefore closer to the rim of a potentially still existent plateau. At the same time, the overly strong stabilization of the Z-TBA isomer, induced by the increased vdW attraction between the side groups, pushes the excited states further down in energy at this point, thereby effectively removing the excited-state gradient that was found for Z-Ab before.

The above presented results may also help to settle the controversy over the prevalence of rotation or inversion motion during photo-isomerization. In a recent experimental study, a dominance of an inversion-based mechanism has been proposed [257]. The authors base this interpretation on the observation of a selection rule to photo-switching that applies differently to different chiral island domains of TBA on Au(111). They rationalize this effect by an initially planar linearization of one CCN bond angle α and two subsequent channels towards the Z-TBA structure. In that way, E-TBA of one racemic type may convert into a left-handed and a right-handed Z-TBA molecule by changing the handedness of the azo-bridge. As a second argument, such a pathway would additionally maximize the van der Waals interaction of both phenyl rings with the surface as much as possible during the isomerization process. The here presented ground- and excited-state potential energy curves do not support this statement. Surface adsorption only shows minimal effects on the topology of the potential energy surfaces along inversion. Motion following an excited-state inversion pathway, regardless of intramolecular or substrate-mediated, would experience a small barrier and no significant gradient that may activate the necessary vibrational modes. In constrast, upon adsorption the rotational pathway becomes the energetically most favourable in ground and excited states. Low lying vibrational modes do contribute to vertical wagging modes of the azo-bridge that may initiate a rotational motion, whereas no such low lying modes where found that contribute to asymetric phenyl inversion [199]. Owing to the covalent contribution at increasing rotational distortion, the molecular adsorption energy is maximized along the rotational pathway. In summary, the current understanding on the basis of the here presented results can only be that rotation is the dominating motion that drives the isomerization process. This does, however, not mean that bending angle motion via a breathing mode will not contribute to the dynamical process and the intramolecular energy dissipation. The corresponding chiral selectivity found by Comstock *et al.* [257] can be understood by taking a glimpse into the dynamics of the gas-phase or solvent mechanism. Weingart *et al.* [187] have found that also rotational isomerization can generate two different pro-chiral Z-Ab variants by either clockwise or anti-clockwise rotation of the azo-bridge. This finding is based on the fact that motion during isomerization is dominated by the light-weight azo-bridge. Translated to the surface situation, that could mean that during a wagging motion of the molecule, an asymetric vertical rotation of the two nitrogen atoms (much like the pedals of a bicycle when viewed from ahead) may change the corresponding handedness.

The above presented data therefore provide a detailed rationale of the geometric and electronic details that decide upon adsorbed molecular switching. Nevertheless, one should be wise enough to only take the interpetations for what they are: *a posteriori* rationalizations of experimental findings on the basis of purely static energetics. From such a study no detailed knowledge on the actual time-dependent nuclear dynamics and the underlying non-adiabatic electronic changes can be found. Such an understanding can only be obtained in an explicit *ab-initio* based molecular simulation of the switching event, which is a challenging task considering the sheer size of the system and the assoziated computational cost, and may only be done with considerable reduction in parameter space and complexity. When designing such a simulation, a full knowledge of the ground- and excited-state energetics of the relevant degrees of freedom may nevertheless very well come in handy, as will be seen in the next chapter.

13 Outlook on Explicit Excited State Dynamics Simulations

In this chapter a detailed outlook is attempted on the necessary ingredients for a simulation of the explicit non-adiabatic dynamics involved in photo-induced molecular switching on metal surfaces.

13.1 Requirements to a Dynamical Simulation of Photo-Induced Molecular Switching

Azobenzene is, in all possible variants of its function, one of the best studied molecules in chemistry. In the early days of chemistry, this owed to its great value as a chromophore in the dye industry. In our comparatively modern days, it additionally owes to the exciting photophysical and photochemical properties that can be associated with its light-absorbance. Although a plethora of spectroscopic measurements, spanning over decades, has characterized the light-response and photoisomerization in great detail (see chapter 5), a clear understanding of the detailed molecular dynamics that are associated with the switching process could only be established with *ab-initio* simulation techniques that emerged during the last 20 years[1]. The long-standing interest and large pool of experimental data has made Azobenzene or diazenes an ideal playground for the development and testing of the aforementioned methods [161, 177, 191], which have grown to standard tools in gas-phase and solvent photochemistry by now [322, 323]. In the case of surface-adsorbed photodynamics, such tools are not yet fully established. Whereas a variety of works has already applied the above mentioned tools in the description of photodynamics on insulating or semi-conducting surfaces [324, 325], corresponding tools can not fully account for the omnipresent non-adiabaticity in dynamical events on metal-surfaces [39, 326]. Nevertheless, some studies have successfully adressed a non-adiabatic description at metal surfaces [255, 327] and recent methodological improvements enabled a very accurate description of metal surface impingement of a diatomic molecule [328, 329]. On the basis of the above works, a proposal to a potential approach for surface-adsorbed Ab switching is given in this chapter.

The by now gathered experimental and computational findings regarding the photo-induced isomerization of Azobenzenes on coinage metals suggest that a potential explicit dynamical simulation can by no means be called an easy task. A full description of the dynamics involving all nuclear degrees of freedom is virtually impossible. The high computational cost, dictated by the large system size, necessicates simplifications and reductions in parameter space. A potential modelling approach also has to be able to describe the non-adiabatic interactions between adsorbate and substrate electronic degrees of freedom, which are likely to quench an excited state within a few fs. To design an approach that is both computationally efficient

[1] The understanding of the dynamical details of photo-induced isomerization can, by no means, be called complete at this point in time. It might, considering the ever growing scientific appetite for more detail, most probably never be.

and physically accurate, a careful choice of approximations has to be undertaken. In order to establish such an approach, one has to define

- the number of degrees of freedom that are necessary and the type of representation of the ground- and excited-state potential energy surfaces involved,
- the non-adiabatic propagation technique of the nuclear degrees of freedom,
- the description of the coupling between electronic states of the adsorbate and the substrate, and
- the simulation setup and initial conditions that enable to generate meaningful data and finally also the questions that can be answered with such an approach.

13.2 A Minimal Model System to Azobenzene Molecular Switching - Constructing Analytical Representations

In current explicit dynamics approaches of gas-phase molecules, the *ab-initio* energetics are often calculated on-the-fly (i.e. energy, forces, and couplings are evaluated in every time step for the corresponding atomic positions). This has become computationally tractable for small to medium-sized molecules only in recent years. Another alternative to this is to map the *ab-initio* energetics onto analytical model potentials or numerical representations of potential energy surfaces [330]. In this case the parameter space that is explicitly considered is restricted to only few dimensions ($\leq$10). However, this approach can be made more efficient by the use of internal and symmetry-adapted coordinates. In accordance with that, it has to be assumed that the isomerization dynamics are mainly governed by the active involvement of only few vibrational modes.

For the specific case of Azobenzene isomerization on coinage metals, the system size renders an on-the-fly evaluation of the DFT energetics absolutely intractable at the time. One therefore has to select a restricted set of degrees of freedom in which explicit time propagation can be performed. The absolutely minimal subset of degrees of freedom (DOF), in which a photo-induced switching of gas-phase Ab can be described includes the central dihedral angle ω and the two central bending angles α and α'. Including these DOFs, such a coarse-grained model should be able to describe the central properties of the switching process, namely the pedal motion of the azo-bridge that is induced by photo-excitation and the subsequent rotational isomerization. However, the neglect of the explicit dynamics of all other nuclei will prevent the correct description of energy dissipation into other molecular degrees of freedom and therefore lead to systematically overestimated switching rates, excited state lifetimes, and also recurrence probabilities. For a more realistic description one would also have to include, in a next step, the central NN and CN bond stretches and phenyl ring twisting angles (β, β'). Nevertheless, reduction to a 3-dimensional parameter space is a tempting option, due to the efficient and simple mapping and straightforward model construction at such a low dimensionality (see Fig. 13.1).

In order to proof this statements, such a 3-dimensional model potential has been generated for the gas-phase Ab molecule. Corresponding calculations have been performed with the FHI-AIMS code employing a PBE-GGA functional and a standard 'tier2' basis set [204]. For a selected fixed set of the three angular parameters, all other DOFs have been optimized in the ground state (for more details see chapter 6 and appendix A.2). Excited-state energies have been calculated with ΔSCF on top of these ground-state geometries. From the analysis of the

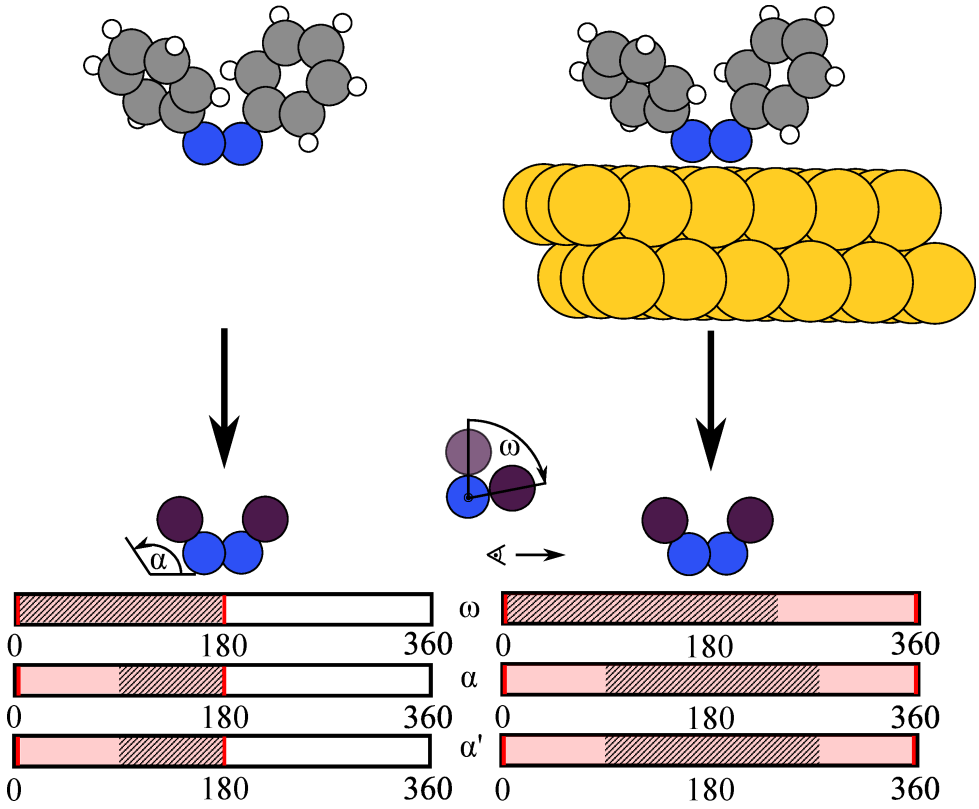

Figure 13.1: Schematic view of the reduction of explicit parameters down to the central dihedral angle ω and the two bending angles α and α'. All other coordinates are optimized for fixed (ω, α, and α') and the atoms of the phenyl ring are coarse-grained to an effective particle of equal mass, thereby moving from the description in the top to the description in the bottom of the figure. Also shown is the parameter space of ω, α, and α' that has to be considered. Only red shaded regions are symmetrically unique and only hatched regions are believed to yield energies that are relevant in the photo-isomerization process. Angles are given in degrees.

PES topologies in chapter 6 it can be savely assumed that the error due to missing excited-state optimization will not qualitatively hamper the description. Fig. 13.1 shows the region of parameter space which has been sampled. Only values of ω between 0 and 180° and α/α' between 90 and 180° have been considered due to symmetry. The high symmetry and equivalence of the two bending angles can be extensively used (see table 13.1 for the set of equivalent points on the PES). An analytical representation of the data set has been generated with multi-layered Radial Basis Functions [331] (RBF), employing the numerical library ALGLIB [332] by S. Bochkanov [2]. The accuracy of the RBF representation has been evaluated by Root Mean Square Deviation (RMSD)

$$\mathrm{RMSD} = \sqrt{\frac{1}{N}\sum_{i=1}^{N}(E_{\mathrm{ref}}(i) - E_{\mathrm{RBF}}(i))^2}, \tag{13.1}$$

where the sum runs over points of a reference test set with N=20. With 320 irreducible data points (or $16 \cdot 320$ reducible data points), the RMSD of the model potential is below 15 meV for

[2] The PESs have been constructed using 6 layers, a base radius of 60 degrees, and a tuning parameter of $\lambda = 0.0001$.

Table 13.1: Summary of equivalent points in the 3-dimensional parameter space for a given set of ω, α, α'. For every such set, 15 other equivalent sets exist.

data point	ω	α	α'
equivalent points	180-ω	360-α	α'
	180-ω	α	360-α'
	ω	360-α	360-α'
	360-ω	α	α'
	180+ω	360-α	α'
	180+ω	α	360-α'
	360-ω	360-α	360-α'
	ω	α'	α
	180-ω	360-α'	α
	180-ω	α'	360-α
	ω	360-α'	360-α
	360-ω	α'	α
	180+ω	360-α'	α
	180+ω	α'	360-α
	360-ω	360-α'	360-α

the ground state and the first excited (S1) state, and below 50 meV for the second excited state (S2), which is deemed accurate enough for a proof of principle.

Fig. 13.2 presents 2-dimensional cuts of the 3-dimensional analytical model of gas-phase Azobenzene. Going from top to bottom, one moves from ground to the excited states for the same PES cut. When going from left to right within a row, the α' value is varied for the same state. The PES cuts appear as smooth potential energy surfaces. In the ground state, the two barriers along rotation ($\omega = 90, 270$) and inversion ($\alpha = 180$) are nicely reproduced. One can also find that the overall corrugation of the surface is slowly reduced by increasing α and α'. In the extreme case of a linearised CNNC dihedral (top right plot), no corrugation along ω can be found in this PES cut. For the here presented model, derivatives with respect to the three DOFs can be evaluated numerically with minimal computational overhead. Corresponding forces are then expressed in the set of internal coordinates (ω, α, and α') and can be transformed into cartesian space via a Wilson B-matrix transformation [333]. Such a transformation can also be done for all other vector quantities, such as the non-adiabatic couplings [334]. The explicit treatment of the two heavily discussed rotation and inversion DOFs may enable a very basic description of the dynamical processes that are involved.

Similarly as in the gas-phase, one may propose a 3-dimensional model for isomerization of the surface-adsorbed species. In this case, not only the other intramolecular DOFs are optimized and neglected, but also the substrate degrees of freedom. This results in the fact that effects of hybridization and interaction with the metal electronic structure are only accounted for by their effect on the ground and excited states of the molecule; their dynamical involvement in terms of explicit non-adiabatic decay via such states is neglected. Such a harsh model might still yield a qualitatively correct description of the isomerization and excited-state lifetime, if the explicit dissipation of energy through all important channels and the excited-state lifetime reduction is captured in some fashion. This includes the dissipiation of energy via excitation of electron-hole pairs in the substrate (equivalent to the above mentioned decay) [288] and via other molecular modes or the substrate phonons. A widely used approach to account for the energy sink that electron-hole pair excitations represent, is hereby done by introducing an electronic friction force

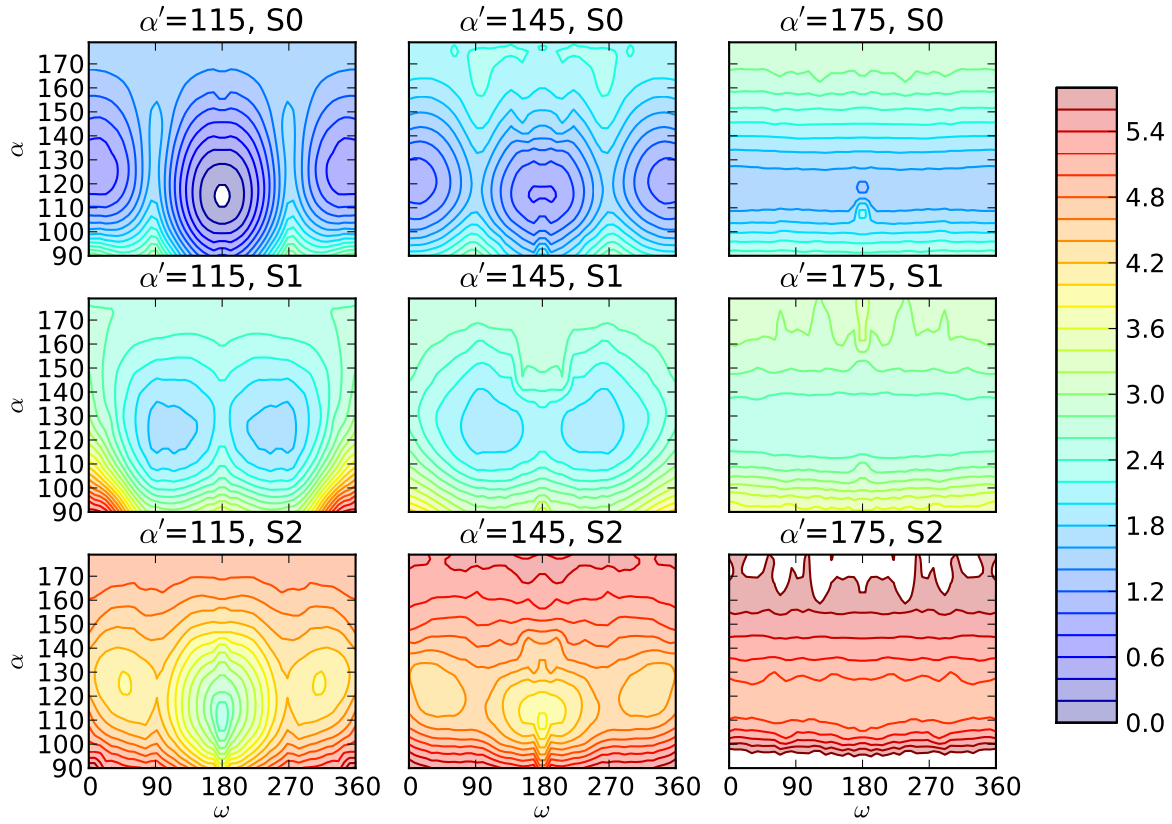

Figure 13.2: 2-dimensional PES cuts of an analytical model of gas-phase Azobenzene molecular switching. In every column contour plots of the ground (S0), first (S1), and second excited states are shown as function of α and ω, while α' is fixed to a value. Contour lines mark an energy difference of 0.2 eV. White spaces mark regions with energies above 6 eV.

[321, 335] that acts on the nuclei.

The most relevant other degree of freedom that will be important to the switching mechanism is the vertical distance from the substrate, which will sensitively control the lifetime of the excited states and may vary significantly during the isomerization. This is a DOF, which could be added to an existing model by adding an effective binding energy function to the 3-dimensional PES. In general, the necessity to explicitly include further degrees of freedom will have to be evaluated in a trial-and-error fashion, where gas-phase simulations and experimental data serve as benchmark reference.

13.3 Possible Approaches towards Non-Adiabatic Dynamics on Metal Surfaces

When simulating molecular motion of non-adiabatic processes in isolated molecules, applications employing mixed-quantum classical descriptions presently outweigh full quantum descriptions of both electrons and nuclei. These are applicable approaches if the motion of the nuclei is not dominated by quantum effects (e.g. if it is not dominated by fast, reactive hydrogen motion).

Examples for such mixed quantum-classical approaches are Ehrenfest dynamics [336] or Tully's fewest-switches surface-hopping approach (TSH) [323, 337]. Both have also already been transferred and successfully applied to the simulation of energy transfer to metal surfaces [327, 338]. However, Ehrenfest or Mean-Field dynamics is not a well suited approach for Azobenzene switching, due to its inability to describe branching processes [337], such as involved in the switching between two isomers. Here, TSH has emerged as the state-of-the-art approach and has been used extensively for the simulation of Azobenzene photoswitching [174, 177, 187]. Specifically in the context of metal surface mounted dynamics, full quantum treatment of the nuclear motion via wavepacket propagation or density-matrix methods [256] is also widely employed, however, only for strongly simplified models of the corresponding processes.

In the TSH approach [337], the nuclear motion is described in terms of classical motion on trajectories. The non-adiabaticity is captured via trajectory hops between the electronic states on which they evolve. Averaging over a large number of trajectories will yield a description equivalent to a wavepacket propagation.

The corresponding time-dependent evolution of the electronic wave fuction along this trajectory is described by the electronic Hamiltonian as it emerges from the Born-Oppenheimer separation (see eq. 2.7 in chapter 2.2) [323, 337, 339].

The electonic subsystem evolves in time following the time-dependent Schrödinger equation

$$\left(i\frac{d}{dt} - \hat{H}_{\text{elec}}\right)\Psi(\mathbf{r},\mathbf{R},t) = 0, \tag{13.2}$$

where $\hat{H}_{\text{elec}}$ is the Hamiltonian as defined in eq. 2.7 and $\Psi(\mathbf{r},\mathbf{R},t)$ is the time-dependent electronic wave function that can be written as a linear combination of adiabatic electronic states $\Phi_i(\mathbf{r};\mathbf{R}(t))$ (solutions of the time-independent electronic Schrödinger eq. 2.7):

$$\Psi(\mathbf{r},\mathbf{R},t) = \sum_j c_j(t)\Phi_j(\mathbf{r};\mathbf{R}(t)). \tag{13.3}$$

Inserting this expression 13.3 into eq. 13.2, multiplying from the left with an electronic wave function $\langle\Phi_i|$, and integrating over electronic degrees of freedom, one arrives at the following set of differential equations for the coefficients (in Dirac notation):

$$i\sum_j \langle\Phi_i|\frac{d}{dt}c_j|\Phi_j\rangle - \sum_j \langle\Phi_i|\hat{H}_{\text{elec}}|\Phi_j\rangle\, c_j = 0. \tag{13.4}$$

Accounting for orthonormality $\langle\Phi_i|\Phi_j\rangle = \delta_{ij}$ and employing the product rule of differentiation, this can be rewritten as

$$i\frac{d}{dt}c_i - E_i^{\text{elec}}c_i + i\sum_j \langle\Phi_i|\frac{d}{dt}\Phi_j\rangle = 0, \tag{13.5}$$

where E_i^{elec} is the i-th electronic state. This can be rewritten further by using the chain rule

$$\langle\Phi_i|\frac{d}{dt}\Phi_j\rangle = \langle\Phi_i|\nabla\Phi_j\rangle\,\frac{d}{dt}\mathbf{R} \tag{13.6}$$

to yield

$$i\frac{d}{dt}c_i - E_i^{\text{elec}}c_i + i\sum_j \langle\Phi_i|\nabla|\Phi_j\rangle\cdot\mathbf{v} = 0, \tag{13.7}$$

where $\mathbf{v}$ are the velocities of the nuclei at positions $\mathbf{R}$. This differential equation for the coefficients c_i defines the density matrix of the electronic states via

$$a_{ij}(t) = c_i^*(t)c_j(t). \tag{13.8}$$

The state populations are given by the diagonal elements of this matrix. The terms

$$\langle \Phi_i | \nabla | \Phi_j \rangle = \mathbf{d}_{ij} \tag{13.9}$$

are so-called non-adiabatic coupling vectors and are the semi-classical analogues to the non-adiabatic coupling operators defined in eq. 2.14 of chapter 2.2. While the nuclei evolve on one single electronic state, the density matrix is propagated using the above equations and used to evaluate the probability of switching to another state. There are different ways of defining the hopping probability from a state i to a state j, the most common one being Tully's fewest switches-criterion:

$$P_{i \to j} = \max \left[0, \frac{2\Delta t}{a_{ii}} \mathrm{Re}(a_{ij}) \mathbf{d}_{ij} \cdot \mathbf{v}) \right], \tag{13.10}$$

where Δt is the time interval in which this hop may occur. Such a hop can only be allowed if the kinetic energy is sufficient to overcome the energy gap between initial and final state. After a successful hop, the velocities have to be rescaled along the non-adiabatic coupling vectors to ensure energy conservation. Further details on the hopping probability and the possible approaches to the calculation of non-adiabatic couplings (NACS) will be given in the next section. The TSH approach has been implemented in the ASE package in order to be used with analytical model potentials (for more details see appendix A.4).

Due to its numerical simplicity TSH is a particularly appealing technique for describing the nuclear motion in non-adiabatic processes. However, the fact that the motion of the nuclei evolves only on one state at a time creates artificial coherence between the states. [340] This is specifically an issue for systems, where branching can occur. Corrections to this have been proposed by Zhu *et al.* [341], Stock and Thoss [342], or through the very recent work of Shenvi, Subotnik, and Yang, which either corrects for decoherence via a probability of wavepaket collapse [343] or via propagation of simultaneous trajectories on all states [344]. The same authors have also recently suggested a simple phase-correction scheme that significantly improves results obtained with original TSH [345].

13.4 Non-Adiabatic Coupling Models

A remaining problem of TSH, especially in the context of metal-surface mounted processes, is the restriction to only few explicitly treated non-adiabatic states. For the correct description of non-adiabatic processes on metal surfaces, one would have to include all intermediate electronic states and their couplings; a task of unperceivable complexity. Possible approaches that circumvent this problem have been proposed and can be summarized to the following three categories: The simplest possible approach is to only retain a small amount of electronic states explicitly and include the substrate effects implicitly via a modified coupling between these states [255]. In a completely different approach, the non-adiabatic energy dissipation to the metal DOFs can be described with the help of Langevin dynamics and a random friction force [321]. Very recently, a third route has been proposed by Shenvi and Tully [328] - so-called independent-electron surface hopping. The authors employ a much simplified Newns-Anderson type model Hamiltonian and include a discretized set of dispersion-free substrate bands within which an excited state can decay via a ladder-climbing process.

An intriguing option is to combine the first and the second approach. This would amount to describing the coupling between and the dynamics on a few selected states explicitly, while capturing the non-adiabatic effects of the substrate, be they electronic or vibrational in nature, with an energy-dissipation sink described by one or several friction components. In this way, the excited state PESs obtained with leΔSCF could be combined with a substrate-dependent

non-adiabatic energy sink. Corresponding friction could be designed to act differently depending on the active PES. A similar combination of IESH and Langevin thermostats has recently been attempted by Shenvi and Tully [346].

A generalized Langevin formalism [321, 347, 348] provides a simple way to introduce the effects of not explicitly treated DOFs via effective friction and fluctuation terms. The corresponding equation of motion for atom I reads

$$M_I \frac{d^2}{dt^2}\mathbf{R}_I = \mathbf{F}_I - \sum_j K_{IJ}\frac{d}{dt}\mathbf{R}_J + S_I(t), \tag{13.11}$$

where the first term represents the forces due to the potential energy surface through which the nuclear motion is currently dominated. The second term is the friction force on this atom that is induced by all other atoms J, and S_I is a stochastic fluctuating force that satisfies

$$\langle S_I(t) S_J(t')\rangle = k_B T K_{IJ}\delta(t-t'), \tag{13.12}$$

the $\langle \ldots \rangle$ expresses a thermal average. K_{IJ} is a matrix in the available atomic DOFs that describes the friction force. Assuming time-independence of this matrix and a smooth DOS around the Fermi level, K_{IJ} can be approximated as [321]

$$K_{IJ} = \pi \mathrm{Tr}[\mathbf{P}(\epsilon_F)\mathbf{G}^I\mathbf{P}(\epsilon_F)\mathbf{G}^J], \tag{13.13}$$

where $\mathbf{P}(\epsilon_F)$ is the local density-of-states at the Fermi level, and $\mathbf{G}^I$ is defined as

$$G^I_{ai} = \frac{\langle\Psi_a|\nabla_I H|\Psi_i\rangle - \epsilon_F \langle\Psi_a|\nabla_I\Psi_i\rangle}{\epsilon_a - \epsilon_i}. \tag{13.14}$$

In eq. 13.14, ϵ_i and ϵ_a refer to the energies of electronic state i and a with corresponding wave functions Ψ_i and Ψ_a, respectively. To a reasonable approximation the plethora of excited states of the metal substrate can be replaced by the occupied and unoccupied non-interacting KS reference states ψ_i and ψ_a and their corresponding orbital eigenenergies. Employing the relation [349, 350]

$$\langle\Psi_a|\nabla_I\Psi_i\rangle = \frac{\langle\Psi_a|\nabla_I H|\Psi_i\rangle}{\epsilon_a - \epsilon_i} \tag{13.15}$$

the above eq. 13.14 can be rewritten as

$$G^I_{ai} = \mathbf{d}^I_{ai}\cdot\left(1 - \frac{\epsilon_F}{\epsilon_a - \epsilon_i}\right). \tag{13.16}$$

Other approaches of varying intricacy have also been given in literature on how to calculate this matrix from *ab-initio* data [351, 352].

Regardless of the additional or implicit account of non-adiabatic coupling of the adsorbate with the substrate degrees of freedom, the TSH formalism depends on a known expression for the NACs $\mathbf{d}_{ij}$ or the hopping probability $P_{i\to j}$. The calculation of NACs is, to say the least, an intricate task. Employing eq. 13.9, this could for a long time only be done for configuration interaction-based wave function techniques [353, 354]. Within dynamics simulations, the NAC between the ground and excited state can always be approximated by finite time differences between ground- and excited-state wavefunctions at different points in time [355–357]. However, in this case the wave functions have to be available during the time propagation, which is not the case when using precalculated potentials. For lrTD-DFT, analytical expressions for NACs have been proposed recently [222, 358, 359], which also extend to NACs between excited states

[350]. In the specific case of ΔSCF-based dynamics, NAC formulations have been given, based on a single set of reference KS states that has been evaluated with a transition-state density (i.e. a linear combination of two states) [349, 360, 361]. According to such an approach, the NACs from leΔSCF could also be evaluated[3]. These methods all necessitate NACs being evaluated during the dynamics or before hand, in order to then be fitted to analytical expressions. This might indeed pose a potential way to calculate the NACs between the ground state of Ab and its intramolecular excited states.

In the case of non-adiabatic molecular dynamics on metal surfaces, only approaches have to date been formulated, which are based on simple model Hamiltonians or more modest approximations to non-adiabatic couplings. One of which is the *sudden transition and averaging* (STA) [256, 362, 363] approach that is often used in the context of substrate-mediated photodynamics, specifically for mechanisms following a Menzel-Gomer-Redhead model (such as the one proposed for TBA on Au(111)) [252, 253]. In this approach one runs many semi-classical trajectories, each with a different excited state lifetime τ_n. After vertical excitation to the excited state, the system propagates for a time τ_n and deexcites back to the ground state. Observables are computed by averaging over different lifetimes τ_n. If τ_n is chosen in equidistant steps, the quantum yield and final state distribution can be calculated as

$$\langle O \rangle (t) = \sum_{n=1}^{N} w_n \langle O_{\tau_n}(t) \rangle , \tag{13.17}$$

where the different lifetimes are weighted via

$$w_n = \frac{e^{-\tau_n/\tau}}{\sum_{n=1}^{N} e^{-\tau_n/\tau}}. \tag{13.18}$$

τ is an assumed excited-state lifetime. The weighting accounts for the exponential decay of the excited state. The benefit of this approach is that no further thought has to go into the description of the hopping probabilities and NACs. Nevertheless, an excited-state lifetime has to be assumed and a large amount of trajectories has to be run to converge the results.

NACs between states that are well separated in energy can be approximated as mere functions of energies and forces. At well enough separation one may assume that couplings between states i and j are not affected by the changes in other states. Therefore the evaluation of NACs between several states may be approximated by expression as independent two-state problems. In a two state system, if both diabatic and adiabatic sets of energies are known, the NACs can be calculated by matrix inversion [327]. However, this is not the case for our system Azobenzene on Au(111) as calculated with leΔSCF. Nevertheless, if only the adiabatic energies are known, the NACs can still be calculated, but a functional form of the diabatic coupling has to be assumed. The corresponding coupling can be written as

$$\mathbf{d}_{ij} = \pm \frac{V_{ij}}{(\epsilon_j - \epsilon_i)^2} \frac{(\epsilon_j - \epsilon_i)(\mathbf{F}_i - \mathbf{F}_j)}{\sqrt{(\epsilon_j - \epsilon_i)^2 - 4V_{ij}^2}} \mp \frac{V_{ij}(\nabla V_{ij})}{(\epsilon_j - \epsilon_i)^2} \left(\frac{(\epsilon_j - \epsilon_i)^2 - 4V_{ij}^2 + 4V_{ij}}{\sqrt{(\epsilon_j - \epsilon_i)^2 - 4V_{ij}^2}} \right), \tag{13.19}$$

where ϵ_i and ϵ_j are the adiabatic energies of state i and j, $\mathbf{F}_i$ and $\mathbf{F}_j$ are the corresponding nuclear forces, and V_{ij} is the diabatic coupling strength. For a derivation of this equation, see appendix B. This diabatic coupling strength can be assumed as constant or as a function of energetic state separation (in both cases the second term vanishes). In order to accurately describe NACs of molecular systems, the employed form of V_{ij} has to be benchmarked against NACs calculated from explicit *ab-initio* calculations.

[3] With the restrictions given by the additional 'Pulay'-terms that arise.

Ideally one would like to avoid the calculation of NAC elements completely. In the following a few simple approximations to NACs will be given. An early model to the transition probability between two states has been derived by Landau and Zener [364, 365]:

$$P_{i\to j} = \exp\left[-\frac{2\pi V_{ij}^2}{\mathbf{v}\cdot\partial(H_{ii}-H_{jj})/\partial\mathbf{R}}\right], \tag{13.20}$$

where H_{ii}, H_{jj}, and V_{ij} are the diabatic on and off-diagonal elements of the Hamiltonian. This strictly only applies to the diabatic representation in one-dimensional systems. A corresponding model in the adiabatic representation has been derived by Desouter-Lecomte and Lorquet [366][4]:

$$P_{i\to j} = \exp\left[-\frac{2\pi(\epsilon_j-\epsilon_i)}{\mathbf{v}\cdot\mathbf{d}_{ij}}\right]. \tag{13.21}$$

Again this only holds strictly for the one-dimensional case, however, with significantly underestimated transition probabilities [367] and it additionally bears the problem of explicit dependence on the NACs.

A very appealing approximation to the transition probability between two states has been given by Miller and George [368]:

$$P_{i\to j} = \exp\left[-\frac{4(\epsilon_i-\epsilon_j)}{3}\left(\frac{2(\epsilon_i-\epsilon_j)}{d^2(\epsilon_i-\epsilon_j)/dt^2}\right)^{1/2}\right]. \tag{13.22}$$

This form of the transition probability has already been successfully applied for non-adiabatic dynamics simulations of large molecules on semiconducting surfaces [369]. In simulating surface impingement reactions, very often the coupling between adsorbate and substrate degrees of freedom is modelled as vanishing with increasing surface distance, either exponentially or following other simple functional forms [324, 328, 329].

The large number of approximations that have to be employed to render simulations of TBA photodynamics on Au(111) tractable, makes very minimal models of coupling a reasonable starting point. On the basis of such a modelling and a constant benchmark to higher-level approaches and experiment, the NAC description can be systematically escalated towards more sophisticated descriptions.

13.5 Putting it all Together - What Answers can we Expect?

From the above considerations, an absolutely minimal description of photo-induced Azobenzene switching at coinage metal surfaces can be formulated: The nuclear DOFs that absolutely have to be included are the rotation and inversion angles around the central azo-bridge. In further steps, the vertical adsorption height and the intra-molecular bond stretches of this minimal model might have to be included. In such a reduced space of parameters, analytical representations of the energetics as described by DFT and leΔSCF-DFT can be constructed. The immense computational expense of this endeavour will only enable a coarse sampling of the involved DOFs. Employing the TSH approach, a large number of trajectories can efficiently be simulated on these explicit PESs. Ideally, these trajectories start from a random sampling of phase space around the ground-state minimum. This can be achieved by sequential snapshots of ground-state trajectories or by a canonical Wigner distribution around the minimum. Simulations start at the excited-state PESs with the corresponding ground-state thermalized positions and momenta

[4] This work also includes an excellent summary and comparison of different one-dimensional coupling models.

(Franck-Condon excitation). The coupling between states can in a first step be accounted for by a given lifetime and the STA approach. A natural next step would be the calculation of coupling between the ground and excited states using one of the above mentioned methods and connecting this approach with a Langevin friction force that acts on the adsorbate nuclei.

Such an approach is highly error-prone and a significant number of tests and benchmarks will be necessary to enable an assessment of the reliability. For example, the reduced parameter space in which the dynamics occur, will not correctly describe the non-equilibrium energy distribution and dissipation into all molecular modes and substrate degrees of freedom. The result will be an artificially fast switching process, possibly also exhibiting biased switching rates. The extent by which energy is dissipated into intramolecular modes, that are not being explicitly accounted, can be evaluated by simultaneous molecular dynamics simulations of the reduced gas-phase model that was presented in section 13.2 and a full on-the-fly *ab-initio* model of gas-phase Azobenzene. Adiabatic excited-state trajectories, which have been prepared in the above mentioned way, will enable to extract the corresponding time to reach the mid-rotation point and the involved dynamical changes to the molecule and the energy content in the molecular modes. The differences in energy distribution and reaction time will enable a better assessment of the quality of the model. These findings together with the large literature knowledge on Ab dynamics can then be incorporated into improved coupling models, which account for the intramolecular energy dissipation by a friction component on the nuclear motion. The effect of energy dissipation due to induced substrate nuclear motion and low-lying electron-hole pairs can also be accounted for by a friction force. Corresponding models have been formulated in literature [352, 370–373].

After such a detailed reliability test both proposed mechanisms, an intramolecular excitation and a substrate-mediated excitation, can be investigated. While the above mentioned friction components for energy dissipation into intramolecular and substrate degrees of freedom can be assumed identical in both cases, however, the explicit coupling between the excited and the ground state may be very different. The expected lifetime for intramolecular excited electrons will be in the order of only a few femtoseconds[5]. The hot holes around the upper *d*-band edge, discussed in the case of the substrate-mediated excitation process, can have lifetimes of the order of 25 fs in coinage metals [251, 375–377], which are considerably higher than the lifetimes of excited electrons of equal energy [378, 379]. The rather short lifetimes that are expected for intramolecular excitations together with the strong experimental evidence towards a substrate-mediated mechanism suggest that explicit simulations on the former are not an ideal choice.

A detailed simulation study of the substrate-mediated mechanism will initially have to be conducted for Ab adsorbed on Au(111). A large number of trajectories with varying lifetime (or coupling) will enable to identify if a significant switching probability can be achieved at realistic excited-state lifetimes. The very much similar form of the S1 and cationic resonance state PES for Ab on Au(111) may additionally allow interpretations towards the intramolecular mechanism for very small lifetimes. Subsequently, the dependence of the resulting E/Z ratio and quantum yield on the temperature can be studied by varying different initial conditions. From this, answers with respect to the experimentally observed temperature dependence and suspected vibrational activation can be expected. In addition, the rotation-inversion controversy of the nuclear dynamics may be adressed by a selective initial population of the rotation or inversion vibrational modes.

In a second step, a comparison between the dynamics of Ab and TBA adsorbed to Au(111)

[5] This can be estimated from similar electron excitation processes on surfaces, such as photodesorption of NH_3 on Cu(111) [255, 374] and the lifetime of such excitations (<10 fs) in 2PPE spectra of TBA on Au(111) [247], pp. 61-71.

has to follow. The functionalization-induced changes in the excited-state PES that were identified in chapter 12 will carry over to changes in the switching probability and E/Z ratio. Correspondingly, simulations at the same initial conditions and lifetimes as were used for Ab on Au(111) will reveal these changes and might also enable to pinpoint the experimentally observed photo-induced switching of TBA to exactly these topological modifications, thereby adressing the effect of molecule functionalization on the molecular switching mechanism.

All in all, a step by step approach along the lines detailed above will shine light on the main questions that are still to answer. A large part of the understanding that can be gained, will enter *via* the assessment of the reliability and applicability of the approximations and physical models that are used in describing the coupling. The reward of a full qualitative understanding of the switching mechanism may therefore already be granted on the journey and not just at the designated destination.

14 Conclusions

The ongoing efforts for further miniaturization of electronic building blocks have slowly reached the point, where the individual control of single molecules is the main focus of attention for future device design. With this shift in attention and scale, also the means of fabrication have to shift. The standard construction procedures for the current main building-block in electronics, the field-effect transistor, are well understood and have permanently been optimized and changed over the last decades to achieve a size reduction by orders of magnitude. When reaching the regime of single functional molecules, very novel approaches to device construction have to be pursued. This implies that the parameters determining successful assembly of a device, such as the embedding of functional molecules into a matrix, have to be studied from scratch. The variables that decide on the envisioned molecular function include changes in the environment or substrate and differing molecular functionalization. Mastering the production of a molecular based functional device amounts to nothing more and nothing less than being able to balance all quantum molecular interactions that are located in the atomistic world by techniques that are located in the macroscopic world.

This thesis has attempted to contribute to this task by seeking a full understanding of substrate-mounted molecular function on the basis of an atomistic first-principles parameter-free description. This is best done for a well-studied prototypical system, in this case here, the photo-induced isomerization dynamics of Azobenzene adsorbed to coinage metal surfaces. As already stated, the underlying aspiration was, that a potentially gained understanding might support new forms of rational device design. In the course of this, a methodological basis had to be found that enables a reliable description of the molecular geometry and energetics in the ground and in the electronically excited states. This can only be done by firm knowledge of the current literature associated with the molecular mechanism in gas-phase and in chemically active environments, as well as by close collaboration with experimental studies that act as a benchmark reference. Consequently, employing such methodology, the effects of the substrate and molecular functionalization on the structure and stability of the isomerization intermediates has to be analyzed in order to then do the same with excited states that may be involved in a photo-induced switching mechanism. This can then serve as a basis for a modelling approach that takles the explicit nuclear dynamics and transient electronic changes that determine the molecular switching process.

The choice of methodology fell on semi-local approximations to Density-Functional Theory for their highly efficient and reliable description of coinage metal surfaces. However, this approach suffers on the one hand from an insufficient description of dispersion interactions, which are essential for a correct description of the structure and energetics of the adsorbate-substrate complex, and on the other hand from a complicated starting point to an excited-state description that is feasible for such large systems.

Employing a recent dispersion correction to DFT (DFT+vdw$^{\text{surf}}$) that incorporates the effects of collective many-body substrate response, a highly accurate structural model for Azobenzene adsorption could be found. This is supported by an excellent agreement with recent experiments (see chapter 9). To reach this level of accuracy the geometrical effects due to lateral

interactions in highly dense molecular overlayers and the effects due to vibrational anharmonicity at the experimental conditions had to be accounted for. Azobenzene adsorbed to Ag(111) exhibits highly unusual and unexpected structural changes as a function of surface coverage for the vertical positioning on the surface, but also for intramolecular degrees of freedom. It is due to the accurate structural description of the DFT+vdw$^{\text{surf}}$ approach that the experimental analysis has been refined. At this accuracy, both experiment and theory act as benchmark for each other. The effects of anharmonicity to the geometry have only been accounted for by modelling vibrations as uncoupled anharmonic oscillators. In order to further refine this approach the effects of additional coupling between these modes and the agreement with explicit *ab-initio* molecular dynamics calculations have to be investigated in the future.

The adsorbate geometries and ground-state energetics along important isomerization pathways have been investigated, yielding remarkable implications for the isomerization ability of Azobenzene (see chapter 10). When breaking the double bond along a rotational motion between E and Z-Azobenzene, the molecule passes from its almost purely physisorbed state via a strongly bound, chemisorbed intermediate to the, again, dominantly physisorbed Z state. This extreme change of bonding character along a reaction coordinate was absolutely unexpected, but is in fact very general for surface-mounted double bond breaking and easy to understand from a chemist's perspective. The resulting unbalanced changes to the relative energetics render a photoinduced isomerization of Azobenzenes on surfaces more reactive than Au(111) virtually impossible. Furthermore, the addition of bulky functional side groups to the molecule does not affect this situation at all. The unbalanced stabilization of different geometries involved in the isomerization procedure can not be correctly counteracted by substrate and molecule modifications that only target the end points of the reaction. Therefore, the currently employed device design strategies are not sufficient and a paradigm shift is due. A successful device design on the basic level of assuring the necessary stability prerequisites has to target all adsorbate states involved in the switching process by controlling factors such as surface electronegativity, lateral interaction strengths, and steric hindrance. Possible state-selective techniques may involve the use of coadsorbates or substrate alloys. Coadsorbates can act as strong substrate electron acceptors or may selectively affect certain geometries via dipole-dipole interactions or steric hindrance, while alloys may yield a better control over the substrate electronegativity. In the specific case of Azobenzene, a future point to investigate might be the yet insufficiently studied coverage dependence of the ground-state stabilities.

The second shortcoming of current DFT approaches in the context of this work, namely the missing efficient excited-state approach, deserved a step back to the reduced complexity of the isolated molecule. A survey on literature revealed that not many accurate methods exist that can be transferred to the adsorbate case, where they describe molecular electronic excitations and charge-transfer excitations from or to the substrate on equal footing; an absolute necessity in the context of the mechanisms discussed for metal-adsorbed Azobenzene. Owing to these constraints and very recent extensions of ΔSCF into these directions, this method emerged as a candidate and was tested for its ability to describe low lying excited-state potential energy surfaces of the gas-phase molecule (see chapter 6), which it successfully does. The topologies along the dominant excited-state pathways are perfectly described. Notwithstanding the absolute excitation energies are systematically underestimated with semi-local xc-functional approximations; a fact that, in the context of metal surface-adsorption, cannot be remedied by mere admixture of Hartree-Fock exchange. In the future it might be remedied by employing additional orbital dependent penalty potentials as discussed in appendix D, more sophisticated versions of ensemble DFT [380], or novel Koopman's compliant density-functional theory approximations [381, 382]

Within this work, the linear expansion ΔSCF approach of Gavnholt *et al.* [29] has been extended to represent a general purpose efficient approach to the calculation of molecular ex-

citations in the limit of weak hybridization or hybridization to metals in the wide band limit (see chapter 11). It is able to describe the major qualitative physical effects that govern intramolecular excitations and substrate-mediated charge-transfer for large-scale adsorbates on metal surfaces, but is not limited to such systems. In this way, both previously defined drawbacks to DFT as a method for the modelling task of this work have been lifted.

The starting point for this investigation was given by experimental findings that suggest a rather different electronic mechanism for the surface-mounted photoswitching than for the isolated molecular case. A photoisomerization yield that is rather constant over a broad range of photon incidence energies and that strongly depends on substrate temperature has triggered the belief that substrate-mediated charge transfer is the dominant mechanism [28]. Correspondingly, the prerequisites for both intramolecular and substrate-mediated excitation mechanisms have been investigated.

The calculated intramolecular excited-state potential energy surfaces in the context of the traditional gas-phase isomerization mechanism suggest a strong reduction of the maximally achievable photostationary E/Z ratio and a strong reduction of isomerization efficiency just in terms of the absorbance. This is without even accounting for the fact that the mechanism does not explain the experimentally observed behavior. On this basis, a dominance of this pathway has to be excluded, however, without doubting its principal feasibility on surfaces.

The necessary prerequisites to a substrate-mediated mechanism, where a short-lived excitation induces the necessary molecular motion, are significant vibronic coupling in the Franck-Condon regions of the molecular ionic resonance states and a balance between kinetic excess energy, ground state stability, and barrier height. Either one of these prerequisites is destroyed by a chemically active surface or a strong stabilization at the surface. However, in the case of TBA on Au(111) a successful switching on the basis of a short-lived ionic resonance can be rationalized in terms of the here presented excited-state topologies. A rather intriguing point to mention is that also too weak coupling to the surface can inhibit such a mechanism due to an insurmountable remaining barrier and insufficiently stabilized ionic resonances. It is exactly this sensitive balance between overly strong and insufficient coupling to the surface, which seems to be achieved coincidentally for TBA on Au(111) and which makes the design of functioning switches such an intricate task.

Employing the herewith established methodology, clear step-by-step paths to an explicit dynamical treatment of increasing complexity for the switching function emerge (see chapter 13), where at every step, the quality of the description of coupling to the surface degrees of freedom (via electron-hole pair and phonon excitation) should be assessed. In this way, using first-principles parameter-free modelling, a complete picture can be drawn and highly relevant details of molecular function in complex environments can be described. The selected example of photo-induced Azobenzene isomerization on coinage metals furthermore shows that after several decades there is still a lot of insight to be gained in the field of photochemistry on metal surfaces and its great potential in heterogeneous catalysis is yet to be recognized sufficiently.

Further proceedings will have to include similar systematic studies on the effects of coadsorption, semiconductor-gated metal surfaces, or other forms of molecule embedding as alternative to mere adsorption. Only if the key variables that determine the existence and efficiency of selectively inducible molecular motion are clear, can such molecules be integrated into technological devices. An often forgotten point in basic research studies is that the so gained rationale has to be portable to a simple set of rules for device fabrication. Although the author of this work is highly doubtful about molecular devices of the kind studied in this work as being technologically relevant in the course of his lifetime, he is more than willing to further contribute a significant amount of his time, just to find himself disproven.

Appendices

A Software used in this Work

A.1 The TURBOMOLE and GAMESS packages

TURBOMOLE [211, 383] and GAMESS [212] are all-electron computational chemistry packages employing localized orbital basis sets of the Gaussian-type [384]. Both codes have a long development history and have been mainly designed for use on workstation computers. Especially TURBOMOLE is designed for this type of hardware and features low memory and disk requirements and highly efficient integral evaluation for SCF calculations of the Hartree-Fock [385] and DFT type [386]. Thereby heavy use is made of the Resolution of Identity approximation (RI) [387, 388]. In this approach, the electron density is approximated by an atom-centered auxiliary basis set $\{\alpha\}$

$$\rho(\mathbf{r}) \approx \sum_{\alpha} c_{\alpha}\alpha(\mathbf{r}). \tag{A.1}$$

and by expressing the Coulomb operator (or Hartree term) in Hartree-Fock or KS-DFT in terms of this basis, the evaluation of four-center-two-electron integrals can be avoided on behalf of a large number of well-understood two-electron integrals. In TURBOMOLE, this highly efficient modification can be employed for the calculation of ground state properties with HF and DFT, but also for use in excited state calculations with lrTD-DFT [214] and Coupled Cluster (RI-CC2) [46, 47] calculations.

In this thesis, use of TURBOMOLE and GAMESS has been made in chapter 6 and chapter 13. In all cases, the Ahlrichs class of triple [389, 390] to quadruple [391] zeta gaussian basis sets has been used. The contributions due to the xc-functional have been calculated on a default 'm3' grid. Ground- and excited-state calculations have been converged at standard electronic structure settings, with the exception of tightened density convergence. In the case of GAMESS only use of the CAM-B3LYP functional has been made [65]. Non-adiabatic coupling elements to the lrTD-DFT excitations have been calculated for testing purposes using the module by Send and Furche [392].

A.2 The FHI-AIMS package

FHI-AIMS is an all-electron multi-purpose electronic structure code based on numeric atomic-centered orbitals (NAOs) [204]. Herefore, the radial shape of an atomic basis function is numerically tabulated. This enables a correct description of the nuclear potential close to the nucleus and at large distances. Both these regimes otherwise need extensive contracted linear combinations of GTOs to be described properly. The corresponding basis sets are strictly local and lead to quickly convergent results with respect to the number of basis functions. However, the numerical evaluation of integrals is more intricate than in the case of GTOs. The NAO basis set definition starts from a minimal basis, which comprises the occupied atomic states of the corresponding free atom. Additional basis functions are hirarchically structured in groups containing functions of different angular momenta, so-called 'tiers'. A level-by-level increase of 'tier' yields a systematic way to converge results.

In this work (mainly chapter 6), FHI-AIMS has been used for optimizations, ground state energy and force evaluations using local, semi-local, and hybrid xc-functionals [393]. Optimizations have been performed using at least a 'tier2' level at otherwise standard tight numerical settings, whereas energy evaluations have been done at 'tier3' level. Typical electronic convergence settings were dominated by a total energy convergence criterion of 10^{-6} eV. ΔSCF calculations have been performed with an occupation constraint module, implemented by Matthias Gramzow, Fritz-Haber Institut Berlin.

Implementations to FHI-AIMS

In order to facilitate convergence of the ΔSCF excited state calculations at near degeneracy situations, an addition to the occupation constraint was made. At near degeneracies of a constrained KS state with other states, the occupation constraint is 'distributed' between degenerate states. This constraint smearing is defined by a gaussian distribution with a given width (input parameter *force_occupation_smearing*).

A.3 The CASTEP package

The CASTEP code[1] is an electronic structure code, designed for the calculation of condensed matter systems [258, 394]. It employs a pseudopotential plane wave basis. Its original development started in the early 1990's [259]. Many different contributions led to a quick growth of functionality. The code was written in FORTRAN 77 and had no modular structure or clear coding guidelines. Therefore, starting from 1999 the code was completely redesigned in a modular structure (see Fig. A.1), written in FORTRAN 95, which extremely facilitates contribution to the code. The Kohn-Sham wavefunctions are expanded in a plane wave basis set on the basis of Bloch's theorem (see chapter 4). The attractive potential between electrons and nuclei is approximated with *ab-initio* pseudopotentials of the norm-conserving [130] or ultrasoft [131, 311] kind. Specifically to mention are the highly efficient direct minimization techniques with which the Kohn-Sham equations are solved for the wave functions, eigenvalues and the density [259]. For systems that exhibit pathological convergence issues, a robust Ensemble DFT solver is implemented [395]. The plane wave basis is expanded on a reciprocal space grid and a real space grid, which can be transformed efficiently via a Fast Fourier Transform. The Hamiltonian can be split into parts, which are easy to solve on a reciprocal space grid (e.g. applying the kinetic energy functional) and parts which are more easy to solve in real space (e.g. constructing the density from the wave functions).

In this work, heavy use has been made of the 'density mixing' [301, 396] solver in CASTEP and the standard library ultrasoft pseudopotentials optimized for use with PBE that ship with CASTEP. The corresponding mixing was performed with the scheme developed by Pulay [397]. In all ground state calculations, the electronic structure was converged to a total energy difference of 10^{-8}eV. Convergence was eased with a Gaussian smearing of 0.15 eV. Molecular geometries were optimized with the optimizer based on delocalized internal coordinates [263] down to a maximum force component of 25 meV/Å per atom, an energy difference criterion of 2×10^{-5}eV per atom, and a maximum step size of 10^{-3}Å. All other computational settings have been specified in the respective results chapters of this thesis (see chapter 8). Due to the use of dispersion correction methods [77, 85, 196] that rely on the atoms-in-molecules density partitioning scheme by Hirshfeld [78] and semi-local GGA functionals, the cutoff of the real

[1] www.castep.org

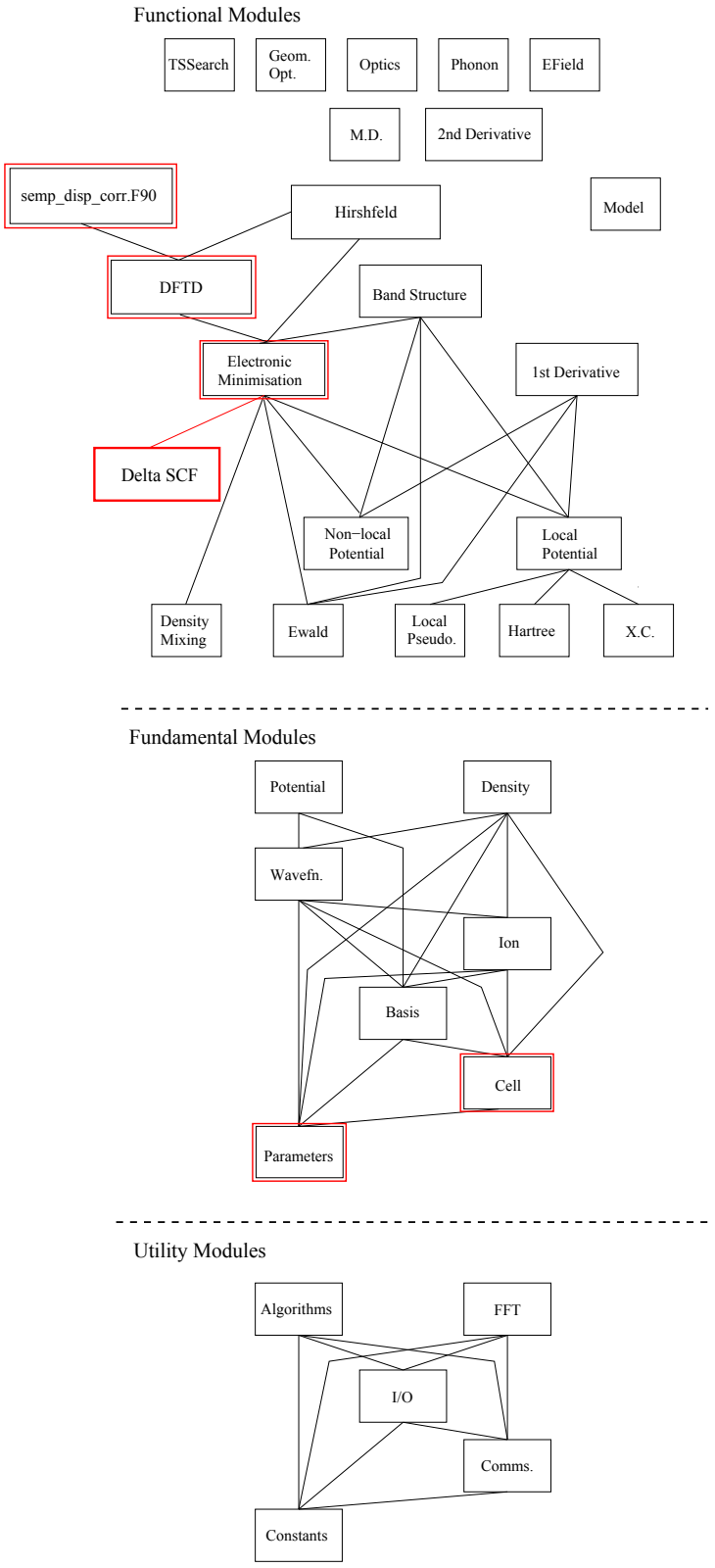

Figure A.1: Module structure of CASTEP. Modifications to the code during this thesis have been made in the red marked modules. The module 'Delta SCF' has been designed from scratch. The basic diagram has been taken from the CASTEP specifications.

space grid on which the density is mapped was chosen to be two times the length of the largest wave vector that was included in the plane wave series.

Implementations in CASTEP

All modifications that have been made to the code are specified in Fig. A.1 by red squares. Within the work of chapter 8, the novel dispersion correction scheme vdw^{surf} [85] has been implemented. The dispersion correction module in CASTEP (developed by Erik McNellis and Jörg Meyer) is composed of a stand-alone code for the calculation of pairwise interactions in solids (semp_disp_corr.F90) and an interface module (dftd.F90) that combines this code with CASTEP. This code enables to selectively include or neglect vdW interactions with different schemes (incl. vdw(TS) [77]) in certain directions along the lattice parameters and also between specified groups of atoms and their images. The new vdW parameters devised by Ruiz *et al.* [85] have been introduced to semp_disp_corr.F90. Additionally the rescaling of the C_6 coefficients in vdw^{surf} necessitates a bulk reference atomic volume instead of a free atomic volume in vdw(TS). The corresponding pre-calculated ratio between free and bulk atomic volume can be given as input to dftd.F90 via the existing secondary input file *.sedc_pbc. Additionally, the functionality of neglecting selected vdW interactions *within* the unit cell has been added. Thereby, the vdW interactions within a specified group of atoms can be neglected without modifying the interactions with all other atoms and also the complete vdW contributions due to this group can be removed.

In chapter 11 the leΔSCF scheme to calculate excited states of adsorbates has been introduced. This has been implemented via the deltscf.F90 module. This module contains subroutines that are called within the self consistent field algorithm in electronics.F90 and are necessary to initialize the ΔSCF (both simple ΔSCF and leΔSCF) procedure, to read a given set of reference wave functions ϕ_c, to calculate the projections, and to construct the reshaped orbital space during each SCF step. The occupations are modified after the wave function optimization and during the calculation of the Fermi energy.

The deltascf.F90 module also contains routines that can be accessed by the CASTEP main code directly after finalization of all tasks. These routines enable the calculation of Molecular Orbital projected Density-of-State coefficients (MOpDOS). For this purpose, specified reference orbitals are read, the overlap with the converged wave functions is calculated, and coefficients are written to file. The corresponding coefficients are read by a post-processing tool 'MolPDOS.F90', which has been integrated into the CASTEP suite and uses some CASTEP module functions. MolPDOS.F90 processes the coefficients, together with the standard Density-of-States information to generate the projected MOpDOS visualization data.

In appendix D, a ΔSCF derived scheme for correcting adsorbate orbital energies and positions has been suggested employing an additional orbital-dependent potential term to the Hamiltonian. This scheme uses the same projections as the two above mentioned approaches. Corresponding subroutines have been added to enable evaluation of this additional term to the Hamiltonian and its self consistent effect on the wave functions and band energies.

A.4 The ASE package

The Atomic Simulation Environment (ASE) [206, 398] is an object-oriented simulation tool with the aim of producing one common infrastructure for setting up, steering, and analyzing atomistic simulations. It is written in Python scripting language and includes a large number of interfaces to common simulation packages, both *ab-initio* and molecular mechanics based (e.g. interfaces to FHI-AIMS, CASTEP, TURBOMOLE). These interfaces are termed "calculators"

and handle the file Input and Output of the program packages and deliver energy, forces, and other properties to ASE. It contains a variety of subroutines that enables the construction of atomistic models of surfaces, bulk structures, and molecules, as well as routines for optimization, molecular dynamics, and data analysis.

In this thesis, ASE has been used to construct structural models of adsorbate-substrate complexes, as well as to visualize them. Furthermore the optimization routines of ASE have been heavily used in chapters 6, 11, 12, and 13.

Implementations in ASE

In the context of the work in chapter 6, constraint optimizations were necessary. This refers to the optimization of a molecular geometry under the constraint of a fixed internal degree of freedom, such as a dihedral angle or a bending angle. To enable this procedure, a new class of constraints has been implemented to the "constraints" module of ASE - the *FixInternals* constraint. Thereby a fixed set of internal degrees of freedom [333] is forced to determined values by a self-consistent SHAKE algorithm [207]. The set of internal degrees of freedom may contain any number and combination of dihedral angles, bending angles, and bond stretches. This functionality is available starting from ASE version 3.6.0 (Feb. 24, 2012).

In the course of chapter 13, a mixed-quantum-classical trajectory surface hopping scheme has been implemented to ASE (module "surfacehopping") following the descriptions of Tully's original work [337] and recent reviews [323, 339]. This module is designed to be used with analytical model potentials, but should in principle also enable its use with the implemented calculator interfaces to stand-alone codes in ASE. It collects energies, forces, and non-adiabatic coupling vectors from calculators. The dynamics are simulated in the adiabatic representation. The nuclear dynamics are propagated at different time steps than the coupled differential equations. The latter are interpolated at a smaller time interval with a 4th order Runge-Kutta scheme [120]. The code is able to reproduce the results of Tully [337] for the same one-dimensional model systems. Coherence corrections as defined by Zhu *et al.* [341] have been implemented.

A number of "calculators" has been generated to reproduce one-dimensional model potentials [337, 399]. A calculator interface to the ALGLIB [332] library has been written that enables the construction of up to 3-dimensional model potentials and the calculation of energies, forces, and non-adiabatic couplings therewith.

A.5 Other software used in this thesis

During this thesis, heavy use has been made of the following pieces of software:

Visualization and Molecular Modelling Tools: VMD [400], Aten [401], Avogadro [402], matplotlib

Numerical Tools: python, SciPy, NumPy, ALGLIB [332]

Other Tools: the LaTeX typesetting software, the Arch Linux operating system

B Non-Adiabatic Coupling Elements for a Two-State Model

A two-level electronic system can be described by a Hamiltonian in a diabatic basis of the form

$$H = \begin{pmatrix} a & c \\ c & b \end{pmatrix} \tag{B.1}$$

This matrix can be brought into diagonal form

$$\tilde{H} = \begin{pmatrix} \epsilon_1 & 0 \\ 0 & \epsilon_2 \end{pmatrix} \tag{B.2}$$

by a unitary transformation $\tilde{H} = U^\dagger H U$ with a rotation matrix or eigenvector matrix U with rotation angle α

$$U = \begin{pmatrix} \cos\alpha & -\sin\alpha \\ \sin\alpha & \cos\alpha \end{pmatrix} \qquad \alpha = \arctan\left(\frac{2c}{b-a}\right) \tag{B.3}$$

This diagonal form is then called the adiabatic representation. The adiabatic eigenenergies ϵ_1, ϵ_2 are defined by

$${}_1\epsilon_2 = \frac{a+b}{2} \pm \sqrt{\left(\frac{a+b}{2}\right)^2 - ab + c^2} \tag{B.4}$$

The non-adiabatic coupling matrix elements (see chapter 2.2) are defined as

$$\mathbf{d}_{ij} = \langle \Phi_i | \nabla \Phi_j \rangle = \frac{\langle \Phi_i | \nabla \hat{H} | \Phi_j \rangle}{\epsilon_2 - \epsilon_1} = -\nabla\alpha \tag{B.5}$$

and furthermore

$$\alpha' = \nabla\alpha = \frac{(b-a)\nabla c - c\nabla(b-a)}{(b-a)^2 + 4c^2} \tag{B.6}$$

In the following $\alpha' = f(a,b,c)$ will be expressed as $\alpha' = f(\epsilon_1, \epsilon_2, c)$. When adding and subtracting the two solutions of eq. B.4 one arrives at

$$I: \quad \epsilon_2 + \epsilon_1 = a + b \tag{B.7}$$

$$II: \quad \epsilon_2 - \epsilon_1 = 2\sqrt{\left(\frac{a+b}{2}\right)^2 - ab + c^2} \quad \Big|^2$$

$$(\epsilon_2 - \epsilon_1)^2 = 4\left[\left(\frac{a+b}{2}\right)^2 - ab + c^2\right]$$

$$a^2 + b^2 - 2ab + 4c^2 - (\epsilon_2 - \epsilon_1)^2 = 0 \tag{B.8}$$

When inserting eq. I into eq. II in B.7 one arrives at

$$(\epsilon_1 + \epsilon_2 - b)^2 + b^2 - 2(\epsilon_1 + \epsilon_2 - b)b + 4c^2 - (\epsilon_2 - \epsilon_1)^2 = 0$$

$$4b^2 - 4b(\epsilon_2 + \epsilon_1) + 4c^2 + 4\epsilon_1\epsilon_2 = 0 \tag{B.9}$$

$$\tag{B.10}$$

There are two pairs of solutions to this quadratic equation.

$${}_1b_2 = {}_2a_1 = \frac{\epsilon_2 + \epsilon_1}{2} \pm \sqrt{\left(\frac{\epsilon_2 + \epsilon_1}{2}\right)^2 - \epsilon_1\epsilon_2 - c^2} \tag{B.11}$$

From this result the corresponding difference in eq. B.6 can be calculated

$$(b - a) = \pm 2\sqrt{\left(\frac{\epsilon_2 + \epsilon_1}{2}\right)^2 - \epsilon_1\epsilon_2 - c^2} = \pm\sqrt{(\epsilon_2 - \epsilon_1)^2 - 4c^2} \tag{B.12}$$

The corresponding derivative is

$$\nabla(b - a) = \pm\frac{(\epsilon_2 - \epsilon_1)(\mathbf{F}_1 - \mathbf{F}_2) - 4c \cdot (\nabla c)}{\sqrt{(\epsilon_2 - \epsilon_1)^2 - 4c^2}} \tag{B.13}$$

where $\mathbf{F}_i$ is the nuclear derivative of state ϵ_i. When inserting B.12 and B.13 into eq. B.5 one arrives after simple transformation at

$$\mathbf{d}_{12} = \pm\frac{c}{(\epsilon_2 - \epsilon_1)^2}\frac{(\epsilon_2 - \epsilon_1)(\mathbf{F}_1 - \mathbf{F}_2)}{\sqrt{(\epsilon_2 - \epsilon_1)^2 - 4c^2}} \mp \frac{c(\nabla c)}{(\epsilon_2 - \epsilon_1)^2}\left(\frac{(\epsilon_2 - \epsilon_1)^2 - 4c^2 + 4c}{\sqrt{(\epsilon_2 - \epsilon_1)^2 - 4c^2}}\right) \tag{B.14}$$

C leΔSCF - Contributions to Energy Derivatives

In this appendix the error in energy derivatives that was found for the leΔSCF approach (see chapter 11) is studied.

Linear expansion ΔSCF

In the current CASTEP implementation of leΔSCF the standard ground-state self-consistent field (SCF) DFT calculation is changed in two ways:

1. Constructing a Modified Orbital Space In every SCF step a resonance orbital is constructed as a linear combination with respect to a projection to a reference orbital ϕ_c:

$$|\tilde{\psi}_c^{\mathbf{k}}\rangle = \sum_i^{\text{states}} |\psi_i^{\mathbf{k}}\rangle \langle\psi_i^{\mathbf{k}}|\phi_c^{\mathbf{k}}\rangle \,, \tag{C.1}$$

while at the same time the remaining KS states have to be orthogonalized correspondingly:

$$|\tilde{\psi_i^{\mathbf{k}}}\rangle = |\psi_i^{\mathbf{k}}\rangle - \sum_c^{\text{constr.}} |\phi_c^{\mathbf{k}}\rangle \langle\phi_c^{\mathbf{k}}|\psi_i^{\mathbf{k}}\rangle \,. \tag{C.2}$$

After normalization a reshaped orbital space with a localized resonance state has been constructed. The corresponding states are not eigenstates of the system Hamiltonian and therefore additional force terms arise.

2. Constructing the Density from a non-Fermi Electron Distribution Within this reshaped non-variational orbital space, an excited-state density is constructed by distributing electrons in form of a non-Fermi distribution. This can be done in terms of single state-to-state electron transfer, for example from the highest ground-state occupied orbital to the lowest ground-state unoccupied orbital or by a more complex non-integer distribution of electrons that also accounts for thermal effects or photo-induced electron distributions. In all cases, the electron distribution does not represent an equilibrium ground-state Fermi distribution.

Numerical Tests

Using only the second above mentioned constraint corresponds to a simple ΔSCF treatment. In that case it can be observed that analytical forces correspond to numerical forces when orbital occupations are integer. This shows that minimizing the energy functional with respect to an excited-state Slater determinant yields a variational solution to this approximated excited-state for which the Hellman-Feynman theorem holds. Using only excited-state occupations with non-integer occupations does in fact introduce additional forces, due to the thermal uncertainty

Figure C.1: Binding energy curve of an isolated N_2 molecule. Gradient bars on the potential energy curves depict the nuclear forces at this point. Inset shows a zoom on the first excited state minimum. The vertical dotted line corresponds to the minimum of analytical energy derivatives.

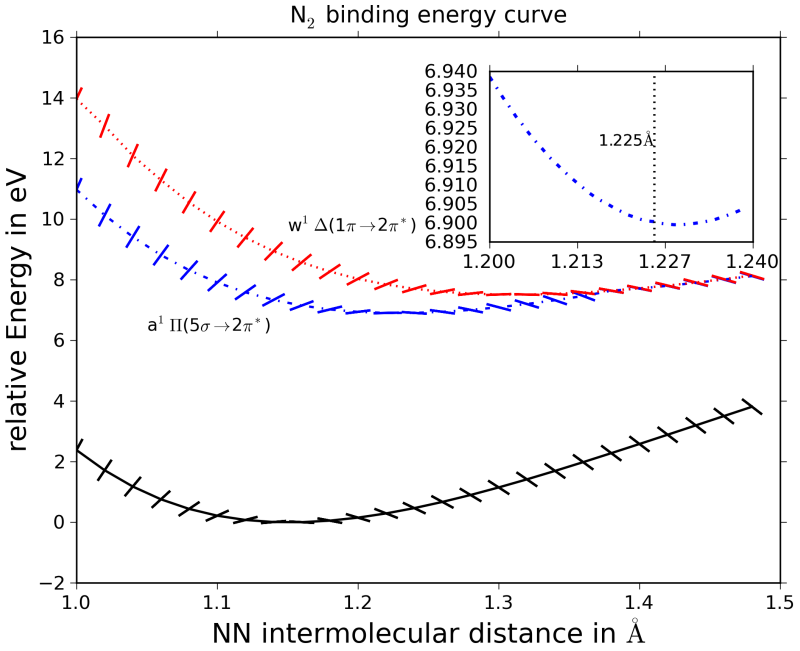

in the energy and the fact that we actually minimize a free-energy functional instead of the electronic energy functional. If this corresponds to a thermal non-zero temperature electron distribution, such errors are very often small and can be accounted for by definition of a free energy functional [301].

Using only the orbital transformation and modification of the eigenstates (the first constraint) without generating an excited-state density the energy does not change when projecting onto virtual states of the system (within 10^{-3} eV in the example case of N_2H_2@Au(111) projecting on to the π^*(LUMO) gas-phase orbital), but forces change significantly. Therefore, the energy and analytical derivatives are not consistent any more. As such, this transformation itself introduces additional force contributions. Due to the projection new variational parameters have been introduced, which change with changing nuclear positions.

Numerical tests on molecular systems (N_2, Azobenzene) have been performed, which also support the above statement for the limit of no hybridization. Figure C.1 shows for an isolated N_2 molecule that the energy and nuclear forces for the ground- and excited-state calculated with leΔSCF agree in the overall picture, but close examination shows that even in such a simple system, where the reference orbitals are identical with the ground-state orbitals of the system under study, when using leΔSCF there is a small error in the analytical forces that corresponds to a distance difference of 0.004 Å and an energy difference of 13 meV. An error of similar size can be found for the second excited state. When going from the limit of no hybridization to an adsorbed system, one finds that, the larger the constrained subspace of the Hilbert space, the bigger the error. For the example of gas-phase N_2 a similar error was found when employing the leΔSCF implementation in GPAW [29], although the absolute errors are different.

When constraining molecular systems with reference orbitals of the same system, the actual rehybridization that is enforced is very small. An error estimate for the ground-state and surface-mediated anionic resonance state of a surface-adsorbate system, where the reference

Figure C.2: Two-dimensional ground-state (left) and excited-state (right) potential energy surfaces of N_2 on Ruthenium (0001) with nuclear gradients visualized as vector field. The two directions are the vertical center of mass distance of the molecule from the surface and the intramolecular atomic distance. The excited-state potential energy surface also shows the ground-state surface in the background.

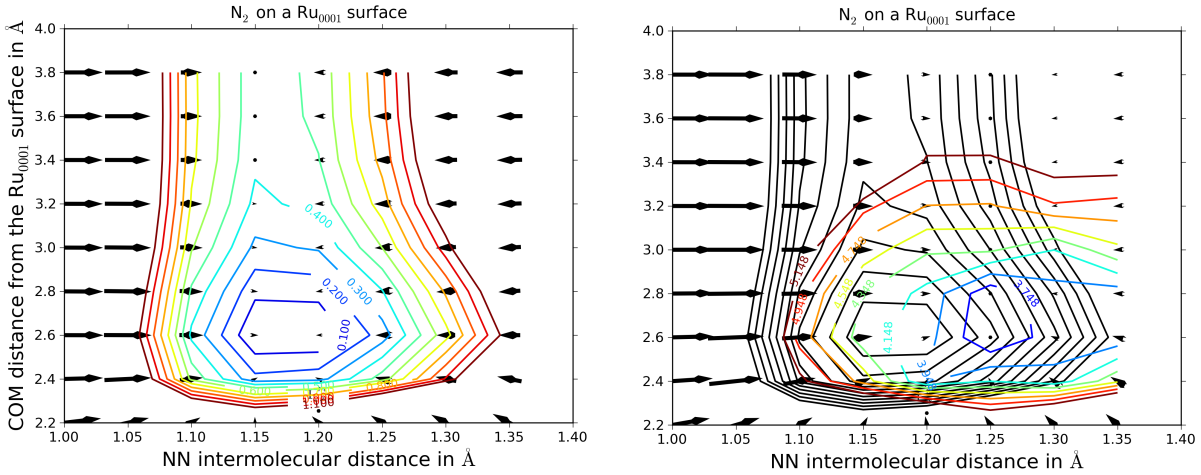

orbital stems from the corresponding gas-phase molecule, was done for N_2 adsorbed upright to Ru(0001), which was also the main test system in the study of Gavnholt *et al.* [29].

Here again the overall potential energy surface does not allow to identify a systematic error (Figure C.2), specifically not for the ground-state. However, numerical and analytical nuclear derivatives differ significantly in absolute values (at an exemplary position the F_z component orthogonal to the surface for the lower lying N atom, numeric: 4.309 eV/Å, analytic: 9.868 eV/Å). Initial comparisons and tests on larger systems, such as surface-adsorbed Azobenzene show that this effect is much larger for high-dimensional systems.

An Approach to Analytical Atomic Forces with leΔSCF:

As shown above the inconsistent force evaluation dominantly stems from the linear combination scheme. We can therefore focus on this issue independently from the ΔSCF occupation constraint. When minimizing the KS-DFT energy functional in the leΔSCF scheme one not only enforces orbital orthonormalization, but also orthonormality with respect to the specified gas-phase molecular orbital.

The standard ground state KS-DFT Lagrangian is given by:

$$L = E_{tot}[\{\psi\}; \mathbf{R}_I] = E^{KS}[\{\psi\}; \mathbf{R}_I] - \sum_i f_i \epsilon_i \left(\langle \psi_i | \psi_i \rangle - 1 \right), \tag{C.3}$$

where the constraint enforces orthonormality for the orbitals that are included in the density evaluation (specified by their occupation f_i and eigenenergy ϵ_i). The forces on the nuclei due to this Lagrangian are[1]

$$\mathbf{F}_I = -\frac{\partial E^{KS}(\mathbf{R}_I)}{\partial \mathbf{R}_I} + \frac{\partial}{\partial \mathbf{R}_I} \sum_i f_i \epsilon_i \langle \psi_i | \psi_i \rangle, \tag{C.4}$$

where the last term vanishes for the variational solution and non-local basis sets (e.g. plane waves). The standard force expression can be found in Martin [57], p.529.

[1] For more detailed derivations see the PhD Thesis of Ralph Gehrke [403].

Now in addition to the orthonormality of KS states, leΔSCF also enforces orthonormalization with respect to a set of arbitrary reference orbitals.

$$\begin{aligned} L^{\text{constr}} &= E_{tot}[\{\psi\};\mathbf{R}_I] + E^{\text{constr}}[\{\psi\};\mathbf{R}_I,\{\phi^c\}] = \\ &= E^{KS}[\{\psi\};\mathbf{R}_I] - \sum_i f_i\epsilon_i\left(\langle\psi_i|\psi_i\rangle - 1\right) - \\ &- \sum_c\sum_i f_i\lambda_i^c\left(\langle\psi_i|\phi_c\rangle - \langle\phi_c|\psi_i\rangle\right) \end{aligned}$$

The constraint enforces that

$$\langle\psi_i|\phi_c\rangle = \langle\phi_c|\psi_i\rangle\,.$$

Keeping in mind that the wavefunctions are complex, this is only true if the overlap integrals are either zero or one. This describes a transformation of the orbital space to one where KS states are orthonormal with respect to this one state $|\phi_c\rangle$. Now if we vary the wavefunctions with respect to $\langle\psi_i|$ we arrive at the following system of equations

$$\frac{\delta L}{\delta\langle\psi_i|} = \sum_i f_i\left\{\hat{H}\,|\psi_i\rangle - \epsilon_i\,|\psi_i\rangle - \sum_c\lambda_i^c\,|\phi_c\rangle\right\} \stackrel{!}{=} 0$$

The nuclear derivative that corresponds to this constrained DFT term is

$$\begin{aligned} \mathbf{F}_I &= \frac{\partial E^{\text{constr}}[\{\psi\};\mathbf{R}_I,\{\phi^c\}]}{\partial\mathbf{R}_I} = \\ &= \tfrac{\partial}{\partial\mathbf{R}_I}\textstyle\sum_i\lambda_i^c\cdot\left(\langle\psi_i|\phi^c\rangle - \langle\phi^c|\psi_i\rangle\right) \\ &= \textstyle\sum_i\lambda_i^c\cdot\left(\langle\psi_i|\tfrac{\partial}{\partial\mathbf{R}_I}\phi^c\rangle - \langle\tfrac{\partial}{\partial\mathbf{R}_I}\phi^c|\psi_i\rangle\right) \end{aligned}$$

To include these force contributions one needs to evaluate the λ_i^cs and the nuclear derivative with respect to the overlap integrals. During a ΔSCF run, the unconstrained Hamiltonian is diagonalized in every SCF step and afterwards the linear expansion constraint is applied. The difference between the eigenvalues before and after applying this constraint should give at least an estimate of λ_i^c.

$$\lambda_i^c = \underbrace{<\psi_i^{\text{after}}|\hat{H}|\psi_i^{\text{after}}>}_{\tilde{\epsilon}_i} - \underbrace{<\psi_i^{\text{pre}}|\hat{H}|\psi_i^{\text{pre}}>}_{\epsilon_i} \tag{C.5}$$

The nuclear derivatives on the overlap integrals reduce to the position dependence of the plane wave expansion coefficients (see appendix D). These 'Pulay'-like terms have not yet been reported for plane waves and no clear solution to their evaluation is known.

D DFT+U(MO): Self-Interaction Correction with an Orbital-Dependent Penalty Functional

A general methodological problem for the DFT description of surface adsorption phenomena are the different requirements to the theory posed by the different subsystems. While the electronic structure of a typical metal surface is dominated by delocalized smooth electronic states, where correlation and specifically exchange effects are strongly screened and only act very locally, the finite molecular states of the adsorbate experience a strong exchange contribution that leads to a large fundamental gap. In almost all cases, the electronic structure that is formed after hybridization still experiences these features and a correct description of the adsorbate-surface interaction crucially depends on correctly capturing the localized nature of adsorbate and delocalized nature of substrate states. This poses a great challenge to currently used exchange-correlation functional approximations, such as typically employed semi-local xc-functionals, which yield a good description of the band structure of main group metals and coinage metals, but, due to their inherent self-interaction error, give a bad description of isolated molecules, semi-conductors, and transition metal compounds (see Gross [262], pp. 57 ff.).

In the case of isolated molecules and also semi-conductor surfaces this self-interaction error can be reduced by admixture of exact Hartree-Fock exchange to the xc-functional approximation [61, 62] or the use of many-body perturbation theory approaches such as the GW method [295, 296].

When treating transition metal surfaces or also large band-gap semi-conductor surfaces, for a long time a more modest approach has been used, namely an empirical self-interaction correction approach based on explicit orbital dependence. This approach is generally termed LDA+U or DFT+U, specifically referring to the additional parametrized potential that is added to the standard DFT description [315, 317, 404, 405]. The semi-local self-interaction error prone functionals do not correctly predict the strong splitting in occupied and unoccupied d and f states, thereby resulting in artificial, often non-integer occupation of a large part of the corresponding bands. In order to correctly predict magnetic properties and the correct chemisorption behavior of certain species this integer occupation can be enforced by a DFT+U potential of the following form [209, 406]

$$E_U = \sum_I \frac{U^I}{2} \sum_\sigma \mathrm{Tr}[\mathbf{n}^{I\sigma}(\mathbf{1} - \mathbf{n}^{I\sigma})], \tag{D.1}$$

where the sum runs over all ions I and spin channels σ, U^I is an ion-dependent empirical

parameter, and $\mathbf{n}^{I\sigma}$ is an occupation matrix defined as

$$n^{I\sigma}_{mm'} = \sum_{\mathbf{k},\nu} f_\nu \langle \psi^\sigma_{\mathbf{k}\nu} | \phi^I_m \rangle \langle \phi^I_{m'} | \psi^\sigma_{\mathbf{k}\nu} \rangle , \tag{D.2}$$

where $\mathbf{k}$ specifies the crystal momentum, ν the band index, and ϕ_m and $\phi_{m'}$ specify atom-centered orbitals in a certain sub-space $\{m\}$, for example the space of d-orbitals.

At a specified value of U^I this constraint-functional is minimal when the occupation matrix equals its own square, *i.e.* when the occupation matrix is idempotent. This statement is identical to only allowing integer diagonal elements and therefore integer occupations of the d-orbitals.

Following the ideas of Kresse *et al.* that have been employed in the case of CO adsorption on Pt(111)[313], the self-interaction error in molecular states of adsorbates can be tackled by employing such a constraint functional not to atomic reference states, but to molecular gas-phase reference states, such as the ones presented in chapter 11.2 (in the following this approach will be termed DFT+U(MO)). The corresponding occupation 'matrix' can be defined as

$$n_c = \sum_{\mathbf{k},\nu} \langle \psi_{\mathbf{k}\nu} | \phi_c \rangle \langle \phi_c | \psi_{\mathbf{k}\nu} \rangle = \sum_{\mathbf{k},\nu} \bar{n}^{\mathbf{k},\nu}_c, \tag{D.3}$$

where every reference molecular orbital ϕ_c specifies a one-orbital subspace. To simplify things we neglect spin for the moment. Correspondingly, n_c represents the effective occupation of this orbital ϕ_c. Similar to eq. D.1 one can define the following constraint functional

$$E^{\mathrm{U,I}}_c = \frac{U}{2} n_c (1 - n_c), \tag{D.4}$$

which enforces integer occupations in the reference gas-phase molecular orbital ϕ_c. At positive values of U this functional is minimal at zero occupation of ϕ_c, at negative values the lowest value is achieved at full occupation. After variation with respect to the density one arrives at the constraint potential

$$\hat{V}^{\mathrm{U,I}}_c = \frac{\delta E^{\mathrm{U,I}}_c}{\delta \rho} = \frac{U}{2} (1 - 2n_c) \, |\phi_c\rangle \langle \phi_c| \, . \tag{D.5}$$

From this it can be seen that this additional potential to the Hamiltonian gives a contribution depending on the overlap with ϕ_c. Finding the optimal parameter of U to satisfy the idempotency constraint can be done in a second self-consistency loop in which U is varied.

This constraint can be used to lift artificially strong hybridization of adsorbate electronic states with surface states and also to enforce or remove charge-transfer to or from these states. However, of much larger interest in the context of a self-interaction-correction to adsorbate electronic states is a functional along the lines of constrained DFT [106] in the following form:

$$E^{\mathrm{U,II}}_c = \frac{U}{2} (n_c - N_c), \tag{D.6}$$

where n_c specifies the above mentioned occupation of ϕ_c and N_c is the envisioned electron occupation to be constrained. This functional is optimal when the occupation N_c is reached, which again would be achieved by optimizing the Lagrange parameter U correspondingly. The potential connected to this functional is

$$\hat{V}^{\mathrm{U,II}}_c = \frac{U}{2} \cdot |\phi_c\rangle \langle \phi_c| \tag{D.7}$$

This potential shifts bands according to their overlap with ϕ_c. Positive values of U increase the eigenvalues of bands that overlap with ϕ_c, negative ones decrease them. This constraint can

be used to enforce a certain occupation N_c, and therefore analyse the effect of self-interaction error correction on the observed charge transfer between the adsorbate and the substrate, as has been done in a similar fashion in Kresse *et al.* [313]. For large-scale systems this enables an assessment of how sensitively the adsorbate binding behavior obtained from semi-local xc-functionals depends on the associated self-interaction error and the therewith underestimated HOMO-LUMO gap of the molecule.

Much more connected to the topic of this thesis, such an approach could also be used in connection with the highly efficient leΔSCF scheme. The approach as presented and used in this work yields qualitatively correct excited-state potential energy surfaces, but due to the self-interaction error inherent to semi-local xc-functionals that are used for adsorption on metal surfaces, systematically too low absolute excitation energies. Although such a correction is highly empirical and corresponding sets of constraints and U parameters have to be specified from scratch for every individual system, it enables a very efficient calculation of excitation energies for large adsorbate systems with only minimal losses in accuracy. A corresponding DFT+U(MO) treatment will be presented at the end of this appendix for the excited-state isomerization of gas-phase Azobenzene.

Similar correction schemes have been used in a series of works of Flores, Ortega, and co-workers [407–409] in the context of band-level alignment of organic electronics. The authors employed a scissors-operator of the following kind to correct the molecule HOMO-LUMO gap with a constant value U:

$$\hat{V}^{\text{scissors}} = \frac{U}{2} \sum_{\mu_i,\nu_i} \left[|\mu_i\rangle \langle\mu_i| - |\nu_i\rangle \langle\nu_i| \right] \tag{D.8}$$

The sum runs over all pairs of occupied and virtual orbitals. One single parameter U corrects the gap between occupied and unoccupied states. Additionally, the authors also correct for the charging of the molecule by systematically shifting the whole molecular level spectrum with respect to the Fermi level of the metal surface employing following potential:

$$\hat{V}_{\alpha}^{\text{shift}} = \epsilon_{\alpha} \sum_{\beta} |\beta\rangle \langle\beta| \,, \tag{D.9}$$

where β runs over all molecular levels. This highly empirical way of correcting the shortcomings of semi-local xc-functionals in describing molecular resonances can yield a very accurate description of adsorbate electronic structure, but only for equilibrium geometries. In a wider context of surface reactions and excited-state dynamics a global scissors operator could not describe state crossings.

Nuclear Forces due to the Constraint Potentials Due to the fact that the Hamiltonian and the constraint potential are known and eigenvalues and eigenfunctions are calculated self-consistently, the Hellmann-Feynman [410, 411] theorem holds and in principal one should be able to calculate the forces on the atoms due to this constraint.

The corresponding force expressions for the two potentials that have been presented here are

$$\mathbf{F}_{c,\mathbf{R}}^{\text{U,I}} = \frac{\partial E_c^{\text{U,I}}}{\partial \mathbf{R}} = \frac{U}{2} \cdot \sum_{\mathbf{k}\nu} f_{\mathbf{k}\nu} (1 - 2n_c^{\mathbf{k}\nu}) \frac{\partial \bar{n}_c^{\mathbf{k}\nu}}{\partial \mathbf{R}} \tag{D.10}$$

and

$$\mathbf{F}_{c,\mathbf{R}}^{\text{U,II}} = \frac{\partial E_c^{\text{U,II}}}{\partial \mathbf{R}} = \frac{U}{2} \cdot \sum_{\mathbf{k}\nu} f_{\mathbf{k}\nu} \frac{\partial \bar{n}_c^{\mathbf{k}\nu}}{\partial \mathbf{R}}, \tag{D.11}$$

where $\mathbf{R}$ specifies nuclear coordinates and $f_{\mathbf{k}\nu}$ is the occupation of band $\psi_{\mathbf{k}\nu}$. The remaining issue is to find the derivative of $n_c^{\mathbf{k}\nu}$ with respect to $\mathbf{R}$, which can be rewritten in the following way:

$$\frac{\partial \bar{n}_c^{\mathbf{k}\nu}}{\partial \mathbf{R}} = \frac{\partial \left(\langle \psi_{\mathbf{k}\nu} | \phi_c \rangle \langle \phi_c | \psi_{\mathbf{k}\nu} \rangle \right)}{\partial \mathbf{R}} = \left(\frac{\partial}{\partial \mathbf{R}} \langle \psi_{\mathbf{k}\nu} | \phi_c \rangle \right) \langle \phi_c | \psi_{\mathbf{k}\nu} \rangle + \langle \psi_{\mathbf{k}\nu} | \phi_c \rangle \left(\frac{\partial}{\partial \mathbf{R}} \langle \phi_c | \psi_{\mathbf{k}\nu} \rangle \right) \tag{D.12}$$

with

$$\frac{\partial}{\partial \mathbf{R}} \langle \psi_{\mathbf{k}\nu} | \phi_c \rangle = \langle \psi_{\mathbf{k}\nu} | \frac{\partial}{\partial \mathbf{R}} | \phi_c \rangle \,. \tag{D.13}$$

The last equality in eq D.13 stems from the fact that forces are always evaluated at the end of a calculation at which point the $\psi_{\mathbf{k}\nu}$ are self-consistent variational solutions to the Hamiltonian, therefore the derivatives of $\psi_{\mathbf{k}\nu}$ with respect to $\mathbf{R}$ vanish. This does however not hold for the derivative of ϕ_c with respect to $\mathbf{R}$. The results strongly depend on the position of the non-variational reference orbital ϕ_c with respect to the atomic nuclei. Such 'Pulay'-like terms [412] are very uncommon in pseudopotential-plane-wave approaches, but arise naturally when using localized basis sets or augmented plane wave approaches [413]. Therefore possible paths to evaluate such integrals, either numerically or via a pertubative treatment could be found in the corresponding literature.

Example: Correcting ΔSCF Excitation Energies of Gas Phase Azobenzene using DFT+U(MO)

As mentioned in chapter 6 of this thesis, the ΔSCF approach yields a good account of the qualitative features of excited-state potential energy surfaces involved in the photo-isomerization process of gas-phase Azobenzene. Unfortunately, the absolute excitation energies are systematically too low due to the inherent self-interaction error of the employed semi-local GGA-PBE functional [60]. In the context of surface adsorbed molecular switching, admixing exact-exchange is no option to correct for this shortcoming due to its undesirable effect on the envisioned surface electronic structure [224, 314]. However the above introduced empirical correction scheme might pose an efficient approach to achieve an improved description of absolute excitation energies of surface adsorbed organic molecules.

In the following the differences between ΔSCF excitation energies on the basis of GGA-PBE and GGA-PBE+U(MO) will be tested. For this purpose ΔSCF(GGA-PBE+U(MO)) excitation energies of the minimum energy path geometries of gas-phase Ab along rotation and inversion from chapter 6 are calculated. The therefor employed constraint potential is the one defined in eq. D.6. The corresponding reference orbitals ϕ_c are the optimized ground state KS orbitals of gas-phase Ab calculated with GGA-PBE. Constraints have been applied to the frontier orbitals HOMO-4 to HOMO-1 and LUMO to LUMO+3. The used U values can be found in table D.1. The calculations have been performed in a (20Å×20Å×20Å) supercell employing a 350 eV plane-wave cutoff, standard library pseudopotentials and by only considering the electronic structure at the Γ-point. Excited-state energies have been calculated using the leΔSCF scheme as presented in chapter 11. The reference orbitals used for the leΔSCF part are the excited-state orbitals optimized for every corresponding state as calculated by ΔSCF(GGA-PBE). To clarify, the +U-correction is based on projections on the ground-state orbitals, the leΔSCF calculations are based on projections on the optimized excited-state orbitals (calculated via simple ΔSCF) corresponding to the envisioned excitation.

Table D.1: List of employed U values in the calculation of ΔSCF(GGA-PBE+U(MO)) excitations of Azobenzene shown in Fig. D.1.

Orbital	U value in eV
HOMO-4	-0.90
HOMO-3	-0.90
HOMO-2	-0.90
HOMO-1	-0.90
HOMO	0.00
LUMO	1.45
LUMO+1	1.45
LUMO+2	1.45
LUMO+3	1.45

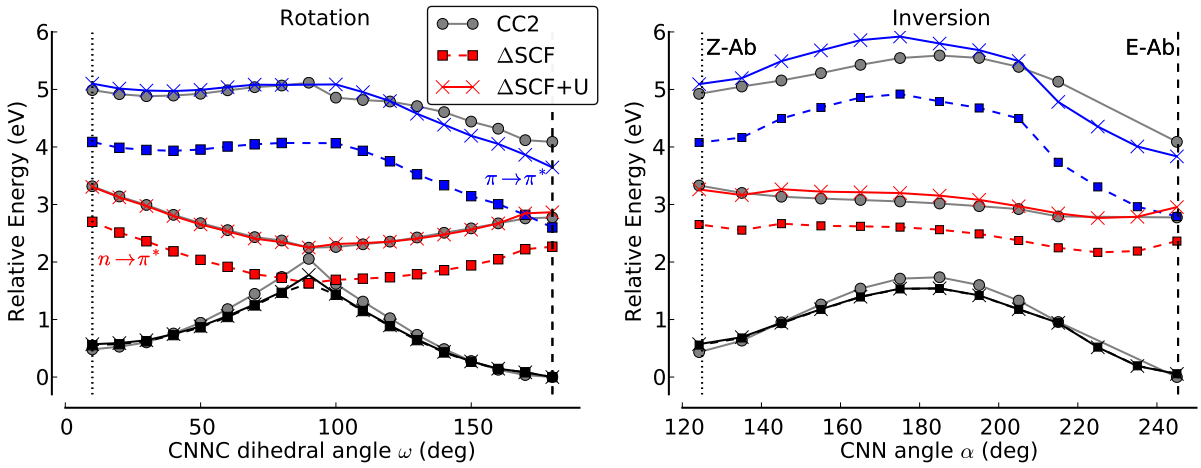

Figure D.1: Ground and excited state energies of gas-phase Azobenzene minimum energy paths along rotation and inversion degrees of freedom (see Fig. 5.2 for definition). Shown are the energies as calculated by RI-CC2 (grey circles), ΔSCF-DFT(GGA-PBE) (squares), and ΔSCF-DFT(GGA-PBE+U(MO)) for the ground state (black), first (red), and second (blue) excited state.

Figure D.1 shows ground- and excited-state energies for the minimum energy paths of Azobenzene along rotation and inversion degrees of freedom. The corresponding energies of the first and second excited states as calculated with ΔSCF(GGA-PBE) are systematically too low when compared to RI-CC2 results. However the qualitative features such as barriers, relative energies, and the state crossing between ground state and first excited-state at mid-rotation are correctly reproduced. When calculating the leΔSCF energies on the basis of the GGA-PBE+U(MO) method with the U constraints as listed in Table D.1 one arrives at the results represented by crosses and straight lines in Fig. D.1. The relative ground-state energetics are almost completely unaffected by the constraint-potential, with the exception of the mid-rotation point. The corresponding barrier with respect to E-Ab is slightly increased (1.78 eV) compared to the standard DFT value of 1.74 eV, but not enough to reach the CC2 value of 2.05 eV. In contrast to this, both excited-state potential energy surfaces are systematically shifted towards higher energies and now almost match the Coupled Cluster results in terms of absolute ener-

gies, but also in relative energies within an excited-state. The fact that with this U-scheme the excited-state energies are systematically shifted, but the ground-state is unaffected leads to an effective removal of the state crossing at the 90° mid-rotation point. The removal of this efficient radiationless de-excitation channel has drastic implications to the photoisomerization dynamics. It should be noted here that systematically exploring different combination of U-constraints, it should be possible to find a correction that also increases the mid-rotation barrier and does not lift the state crossing.

It can be summarized that an effective self-interaction correction approach such as the DFT+U(MO) method that modifies orbital energies is able to yield correct absolute excitation energies over a large range of different geometries and will also be able to correct the KS orbital positioning of large organic molecules on metal surfaces. However, in the special case of photochemical processes that include conical intersection points, such as the mid-rotation point in gas-phase Ab, an unbalanced modification of the excited-state surfaces and the ground-state can destroy the main feature that governs the photochemical behavior of the molecule. Therefore, such an approach also has to modify the ground-state energetics correspondingly. In the special case of Azobenzene, this could eventually be achieved by a significant upward shift of the highest occupied molecular orbital. In general, this group of constraint potentials has to be tested in more detail, to assess their applicability to excited-state treatments.

List of Publications

Publications, which are directly related to this thesis:

12. G. Mercurio, R.J. Maurer, S. Hagen, F. Leyssner, J. Meyer, P. Tegeder, S. Soubatch, K. Reuter, and F.S. Tautz, "X-ray standing wave simulations based on Fourier vector analysis as a method to retrieve complex molecular adsorption geometries", *Frontiers in Physics*, **2**, 2 (2014), DOI: 10.3389/fphy.2014.00002.

11. R.J. Maurer, and K. Reuter, "Excited-state potential-energy surfaces of metal-adsorbed organic molecules from linear expansion Δ-self-consistent field density-functional theory (ΔSCF-DFT)", *J. Chem. Phys.* **139**, 014708 (2013), DOI: 10.1063/1.4812398.

10. G. Mercurio, R.J. Maurer, W. Liu, S. Hagen, F. Leyssner, P. Tegeder, J. Meyer, A. Tkatchenko, S. Soubatch, K. Reuter, and F.S. Tautz, "Quantification of finite-temperature effects on adsorption geometries of π-conjugated molecules: Azobenzene/Ag(111)", *Phys. Rev. B* **88**, 035421 (2013), DOI: 10.1103/PhysRevB.88.035421.

9. R.J. Maurer and K. Reuter, "Bistability Loss as a Key Feature in Azobenzene (Non-) Switching on Metal Surfaces", *Angew. Chem. Int. Ed.* **51**, 12009–12011 (2012), DOI: 10.1002/anie.201205718.

8. R.J. Maurer, and K. Reuter, "Assessing computationally efficient isomerization dynamics: ΔSCF density-functional theory study of azobenzene molecular switching.", *J. Chem. Phys.*, **135**, 224303 (2011), DOI: 10.1063/1.3664305.

Other publications:

7. T.G. Gopakumar, T. Davran-Candan, J. Bahrenburg, R.J. Maurer, F. Temps, K. Reuter, and R. Berndt, "Broken Symmetry of an Adsorbed Molecular Switch Determined by Scanning Tunneling Spectroscopy", *Angew. Chem. Int. Ed.* **52**, 11007–11010 (2013), DOI: 10.1002/anie.201305027.

6. R.J. Maurer, A.F. Sax, and V. Ribitsch, "Molecular simulation of surface reorganization and wetting in crystalline cellulose I and II", *Cellulose* **20**, 25-42 (2013), DOI: 10.1007/s10570-012-9835-9.

5. S. Engelskirchen, R. Maurer, T. Levy, R. Berghaus, H. Auweter, and O. Glatter, "Highly concentrated emulsified microemulsions as solvent-free plant protection formulations.", *J. Colloid Interface Sci.* **388**, 151–161 (2012), DOI: 10.1016/j.jcis.2012.06.084.

4. S. Engelskirchen, R. Maurer, T. Levy, R. Berghaus, H. Auweter, and O. Glatter, "Emulsified Microemulsions as Solvent-free Carrier for an Amorphous Solid Plant Protection Agent", *Chem. Lett.* **41**, 1125–1127 (2012), DOI: 10.1246/cl.2012.1125.

3. S. Engelskirchen, R. Maurer, and O. Glatter, "Effect of glycerol addition on the internal structure and thermal stability of hexosomes prepared from phytantriol", *Colloids Surf., A* **41**, 95–100 (2011), DOI: 10.1016/j.colsurfa.2011.10.001.

2. R.J. Maurer and A.F. Sax, "Molecular dynamics of cellulose crystal surfaces with ChemShell", *Proc. Comp. Sci.* **1**, 1149–1154 (2010), DOI: 10.1016/j.procs.2010.04.128.

1. R.J. Maurer and A.F. Sax, "Solvation of carbon nanotubes by aniline calculated with density functional tight binding", *Phys. Chem. Chem. Phys.: PCCP* **12**, 9893–9899 (2010), DOI: 10.1039/c001066a.

List of Figures

List of Tables

Bibliography

[1] C Joachim, J. Gimzewski, and A. Aviram, *Electronics using hybrid-molecular and mono-molecular devices*, Nature **408**, 541 (2000), (cit. on pp. 1, 57).

[2] M.-M. Russew and S. Hecht, *Photoswitches: from molecules to materials.* Adv. Mat. **22**, 3348 (2010), (cit. on p. 1).

[3] Y Cui, Q Wei, H Park, and C. M. Lieber, *Nanowire nanosensors for highly sensitive and selective detection of biological and chemical species.* Science **293**, 1289 (2001), (cit. on p. 1).

[4] K. Uchida, N. Izumi, S. Sukata, Y. Kojima, S. Nakamura, and M. Irie, *Photoinduced reversible formation of microfibrils on a photochromic diarylethene microcrystalline surface.* Angew. Chem. Int. Ed. **45**, 6470 (2006), (cit. on pp. 1, 57).

[5] V Balzani, A Credi, F. Raymo, and J. Stoddart, *Artificial Molecular Machines.* Angew. Chem. Int. Ed. **39**, 3348 (2000), (cit. on p. 1).

[6] B. L. Feringa, *Molecular Switches*, Wiley-VCH, Weinheim, 2001, ISBN: 3527299653, (cit. on pp. 1, 37).

[7] T. Ikeda and O Tsutsumi, *Optical Switching and Image Storage by Means of Azobenzene Liquid-Crystal Films*, Science **268**, 1873 (1995), (cit. on pp. 1, 57).

[8] N. Katsonis, T. Kudernac, M. Walko, S. J. van der Molen, B. J. van Wees, and B. L. Feringa, *Reversible Conductance Switching of Single Diarylethenes on a Gold Surface*, Adv. Mat. **18**, 1397 (2006), (cit. on pp. 1, 57).

[9] G. Schulze, K. J. Franke, and J. I. Pascual, *Induction of a Photostationary Ring-OpeningRing-Closing State of Spiropyran Monolayers on the Semimetallic Bi(110) Surface*, Phys. Rev. Lett. **109**, 026102 (2012), (cit. on p. 2).

[10] M. Comstock, J. Cho, A. Kirakosian, and M. Crommie, *Manipulation of azobenzene molecules on Au(111) using scanning tunneling microscopy*, Phys. Rev. B **72**, 153414 (2005), (cit. on pp. 2, 57).

[11] S Venkataramani, U Jana, M Dommaschk, F. D. Sönnichsen, F Tuczek, and R Herges, *Magnetic bistability of molecules in homogeneous solution at room temperature.* Science **331**, 445 (2011), (cit. on p. 2).

[12] C. Wäckerlin, D. Chylarecka, A. Kleibert, K. Müller, C. Iacovita, F. Nolting, T. A. Jung, and N. Ballav, *Controlling spins in adsorbed molecules by a chemical switch.* Nature Commun. **1**, 61 (2010), (cit. on p. 2).

[13] S. Hagen, F. Leyssner, D. Nandi, M. Wolf, and P. Tegeder, *Reversible switching of tetra-tert-butyl-azobenzene on a Au (1 1 1) surface induced by light and thermal activation*, Chem. Phys. Lett. **444**, 85 (2007), (cit. on pp. 2, 58, 59, 83, 117, 120).

[14] B.-Y. Choi, S.-J. Kahng, S. Kim, H. Kim, H. Kim, Y. Song, J. Ihm, and Y. Kuk, *Conformational Molecular Switch of the Azobenzene Molecule: A Scanning Tunneling Microscopy Study*, Phys. Rev. Lett. **96**, 156106 (2006), (cit. on pp. 2, 57, 58, 86).

[15] R. A. van Delden, M. K. J. ter Wiel, M. M. Pollard, J. Vicario, N. Koumura, and B. L. Feringa, *Unidirectional molecular motor on a gold surface.* Nature **437**, 1337 (2005), (cit. on p. 2).

[16] N Katsonis, M Lubomska, M Pollard, B Feringa, and P Rudolf, *Synthetic light-activated molecular switches and motors on surfaces*, Progr. Surf. Sci. **82**, 407 (2007), (cit. on pp. 2, 57).

[17] G. S. Kottas, L. I. Clarke, D. Horinek, and J. Michl, *Artificial molecular rotors.* Chem. Rev. **105**, 1281 (2005), (cit. on p. 2).

[18] T. Kudernac, N. Ruangsupapichat, M. Parschau, B. Maciá, N. Katsonis, S. R. Harutyunyan, K.-H. Ernst, and B. L. Feringa, *Electrically driven directional motion of a four-wheeled molecule on a metal surface.* Nature **479**, 208 (2011), (cit. on p. 2).

[19] G. S. Hartley, *The Cis-form of Azobenzene*, Nature **140**, 281 (1937), (cit. on pp. 2, 37, 38).

[20] H. Rau, *Spectroscopic Properties of Organic Azo Compounds*, Angew. Chem. Int. Ed. **12**, 224ß235 (1973), (cit. on pp. 2, 37, 38).

[21] M. Comstock, N. Levy, A. Kirakosian, J. Cho, F. Lauterwasser, J. Harvey, D. Strubbe, J. Fréchet, D. Trauner, S. Louie, and Others, *Reversible photomechanical switching of individual engineered molecules at a metallic surface*, Phys. Rev. Lett. **99**, 38301 (2007), (cit. on pp. 2, 57, 58, 120).

[22] M. Alemani, S. Selvanathan, F. Ample, M. V. Peters, K.-H. Rieder, F. Moresco, C. Joachim, S. Hecht, and L. Grill, *Adsorption and Switching Properties of Azobenzene Derivatives on Different Noble Metal Surfaces: Au(111), Cu(111), and Au(100)*, J. Phys. Chem. Lett. **112**, 10509 (2008), (cit. on pp. 2, 58).

[23] C. Bronner, M. Schulze, S. Hagen, and P. Tegeder, *Electronic structure of adsorbate / substrate complexes : influence on the photoisomerization ability*, N. J. Phys. **14**, 043023 (2012), (cit. on pp. 2, 59, 60, 83, 117).

[24] C. Gahl, K. Ishioka, Q. Zhong, A. Hotzel, and M. Wolf, *Structure and dynamics of excited electronic states at the adsorbate/metal interface: C6F6/Cu(111)*, Faraday Discuss. **117**, 191 (2000), (cit. on p. 2).

[25] P. S. Kirchmann, P. a. Loukakos, U Bovensiepen, and M Wolf, *Ultrafast electron dynamics studied with time-resolved two-photon photoemission: intra- and interband scattering in C6F6/Cu(111)*, New J. Phys. **7**, 113 (2005), (cit. on p. 2).

[26] S. Hagen, P. Kate, F. Leyssner, D. Nandi, M. Wolf, and P. Tegeder, *Excitation mechanism in the photoisomerization of a surface-bound azobenzene derivative: Role of the metallic substrate.* J. Chem. Phys. **129**, 164102 (2008), (cit. on pp. 2, 58–60, 111, 112).

[27] E. R. McNellis, G. Mercurio, S. Hagen, F. Leyssner, J. Meyer, S. Soubatch, M. Wolf, K. Reuter, P. Tegeder, and F. S. Tautz, *Bulky spacer groups - A valid strategy to control the coupling of functional molecules to surfaces?*, Chem. Phys. Lett. **499**, 247 (2010), (cit. on pp. 2, 41, 59, 61, 65, 69, 71, 72, 83, 92).

[28] M. Wolf and P. Tegeder, *Reversible molecular switching at a metal surface: A case study of tetra-tert-butyl-azobenzene on Au(111)*, Surf. Sci. **603**, 1506 (2009), (cit. on pp. 2, 59, 60, 83, 93, 111, 116, 117, 122, 139).

[29] J. Gavnholt, T. Olsen, M. Engelund, and J. Schiøtz, *Δ self-consistent field method to obtain potential energy surfaces of excited molecules on surfaces*, Phys. Rev. B **78**, 075441 (2008), (cit. on pp. 3, 41, 98, 100, 101, 103, 108, 138, 152, 153).

[30] A Szabo and N. Ostlund, *Modern quantum chemistry - introduction to advanced electronic structure theory*, First Edit, McGraw-Hill, New York, 1989, ISBN: 0486691861, (cit. on pp. 7, 9, 16, 97).

[31] A. L. Fetter and J. D. Walecka, *Quantum Theory of Many-Particle Systems*, McGraw-Hill, New York, 1971, ISBN: 0486428273, (cit. on p. 7).

[32] R. G. Parr and W. Yang, *Density-Functional Theory of Atoms and Molecules*, Oxford University Press, New York, 1989, ISBN: 978-0195092769, (cit. on pp. 7, 17).

[33] D. A. McQuarrie and J. D. Simon, *Physical Chemistry: A Molecular Approach*, University Science Books, 1997, ISBN: 978-0935702996, (cit. on p. 7).

[34] W. Kutzelnigg, *Einführung in die Theoretische Chemie, Band 1*, Wiley-VCH, Weinheim, 1975, ISBN: 3527254595, (cit. on pp. 7, 11).

[35] E. Schrödinger, *Quantisierung als Eigenwertproblem*, Annalen der Physik **384**, 361 (1926), (cit. on p. 7).

[36] M. Born and R. Oppenheimer, *Zur Quantentheorie der Molekeln*, Annalen der Physik **389**, 457 (1927), (cit. on p. 8).

[37] W. Kutzelnigg, *The adiabatic approximation I. The physical background of the Born-Handy ansatz*, Mol. Phys. **90**, 909 (1997), (cit. on p. 9).

[38] M. Born and K. Huang, *Dynamical Theory of Crystal Lattices*, Oxford University Press, Oxford, 1955, ISBN: 9780198503699, (cit. on p. 9).

[39] A. M. Wodtke, J. C. Tully, and D. J. Auerbach, *Electronically non-adiabatic interactions of molecules at metal surfaces: Can we trust the BornOppenheimer approximation for surface chemistry?*, Int. Rev. Phys. Chem. **23**, 513 (2004), (cit. on pp. 9, 125).

[40] G. A. Worth and L. S. Cederbaum, *Beyond Born-Oppenheimer: molecular dynamics through a conical intersection.* Ann. Rev. Phys. Chem. **55**, 127 (2004), (cit. on p. 9).

[41] H. A. Bethe and E. E. Salpeter, *Quantum Mechanics of One- and Two-Electron Atoms*, Academic Press, New York, 1957, ISBN: 978-0486466675, (cit. on p. 11).

[42] L. Genovese, A. Neelov, S. Goedecker, T. Deutsch, S. A. Ghasemi, A. Willand, D. Caliste, O. Zilberberg, M. Rayson, A. Bergman, and R. Schneider, *Daubechies wavelets as a basis set for density functional pseudopotential calculations.* J. Chem. Phys. **129**, 014109 (2008), (cit. on p. 12).

[43] R. D. Mattuck, *A Guide to Feynman Diagrams in the Many-Body Problem*, McGraw-Hill, New York, 1976, ISBN: 9780486670478, (cit. on p. 13).

[44] R. Bartlett and M. Musia, *Coupled-cluster theory in quantum chemistry*, Rev. Mod. Phys **79**, 291 (2007), (cit. on p. 15).

[45] K. Raghavachari, G. W. Trucks, J. A. Pople, and M. Head-Gordon, *A fifth-order perturbation comparison of electron correlation theories*, Chem. Phys. Lett. **157**, 479 (1989), (cit. on p. 16).

[46] O Christiansen, H. Koch, and P. Jørgensen, *The second-order approximate coupled cluster singles and doubles model CC2*, Chem. Phys. Lett. **243**, 409 (1995), (cit. on pp. 16, 42, 43, 106, 143).

[47] C. Hättig and F. Weigend, *CC2 excitation energy calculations on large molecules using the resolution of the identity approximation*, J. Chem. Phys. **113**, 5154 (2000), (cit. on pp. 16, 42, 43, 143).

[48] W. Koch and M. C. Holthausen, *A Chemist's Guide to Density Functional Theory*, Second Edi, Wiley-VCH, Weinheim, 2001, ISBN: 3527303723, (cit. on pp. 17, 21).

[49] R. Dreizler and E. Gross, *Density Functional Theory*, Springer, Berlin Heidelberg, 1990, ISBN: 9780306449055, (cit. on p. 17).

[50] C. A. Ullrich, *Time-Dependent Density-Functional Theory*, Oxford University Press, New York, 2012, ISBN: 978-0199563029, (cit. on p. 17).

[51] P. Hohenberg and W. Kohn, *Inhomogeneous Electron Gas*, Phys. Rev. **136**, B864 (1964), (cit. on pp. 18, 97, 98).

[52] M. Levy, *Universal Variational Functionals of Electron Densities, First-Order Density Matrices, and Natural Spin-Orbitals and Solution of the v-Representability Problem*, Proc. Natl. Acad. Sci. U.S.A. **76**, 6062 (1979), (cit. on p. 19).

[53] M. Levy, *Electron densities in search of Hamiltonians*, Phys. Rev. A **26**, 1200 (1982), (cit. on p. 19).

[54] J. T. Chayes, L. Chayes, and M. B. Ruskai, *Density functional approach to quantum lattice systems*, J. Stat. Phys. **38**, 497 (1985), (cit. on p. 20).

[55] W. Kohn and L. J. Sham, *Self-Consistent Equations Including Exchange and Correlation Effects*, Phys. Rev. **140**, A1133 (1965), (cit. on pp. 20, 22, 97, 99).

[56] P. Gori-Giorgi and M. Seidl, *Density functional theory for strongly-interacting electrons: perspectives for physics and chemistry.* Phys. Chem. Chem. Phys.: PCCP **12**, 14405 (2010), (cit. on p. 20).

[57] R. M. Martin, *Electronic Structure: Basic theory and practical methods*, Cambridge University Press, Cambridge, 2011, ISBN: 978-0521534406, (cit. on pp. 22, 32, 153).

[58] S. H. Vosko, L Wilk, and M Nusair, *Accurate spin-dependent electron liquid correlation energies for local spin density calculations: a critical analysis*, Can. J. Phys. **58**, 1200 (1980), (cit. on p. 22).

[59] D. Ceperley and B. Alder, *The ground state of the electron gas by a stochastic method*, Phys. Rev. Lett. **45**, 566 (1980), (cit. on p. 22).

[60] J. P. Perdew, K. Burke, and M. Ernzerhof, *Generalized Gradient Approximation Made Simple*, Phys. Rev. Lett. **77**, 3865 (1996), (cit. on pp. 23, 42, 65, 158).

[61] A. D. Becke, *A new mixing of HartreeFock and local density-functional theories*, J. Chem. Phys. **98**, 1372 (1993), (cit. on pp. 23, 42, 155).

[62] C. Adamo and V. Barone, *Toward reliable density functional methods without adjustable parameters: The PBE0 model*, J. Chem. Phys. **110**, 6158 (1999), (cit. on pp. 23, 155).

[63] P. J. Stephens, F. J. Devlin, C. F. Chabalowski, and M. J. Frisch, *Ab Initio Calculation of Vibrational Absorption and Circular Dichroism Spectra Using Density Functional Force Fields*, J. Phys. Chem. **98**, 11623 (1994), (cit. on pp. 23, 42).

[64] R. Baer, E. Livshits, and U. Salzner, *Tuned range-separated hybrids in density functional theory.* Annu. Rev. Phys. Chem. **61**, 85 (2010), (cit. on p. 23).

[65] T. Yanai, D. P. Tew, and N. C. Handy, *A new hybrid exchangecorrelation functional using the Coulomb-attenuating method (CAM-B3LYP)*, Chem. Phys. Lett. **393**, 51 (2004), (cit. on pp. 23, 43, 143).

[66] A. Heßelmann and A. Görling, *Random-phase approximation correlation methods for molecules and solids*, Mol. Phys. **109**, 2473 (2011), (cit. on p. 23).

[67] X. Ren, P. Rinke, C. Joas, and M. Scheffler, *Random-phase approximation and its applications in computational chemistry and materials science*, J. Mater. Sci. **47**, 7447 (2012), (cit. on p. 23).

[68] K. J. H. Giesbertz, R. van Leeuwen, and U. von Barth, *Towards nonlocal density functionals by explicit modeling of the exchange-correlation hole in inhomogeneous systems*, Phys. Rev. A **87**, 022514 (2013), (cit. on p. 23).

[69] S. Kristyán and P. Pulay, *Can (semi)local density functional theory account for the London dispersion forces?*, Chem. Phys. Lett. **229**, 175 (1994), (cit. on p. 24).

[70] A. D. Becke and E. R. Johnson, *Exchange-hole dipole moment and the dispersion interaction.* J. Chem. Phys. **122**, 154104 (2005), (cit. on p. 24).

[71] E. R. Johnson, I. D. Mackie, and G. A. DiLabio, *Dispersion interactions in density-functional theory*, J. Phys. Org. Chem. **22**, 1127 (2009), (cit. on p. 24).

[72] J. Klimeš and A. Michaelides, *Perspective: Advances and challenges in treating van der Waals dispersion forces in density functional theory.* J. Chem. Phys. **137**, 120901 (2012), (cit. on pp. 24, 63).

[73] J. P. Perdew, *Jacobs ladder of density functional approximations for the exchange-correlation energy*, AIP Conference Proceedings **577**, 1 (2001), (cit. on p. 24).

[74] S. Grimme, *Accurate description of van der Waals complexes by density functional theory including empirical corrections.* J. Comput. Chem. **25**, 1463 (2004), (cit. on p. 24).

[75] S. Grimme, *Semiempirical GGA-type density functional constructed with a long-range dispersion correction*, J. Comput. Chem. **16**, 1787 (2006), (cit. on p. 24).

[76] S. Grimme, J. Antony, S. Ehrlich, and H. Krieg, *A consistent and accurate ab initio parametrization of density functional dispersion correction (DFT-D) for the 94 elements H-Pu.* J. Chem. Phys. **132**, 154104 (2010), (cit. on p. 24).

[77] A. Tkatchenko and M. Scheffler, *Accurate Molecular Van Der Waals Interactions from Ground-State Electron Density and Free-Atom Reference Data*, Phys. Rev. Lett. **102**, 073005 (2009), (cit. on pp. 24, 63, 65, 73, 144, 146).

[78] F. L. Hirshfeld, *Bonded-atom fragments for describing molecular charge densities*, Theor. Chim. Acta. **44**, 129 (1977), (cit. on pp. 24, 65, 144).

[79] E. R. Johnson and A. D. Becke, *A post-Hartree-Fock model of intermolecular interactions.* J. Chem. Phys. **123**, 24101 (2005), (cit. on p. 24).

[80] A. Olasz, K. Vanommeslaeghe, A. Krishtal, T. Veszprémi, C. Van Alsenoy, and P. Geerlings, *The use of atomic intrinsic polarizabilities in the evaluation of the dispersion energy.* J. Chem. Phys. **127**, 224105 (2007), (cit. on p. 24).

[81] W. Liu, J. Carrasco, B. Santra, A. Michaelides, M. Scheffler, and A. Tkatchenko, *Benzene adsorbed on metals: Concerted effect of covalency and van der Waals bonding*, Phys. Rev. B **86**, 245405 (2012), (cit. on pp. 25, 64, 73).

[82] M. Dion, H. Rydberg, E. Schröder, D. Langreth, and B. Lundqvist, *Van der Waals Density Functional for General Geometries*, Phys. Rev. Lett. **92**, 246401 (2004), (cit. on p. 25).

[83] G. Román-Pérez and J. Soler, *Efficient Implementation of a van der Waals Density Functional: Application to Double-Wall Carbon Nanotubes*, Phys. Rev. Lett. **103**, 1 (2009), (cit. on p. 25).

[84] J. Klimeš, D. R. Bowler, and A. Michaelides, *Van der Waals density functionals applied to solids*, Phys. Rev. B **83**, 195131 (2011), (cit. on p. 25).

[85] V. Ruiz, W. Liu, E. Zojer, M. Scheffler, and A. Tkatchenko, *Density-Functional Theory with Screened van der Waals Interactions for the Modeling of Hybrid Inorganic-Organic Systems*, Phys. Rev. Lett. **108**, 146103 (2012), (cit. on pp. 25, 63–65, 72, 73, 144, 146).

[86] E. Lifshitz, *The Theory of Molecular Attractive Forces between Solids*, Sov. Phys. JETP 2 **2**, 73 (1956), (cit. on p. 25).

[87] E. Zaremba and W. Kohn, *Van der Waals interaction between an atom and a solid surface*, Phys. Rev. B **13**, 2270 (1976), (cit. on p. 25).

[88] N. B. Slater, *Classical Motion under a Morse Potential*, Nature **180**, 1352 (1957), (cit. on pp. 25, 78, 81).

[89] O. Gunnarsson and B. Lundqvist, *Exchange and correlation in atoms, molecules, and solids by the spin-density-functional formalism*, Phys. Rev. B **13**, 4274 (1976), (cit. on pp. 25, 26, 42, 98, 99).

[90] T. Ziegler, A. Rauk, and E. J. Baerends, *On the calculation of multiplet energies by the hartree-fock-slater method*, Theor. Chim. Acta **43**, 261 (1977), (cit. on pp. 25, 26, 42, 43, 98, 99).

[91] U. von Barth, *Local-density theory of multiplet structure*, Phys. Rev. A **20**, 1693 (1979), (cit. on pp. 25, 26, 42).

[92] E. Clementi, C. Roothaan, and M. Yoshimine, *Accurate Analytical Self-Consistent Field Functions for Atoms. II. Lowest Configurations of the Neutral First Row Atoms*, Phys. Rev. **127**, 1618 (1962), (cit. on pp. 25, 98).

[93] J. Janak, *Proof that dE/dni=ei in density-functional theory*, Phys. Rev. B **18**, 7165 (1978), (cit. on p. 25).

[94] J. C. Slater, *Statistical Exchange-Correlation in the Self-Consistent Field*, Adv. Quantum Chem. **6**, 1 (1972), (cit. on p. 26).

[95] R. Jones and O Gunnarson, *The density functional formalism, its applications and prospects*, Rev. Mod. Phys **61**, 689 (1989), (cit. on pp. 26, 42).

[96] T. Baruah and M. R. Pederson, *DFT Calculations on Charge-Transfer States of a Carotenoid-Porphyrin-C 60 Molecular Triad*, J. Chem. Theory Comput. **5**, 834 (2009), (cit. on pp. 26, 98).

[97] T. Kowalczyk, S. R. Yost, and T. Van Voorhis, *Assessment of the ΔSCF density functional theory approach for electronic excitations in organic dyes.* J. Chem. Phys. **134**, 054128 (2011), (cit. on pp. 26, 49, 98, 99, 103).

[98] T. Baruah, M. Olguin, and R. R. Zope, *Charge transfer excited state energies by perturbative delta self consistent field method.* J. Chem. Phys. **137**, 084316 (2012), (cit. on pp. 26, 98, 99, 103).

[99] M. Levy and A. Nagy, *Variational Density-Functional Theory for an Individual Excited State*, Phys. Rev. Lett. **83**, 4361 (1999), (cit. on p. 26).

[100] P. Ayers and M. Levy, *Time-independent (static) density-functional theories for pure excited states: Extensions and unification*, Phys. Rev. A **80**, 012508 (2009), (cit. on pp. 26, 98).

[101] P. W. Ayers, M. Levy, and A. Nagy, *Time-independent density-functional theory for excited states of Coulomb systems*, Phys. Rev. A **85**, 042518 (2012), (cit. on p. 26).

[102] A. Görling, *Density-functional theory beyond the Hohenberg-Kohn theorem*, Phys. Rev. A **59**, 3359 (1999), (cit. on pp. 27, 42, 98).

[103] A. Theophilou, *The energy density functional formalism for excited states*, J. Phys. C: Solid State Phys. **12**, 5419 (1979), (cit. on p. 27).

[104] E. Gross, L. Oliveira, and W. Kohn, *Density-functional theory for ensembles of fractionally occupied states. I. Basic formalism*, Phys. Rev. A **37**, 2809 (1988), (cit. on pp. 27, 98).

[105] L. Oliveira, E. Gross, and W. Kohn, *Density-functional theory for ensembles of fractionally occupied states. II. Application to the He atom*, Phys. Rev. A **37**, 2821 (1988), (cit. on p. 27).

[106] P. Dederichs, S Blügel, R Zeller, and H Akai, *Ground states of constrained systems: Application to cerium impurities*, Phys. Rev. Lett. **53**, 2512 (1984), (cit. on pp. 27, 98, 156).

[107] B. Kaduk, T. Kowalczyk, and T. Van Voorhis, *Constrained density functional theory.* Chem. Rev. **112**, 321 (2012), (cit. on pp. 27, 98).

[108] H. Oberhofer and J. Blumberger, *Charge constrained density functional molecular dynamics for simulation of condensed phase electron transfer reactions.* J. Chem. Phys. **131**, 064101 (2009), (cit. on pp. 27, 98).

[109] Q. Wu and T. Van Voorhis, *Direct calculation of electron transfer parameters through constrained density functional theory.* J. Phys. Chem. A **110**, 9212 (2006), (cit. on pp. 27, 98).

[110] Q. Wu and T. Van Voorhis, *Extracting electron transfer coupling elements from constrained density functional theory*, J. Chem. Phys. **125**, 164105 (2006), (cit. on p. 27).

[111] J. Behler, B. Delley, K. Reuter, and M. Scheffler, *Nonadiabatic potential-energy surfaces by constrained density-functional theory*, Phys. Rev. B **75**, 115409 (2007), (cit. on pp. 27, 98, 99).

[112] C.-L. Cheng, Q. Wu, and T. Van Voorhis, *Rydberg energies using excited state density functional theory.* J. Chem. Phys. **129**, 124112 (2008), (cit. on p. 27).

[113] T. Ziegler, M. Seth, M. Krykunov, and J. Autschbach, *A revised electronic Hessian for approximate time-dependent density functional theory.* J. Chem. Phys. **129**, 184114 (2008), (cit. on p. 28).

[114] T. Ziegler, M. Seth, M. Krykunov, J. Autschbach, and F. Wang, *On the relation between time-dependent and variational density functional theory approaches for the determination of excitation energies and transition moments.* J. Chem. Phys. **130**, 154102 (2009), (cit. on pp. 28, 98).

[115] J. Cullen, M. Krykunov, and T. Ziegler, *The formulation of a self-consistent constricted variational density functional theory for the description of excited states*, Chem. Phys. **391**, 11 (2011), (cit. on pp. 28, 98).

[116] T. Ziegler, M. Krykunov, and J. Cullen, *The Application of Constricted Variational Density Functional Theory to Excitations Involving Electron Transitions from Occupied Lone-Pair Orbitals to Virtual π^* Orbitals*, J. Chem. Theory Comput. **7**, 2485 (2011), (cit. on pp. 28, 98).

[117] T. Ziegler, M. Krykunov, and J. Cullen, *The implementation of a self-consistent constricted variational density functional theory for the description of excited states.* J. Chem. Phys. **136**, 124107 (2012), (cit. on pp. 28, 98).

[118] S. Hirata and M. Head-Gordon, *Time-dependent density functional theory within the Tamm-Dancoff approximation*, Chem. Phys. Lett. **314**, 291 (1999), (cit. on p. 28).

[119] M. Casida, K. Casida, and D. Salahub, *Excited-state potential energy curves from time-dependent density-functional theory: A cross section of formaldehyde's 1A1 manifold*, Int. J. Quantum Chem. **70**, 933 (1998), (cit. on pp. 28, 30, 50).

[120] E. Runge and E. Gross, *Density-functional theory for time-dependent systems*, Phys. Rev. Lett. **52**, 997 (1984), (cit. on pp. 28, 97, 98, 147).

[121] R. van Leeuwen, *Mapping from Densities to Potentials in Time-Dependent Density-Functional Theory*, Phys. Rev. Lett. **82**, 3863 (1999), (cit. on p. 28).

[122] M. J. G. Peach, P. Benfield, T. Helgaker, and D. J. Tozer, *Excitation energies in density functional theory: an evaluation and a diagnostic test.* J. Chem. Phys. **128**, 044118 (2008), (cit. on pp. 30, 49–52, 98).

[123] M. R. Silva-Junior, M. Schreiber, S. P. A. Sauer, and W. Thiel, *Benchmarks for electronically excited states: time-dependent density functional theory and density functional theory based multireference configuration interaction.* J. Chem. Phys. **129**, 104103 (2008), (cit. on pp. 30, 50).

[124] D. Jacquemin, V. Wathelet, E. A. Perpete, and C. Adamo, *Extensive TD-DFT Benchmark: Singlet-Excited States of Organic Molecules*, J. Chem. Theory Comput. **5**, 2420 (2009), (cit. on pp. 30, 49).

[125] P. Wiggins, J. A. G. Williams, and D. J. Tozer, *Excited state surfaces in density functional theory: a new twist on an old problem.* J. Chem. Phys. **131**, 091101 (2009), (cit. on pp. 30, 50, 98).

[126] H. J. Monkhorst and J. D. Pack, *Special points for Brillouin zone integration*, Phys. Rev. B **13**, 5188 (1976), (cit. on pp. 32, 65, 75, 76).

[127] J. Moreno and J. Soler, *Optimal meshes for integrals in real- and reciprocal-space unit cells*, Phys. Rev. B **45**, 13891 (1992), (cit. on p. 32).

[128] M. Probert and M. Payne, *Improving the convergence of defect calculations in supercells: An ab initio study of the neutral silicon vacancy*, Phys. Rev. B **67**, 075204 (2003), (cit. on p. 32).

[129] B. Meyer, *The Pseudopotential Plane Wave Approach*, in *Computational Nanoscience: Do it Yourself!*, ed. by J. Grotendorst, S. Blügel, and D. Marx, John von Neumann Institute for Computing, Jülich, 2006, pp. 71–83, ISBN: 3-00-017350-1 (cit. on p. 33).

[130] L. Kleinman and D. Bylander, *Efficacious Form for Model Pseudopotentials*, Phys. Rev. Lett. **48**, 1425 (1982), (cit. on pp. 33, 144).

[131] D. Vanderbilt, *Soft self-consistent pseudopotentials in a generalized eigenvalue formalism*, Phys. Rev. B **41**, 7892 (1990), (cit. on pp. 33, 64, 144).

[132] H. Rau, *Azo Compounds*, in *Photochromism - Molecules and Systems*, ed. by H. Dürr and H. Bouas-Laurent, Elsevier, Amsterdam, 2003, p. 165, ISBN: 978-0-444-51322-9 (cit. on pp. 37, 38, 40, 58, 111, 115).

[133] E. Mitscherlich, *Ueber die Zusammensetzung des Nitrobenzids und Sulfobenzids*, Annalen der Physik und Chemie **107**, 625 (1834), (cit. on p. 37).

[134] P. W. Hofmann, *Ueber Azobenzol und Benzidin*, Annalen der Chemie und Pharmacie **115**, 362 (1860), (cit. on p. 37).

[135] C. Glaser, *Ueber eine neue Bildungsweise des Azobenzols*, Z. Chemie **9**, 308 (1866), (cit. on p. 37).

[136] I. Hausser, *Die Quantenbilanz der cis-trans-Umwandlung von Azobenzol*, Naturwissenschaften **36**, 315 (1949), (cit. on p. 37).

[137] C. A. Winkler, J. Halpern, and G. W. Brady, *The Cis - Trans Isomerization of Azobenzene in Solution*, Can. J. Res. **28b**, 140 (1950), (cit. on p. 37).

[138] P. P. Birnbaum and D. W. G. Style, *The photo-isomerization of some azobenzene derivatives*, Trans. Faraday Soc. **50**, 1192 (1954), (cit. on p. 37).

[139] M. Tsuda and K. Kuratani, *Isomerization of cis-Azobenzene in the Solid Phase*, Bull. Chem. Soc. Jpn. **37**, 1284 (1964), (cit. on p. 37).

[140] H. Stegemeyer, *On the Mechanism of Photochemical cis trans Isomerization*, J. Phys. Chem. **66**, 2555 (1962), (cit. on p. 37).

[141] W. M. Gelbart, *Some Formal Results in a Theory of Molecular Rearrangements: Photoisomerism*, J. Chem. Phys. **50**, 4775 (1969), (cit. on p. 37).

[142] G. Zimmerman, L.-Y. Chow, and U.-J. Paik, *The Photochemical Isomerization of Azobenzene1*, J. Am. Chem. Soc. **80**, 3528 (1958), (cit. on pp. 37, 38).

[143] L. B. Jones and G. S. Hammond, *Mechanisms of Photochemical Reactions in Solution. XXX.1 Photosensitized Isomerization of Azobenzene*, J. Am. Chem. Soc. **87**, 4219 (1965), (cit. on p. 37).

[144] C. J. Brown, *A refinement of the crystal structure of azobenzene*, Acta Crystallogr. **21**, 146 (1966), (cit. on p. 37).

[145] A. Mostad and C. Rø mming, *A refinement of the crystal structure of cis-azobenzene*, Acta Chem. Scand **25**, 3561 (1971), (cit. on pp. 37, 47).

[146] F.-W. Schulze, H.-J. Petrick, H. K. Cammenga, and H. Klinge, *Thermodynamic Properties of the Structural Analogues Benzo[c]cinnoline, Trans-azobenzene, and Cis-azobenzene*, Z. Phys. Chem. **107**, 1 (1977), (cit. on p. 37).

[147] J Andersson, R Petterson, and L Tegner, *Flash photolysis experiments in the vapour phase at elevated temperatures I: spectra of azobenzene and the kinetics of its thermal cis-trans isomerization*, J. Photochem. **20**, 17 (1982), (cit. on pp. 37, 38, 48, 115).

[148] E. R. Talaty and J. C. Fargo, *Thermal cis?trans-isomerization of substituted azobenzenes: a correction of the literature*, Chem. Commun. 65 (1967), (cit. on p. 37).

[149] P. P. Birnbaum, J. H. Linford, and D. W. G. Style, *The absorption spectra of azobenzene and some derivatives*, Trans. Faraday Soc. **49**, 735 (1953), (cit. on pp. 37, 38).

[150] J. Schulze, F. Gerson, J. N. Murrell, and E. Heilbronner, *Elektronenstruktur und physikalisch-chemische Eigenschaften von Azo-Verbindungen. Teil IX: Die Absorptionsspektren der Benzologen des Azobenzols, des Benzalanilins und des Stilbens*, Helv. Chim. Acta **44**, 428 (1961), (cit. on p. 37).

[151] P. Bortolus and S. Monti, *Cis-trans photoisomerization of azobenzene. Solvent and triplet donors effects*, J. Phys. Chem. **83**, 648 (1979), (cit. on p. 38).

[152] N Siampiringue, G. Guyota, S. Monti, and Bortolus P., *The cis trans photoisomerization of azobenzene: an experimental re-examination*, J. Photochem. **37**, 185 (1987), (cit. on p. 38).

[153] J. Bao and P. M. Weber, *Electronic effects on photochemistry: the diverse reaction dynamics of highly excited stilbenes and azobenzene.* J. Am. Chem. Soc. **133**, 4164 (2011), (cit. on p. 38).

[154] H. Rau and E. Lueddecke, *On the rotation-inversion controversy on photoisomerization of azobenzenes. Experimental proof of inversion*, J. Am. Chem. Soc. **104**, 1616 (1982), (cit. on p. 38).

[155] J. Bouwstra, A Schouten, and J Kroon, *Structural studies of the system trans-azobenzene / trans-stilbene. I. A reinvestigation of the disorder in the crystal structure of trans-azobenzene, C12H10N2*, Acta Crystallogr., Sect. C: Cryst. Struct. Commun. **39**, 1121 (1983), (cit. on pp. 38, 47).

[156] H Rau, *Further evidence for rotation in the π,π* and inversion in the n,π* photoisomerization of azobenzenes*, J. Photochem. **26**, 221 (1984), (cit. on p. 38).

[157] G. Kumar and D. Neckers, *Photochemistry of azobenzene-containing polymers*, Chem. Rev. **89**, 1915 (1989), (cit. on p. 38).

[158] I. K. Lednev, T.-Q. Ye, R. E. Hester, and J. N. Moore, *Femtosecond Time-Resolved UVVisible Absorption Spectroscopy of trans -Azobenzene in Solution*, J. Phys. Chem. **100**, 13338 (1996), (cit. on p. 38).

[159] T. Nägele, R. Hoche, W. Zinth, and J. Wachtveitl, *Femtosecond photoisomerization of cis-azobenzene*, Chem. Phys. Lett. **272**, 489 (1997), (cit. on pp. 38, 39).

[160] T Fujino, S. Y. Arzhantsev, and T Tahara, *Femtosecond/picosecond time-resolved spectroscopy of trans-azobenzene: isomerization mechanism following S 2 (ππ*) S 0 photoexcitation*, Bull. Chem. Soc. Jpn. **75**, 1031 (2002), (cit. on pp. 38, 39).

[161] T. Schultz, J. Quenneville, B. Levine, A. Toniolo, T. J. Martínez, S. Lochbrunner, M. Schmitt, J. P. Shaffer, M. Z. Zgierski, and A. Stolow, *Mechanism and dynamics of azobenzene photoisomerization.* J. Am. Chem. Soc. **125**, 8098 (2003), (cit. on pp. 38–40, 125).

[162] H Satzger, S Spörlein, C Root, J Wachtveitl, W Zinth, and P Gilch, *Fluorescence spectra of trans- and cis-azobenzene emission from the FranckCondon state*, Chem. Phys. Lett. **372**, 216 (2003), (cit. on pp. 38, 40).

[163] H. Satzger, C. Root, and M. Braun, *Excited-State Dynamics of trans - and cis -Azobenzene after UV Excitation in the ππ* Band*, J. Phys. Chem. A **108**, 6265 (2004), (cit. on pp. 38, 40).

[164] C.-W. Chang, Y.-C. Lu, T.-T. Wang, and E. W.-G. Diau, *Photoisomerization dynamics of azobenzene in solution with S1 excitation: a femtosecond fluorescence anisotropy study.* J. Am. Chem. Soc. **126**, 10109 (2004), (cit. on p. 38).

[165] H. M. D. Bandara, T. R. Friss, M. M. Enriquez, W. Isley, C. Incarvito, H. A. Frank, J. Gascon, and S. C. Burdette, *Proof for the Concerted Inversion Mechanism in the trans-cis Isomerization of Azobenzene Using Hydrogen Bonding To Induce Isomer Locking.* J. Org. Chem. **75**, 4817 (2010), (cit. on p. 38).

[166] S. Monti, G. Orlandi, and P. Palmieri, *Features of the photochemically active state surfaces of azobenzene*, Chem. Phys. **71**, 87 (1982), (cit. on pp. 38, 40).

[167] P. Cattaneo and M. Persico, *An abinitio study of the photochemistry of azobenzene*, Phys. Chem. Chem. Phys.: PCCP **1**, 4739 (1999), (cit. on pp. 38, 40, 84).

[168] T. Ishikawa, T. Noro, and T. Shoda, *Theoretical study on the photoisomerization of azobenzene*, J. Chem. Phys. **115**, 7503 (2001), (cit. on pp. 38–40).

[169] A. Cembran, F. Bernardi, M. Garavelli, L. Gagliardi, and G. Orlandi, *On the mechanism of the cis-trans isomerization in the lowest electronic states of azobenzene: S0, S1, and T1.* J. Am. Chem. Soc. **126**, 3234 (2004), (cit. on pp. 38, 40, 46, 47, 84).

[170] H. Fliegl, A. Köhn, C. Hättig, and R Ahlrichs, *Ab initio calculation of the vibrational and electronic spectra of trans- and cis-azobenzene.* J. Am. Chem. Soc. **125**, 9821 (2003), (cit. on pp. 38, 42, 43, 45, 49).

[171] E. Wei-Guang Diau, *A New Trans-to-Cis Photoisomerization Mechanism of Azobenzene on the S 1 (n,π*) Surface*, J. Phys. Chem. A **108**, 950 (2004), (cit. on pp. 38, 46, 84).

[172] L. Gagliardi, G. Orlandi, F. Bernardi, A. Cembran, and M. Garavelli, *A theoretical study of the lowest electronic states of azobenzene: the role of torsion coordinate in the cis?trans photoisomerization*, Theor. Chem. Acc. **111**, 363 (2004), (cit. on p. 38).

[173] M. L. Tiago, S. Ismail-Beigi, and S. G. Louie, *Photoisomerization of azobenzene from first-principles constrained density-functional calculations.* J. Chem. Phys. **122**, 094311 (2005), (cit. on pp. 38, 40, 42, 46, 49–51, 53).

[174] A Toniolo, C Ciminelli, M Persico, and T. J. Martínez, *Simulation of the photodynamics of azobenzene on its first excited state: comparison of full multiple spawning and surface hopping treatments.* J. Chem. Phys. **123**, 234308 (2005), (cit. on pp. 38, 40, 130).

[175] G. Füchsel, T. Klamroth, and J. Dokić, *On the electronic structure of neutral and ionic azobenzenes and their possible role as surface mounted molecular switches*, J. Phys. Chem. B **110**, 16337 (2006), (cit. on pp. 38, 117).

[176] C. R. Crecca and A. E. Roitberg, *Theoretical study of the isomerization mechanism of azobenzene and disubstituted azobenzene derivatives.* J. Phys. Chem. A **110**, 8188 (2006), (cit. on pp. 38, 40, 46, 84).

[177] G. Granucci and M. Persico, *Excited state dynamics with the direct trajectory surface hopping method: azobenzene and its derivatives as a case study*, Theor. Chim. Acc. **117**, 1131 (2006), (cit. on pp. 38, 40, 125, 130).

[178] I. Conti, M. Garavelli, and G. Orlandi, *The different photoisomerization efficiency of azobenzene in the lowest n pi* and pi pi* singlets: the role of a phantom state.* J. Am. Chem. Soc. **130**, 5216 (2008), (cit. on pp. 38–40, 45, 47, 48, 84).

[179] S. Yuan, Y. Dou, W. Wu, Y. Hu, and J. Zhao, *Why Does trans-Azobenzene Have a Smaller Isomerization Yield for pipi* Excitation Than for npi* Excitation?*, J. Phys. Chem. A **112**, 13326 (2008), (cit. on pp. 38, 40).

[180] T. Cusati, G. Granucci, M. Persico, and G. Spighi, *Oscillator strength and polarization of the forbidden n-pi* band of trans-azobenzene: a computational study.* J. Chem. Phys. **128**, 194312 (2008), (cit. on p. 38).

[181] J. Shao, Y. Lei, Z. Wen, Y. Dou, and Z. Wang, *Nonadiabatic simulation study of photoisomerization of azobenzene: detailed mechanism and load-resisting capacity.* J. Chem. Phys. **129**, 164111 (2008), (cit. on pp. 38, 40, 84).

[182] Y. Ootani, K. Satoh, A. Nakayama, T. Noro, and T. Taketsugu, *Ab initio molecular dynamics simulation of photoisomerization in azobenzene in the n pi* state.* J. Chem. Phys. **131**, 194306 (2009), (cit. on pp. 38, 40).

[183] M. Böckmann, N. Doltsinis, and D. Marx, *Azobenzene photoswitches in bulk materials*, Phys. Rev. E **78**, 036101 (2008), (cit. on p. 38).

[184] G. Tiberio, L. Muccioli, R. Berardi, and C. Zannoni, *How does the trans-cis photoisomerization of azobenzene take place in organic solvents?*, ChemPhysChem **11**, 1018 (2010), (cit. on p. 38).

[185] M. Pederzoli, J. Pittner, M. Barbatti, and H. Lischka, *Nonadiabatic Molecular Dynamics Study of the cis-trans Photoisomerization of Azobenzene Excited to the S(1) State.* J. Phys. Chem. A **115**, 11136 (2011), (cit. on pp. 38, 40).

[186] T. Cusati, G. Granucci, E. Martínez-n, F. Martini, and M. Persico, *Semiempirical Hamiltonian for Simulation of Azobenzene Photochemistry*, J. Phys. Chem. A **116**, 98 (2012), (cit. on p. 38).

[187] O. Weingart, Z. Lan, and A. Koslowski, *Chiral Pathways and Periodic Decay in cis-Azobenzene Photodynamics*, J. Phys. Chem. Lett. **2**, 1506 (2011), (cit. on pp. 38, 40, 123, 130).

[188] N. Tamai and H. Miyasaka, *Ultrafast Dynamics of Photochromic Systems*, Chem. Rev. **100**, 1875 (2000), (cit. on p. 38).

[189] D. Yarkony, *Diabolical conical intersections*, Rev. Mod. Phys. **68**, 985 (1996), (cit. on p. 39).

[190] G. Floß, G. Granucci, and P. Saalfrank, *Surface hopping dynamics of direct trans cis photoswitching of an azobenzene derivative in constrained adsorbate geometries.* J. Chem. Phys. **137**, 234701 (2012), (cit. on pp. 39, 40, 115).

[191] C. Ciminelli, G. Granucci, and M. Persico, *The photoisomerization mechanism of azobenzene: a semiclassical simulation of nonadiabatic dynamics.* Chem. Eur. J. **10**, 2327 (2004), (cit. on pp. 39, 40, 125).

[192] C. Nonnenberg, H. Gaub, and I. Frank, *First-principles simulation of the photoreaction of a capped azobenzene: the rotational pathway is feasible.* ChemPhysChem **7**, 1455 (2006), (cit. on p. 40).

[193] M. Böckmann, N. L. Doltsinis, and D. Marx, *Nonadiabatic hybrid quantum and molecular mechanic simulations of azobenzene photoswitching in bulk liquid environment.* J. Phys. Chem. A **114**, 745 (2010), (cit. on pp. 40, 84).

[194] J. Gamez, O. Weingart, A. Koslowski, and W. Thiel, *Cooperating Dinitrogen and Phenyl Rotations in trans- Azobenzene Photoisomerization*, J. Chem. Theory Comput. **8**, 2352 (2012), (cit. on p. 40).

[195] R. J. Maurer and K. Reuter, *Assessing computationally efficient isomerization dynamics: ΔSCF density-functional theory study of azobenzene molecular switching.* J. Chem. Phys. **135**, 224303 (2011), (cit. on pp. 41, 84, 98, 99, 103, 106, 115, 116).

[196] E. R. McNellis, J. Meyer, and K. Reuter, *Azobenzene at coinage metal surfaces: Role of dispersive van der Waals interactions*, Phys. Rev. B **80**, 205414 (2009), (cit. on pp. 41, 53, 61, 63, 65, 67, 68, 144).

[197] E. McNellis, J. Meyer, A. Baghi, and K. Reuter, *Stabilizing a molecular switch at solid surfaces: A density functional theory study of azobenzene on Cu(111), Ag(111), and Au(111)*, Phys. Rev. B **80**, 035414 (2009), (cit. on pp. 41, 61, 63, 65–68, 84, 89, 104, 108).

[198] G. Mercurio, E. McNellis, I. Martin, S. Hagen, F. Leyssner, S. Soubatch, J. Meyer, M. Wolf, P. Tegeder, F. Tautz, and R. K., *Structure and energetics of azobenzene on Ag (111): benchmarking semiempirical dispersion correction approaches*, Phys. Rev. Lett. **104**, 36102 (2010), (cit. on pp. 41, 59, 61, 63, 71–74, 82).

[199] E. R. McNellis, C. Bronner, J. Meyer, M. Weinelt, P. Tegeder, and K. Reuter, *Azobenzene versus 3,3',5,5'-tetra-tert-butyl-azobenzene (TBA) at Au(111): characterizing the role of spacer groups.* Phys. Chem. Chem. Phys.: PCCP **12**, 6404 (2010), (cit. on pp. 41, 59, 61, 63, 65, 71, 90, 123).

[200] Q. Wu and T. Van Voorhis, *Direct optimization method to study constrained systems within density-functional theory*, Phys. Rev. A **72**, 024502 (2005), (cit. on p. 41).

[201] J. Behler, K. Reuter, and M. Scheffler, *Nonadiabatic effects in the dissociation of oxygen molecules at the Al (111) surface*, Phys. Rev. B **77**, 115421 (2008), (cit. on pp. 41–43, 49, 98).

[202] A Hellman, B Razaznejad, and B. I. Lundqvist, *Potential–energy surfaces for excited states in extended systems.* J. Chem. Phys. **120**, 4593 (2004), (cit. on pp. 41, 98, 99).

[203] M. Casida, *Time-dependent density-functional theory for molecules and molecular solids*, J. Mol. Struct.: THEOCHEM **914**, 3 (2009), (cit. on pp. 42, 50, 97).

[204] V. Blum, R. Gehrke, F. Hanke, P. Havu, V. Havu, X. Ren, K. Reuter, and M. Scheffler, *Ab initio molecular simulations with numeric atom-centered orbitals*, Comp. Phys. Commun. **180**, 2175 (2009), (cit. on pp. 42, 126, 143).

[205] J. P. Perdew and Y. Wang, *Accurate and simple analytic representation of the electron-gas correlation energy*, Phys. Rev. B **45**, 13244 (1992), (cit. on p. 42).

[206] S. Bahn and K. Jacobsen, *An object-oriented scripting interface to a legacy electronic structure code*, Comput. Sci. Eng. **4**, 56 (2002), (cit. on pp. 42, 146).

[207] D. Dubbeldam, G. A. E. Oxford, R. Krishna, L. J. Broadbelt, and R. Q. Snurr, *Distance and angular holonomic constraints in molecular simulations.* J. Chem. Phys. **133**, 034114 (2010), (cit. on pp. 42, 147).

[208] O. Gunnarsson and R. O. Jones, *Extensions of the LSD approximation in density functional calculations*, J. Chem. Phys. **72**, 5357 (1980), (cit. on p. 42).

[209] B. Himmetoglu, A. Marchenko, I. Dabo, and M. Cococcioni, *Role of electronic localization in the phosphorescence of iridium sensitizing dyes.* J. Chem. Phys. **137**, 154309 (2012), (cit. on pp. 43, 49, 98, 99, 103, 155).

[210] R Bauernschmitt and R Ahlrichs, *Treatment of electronic excitations within the adiabatic approximation of time dependent density functional theory*, Chem. Phys. Lett. **256**, 454 (1996), (cit. on p. 43).

[211] R Ahlrichs, M Bär, M Häser, H. Horn, and C Kölmel, *Electronic structure calculations on workstation computers: The program system turbomole*, Chem. Phys. Lett. **162**, 165 (1989), (cit. on pp. 43, 143).

[212] M. W. Schmidt, K. K. Baldridge, J. A. Boatz, S. T. Elbert, M. S. Gordon, J. H. Jensen, S. Koseki, N. Matsunaga, K. A. Nguyen, S. Su, T. L. Windus, M. Dupuis, and J. A. Montgomery, *General atomic and molecular electronic structure system*, J. Comput. Chem. **14**, 1347 (1993), (cit. on pp. 43, 143).

[213] F Weigend, M Häser, H Patzelt, and R Ahlrichs, *RI-MP2: optimized auxiliary basis sets and demonstration of efficiency*, Chem. Phys. Lett. **294**, 143 (1998), (cit. on p. 43).

[214] R Bauernschmitt, M Häser, O Treutler, and R Ahlrichs, *Calculation of excitation energies within time-dependent density functional theory using auxiliary basis set expansions*, Chem. Phys. Lett. **264**, 573 (1997), (cit. on pp. 43, 143).

[215] E. V. Brown and G. R. Granneman, *Cis-trans isomerism in the pyridyl analogs of azobenzene. Kinetic and molecular orbital analysis*, J. Am. Chem. Soc. **97**, 621 (1975), (cit. on p. 47).

[216] A Biancalana, *Direct observation of a 220 cm-1 structure in the lowest ππ* absorption band in the vapour phase of trans-azobenzene*, Spectrochim. Acta, Part A **55**, 2883 (1999), (cit. on p. 48).

[217] D. J. Tozer and N. C. Handy, *Improving virtual KohnSham orbitals and eigenvalues: Application to excitation energies and static polarizabilities*, J. Chem. Phys. **109**, 10180 (1998), (cit. on pp. 50, 103, 106).

[218] M. J. Allen and D. J. Tozer, *KohnSham calculations using hybrid exchange-correlation functionals with asymptotically corrected potentials*, J. Chem. Phys. **113**, 5185 (2000), (cit. on p. 50).

[219] M. Gruning, O. V. Gritsenko, S. J. A. van Gisbergen, and E. J. Baerends, *Shape corrections to exchange-correlation potentials by gradient-regulated seamless connection of model potentials for inner and outer region*, J. Chem. Phys. **114**, 652 (2001), (cit. on p. 50).

[220] M Wanko, M Garavelli, F. Bernardi, T. A. Niehaus, T Frauenheim, and M Elstner, *A global investigation of excited state surfaces within time-dependent density-functional response theory.* J. Chem. Phys. **120**, 1674 (2004), (cit. on p. 50).

[221] J. Plotner, D. J. Tozer, and A. Dreuw, *Dependence of Excited State Potential Energy Surfaces on the Spatial Overlap of the KohnSham Orbitals and the Amount of Nonlocal HartreeFock Exchange in Time-Dependent Density Functional Theory*, J. Chem. Theory Comput. **6**, 2315 (2010), (cit. on pp. 50, 103).

[222] Q. Hu, K. Reuter, and M. Scheffler, *Towards an exact treatment of exchange and correlation in materials: Application to the CO adsorption puzzle and other systems*, Phys. Rev. Lett. **98**, 176103 (2007), (cit. on pp. 54, 105, 116, 132).

[223] E. A. Carter, *Challenges in modeling materials properties without experimental input.* Science **321**, 800 (2008), (cit. on pp. 54, 105).

[224] A Stroppa and G Kresse, *The shortcomings of semi-local and hybrid functionals: what we can learn from surface science studies*, New J. Phys. **10**, 063020 (2008), (cit. on pp. 54, 105, 116, 158).

[225] W. R. Browne and B. E. N. L. Feringa, *Making molecular machines work*, Nat. Nanotechnol. **1**, 25 (2006), (cit. on p. 57).

[226] A. Coskun, M. Banaszak, R. D. Astumian, J. F. Stoddart, and B. a. Grzybowski, *Great expectations: can artificial molecular machines deliver on their promise?*, Chem. Soc. Rev. **41**, 19 (2012), (cit. on p. 57).

[227] T. Hugel, N. B. Holland, A. Cattani, L. Moroder, M. Seitz, and H. E. Gaub, *Single-molecule optomechanical cycle.* Science **296**, 1103 (2002), (cit. on p. 57).

[228] R Rosario, G Devens, A. A. Garcia, M Hayes, J. L. Taraci, T Clement, J. W. Dailey, and S. T. Picraux, *Lotus Effect Amplifies Light-Induced Contact Angle Switching*, J. Phys. Chem. B **108**, 12640 (2004), (cit. on p. 57).

[229] M. Zharnikov, G. Pace, V. Ferri, C. Grave, M. Elbing, C. V. Ha, M. Mayor, M. A. Rampi, and P. Samor, *Cooperative light-induced molecular movements of highly ordered azobenzene self-assembled monolayers*, PNAS **104**, 9937 (2007), (cit. on p. 57).

[230] C. A. Mirkin and M. A. Ratner, *Molecular electronics*, Annu. Rev. Phys. Chem. **43**, 719 (1992), (cit. on p. 57).

[231] Z. F. Liu, K. Hashimoto, and A. Fujishima, *Photoelectrochemical information storage using an azobenzene derivative*, Nature **347**, 658 (1990), (cit. on p. 57).

[232] M. Irie, *Diarylethenes for Memories and Switches*, Chem. Rev. **100**, 1685 (2000), (cit. on p. 57).

[233] A. Kirakosian, M. Comstock, J. Cho, and M. Crommie, *Molecular commensurability with a surface reconstruction: STM study of azobenzene on Au(111)*, Phys. Rev. B **71**, (2005), (cit. on p. 57).

[234] J. Henzl, M. Mehlhorn, H. Gawronski, K.-H. Rieder, and K. Morgenstern, *Reversible cis-trans isomerization of a single azobenzene molecule.* Angew. Chem. Int. Ed. **45**, 603 (2006), (cit. on pp. 57, 58).

[235] J. Henzl, P. Puschnig, C. Ambrosch-Draxl, A. Schaate, B. Ufer, P. Behrens, and K. Morgenstern, *Photoisomerization for a molecular switch in contact with a surface*, Phys. Rev. B **85**, 1 (2012), (cit. on pp. 57, 58).

[236] K. Morgenstern, *Switching individual molecules by light and electrons: From isomerisation to chirality flip*, Progr. Surf. Sci. **86**, 115 (2011), (cit. on pp. 57, 58).

[237] M. Alemani, M. V. Peters, S. Hecht, K.-H. Rieder, F. Moresco, and L. Grill, *Electric field-induced isomerization of azobenzene by STM.* J. Am. Chem. Soc. **128**, 14446 (2006), (cit. on p. 58).

[238] C. Dri, M. V. Peters, J. Schwarz, S. Hecht, and L. Grill, *Spatial periodicity in molecular switching.* Nature Nanotech. **3**, 649 (2008), (cit. on p. 58).

[239] J. Cho, L Berbil-Bautista, N. Levy, D. Poulsen, J. M. J. Fréchet, and M. F. Crommie, *Functionalization, self-assembly, and photoswitching quenching for azobenzene derivatives adsorbed on Au(111).* J. Chem. Phys. **133**, 234707 (2010), (cit. on p. 58).

[240] P. Tegeder, S. Hagen, F. Leyssner, M. Peters, S. Hecht, T. Klamroth, P. Saalfrank, and M. Wolf, *Electronic structure of the molecular switch tetra-tert-butyl-azobenzene adsorbed on Ag(111)*, Appl. Phys. A **88**, 465 (2007), (cit. on pp. 58–60, 83, 91).

[241] F. Leyssner, S. Hagen, L. Ovari, J. Dokic, P. Saalfrank, M. V. Peters, S. Hecht, T. Klamroth, and P. Tegeder, *Photoisomerization Ability of Molecular Switches Adsorbed on Au(111): Comparison between Azobenzene and Stilbene Derivatives*, J. Phys. Chem. C **114**, 1231 (2010), (cit. on pp. 58, 59, 117).

[242] C. Gahl, D. Brete, F. Leyssner, M. Koch, E. R. McNellis, J. Mielke, R. Carley, L. Grill, K. Reuter, P. Tegeder, and M. Weinelt, *Coverage- and temperature-controlled isomerization of an imine derivative on Au(111).* J. Am. Chem. Soc. **135**, 4273 (2013), (cit. on p. 58).

[243] M. J. Comstock, N. Levy, J. Cho, L. Berbil-Bautista, M. F. Crommie, D. A. Poulsen, and J. M. J. Frechet, *Measuring reversible photomechanical switching rates for a molecule at a surface*, Appl. Phys. Lett. **92**, 123107 (2008), (cit. on pp. 58, 59, 83, 112, 116).

[244] R. Schmidt, S. Hagen, D. Brete, R. Carley, C. Gahl, J. Dokić, P. Saalfrank, S. Hecht, P. Tegeder, and M. Weinelt, *On the electronic and geometrical structure of the trans-and cis-isomer of tetra-tert-butyl-azobenzene on Au (111)*, Phys. Chem. Chem. Phys.: PCCP **12**, 4488 (2010), (cit. on p. 59).

[245] S. Hagen, P. Kate, M. V. Peters, S. Hecht, M. Wolf, and P. Tegeder, *Kinetic analysis of the photochemically and thermally induced isomerization of an azobenzene derivative on Au(111) probed by two-photon photoemission*, Appl. Phys. A **93**, 253 (2008), (cit. on p. 59).

[246] J. Dokić, M. Gothe, J. Wirth, M. V. Peters, J. Schwarz, S. Hecht, and P. Saalfrank, *Quantum chemical investigation of thermal cis-to-trans isomerization of azobenzene derivatives: substituent effects, solvent effects, and comparison to experimental data.* J. Phys. Chem. A **113**, 6763 (2009), (cit. on p. 59).

[247] S. Hagen, *Isomerization behavior of photochromic molecules in direct contact with noble metal surfaces*, PhD thesis, Free University of Berlin, 2009, (cit. on pp. 59, 135).

[248] L. Ovari, M. Wolf, and P. Tegeder, *Reversible Changes in the Vibrational Structure of Tetra-tert-butylazobenzene on a Au(111) Surface Induced by Light and Thermal Activation*, J. Phys. Chem. C **111**, 15370 (2007), (cit. on p. 59).

[249] L. Óvári, J. Schwarz, M. V. Peters, S. Hecht, M. Wolf, and P. Tegeder, *Reversible isomerization of an azobenzene derivative adsorbed on Au(111): Analysis using vibrational spectroscopy*, Int. J. Mass Spectrom. **277**, 223 (2008), (cit. on p. 59).

[250] E. R. McNellis, *First-Principles Modeling of Molecular Switches at Surfaces*, PhD thesis, Free University of Berlin, 2009, (cit. on pp. 59, 61, 63, 65).

[251] I. Campillo, A. Rubio, J. Pitarke, A. Goldmann, and P. Echenique, *Hole Dynamics in Noble Metals*, Phys. Rev. Lett. **85**, 3241 (2000), (cit. on pp. 59, 135).

[252] D. Menzel and R. Gomer, *Desorption from Metal Surfaces by Low-Energy Electrons*, J. Chem. Phys. **41**, 3311 (1964), (cit. on pp. 60, 112, 133).

[253] P. A. Redhead, *Interaction of slow electrons with chemisorbed oxygen*, Can. J. Phys. **42**, 886 (1964), (cit. on pp. 60, 133).

[254] X.-L. Zhou, X.-Y. Zhu, and J. White, *Photochemistry at adsorbate/metal interfaces*, Surf. Sci. Rep. **13**, 73 (1991), (cit. on pp. 60, 112).

[255] T. Hertel, M. Wolf, and G. Ertl, *UV photostimulated desorption of ammonia from Cu(111)*, J. Chem. Phys. **102**, 3414 (1995), (cit. on pp. 60, 112, 125, 131, 135).

[256] H. Guo, P. Saalfrank, and T. Seideman, *Theory of photoinduced surface reactions of admolecules*, Progr. Surf. Sci. **62**, 239 (1999), (cit. on pp. 60, 112, 130, 133).

[257] M. Comstock, D. Strubbe, L. Berbil-Bautista, N. Levy, J. Cho, D. Poulsen, J. Fréchet, S. Louie, and M. Crommie, *Determination of Photoswitching Dynamics through Chiral Mapping of Single Molecules Using a Scanning Tunneling Microscope*, Phys. Rev. Lett. **104**, 178301 (2010), (cit. on pp. 61, 123).

[258] S. Clark, M. Segall, C. Pickard, P. Hasnip, M. Probert, K. Refson, and M. Payne, *First principles methods using CASTEP*, Z. Kristallogr. **220**, 567 (2005), (cit. on pp. 64, 104, 144).

[259] M. C. Payne, T. A. Arias, and J. D. Joannopoulos, *Iterative minimization techniques for ab initio total-energy calculations: molecular dynamics and conjugate gradients*, Rev. Mod. Phys **64**, 1045 (1992), (cit. on pp. 64, 104, 144).

[260] J. E. Peralta, J. Uddin, and G. E. Scuseria, *Scalar relativistic all-electron density functional calculations on periodic systems.* J. Chem. Phys. **122**, 84108 (2005), (cit. on p. 65).

[261] A. Zangwill, *Physics at surfaces*, Cambridge University Press, Cambridge, 1996, ISBN: 9780521347525, (cit. on p. 65).

[262] A Gross, *Theoretical Surface Science: A Microscopic Perspective*, Springer, 2009, ISBN: 978-3540689669, (cit. on pp. 65, 99, 155).

[263] J. Andzelm and R. King-Smith, *Geometry optimization of solids using delocalized internal coordinates*, Chem. Phys. Lett. **335**, 321 (2001), (cit. on pp. 65, 84, 144).

[264] J. M. Gottfried, E. K. Vestergaard, P. Bera, and C. T. Campbell, *Heat of adsorption of naphthalene on Pt(111) measured by adsorption calorimetry.* J. Phys. Chem. B **110**, 17539 (2006), (cit. on p. 72).

[265] C. T. Campbell and J. R. V. Sellers, *The entropies of adsorbed molecules.* J. Am. Chem. Soc. **134**, 18109 (2012), (cit. on p. 72).

[266] J. Zegenhagen, *Surface structure determination with X-ray standing waves*, Surf. Sci. Rep. **18**, 202 (1993), (cit. on pp. 72, 74, 81).

[267] G. Mercurio, R. J. Maurer, W. Liu, S. Hagen, F. Leyssner, P. Tegeder, J. Meyer, A. Tkatchenko, S. Soubatch, K. Reuter, and F. S. Tautz, *Quantification of finite-temperature effects on adsorption geometries of π-conjugated molecules: Azobenzene/Ag(111)*, Phys. Rev. B **88**, 035421 (2013), (cit. on pp. 73, 74, 81).

[268] G. Mercurio, R. J. Maurer, S. Hagen, F. Leyssner, J. Meyer, P. Tegeder, S. Soubatch, K. Reuter, and F. S. Tautz, *X-ray standing wave simulations based on Fourier vector analysis as a method to retrieve complex molecular adsorption geometries*, Front. Phys. 2 (2014), (cit. on pp. 73, 74, 81).

[269] L. Romaner, G. Heimel, J.-L. Brédas, A. Gerlach, F. Schreiber, R. Johnson, J. Zegenhagen, S. Duhm, N. Koch, and E. Zojer, *Impact of Bidirectional Charge Transfer and Molecular Distortions on the Electronic Structure of a Metal-Organic Interface*, Phys. Rev. Lett. **99**, 256801 (2007), (cit. on p. 73).

[270] N. Koch, A. Gerlach, S. Duhm, H. Glowatzki, G. Heimel, A. Vollmer, Y. Sakamoto, T. Suzuki, J. Zegenhagen, J. P. Rabe, and F. Schreiber, *Adsorption-induced intramolecular dipole: correlating molecular conformation and interface electronic structure.* J. Am. Chem. Soc. **130**, 7300 (2008), (cit. on p. 73).

[271] N. Atodiresei, V. Caciuc, P. Lazić, and S. Blügel, *Chemical versus van der Waals Interaction: The Role of the Heteroatom in the Flat Absorption of Aromatic Molecules C6H6, C5NH5, and C4N2H4 on the Cu(110) Surface*, Phys. Rev. Lett. **102**, 136809 (2009), (cit. on p. 73).

[272] F. Mittendorfer, A. Garhofer, J. Redinger, J. Klimeš, J. Harl, and G. Kresse, *Graphene on Ni(111): Strong interaction and weak adsorption*, Phys. Rev. B **84**, 201401 (2011), (cit. on p. 73).

[273] W. Liu, A. Savara, X. Ren, W. Ludwig, K.-H. Dostert, S. Schauermann, A. Tkatchenko, H.-J. Freund, and M. Scheffler, *Toward Low-Temperature Dehydrogenation Catalysis: Isophorone Adsorbed on Pd(111)*, J. Phys. Chem. Lett. **3**, 582 (2012), (cit. on p. 73).

[274] P. Sony, P. Puschnig, D. Nabok, and C. Ambrosch-Draxl, *Importance of Van Der Waals Interaction for Organic Molecule-Metal Junctions: Adsorption of Thiophene on Cu(110) as a Prototype*, Phys. Rev. Lett. **99**, 176401 (2007), (cit. on p. 73).

[275] A. Tkatchenko, L. Romaner, O. Hofmann, E. Zojer, C. Ambrosch-Draxl, and M. Scheffler, *Van der Waals interactions between organic adsorbates and at organic/inorganic interfaces*, MRS Bulletin **35**, 435 (2010), (cit. on p. 73).

[276] W. A. Al-Saidi, H. Feng, and K. A. Fichthorn, *Adsorption of polyvinylpyrrolidone on Ag surfaces: insight into a structure-directing agent.* Nano Lett. **12**, 997 (2012), (cit. on p. 73).

[277] C. Wagner, N. Fournier, F. S. Tautz, and R. Temirov, *Measurement of the Binding Energies of the Organic-Metal Perylene-Teracarboxylic-Dianhydride/Au(111) Bonds by Molecular Manipulation Using an Atomic Force Microscope*, Phys. Rev. Lett. **109**, 076102 (2012), (cit. on p. 73).

[278] D. P. Woodruff, *Surface structure determination using x-ray standing waves*, Rep. Prog. Phys. **68**, 743 (2005), (cit. on p. 74).

[279] G. Mercurio, *Study of Molecule-Metal Interfaces by Means of the Normal Incidence X-Ray Standing Wave Technique*, PhD thesis, RWTH Aachen, 2012, (cit. on p. 74).

[280] G. Mercurio, O. Bauer, M. Willenbockel, N. Fairley, W. Reckien, C. H. Schmitz, B. Fiedler, S. Soubatch, T. Bredow, M. Sokolowski, and F. S. Tautz, *Adsorption height determination of nonequivalent C and O species of PTCDA on Ag(110) using x-ray standing waves*, Phys. Rev. B **87**, 045421 (2013), (cit. on p. 74).

[281] A. Tkatchenko and O. von Lilienfeld, *Popular Kohn-Sham density functionals strongly overestimate many-body interactions in van der Waals systems*, Phys. Rev. B **78**, 045116 (2008), (cit. on p. 81).

[282] A. Tkatchenko, R. DiStasio, R. Car, and M. Scheffler, *Accurate and efficient method for many-body van der Waals interactions*, Phys. Rev. Lett. **108**, 236402 (2012), (cit. on p. 81).

[283] D. P. Woodruff, B. C. C. Cowie, and A. R. H. F. Ettema, *Surface structure determination using X-ray standing waves: a simple view*, J. Phys.: Condens. Matter **6**, 10633 (1994), (cit. on p. 81).

[284] V. F. Sears and S. A. Shelley, *DebyeWaller factor for elemental crystals*, Acta Crystallogr., Sect. A **47**, 441 (1991), (cit. on p. 81).

[285] R. J. Maurer and K. Reuter, *Bistability Loss as a Key Feature in Azobenzene (Non-) Switching on Metal Surfaces*, Angew. Chem. Int. Ed. **51**, 12009 (2012), (cit. on pp. 83, 113).

[286] T. A. Halgren and W. N. Lipscomb, *The synchronous-transit method for determining reaction pathways and locating molecular transition states*, Chem. Phys. Lett. **49**, 225 (1977), (cit. on p. 84).

[287] S. Bell and J. S. Crighton, *Locating transition states*, J. Chem. Phys. **80**, 2464 (1984), (cit. on p. 84).

[288] J. Meyer and K. Reuter, *Electronhole pairs during the adsorption dynamics of O 2 on Pd(100): exciting or not?*, New J. Phys. **13**, 085010 (2011), (cit. on pp. 86, 128).

[289] M. Dewar, *A review of π Complex Theory*, Bull. Soc. Chim. France **18**, C79 (1951), (cit. on p. 89).

[290] J. Chatt and L. A. Duncanson, *586. Olefin co-ordination compounds. Part III. Infra-red spectra and structure: attempted preparation of acetylene complexes*, J. Chem. Soc. 2939 (1953), (cit. on p. 89).

[291] L. Salem and C. Rowland, *The electronic properties of diradicals*, Angew. Chem. Int. Ed. **11**, 92 (1972), (cit. on p. 89).

[292] P. C. Rusu and G. Brocks, *Surface dipoles and work functions of alkylthiolates and fluorinated alkylthiolates on Au(111).* J. Phys. Chem. B **110**, 22628 (2006), (cit. on p. 93).

[293] P. Rusu and G. Brocks, *Work functions of self-assembled monolayers on metal surfaces by first-principles calculations*, Phys. Rev. B **74**, 073414 (2006), (cit. on p. 93).

[294] R. J. Maurer and K. Reuter, *Excited-state potential-energy surfaces of metal-adsorbed organic molecules from linear expansion Δ-self-consistent field density-functional theory (ΔSCF-DFT)*, J. Chem. Phys. **139**, 014708 (2013), (cit. on pp. 97, 111).

[295] G. Onida, L. Reining, and A. Rubio, *Electronic excitations: density-functional versus many-body Greens-function approaches*, Rev. Mod. Phys. **74**, 601 (2002), (cit. on pp. 97, 155).

[296] L Hedin, *New method for calculating the one-particle Green's function with application to the electron-gas problem*, Phys. Rev **139**, A796 (1965), (cit. on pp. 97, 155).

[297] F Aryasetiawan and O Gunnarsson, *The GW method*, Rep. Prog. Phys. **61**, 237 (1998), (cit. on p. 97).

[298] L. Sham and T. Rice, *Many-Particle Derivation of the Effective-Mass Equation for the Wannier Exciton*, Phys. Rev. **144**, 708 (1966), (cit. on p. 97).

[299] W Hanke and L. Sham, *Local-field and excitonic effects in the optical spectrum of a covalent crystal*, Phys. Rev. B **12**, 4501 (1975), (cit. on p. 97).

[300] M. Weinert and J. Davenport, *Fractional occupations and density-functional energies and forces*, Phys. Rev. B **45**, 13709 (1992), (cit. on p. 98).

[301] G Kresse and J. Furthmüller, *Efficiency of ab-initio total energy calculations for metals and semiconductors using a plane-wave basis set*, Comp. Mat. Sci. **6**, 15 (1996), (cit. on pp. 98, 104, 144, 152).

[302] H. Oberhofer and J. Blumberger, *Electronic coupling matrix elements from charge constrained density functional theory calculations using a plane wave basis set.* J. Chem. Phys. **133**, 244105 (2010), (cit. on p. 98).

[303] S. Kasamatsu, S. Watanabe, and S. Han, *Orbital-separation approach for consideration of finite electric bias within density-functional total-energy formalism*, Phys. Rev. B **84**, 085120 (2011), (cit. on p. 98).

[304] T. Olsen, J. Gavnholt, and J. Schiøtz, *Hot-electron-mediated desorption rates calculated from excited-state potential energy surfaces*, Phys. Rev. B **79**, 035403 (2009), (cit. on pp. 98, 103).

[305] P. Zawadzki, J. Rossmeisl, and K. W. Jacobsen, *Electronic hole transfer in rutile and anatase TiO_{2}: Effect of a delocalization error in the density functional theory on the charge transfer barrier height*, Phys. Rev. B **84**, 121203(R) (2011), (cit. on p. 98).

[306] J. Garcia-Lastra and K. Thygesen, *Renormalization of Optical Excitations in Molecules near a Metal Surface*, Phys. Rev. Lett. **106**, 187402 (2011), (cit. on pp. 98, 108).

[307] J. Mortensen, L. Hansen, and K. Jacobsen, *Real-space grid implementation of the projector augmented wave method*, Phys. Rev. B **71**, 035109 (2005), (cit. on p. 102).

[308] J Enkovaara, C Rostgaard, J. J. Mortensen, J Chen, M Duak, L Ferrighi, J Gavnholt, C Glinsvad, V Haikola, H. A. Hansen, H. H. Kristoffersen, M Kuisma, A. H. Larsen, L Lehtovaara, M Ljungberg, O Lopez-Acevedo, P. G. Moses, J Ojanen, T Olsen, V Petzold, N. a. Romero, J Stausholm-Møller, M Strange, G. A. Tritsaris, M Vanin, M Walter, B Hammer, H Häkkinen, G. K. H. Madsen, R. M. Nieminen, J. K. Nørskov, M Puska, T. T. Rantala, J Schiøtz, K. S. Thygesen, and K. W. Jacobsen, *Electronic structure calculations with GPAW: a real-space implementation of the projector augmented-wave method.* J. Phys.: Condens. Matter **22**, 253202 (2010), (cit. on p. 102).

[309] A. D. Dwyer and D. J. Tozer, *Effect of chemical change on TDDFT accuracy: orbital overlap perspective of the hydrogenation of retinal.* Phys. Chem. Chem. Phys.: PCCP **12**, 2816 (2010), (cit. on p. 103).

[310] R. van Leeuwen and E. J. Baerends, *Exchange-correlation potential with correct assymptotic behavior*, Phys. Rev. A **49**, 2421 (1994), (cit. on p. 103).

[311] P Hasnip and C Pickard, *Electronic energy minimisation with ultrasoft pseudopotentials*, Comp. Phys. Comm. **174**, 24 (2006), (cit. on pp. 104, 144).

[312] P. J. Feibelman, B. Hammer, J. K. Nørskov, F. Wagner, M. Scheffler, R. Stumpf, R. Watwe, and J. Dumesic, *The CO/Pt(111) Puzzle* , J. Phys. Chem. B **105**, 4018 (2001), (cit. on p. 105).

[313] G. Kresse, A. Gil, and P. Sautet, *Significance of single-electron energies for the description of CO on Pt(111)*, Phys. Rev. B **68**, 3 (2003), (cit. on pp. 105, 156, 157).

[314] M Marsman, J Paier, A Stroppa, and G Kresse, *Hybrid functionals applied to extended systems*, J. Phys.: Condens. Matter **20**, 064201 (2008), (cit. on pp. 105, 158).

[315] V. Anisimov and J. Zaanen, *Band theory and Mott insulators: Hubbard U instead of Stoner I*, Phys. Rev. B **44**, (1991), (cit. on pp. 105, 155).

[316] A. Liechtenstein and V. Anisimov, *Density-functional theory and strong interactions: Orbital ordering in Mott-Hubbard insulators*, Phys. Rev. B **52**, 5467 (1995), (cit. on p. 105).

[317] A. Petukhov, I. Mazin, L. Chioncel, and A. Lichtenstein, *Correlated metals and the LDA+U method*, Phys. Rev. B **67**, 153106 (2003), (cit. on pp. 105, 155).

[318] F. Della Sala and A. Görling, *Asymptotic Behavior of the Kohn-Sham Exchange Potential*, Phys. Rev. Lett. **89**, 033003 (2002), (cit. on p. 106).

[319] J. Neaton, M. Hybertsen, and S. Louie, *Renormalization of Molecular Electronic Levels at Metal-Molecule Interfaces*, Phys. Rev. Lett. **97**, 216405 (2006), (cit. on p. 108).

[320] K. Thygesen and A. Rubio, *Renormalization of Molecular Quasiparticle Levels at Metal-Molecule Interfaces: Trends across Binding Regimes*, Phys. Rev. Lett. **102**, 046802 (2009), (cit. on p. 108).

[321] M. Head-Gordon and J. C. Tully, *Molecular dynamics with electronic frictions*, J. Chem. Phys. **103**, 10137 (1995), (cit. on pp. 111, 129, 131, 132).

[322] M. Ben-Nun, J. Quenneville, and T. J. Martínez, *Ab Initio Multiple Spawning: Photochemistry from First Principles Quantum Molecular Dynamics*, J. Phys. Chem. A **104**, 5161 (2000), (cit. on p. 125).

[323] M. Barbatti, *Nonadiabatic dynamics with trajectory surface hopping method*, Wiley Interdiscip. Rev. Comput. Mol. Sci. **1**, 620 (2011), (cit. on pp. 125, 130, 147).

[324] C. Carbogno, A. Groß, and M. Rohlfing, *Ab initio investigation of the laser induced desorption of iodine from KI(100)*, Appl. Phys. A **88**, 579 (2007), (cit. on pp. 125, 134).

[325] M. Mehring and T. Klüner, *Understanding surface photochemistry from first principles: The case of COTiO2(110)*, Chem. Phys. Lett. **513**, 212 (2011), (cit. on p. 125).

[326] J. C. Tully, *Chemical Dynamics at Metal Surfaces*, Annu. Rev. Phys. Chem. **51**, 153 (2000), (cit. on p. 125).

[327] C. Carbogno, J. Behler, K. Reuter, and A. Groß, *Signatures of nonadiabatic O_{2} dissociation at Al(111): First-principles fewest-switches study*, Phys. Rev. B **81**, 035410 (2010), (cit. on pp. 125, 130, 133).

[328] N. Shenvi, S. Roy, and J. C. Tully, *Nonadiabatic dynamics at metal surfaces: independent-electron surface hopping.* J. Chem. Phys. **130**, 174107 (2009), (cit. on pp. 125, 131, 134).

[329] N. Shenvi, S. Roy, and J. C. Tully, *Dynamical steering and electronic excitation in NO scattering from a gold surface.* Science **326**, 829 (2009), (cit. on pp. 125, 134).

[330] A. Sax, *Potential Energy Surfaces: Proceedings of the Mariapfarr Workshop in Theoretical Chemistry*, Springer, Berlin, New York, 1999, ISBN: 3540651063, (cit. on p. 126).

[331] M. Buhmann, *Radial Basis Functions*, Cambridge University Press, Cambridge, 2003, ISBN: 9780521101332, (cit. on p. 127).

[332] S. Bochkanov, *ALGLIB: www.alglib.net* (cit. on pp. 127, 147).

[333] E. Wilson, J. Decius, and P. Cross, *Molecular Vibrations: the theory of Infrared and Raman vibrational spectra*, Dover Publications, New York, 1980, ISBN: 9780486639413, (cit. on pp. 128, 147).

[334] V. Bakken and T. Helgaker, *The efficient optimization of molecular geometries using redundant internal coordinates*, J. Chem. Phys. **117**, 9160 (2002), (cit. on p. 128).

[335] J. Trail, M. Graham, D. Bird, M. Persson, and S. Holloway, *Energy Loss of Atoms at Metal Surfaces due to Electron-Hole Pair Excitations: First-Principles Theory of Chemicurrents*, Phys. Rev. Lett. **88**, 166802 (2002), (cit. on p. 129).

[336] N. Doltsinis, *Molecular Dynamics Beyond the Born-Oppenheimer Approximation: Mixed QuantumClassical Approaches*, in *Computational Nanoscience: Do it Yourself*, ed. by J. Grotendorst, S. Blügel, and D. Marx, John von Neumann Institute for Computing, Jülich, 2006, vol. 31, pp. 389–409, ISBN: 3000173501 (cit. on p. 130).

[337] J. C. Tully, *Molecular dynamics with electronic transitions*, J. Chem. Phys. **93**, 1061 (1990), (cit. on pp. 130, 147).

[338] J. C. Tully, *Electronic and phonon mechanisms of vibrational relaxation: CO on Cu(100)*, J. Vac. Sci. Technol., A **11**, 1914 (1993), (cit. on p. 130).

[339] E. Fabiano, T. Keal, and W. Thiel, *Implementation of surface hopping molecular dynamics using semiempirical methods*, Chem. Phys. **349**, 334 (2008), (cit. on pp. 130, 147).

[340] B. J. Schwartz, E. R. Bittner, O. V. Prezhdo, and P. J. Rossky, *Quantum decoherence and the isotope effect in condensed phase nonadiabatic molecular dynamics simulations*, J. Chem. Phys. **104**, 5942 (1996), (cit. on p. 131).

[341] C. Zhu, A. W. Jasper, and D. G. Truhlar, *Non-Born-Oppenheimer Liouville-von Neumann Dynamics. Evolution of a Subsystem Controlled by Linear and Population-Driven Decay of Mixing with Decoherent and Coherent Switching*, J. Comput. Chem. Theory **1**, 527 (2005), (cit. on pp. 131, 147).

[342] G. Stock and M. Thoss, *Semiclassical Description of Nonadiabatic Quantum Dynamics*, Phys. Rev. Lett. **78**, 578 (1997), (cit. on p. 131).

[343] J. E. Subotnik and N. Shenvi, *A new approach to decoherence and momentum rescaling in the surface hopping algorithm.* J. Chem. Phys. **134**, 024105 (2011), (cit. on p. 131).

[344] N. Shenvi, J. E. Subotnik, and W. Yang, *Simultaneous-trajectory surface hopping: a parameter-free algorithm for implementing decoherence in nonadiabatic dynamics.* J. Chem. Phys. **134**, 144102 (2011), (cit. on p. 131).

[345] N. Shenvi, J. E. Subotnik, and W. Yang, *Phase-corrected surface hopping: correcting the phase evolution of the electronic wavefunction.* J. Chem. Phys. **135**, 024101 (2011), (cit. on p. 131).

[346] N. Shenvi and J. C. Tully, *Nonadiabatic dynamics at metal surfaces: Independent electron surface hopping with phonon and electron thermostats*, Faraday Discuss. **157**, 325 (2012), (cit. on p. 132).

[347] R Zwanzig, *Time-Correlation Functions and Transport Coefficients in Statistical Mechanics*, Annu. Rev. Phys. Chem. **16**, 67 (1965), (cit. on p. 132).

[348] R. Zwanzig, *Nonequilibrium Statistical Mechanics*, Oxford University Press, Oxford, 2001, ISBN: 0198032153, (cit. on p. 132).

[349] S. R. Billeter and D. Egli, *Calculation of nonadiabatic couplings with restricted open-shell Kohn-Sham density-functional theory.* J. Chem. Phys. **125**, 224103 (2006), (cit. on pp. 132, 133).

[350] I. Tavernelli, B. F. E. Curchod, A. Laktionov, and U. Rothlisberger, *Nonadiabatic coupling vectors for excited states within time-dependent density functional theory in the Tamm-Dancoff approximation and beyond.* J. Chem. Phys. **133**, 194104 (2010), (cit. on pp. 132, 133).

[351] Y. Li and G. Wahnström, *Molecular-dynamics simulation of hydrogen diffusion in palladium*, Phys. Rev. B **46**, 14528 (1992), (cit. on p. 132).

[352] J. Juaristi, M. Alducin, R. Muiño, H. Busnengo, and A. Salin, *Role of Electron-Hole Pair Excitations in the Dissociative Adsorption of Diatomic Molecules on Metal Surfaces*, Phys. Rev. Lett. **100**, 116102 (2008), (cit. on pp. 132, 135).

[353] B. H. Lengsfield, P. Saxe, and D. R. Yarkony, *On the evaluation of nonadiabatic coupling matrix elements using SA-MCSCF/CI wave functions and analytic gradient methods. I*, J. Chem. Phys. **81**, 4549 (1984), (cit. on p. 132).

[354] B. H. Lengsfield and D. R. Yarkony, *Nonadiabatic Interactions Between Potential Energy Surfaces: Theory and Applications*, in *Adv. Chem. Phys.* Ed. by M. Baer and C.-Y. Ng, John Wiley & Sons, Inc., Hoboken, NJ, USA, 1992, Advances in Chemical Physics vol. 82, p. 1, ISBN: 9780470141403 (cit. on p. 132).

[355] N. Doltsinis and D. Marx, *Nonadiabatic Car-Parrinello Molecular Dynamics*, Phys. Rev. Lett. **88**, 166402 (2002), (cit. on p. 132).

[356] C. Craig, W. Duncan, and O. Prezhdo, *Trajectory Surface Hopping in the Time-Dependent Kohn-Sham Approach for Electron-Nuclear Dynamics*, Phys. Rev. Lett. **95**, 163001 (2005), (cit. on p. 132).

[357] E. Tapavicza, I. Tavernelli, and U. Rothlisberger, *Trajectory Surface Hopping within Linear Response Time-Dependent Density-Functional Theory*, Phys. Rev. Lett. **98**, 023001 (2007), (cit. on p. 132).

[358] V. Chernyak and S. Mukamel, *Density-matrix representation of nonadiabatic couplings in time-dependent density functional (TDDFT) theories*, J. Chem. Phys. **112**, 3572 (2000), (cit. on p. 132).

[359] I. Tavernelli, E. Tapavicza, and U. Rothlisberger, *Nonadiabatic coupling vectors within linear response time-dependent density functional theory.* J. Chem. Phys. **130**, 124107 (2009), (cit. on p. 132).

[360] I. Frank, J. Hutter, D. Marx, and M. Parrinello, *Molecular dynamics in low-spin excited states*, J. Chem. Phys. **108**, 4060 (1998), (cit. on p. 133).

[361] S. R. Billeter and A. Curioni, *Calculation of nonadiabatic couplings in density-functional theory.* J. Chem. Phys. **122**, 34105 (2005), (cit. on p. 133).

[362] J. W. Gadzuk, *The Semiclassical Way to Molecular Dynamics at Surfaces*, Annu. Rev. Phys. Chem. **39**, 395 (1988), (cit. on p. 133).

[363] G. Boendgen and P. Saalfrank, *STM-Induced Desorption of Hydrogen from a Silicon Surface: An Open-System Density Matrix Study*, J. Phys. Chem. B **102**, 8029 (1998), (cit. on p. 133).

[364] E. Teller, *The Crossing of Potential Surfaces.* J. Phys. Chem. **41**, 109 (1937), (cit. on p. 134).

[365] A. Bjerre and E. Nikitin, *Energy transfer in collisions of an excited sodium atom with a nitrogen molecule*, Chem. Phys. Lett. **1**, 179 (1967), (cit. on p. 134).

[366] M. Desouter-Lecomte and J. C. Lorquet, *Nonadiabatic interactions in unimolecular decay. IV. Transition probability as a function of the Massey parameter*, J. Chem. Phys. **71**, 4391 (1979), (cit. on p. 134).

[367] F. Bernardi, M. Olivucci, and M. A. Robb, *Potential energy surface crossings in organic photochemistry*, Chem. Soc. Rev. **25**, 321 (1996), (cit. on p. 134).

[368] W. H. Miller and T. F. George, *Semiclassical Theory of Electronic Transitions in Low Energy Atomic and Molecular Collisions Involving Several Nuclear Degrees of Freedom*, J. Chem. Phys. **56**, 5637 (1972), (cit. on p. 134).

[369] S. A. Fischer, B. F. Habenicht, A. B. Madrid, W. R. Duncan, and O. V. Prezhdo, *Regarding the validity of the time-dependent Kohn-Sham approach for electron-nuclear dynamics via trajectory surface hopping.* J. Chem. Phys. **134**, 024102 (2011), (cit. on p. 134).

[370] M. Persson and B. Hellsing, *Electronic Damping of Adsorbate Vibrations on Metal Surfaces*, Phys. Rev. Lett. **49**, 662 (1982), (cit. on p. 135).

[371] B Hellsing and M Persson, *Electronic Damping of Atomic and Molecular Vibrations at Metal Surfaces*, Physi. Scripta **29**, 360 (1984), (cit. on p. 135).

[372] G. D. Billing, *Electron-hole pair versus phonon excitation in molecule-surface collisions*, Chem. Phys. **116**, 269 (1987), (cit. on p. 135).

[373] G. Wahnström, *Role of phonons and electronhole pairs in hydrogen diffusion on a corrugated metal surface*, Chem. Phys. Lett. **163**, 401 (1989), (cit. on p. 135).

[374] E. Hasselbrink, M. Wolf, S. Holloway, and P. Saalfrank, *Classical and quantum-mechanical modeling of the stimulated desorption of ammonia from Cu(111)*, Surf. Sci. **363**, 179 (1996), (cit. on p. 135).

[375] P. Echenique, R. Berndt, E. Chulkov, T. Fauster, A. Goldmann, and U. Höfer, *Decay of electronic excitations at metal surfaces*, Surf. Sci. Rep. **52**, 219 (2004), (cit. on p. 135).

[376] E. Knoesel, A. Hotzel, and M. Wolf, *Ultrafast dynamics of hot electrons and holes in copper: Excitation, energy relaxation, and transport effects*, Phys. Rev. B **57**, 12812 (1998), (cit. on p. 135).

[377] H. Petek, H. Nagano, and S. Ogawa, *Hot-electron dynamics in copper revisited: The d-band effect*, Appl. Phys. B **68**, 369 (1999), (cit. on p. 135).

[378] H. Petek, H. Nagano, and S. Ogawa, *Hole Decoherence of d Bands in Copper*, Phys. Rev. Lett. **83**, 832 (1999), (cit. on p. 135).

[379] R. Matzdorf, A. Gerlach, F. Theilmann, G. Meister, and A. Goldmann, *New lifetime estimates for d-band holes at noble metal surfaces*, Appl. Phys. B **68**, 393 (1999), (cit. on p. 135).

[380] E. Pastorczak, N. Gidopoulos, and K. Pernal, *Calculation of electronic excited states of molecules using the Helmholtz free-energy minimum principle*, Phys. Rev. A **062501**, 1 (2013), (cit. on p. 138).

[381] I. Dabo, A. Ferretti, N. Poilvert, Y. Li, N. Marzari, and M. Cococcioni, *Koopmans condition for density-functional theory*, Phys. Rev. B **82**, 115121 (2010), (cit. on p. 138).

[382] I. Dabo, A. Ferretti, C.-H. Park, N. Poilvert, Y. Li, M. Cococcioni, and N. Marzari, *Donor and acceptor levels of organic photovoltaic compounds from first principles.* Phys. Chem. Chem. Phys.: PCCP **15**, 685 (2013), (cit. on p. 138).

[383] *TURBOMOLE V6.2 2010, a development of University of Karlsruhe and Forschungszentrum Karlsruhe GmbH, 1989-2007, TURBOMOLE GmbH, since 2007*, 2010 (cit. on p. 143).

[384] S. F. Boys, *Electronic Wave Functions. I. A General Method of Calculation for the Stationary States of Any Molecular System*, Proc. R. Soc. London, Ser. A **200**, 542 (1950), (cit. on p. 143).

[385] M. Häser and R. Ahlrichs, *Improvements on the direct SCF method*, J. Comput. Chem. **10**, 104 (1989), (cit. on p. 143).

[386] O. Treutler and R. Ahlrichs, *Efficient molecular numerical integration schemes*, J. Chem. Phys. **102**, 346 (1995), (cit. on p. 143).

[387] K. Eichkorn, O. Treutler, H. Öhm, M. Häser, and R. Ahlrichs, *Auxiliary basis sets to approximate Coulomb potentials*, Chem. Phys. Lett. **240**, 283 (1995), (cit. on p. 143).

[388] K. Eichkorn, F. Weigend, O. Treutler, and R. Ahlrichs, *Auxiliary basis sets for main row atoms and transition metals and their use to approximate Coulomb potentials*, Theor. Chem. Acc. **97**, 119 (1997), (cit. on p. 143).

[389] A. Schafer, C. Huber, and R. Ahlrichs, *Fully optimized contracted Gaussian basis sets of triple zeta valence quality for atoms Li to Kr*, J. Chem. Phys. **100**, 5829 (1994), (cit. on p. 143).

[390] F. Weigend and R. Ahlrichs, *Balanced basis sets of split valence, triple zeta valence and quadruple zeta valence quality for H to Rn: Design and assessment of accuracy.* Phys. Chem. Chem. Phys.: PCCP **7**, 3297 (2005), (cit. on p. 143).

[391] F. Weigend, F. Furche, and R. Ahlrichs, *Gaussian basis sets of quadruple zeta valence quality for atoms HKr*, J. Chem. Phys. **119**, 12753 (2003), (cit. on p. 143).

[392] R. Send and F. Furche, *First-order nonadiabatic couplings from time-dependent hybrid density functional response theory: Consistent formalism, implementation, and performance.* J. Chem. Phys. **132**, 044107 (2010), (cit. on p. 143).

[393] X. Ren, P. Rinke, V. Blum, J. Wieferink, A. Tkatchenko, A. Sanfilippo, K. Reuter, and M. Scheffler, *Resolution-of-identity approach to HartreeFock, hybrid density functionals, RPA, MP2 and GW with numeric atom-centered orbital basis functions*, New J. Phys. **14**, 053020 (2012), (cit. on p. 144).

[394] M. Segall, P. Lindan, M. Probert, C. Pickard, P. Hasnip, S. Clark, and M. Payne, *First-principles simulation: ideas, illustrations and the CASTEP code*, J. Phys.: Condens. Matter **14**, 2717 (2002), (cit. on p. 144).

[395] N. Marzari, D. Vanderbilt, and M. Payne, *Ensemble Density-Functional Theory for Ab Initio Molecular Dynamics of Metals and Finite-Temperature Insulators*, Phys. Rev. Lett. **79**, 1337 (1997), (cit. on p. 144).

[396] D. Alfè, *Ab initio molecular dynamics, a simple algorithm for charge extrapolation*, Comp. Phys. Commun. **118**, 31 (1999), (cit. on p. 144).

[397] P. Pulay, *Convergence acceleration of iterative sequences. the case of scf iteration*, Chem. Phys. Lett. **73**, 393 (1980), (cit. on p. 144).

[398] *The Atomic Simulation Environment (ASE)* (cit. on p. 146).

[399] F. Plasser, G. Granucci, J. Pittner, M. Barbatti, M. Persico, and H. Lischka, *Surface hopping dynamics using a locally diabatic formalism: charge transfer in the ethylene dimer cation and excited state dynamics in the 2-pyridone dimer.* J. Chem. Phys. **137**, 22A514 (2012), (cit. on p. 147).

[400] W. Humphrey, A. Dalke, and K. Schulten, *VMD – Visual Molecular Dynamics*, J. Mol. Graphics **14**, 33 (1996), (cit. on p. 147).

[401] T. G. A. Youngs, *Aten - An application for the creation, editing, and visualization of coordinates for glasses, liquids, crystals, and molecules*, J. Comput. Chem. **31**, 639 (2010), (cit. on p. 147).

[402] M. D. Hanwell, D. E. Curtis, D. C. Lonie, T. Vandermeersch, E. Zurek, and G. R. Hutchison, *Avogadro: an advanced semantic chemical editor, visualization, and analysis platform.* J. Cheminf. **4**, 17 (2012), (cit. on p. 147).

[403] R. Gehrke, *First-Principles Basin-Hopping for the Structure Determination of Atomic Clusters*, PhD thesis, 2008, (cit. on p. 153).

[404] S. L. Dudarev, S. Y. Savrasov, C. J. Humphreys, and A. P. Sutton, *Electron-energy-loss spectra and the structural stability of nickel oxide: An LSDA+U study*, Phys. Rev. B **57**, 1505 (1998), (cit. on p. 155).

[405] W. Pickett, S. Erwin, and E. Ethridge, *Reformulation of the LDA+ U method for a local-orbital basis*, Phys. Rev. B **58**, 1201 (1998), (cit. on p. 155).

[406] V. L. Campo and M. Cococcioni, *Extended DFT + U + V method with on-site and inter-site electronic interactions.* J. Phys. Condens. Matter **22**, 055602 (2010), (cit. on p. 155).

[407] E Abad, Y. J. Dappe, J. I. Martínez, F Flores, and J Ortega, *C6H6/Au(111): interface dipoles, band alignment, charging energy, and van der Waals interaction.* J. Chem. Phys. **134**, 044701 (2011), (cit. on p. 157).

[408] J. Martínez, E. Abad, C. González, J. Ortega, and F. Flores, *Theoretical characterization of the TTF/Au (111) interface: STM imaging, band alignment and charging energy*, Org. Electron. **13**, 399 (2012), (cit. on p. 157).

[409] J. Beltrán, F. Flores, J. I. Mart, and J. Ortega, *Energy Level Alignment in Organic Organic Heterojunctions : The*, J. Phys. Chem. C **117**, 3888 (2013), (cit. on p. 157).

[410] H. Hellmann, *Zur Rolle der kinetischen Elektronenenergie für die zwischenatomaren Kräfte*, Z. Phys. A: Hadrons Nucl. **85**, 180 (1933), (cit. on p. 157).

[411] R. Feynman, *Forces in molecules*, Phys. Rev. **56**, 340 (1939), (cit. on p. 157).

[412] P. Pulay, *Ab initio calculation of force constants and equilibrium geometries in polyatomic molecules*, Mol. Phys. **17**, 197 (1969), (cit. on p. 158).

[413] Z. Lin, *Pulay forces in density functional theory for periodic and molecular systems*, Phys. Lett. A **299**, 413 (2002), (cit. on p. 158).

Acknowledgements

This work has been prepared at the Chair of Theoretical Chemistry of Prof. Dr. Karsten Reuter at the Technische Universität München between October 2010 and November 2013. In the course of these three years, I have relied on the courtesy and support of many to which I am grateful. I thereby have accumulated a great deal of intellectual debts.

First, I would like to express my gratitude to Prof. Dr. Karsten Reuter for making this work possible and for his constant support. This includes us having down-to-earth discussions with an aim for the big picture, however, without missing out on the details, but also him being always reachable, whenever he was needed. Especially, the evergrowing group of smart and witty scientists he has summoned to Munich, my colleagues, have made this time highly enjoyable.

I would specifically like to express my gratitude to Ruth Mösch for the personal and professional determination to the office, reaching far beyond the job description. Many thanks go to Dr. Christoph Scheurer, Dr. Jörg Meyer, Max Hoffmann, and Christoph Schober for their technical and computational support, and Dr. Sebastian Matera for help with the ALGLIB library.

Work wouldn't have been so much fun without the sometimes philosophical, sometimes histerical discussions in our small mensa-boycott lunch group: Thanks to Dr. Jelena Jelic, Dr. Tuğba Davran-Candan, Vanessa Bukas, Berna Doğan, Dr. Katharina Diller, and all our part-time guests.

During this work, I had the honor to collaborate with many bright people from other groups. I am grateful for many helpful comments and insightful discussions at various occasions with Christopher Bronner and Felix Leyssner from the group of Prof. Dr. Petra Tegeder, and Dr. Giuseppe Mercurio and Martin Willenbockel from the group of Prof. Dr. F. Stefan Tautz. Many thanks go to Prof. Dr. Petra Tegeder and Prof. Dr. Martin Weinelt for inviting me to Berlin to visit their laboratories and for showing me the technical beauty of surface science experiments.

This work has been generously proof-read in parts or as a whole by Prof. Dr. Karsten Reuter, Dr. Katharina Diller, Katja Maurer, and Georg Michelitsch. For all the errors that remain, I accept responsibility. Typesetting guidance by Simon Rittmeyer is appreciated.

Many thanks go to my family for their support and encouragement.

Finally, I should mention the financial support by the TUM Faculty Graduate Center Chemistry, as well as the computational resources and technical support received from the *Leibnitz Rechenzentrum der Bayerischen Akademie der Wissenschaften* and the *Rechenzentrum Garching der Max-Planck Gesellschaft.*

Es war sehr schön, es hat mich sehr gefreut.